

ISBN 978-82-326-1664-0 (printed version)
ISBN 978-82-326-1665-7 (electronic version)
ISSN 1503-8181

Antonie Oosterkamp

Doctoral Thesis

Doctoral theses at NTNU, 2016:163

Antonie Oosterkamp

**Modelling and Measuring
Transient Flow in Natural
Gas Pipelines**

Effect of Ambient Heat Transfer Models

NTNU
Norwegian University of
Science and Technology
Faculty of Engineering Science and Technology
Department of Energy and Process Engineering

Doctoral theses at NTNU, 2016:163



Norwegian University of
Science and Technology

NTNU



Norwegian University of
Science and Technology

Antonie Oosterkamp

Modelling and Measuring Transient Flow in Natural Gas Pipelines

Effect of Ambient Heat Transfer Models

Thesis for the degree of Philosophiae Doctor

Trondheim, May 2016

Norwegian University of Science and Technology
Faculty of Engineering Science and Technology
Department of Energy and Process Engineering



Norwegian University of
Science and Technology

NTNU

Norwegian University of Science and Technology

Thesis for the degree of Philosophiae Doctor

Faculty of Engineering Science and Technology
Department of Energy and Process Engineering

© Antonie Oosterkamp

ISBN 978-82-326-1664-0 (printed version)
ISBN 978-82-326-1665-7 (electronic version)
ISSN 1503-8181

Doctoral theses at NTNU, 2016:163



Printed by Skipnes Kommunikasjon as

I dedicate this thesis to my parents. Looking back, their encouragement during my childhood and adolescent years were crucial. It is due to their support that I took the path through the higher education system.

Abstract

The central question of this thesis is how and to what extent the representation of ambient heat transfer in the calculation models contributes to observed deviations between modelled and measured flow parameters in natural gas transmission. The focus is on the heat transfer occurring with buried pipelines. The research approach was a combination of model studies with a large experimental component.

The first 12 km of an export gas pipeline was instrumented and used for the experimental investigation of heat transfer behaviour and result verification. This pipeline section contains both onshore and offshore sections. A high accuracy model was made. Real data of the gas flow instrumentation present on the pipeline define the fluid conditions at the model boundaries. At an onshore location, the pipeline and surrounding soil was instrumented. Measurements included pipe wall and soil temperatures, soil humidity and meteorological quantities.

A one-dimensional flow model was used to model the gas flow inside the pipe. This model is coupled to three different external heat transfer models of the ambient domain (pipe wall layers and soil) for comparison. These heat transfer models are 1D steady state, 1D radial unsteady and 2D unsteady description of pipe wall layer and soil. Both conduction and convection heat transfer in the soil layers were investigated. The effect of transient boundary conditions on heat transfer rates and flow parameter calculations were quantified. The developed models were used to analyse and understand the experimental data, to study the effect of different external heat transfer models, the relevant importance of different heat transfer modes, and the boundary condition assumptions on the pipe flow calculations.

The thesis addresses the following research objectives:

- The spatial and temporal formulation of the heat transfer problem: how does the choice of external heat transfer model influence the calculation accuracy of the flow parameters during transient flow? To what degree do the different models capture the physics around the pipeline
- Sensitivities for governing parameters: how do key governing ambient parameters like air/seawater temperature, and the thermal properties of the soil affect the calculation accuracy of the flow parameters?
- The effect of ground water convection and ambient boundary conditions on calculating the flow parameters

The model verification, carried out over an extended period, and the sensitivity studies show that including the heat storage term in the ambient model has the biggest impact on the accuracy of the calculated gas temperatures. The accuracy of gas pressures is much less sensitive for the choice of heat transfer model. A large improvement in the calculation accuracy of gas temperatures is obtained when using an unsteady heat conduction model representing the pipe and soil in radial coordinates. This confirm findings from earlier published work that using such a so called 1D radial unsteady

model of the pipe wall and soil, i.e. including the time dependent heat storage term in the governing heat conduction equation, leads to a major improvement of the calculation of gas temperatures during transient flow. This model was compared to the 2D unsteady model, based on coupling a FLUENT model to the flow model. The heat transfer response obtained with the 1D radial unsteady model was found very similar to the geometrically more accurate 2D unsteady model during transient flow conditions. The 1D radial unsteady model does lead to a gas temperature error in response to the annual periodic ambient temperature. This error was found to be small for a typical export gas pipeline, but can be significant for other configurations. The error introduced by the definition of the ambient soil surface boundary condition was also found to be small compared to the choice of heat transfer model.

The results show that the gas temperature is sensitive to the values of soil thermal conductivity, inner film coefficient and seawater temperature during transient flow. The soil surface boundary conditions have a smaller influence. The sensitivity for the governing parameters of the heat transfer model is strongly dependent on the flow conditions; the resulting deviations in gas temperature are larger during transient flow conditions resulting in large gas temperature fluctuations.

The results also show that the effect of natural convection upon the heat transfer is small for the studied case but that at higher intrinsic permeability of the soil, the role of natural convection will play a significant role. The role of forced convection was found to have a negligible effect.

Soil thermal properties were determined using different methods. The resulting values for thermal conductivity and thermal diffusivity are in agreement with each other to within the measurement accuracy. The measurements in the soil surrounding the pipe show that the thermal properties are mostly constant in time. Some temporal variations were found, but these were not found to make a significant difference on the resulting calculated heat transfer rates and gas temperatures. The experimental results show that the temporal development of soil temperature profiles around the pipe is asymmetrical when comparing the left and right direction. The soil temperatures under the pipe close to the pipe wall were found to be lower than those above the pipe wall, which is opposite of the expectation with a heat conduction model. Both the use of forced and natural convection heat transfer in the model could not explain this difference, but the asymmetry was found not to affect the heat transfer rates significantly within the accuracy of the measurements and calculations.

Comparison to experimental results during a longer time period, showed that using a 1D radial unsteady model leads to good overall agreement in gas temperature, pressure and pipe wall heat transfer. However, incidental, significant, gas temperature and pressure deviations still occur in connection with transient flow conditions. A 1D radial unsteady heat conduction model with constant thermal properties, using air temperature as soil surface boundary condition, will for most practical purposes satisfactorily approximate the more complex physics of the heat and mass transfer in the soil in response to the gas temperature fluctuations and the ambient parameters.

Preface

The thesis presented here is submitted as a partial fulfilment of the requirements to obtain the Philosophiae Doctor degree (PhD) at the Norwegian University of Science and Technology (NTNU) in Trondheim.

The research work was carried out at the Faculty of Engineering Science and Technology at NTNU and at the Karmøy based, Norwegian gas operator company Gassco AS. The Gassco AS funded work was carried out in the period from January 2011 until April 2015. The research work was part of an ongoing research activity at Gassco AS with the overall aim to improve the flow modelling of offshore natural gas pipelines. The main supervisor was Professor Tor Ytrehus (Department of Energy and Process Engineering). Co-supervisors were Dr. Leif Idar Langelandsvik (Gassco AS), and Professor Stein Tore Johansen (NTNU/SINTEF Materials and Chemistry). The research work was conducted as part of my employment as Senior Scientist at Haugesund based Uni Research Polytec.

The main objective of the thesis was to study the effect of the ambient heat transfer model upon accurate calculation of transient flow parameters in natural gas pipelines.

Antonie Oosterkamp
Kopervik, February 2016

Acknowledgements

Finally, I have come to the end of writing my PhD thesis. Having arrived at this stage of the process, I would like to acknowledge and thank those who have made it possible for me to finish.

Firstly, I like to thank my supervisor, Professor Tor Ytrehus for the time and patience he has dedicated to me. He has pointed me in the right direction on those occasions where this was necessary. At the same time, he let me find and follow my own path towards answering the set objectives. I would also like to thank my co-supervisors, Leif Idar Langelandsvik and Stein Tore Johansen for their support. Their advice given along the way has been extremely valuable and important for the progress of the work. Prof Bernhard Muller's advice on certain aspects of computational fluid dynamics is also highly appreciated.

Secondly, I like to thank Gassco AS for providing the funding and a highly interesting topic for research. I also would like to thank Gassco AS for hosting me during these years and allowing me to closely interact with their organisation. Their continuous interest and dedication to my work has been highly appreciated. Special thanks go to Willy Postvoll for actively following up my project. Other people at Gassco I like to thank here are Svein Erik Losnegård and Ben Velde. I am also extremely grateful for Gassco AS allowing me to publish the work.

Thirdly, I like to thank Ottar Borgenvik for allowing me to use his land for instrumenting the gas pipeline and as a base for the experimental set-up.

Fourthly, I like to thank my employer, Uni Research Polytec for enabling me to take this opportunity. Special thanks go to Sigmund Mongstad Hope, for leading the 'Improved flow modelling' project of which my research work formed a part. I also like to thank Richard Markeson for projecting and assisting me to design and install the experimental set up. Torleif Lothe receives my thanks for conducting the seabed temperature measurements with me, and Ole Henrik Segtnan for obtaining the seabed temperature date. The assistance and support from Filip Sund and Øistein Johnsen is also highly appreciated.

During my stays at the faculty, I have very much enjoyed the contact with the staff and the other PhD students. Special thanks go to my PhD colleague Jan Fredrik Helgaker for the fruitful discussions and cooperation.

Finally, I like to thank my dear wife, Ljiljana and my daughters, Natalija, Vera, and Lidia for their support. They patiently allowed for the huge amount of time spent on the work.

Contents

Abstract.....	i
Preface.....	iii
Acknowledgements	v
Contents	vii
List of papers.....	x
Nomenclature	xi
1 Introduction	1
1.1 <i>Background and Motivation</i>	1
1.2 <i>Objective of the thesis</i>	2
1.3 <i>Problem Outline</i>	2
1.4 <i>Research Context</i>	3
1.5 <i>Research Questions</i>	3
1.6 <i>Research Method/Research Design</i>	3
1.7 <i>Contributions</i>	3
1.8 <i>Outline of Thesis</i>	5
2 Problem Description and State of the Art review.....	6
2.1 <i>Problem Description</i>	6
2.2 <i>Modelling of 1D pipe flow of natural gas</i>	7
2.3 <i>Fluid properties of natural gas</i>	8
2.4 <i>Gas to ambient heat transfer-models</i>	9
2.5 <i>Review of relevant literature</i>	15
2.5.1 Steady state conduction heat transfer models.....	15
2.5.2 Unsteady heat transfer models and effect on transient flow.....	17
2.5.3 Analytical solutions	18
2.5.4 Including convective heat transfer.....	19
2.5.5 Annual ambient temperature cycle	19
2.6 <i>Discussion and summary</i>	20
3 Experimental setup.....	22
3.1 <i>Description of pipeline case-Europipe 2</i>	22
3.2 <i>Measurement site at Bokn-experimental installation</i>	23
3.3 <i>Measurement of soil properties at the experimental location</i>	29
3.3.1 Modelling of soil thermal properties	29
3.3.2 Measurement of soil thermal properties	31
3.3.3 Determination of thermal diffusivity from temperature profiles.....	32
3.3.4 Use of TP01 sensors to measure soil thermal properties.....	33
3.3.5 Grain size measurement and porous media parameters.....	33
3.4 <i>Estimation of gas temperature and wall heat flux</i>	35

3.5 Seawater temperatures-model values and measurements	38
3.6 Experimental uncertainty	41
3.6.1 Assessment of uncertainty with soil temperature sensors	41
3.6.2 Assessment of uncertainty with the soil surface temperature sensors.....	43
3.6.3 Positional accuracy of the sensors	43
3.6.4 Dual wave length radiometer.....	44
3.6.5 Soil volumetric water content measurements.....	44
3.6.6 Uncertainty in ambient weather data measurements.	45
3.6.7 Collected SCADA data for the Kårstø-Trosvåg pipeline section...	45
3.6.8 Effect of gas composition.....	46
4 Pipe flow and heat transfer models.....	47
4.1 <i>Pipe flow model</i>	47
4.2 <i>External Heat Transfer Models</i>	49
4.2.1 1D steady model	49
4.2.2 1D radial unsteady model.....	50
4.2.3 2D unsteady model	54
4.3 <i>Europipe 2 flow model – Kårstø-Trosvåg</i>	56
4.4 <i>Porous media models</i>	57
4.5 <i>Forced convection model</i>	59
4.6 <i>Natural convection model</i>	60
4.7 <i>Bokn experimental site model</i>	61
5 Results.....	63
5.1 <i>Analysis of transient flow conditions in Europipe 2</i>	63
5.2 <i>Parametric model studies</i>	66
5.2.1 Rapid Transients: effect of choice of ambient model.....	66
5.2.2 Influence of the annual ambient temperature cycle.....	86
5.3 <i>Soil properties and boundary conditions of the verification models</i>	90
5.3.1 Soil grain size distribution and intrinsic permeability estimation	90
5.3.2 Measurements of the thermal properties of the soil	91
5.3.3 Thermal properties measurement at the experimental site	94
5.3.4 Lower boundary condition.....	95
5.3.5 Inner pipe wall boundary conditions-estimation of inner film coefficient and gas temperature	96
5.3.6 Norkyst 800 data- Accuracy Seawater temperature values used in the verification model.....	97
5.4 <i>Soil Measurement series Bokn-observations</i>	99
5.4.1 Difference between soil surface temperature and air temperature	99
5.4.2 Soil temperature profiles	100
5.4.3 Soil moisture measurements.....	104
5.5 <i>Reproducing measured soil temperature profiles with a 2D heat conduction model of the experimental site</i>	105
5.6 <i>Effect of upper soil boundary conditions</i>	109
5.6.1 Soil-atmosphere boundary.....	109
5.6.2 Soil surface moisture migration.....	113
5.7 <i>Effect of groundwater convection</i>	114

5.8	<i>Verification: long term comparison of heat transfer model performance</i>	120
5.8.1	Comparison of 1D steady and 1D radial unsteady heat transfer model	121
5.8.2	2D unsteady ambient model	127
5.8.3	Sensitivity for thermal properties and boundary conditions.....	130
6	Discussion	135
6.1	<i>The characteristics of rapid flow transients</i>	135
6.2	<i>The influence of the external thermal model on the accuracy of calculate gas pressure and temperature during transient flow</i>	135
6.3	<i>Ambient boundary condition</i>	139
6.4	<i>Ability to represent the effect of the annual ambient temperature cycle</i>	140
6.5	<i>Soil thermal properties</i>	141
6.5.1	The role of soil moisture in gas to ambient heat transfer	142
6.6	<i>Implications</i>	143
7	Conclusion and outlook.....	145
7.1	<i>Conclusions</i>	145
7.2	<i>Outlook</i>	147
8	Summary of research articles.....	149
References		154
Appendix A: Selected papers		159
Appendix B: Derivation of governing equations for 1D flow		256
Appendix C: Calibration coefficients PT100 sensors.		263
Appendix D: Europipe 2- Flow Model Data.....		264
Appendix E: Results from parameteric model studies.....		265
Appendix F: Inner film coefficient.....		272
Appendix G: Measured temperature soil profiles		273
Appendix H: Measured and modelled temperature curves.....		275
Appendix I: Results of sensitivity study on the verification model		281

List of papers

- [a] J.F.Helgaker, A.Oosterkamp, T. Ytrehus. Transmission of Natural Gas through offshore pipelines- effect of unsteady heat transfer model. MekIT'13: Seventh national conference on Computational Mechanics, Akademia Publishing 2013, pp. 113-131.
- [b] A.Oosterkamp, J.F. Helgaker, T.Ytrehus. Modelling of natural gas pipe flow with rapid transients-case study of effect of ambient model. In Energy Procedia, 3rd Trondheim Gas Technology Conference, TGTC-3, Trondheim, 2014, vol. 64, pp. 101-110.
- [c] J.F. Helgaker, A.Oosterkamp, L.I.Langelandsvik, T.Ytrehus. Validation of 1D Flow model for transmission of natural gas through offshore pipelines. Journal of Natural Gas Science and Engineering, 2014, vol. 16, pp. 44-56.
- [d] F.Sund, A.Oosterkamp, S.M. Hope. Pipeline modelling – impact of ambient temperature and heat transfer modelling. ISOPE-2015, Proceedings of the Twenty-fifth (2015) International Offshore and Polar Engineering Conference, Kona, Hawaii Big Island, USA, June 21–26, 2015, vol. 2, pp. 303-309.
- [e] A.Oosterkamp, T.Ytrehus, S. Galtung. ‘Effect of the choice of boundary conditions on modelling ambient to soil heat transfer near a buried pipeline’, International Journal of Applied Thermal Engineering, vol.100, pp. 367-377..
- [f] A.Oosterkamp. ‘Modelling and Measuring Soil Thermal Properties and Soil Heat Transfer of a Natural Gas Pipeline’, Submitted to the International Journal of Polar and Offshore Engineering, September 2015.
- [g] A.Oosterkamp, ‘Heat transfer modelling of natural gas pipe flow-effect of yearly ambient temperature cycles ’, Accepted for presentation at ISOPE 2016, the Twenty-sixth International Offshore and Polar Engineering Conference, Rhodes, Greece.

I am the second author of article [a]. In article [a], I made the 2D heat transfer model and performed the 2D heat transfer calculations. As the first author of article [b], I carried out the work and performed the computations. The pipe flow model used was made by the second author, J.F. Helgaker as well as the 1D radial heat transfer model, which I adapted for use in an extended form. My supervisor, T. Ytrehus, provided ideas and feedback. In article [c], I performed the analysis and discussion on the heat transfer model together with the first author J.F. Helgaker. In article [d], I made the 2D heat transfer model and performed the simulations regarding the effect of the annual ambient temperature cycle. I assisted the first author in the interpretation of the other results. As first author of article [e], I devised the experimental setup and the plan for the numerical investigations. The 1D heat transfer model was made by the co-author, S. Galtung and part of the data analysis and simulation work carried out by him. My supervisor T. Ytrehus gave ideas and feedback. I am the sole author of articles [f] and [g].

Nomenclature

A	cross section [m^2]
A_p	pipe cross section [m^2]
Bi	Biot number
c_v	constant volume heat capacity [$\text{J/kg}\cdot\text{K}$]
c_p	constant pressure heat capacity [$\text{J/kg}\cdot\text{K}$]
c_{pw}	constant pressure heat capacity of water [$\text{J/kg}\cdot\text{K}$]
C_{fc}	scaling coefficient forced convection
C_{nc}	scaling coefficient natural convection
Cp_n	heat capacity of soil constituent n [$\text{J/kg}\cdot\text{K}$]
d_o	pipe outer diameter [m]
D	pipe inner diameter [m]
f	friction factor
f_n	weight factor for DeVries method
Fo	Fourier number
g	gravitational acceleration [m/s^2]
h	hydraulic head [m]
h_i	inner film coefficient [$\text{W/m}^2\text{K}$]
h_o	outer film coefficient [$\text{W/m}^2\text{K}$]
h_s	soil surface heat transfer coefficient [$\text{W/m}^2\text{K}$]
H	distance from centerline of pipe to soil surface [m]
K	hydraulic conductivity [m/s]
KP	kilometer post; distance from pipeline inlet (km)
L	length [m]
\dot{m}	mass flow rate [kg/s]
M	molar mass [kg/mol]
Nu	Nusselt number
p	pressure [N/m^2]
P	period of ambient temperature cycle [s]
Pe	Peclet number
Pr	Prandtl number
q	heat flux [W/m^2]
q_w	wall heat flux [W/m^2]
Q	Darcian flow [m^3/s]
\dot{Q}_m	heat transfer rate per unit length pipe(W/m)
q_{kg}	energy exchanged from the ambient to gas per mass unit [W/kg]
q	net surface radiation [W/m^2]
q_G	soil conduction of thermal energy [W/m^2]
q_H	soil surface convective heat flux [W/m^2]
q_{LE}	soil surface latent heat flux [W/m^2]
r_a	air humidity saturation level
r_e	equivalent wall radius [m]
r_i	pipe inner radius [m]
r_n	inner radius of pipe wall layer n [m]
r_o	pipe outer radius [m]

r_{n+1}	outer radius of pipe wall layer n [m]
r_{sat}	soil humidity saturation level
R	ideal gas constant
Ra	Darcy-Rayleigh number
Re	Reynolds number
s	saturation ratio
S	shape factor
SG	specific gravity
t	time [s]
T	temperature [K]
T_a	air temperature [K]
T_{amb}	ambient temperature [K]
T_{gas}	ambient temperature [K]
T_m	average annual temperature cycle [K]
T_s	soil surface temperature [K]
T_v	virtual temperature [K]
T_{wall}	pipe inner wall temperature [K]
ΔT	amplitude annual temperature cycle [K]
u	velocity [m/s]
U	overall heat transfer coefficient [W/m ² ·K]
U_{wall}	overall heat transfer coefficient [W/m ² ·K]
u_s	ground level velocity [m/s]
v_d	Darcy velocity [m/s]
V_a	volume of air [m ³]
V_s	volume of soil [m ³]
V_w	volume of water [m ³]
x	spatial coordinate [m]
y	spatial coordinate [m]
z	spatial coordinate [m]
Z	compressibility factor
α	thermal diffusivity [m ² s]
α_{eq}	equivalent thermal diffusivity of saturated soil [m ² s]
α_0	transformed pipe surface coordinate
β	coefficient of thermal expansion [K ⁻¹]
β_{aw}	transition parameter Devries method
ϵ	pipe roughness
κ	intrinsic permeability [m ²]
λ	thermal conductivity [W/m·K]
λ_{gas}	thermal conductivity of gas [W/m·K]
λ_i	thermal conductivity of pipe wall layer i [W/m·K]
λ_n	thermal conductivity of soil constituent n [W/m·K]
$\lambda_{seawater}$	thermal conductivity of seawater [W/m·K]
λ_{soil}	thermal conductivity soil [W/m·K]
μ	dynamic viscosity [N·s·m ⁻²]
ν	kinematic viscosity [m ² /s]

ρ	density [kg/m^3]
ρ_{air}	density of air [kg/m^3]
ρ_n	density of soil constituent n [kg/m^3]
ρ_w	density of water [kg/m^3]
σ	dimensionless burial depth
ω	angular velocity [rad/s]
ϕ	porosity
ϕ_n	porosity of soil constituent n
ϕ_L	part of pore space taken up by fluid

1 Introduction

1.1 Background and Motivation

Gassco AS is the operator of 8000 km of gas pipelines owned by Gassled. The majority of these are offshore and are located on the Norwegian Continental Shelf (NCS). These include 600-1000 km long gas export pipelines to Great Britain, Germany, France, and Belgium. Real time calculation models are used to monitor and control the flow of the gas in the pipeline network. Experience shows that under transient flow conditions the calculation results provided by the standard models are less accurate than desired. Even though modelling results are generally accurate enough to warrant safe and reliable gas transport throughout the network, more accurate fluid flow models are still desired.

The export pipelines for gas from the NCS are ranging from 500 to 1200 km length with approximate diameters of 1 meter. Only at the inlet and outlet, there are pressure, flow, and temperature measurements. The state of the fluid in between inlet and outlet is calculated using ‘real time’ computer models. The fluid flow in a pipeline is fully described by the three conservation laws, supplied with an equation of state (EoS) and physical parameters:

- Conservation of mass (continuity)
- Conservation of momentum (Newton’s second law)
- Conservation of energy (first law of thermodynamics)

These three equations, called the Navier Stokes (NS) set of equations, are used to calculate three unknowns; pressure, velocity and temperature of the fluid (Navier [1], Stokes [2]). The equations are known for at least 100 years, but an exact, analytical solution for turbulent flow in three dimensions has not been found so far (Devlin [3]). Within the field of computational fluid dynamics, computer codes have been formulated that for certain problems can resolve the entire turbulent case through so called Direct Numerical Simulation (DNS) of the NS set of equations (Orszag [4]). A rule of thumb is that in order to resolve the flow problem with DNS, the size of the calculation elements must be in order of the smallest Kolmogorov turbulence length scale (Kolmogorov [5]), and the total number of calculation elements necessary to resolve the domain being in order of $Re^{9/4}$ (Zienkiewicz et al. [6]). The Reynolds numbers achieved during pipeline transmission of natural gas are 10^6 - 10^7 , rendering the use of DNS out of reach of the computational capabilities of even the largest computer clusters. Alternatively, the flow in the pipe can be calculated using the three equations with an appropriate turbulence model for closure. However, if representing the flow in three dimensions (3D), a several hundred km long pipeline is still outside the practical limits of computational capacity. In order to calculate the flow field for such a long pipeline, the NS set of equations are reduced to their one-dimensional (1D) form, by assuming constant diameter for each calculation element and representing turbulence through a friction factor formulation (Abbaspour and Chapman [7]).

The PhD work described here is part of a larger Gassco AS project. Through a coordinated research effort, Gassco AS has started a systematic evaluation program to

Introduction

quantify the uncertainty each model simplification and empirical formulation introduces to the calculated pressure, temperature, and velocity fields. Good progress has been made with respect to the steady state flow problem, amongst other through the PhD work of Leif Idar Langelandsvik (Langelandsvik [8]), as well as internally reported research. Apart from the remaining uncertainties about the causes of the deviations in the temperature calculation during steady state ([9]), much larger, and currently not well understood deviations with the models have been identified for transient flow in the network. Investigation into different numerical and modelling related causes of deviation during transient flow were carried out in the PhD work of Jan Fredrik Helgaker (Helgaker [10]). Two types of transient flow regimes can be distinguished in a natural gas network: slow and rapid transients. Rapid transients are associated with upsets in production, major leaks, compressor failure, rapid shut down, or quick flow rate change of the system. Slow transients are the changes in flow, pressure, and temperature due to the packing and unpacking phenomena of gas in the network originating from fluctuations in demand. In this study, we will focus mainly on the rapid transients with a time span from one minute to several hours.

1.2 Objective of the thesis

The objective of this PhD thesis is to study transient flow occurring in long natural gas pipelines. The central question is how and to what extent the representation of ambient heat transfer in the calculation models contributes to the observed deviations between modelled and measured flow parameters. This includes:

- The spatial and temporal formulation of the heat transfer problem: how does the choice of heat transfer model influence the calculation accuracy of the flow parameters during transient flow? To what degree do the different models capture the physics around the pipeline?
- Sensitivities for governing parameters: how do key governing ambient parameters like air and seawater temperature, the thermal properties of the soil affect the calculation accuracy of the flow parameters?
- The effect of ground water convection and ambient boundary conditions on calculating the flow parameters.

In order to do this, the 1D viscous, compressible flow model developed by Helgaker, [10] is used together with different model strategies for ambient heat transfer and compared to experimental results.

1.3 Problem Outline

The research presented here consists of a combination of model studies and field measurements of heat transfer from an actual natural gas pipeline. The research is motivated from actual deviations encountered with the flow modelling of the offshore gas export network for control purposes at Gassco AS. The real time thermo-hydraulic modelling of the gas in the network is highly accurate, granted steady and near steady conditions prevail throughout the pipelines. A reduction in the model's predictive ability for fluid pressures and temperatures is observed when the pipeline inlet flow is

Introduction

fluctuating, thus introducing a high level of transient behaviour. Due to the extent of the pipeline network and the need for real time calculation, the models representing heat transfer to the ambient need to be as simple as possible. It is therefore of interest to gain more knowledge about the effect of these simplifications upon the accuracy of flow parameter calculation during transient flow. There are uncertainties related to governing parameters of the heat transfer problem, i.e. soil thermal properties, pipe burial depth, ambient temperatures, and mode of heat transfer. The effect of these uncertainties on the flow calculation also warrants further investigation.

1.4 Research Context

Understanding the origins of the temperature deviations occurring when calculating transient flow is significant given the network flow is generally transient, the steady state being the exception.

1.5 Research Questions

The following research questions were formulated to cover the objectives:

1. What are the characteristics of transient flow in a real pipeline system? What characterizes the inlet and outlet conditions? How are mass rates, temperatures, and pressures interrelated? What are the rates and extent of inlet flow parameter changes?
2. How does the thermal model affect the accuracy of calculated gas pressure and temperature during transient flow conditions, and, what are the magnitudes of error originating from the heat transfer model compared to the effect of the other governing parameters?
3. To what degree do the different models capture the physical effects around the pipeline?
4. How well does a solely conductive heat transfer model capture the soil temperature profiles around the pipeline? Does ground water convection play a significant role?
5. How do the physical effects at the soil to atmosphere boundary affect the heat transfer between the gas and ambient? Which of these are important?

1.6 Research Method/Research Design

The thesis addresses the aspects of pipeline heat transfer to the ambient and its effect upon calculation accuracy of pipe flow parameters. The study combines computational modelling and field measurements of an actual pipeline case, Europipe 2. Field measurements of soil heat transfer, soil thermal properties, and ambient parameters were carried out. Operational pipe flow data was collected from Gassco AS Supervisor Control and Data Acquisition (SCADA) system. The gathered data was used to study the problem and verify model results.

1.7 Contributions

The following main contributions follow from the results presented in this thesis.

Introduction

1. An experimental setup to study gas to ambient heat transfer of a gas export pipeline was designed, installed, and commissioned. Long-term measurements of weather data, soil temperatures, soil humidity and soil thermal properties were conducted at this experimental site (during 3 years). Different methods were used to obtain a good estimate of the soil thermal properties at the experimental site for use in the models. The setup allowed to collect experimental values for soil temperatures, pipe wall heat transfer rates, and gas temperatures. Seawater bottom temperatures were measured and used to verify the seawater temperatures provided by oceanographic model (Norkyst800) used in the models.
2. A method was designed to couple the pipe flow model to a ‘quasi’ 3D external heat transfer model. The external heat transfer model was implemented in the commercial finite volume code ANSYS FLUENT. Scripts were made to use the two models simultaneously in a transient simulation with coupling between the energy equation of each model during each time step. The performance of such coupled model was compared to the use of two standard external heat transfer models; one based upon solving the transient 1D radial heat conduction equation, and one 1D steady state model.
3. The results confirm findings from earlier publications that the 1D radial unsteady model leads to more accurate prediction of gas temperatures compared to the standard 1D steady model. An explanation for the improvement occurring with the 1D radial unsteady model is forwarded in this thesis. The limits of use of the 1D steady and 1D radial unsteady model under transient flow conditions have been determined and compared to the use of a geometrically more accurate 2D model. This is validated against measurements. It is demonstrated that in most cases using a 2D unsteady ambient model leads to the same response on a transient as with the 1D radial model. The error introduced due to heat storage from the annual ambient air temperature cycle was quantified for relevant cases, using the 1D steady and 1D radial unsteady external heat transfer models.
4. The sensitivity of the gas- to ambient heat transfer for the choice of heat transfer model and the other governing parameters have been determined for a real pipeline case. The results were verified against experimental data.
5. The sensitivities of the heat transfer rates for the other governing parameters like soil thermal conductivity, soil thermal diffusivity, temperature of the lower soil domain boundary, and ambient boundary condition have been determined using both models and measurements from the experimental setup.
6. The results show that the choice of external heat transfer model influences mainly the accuracy of gas temperatures and not the gas pressures in response to an inlet transient. The relative contributions of heat storage in the pipe wall and surrounding soil layers on the heat transfer response during gas temperature fluctuations have been determined. The findings confirm earlier results from literature.
7. The extent to which the ambient boundary condition can be simplified without losing accuracy of heat exchange calculation have been established through modelling and experimental measurements of atmosphere-pipeline-soil thermal interaction.

Introduction

8. The validity of the heat conduction external heat transfer model has been investigated by comparing modelled and measured soil temperatures at the experimental site. The accuracy of heat transfer rates between the ambient and the gas inside the pipeline were determined.
9. An estimation of the contribution from groundwater convection in the soil on the heat transfer between gas and ambient was established for the pipeline case at the experimental site.
10. The ability of the external heat transfer models to correctly calculate heat transfer with annual periodic surface temperature boundary conditions was assessed.

1.8 Outline of Thesis

The thesis has the following organization.

Chapter 2 contains the problem description and the relevant state-of-the art from the literature review. This chapter concludes with a short reflective summary. Chapter 3 describes the Europipe 2 case and measurement site, experimental setup as devised and the experimental methods used. Chapter 4 describes the different numerical models as used for the investigations are documented. Chapter 5 presents the results. First, the flow transients are described. This is followed by results from the model study that includes the effects of choice of heat transfer model and parameter sensitivity. Subsequently the results of experimental determination of soil properties at the measurement site are given, followed by investigation of the seawater temperature development over time. The observations made at the measurement site are presented. Further the verification of results and sensitivity for heat exchange model and parameters obtained with the Europipe2 experimental model are presented. Finally, the results of modelling the measurement site are presented. This includes the sensitivities for boundary condition assumptions and the effect of convective heat transfer.

Chapter 6 provides a discussion on the results. Chapter 7 presents the conclusions and outlook are given. Chapter 8 gives a summary of research articles, which are included in the Appendix A.

2 Problem Description and State of the Art review

In this Chapter, the theory and models used in non-isothermal pipe flow hydraulic calculations are described. Emphasis is put on the formulation of the heat exchange between the gas inside the pipeline and the ambient soil and atmosphere.

2.1 Problem Description

Natural gas from gas fields on the NCS is transported by pipeline or ship to processing facilities. At the process facilities, the gas is processed into heavier fractions (light oils) and sales quality natural gas. A minor portion is liquefied into LNG (Liquefied Natural Gas) and brought to market by ship. Export pipelines to terminals in the United Kingdom, Germany, France, and Belgium transport the majority of the sales gas. At the terminals, the gas is further conditioned for distribution into the national grids. Gassco AS operates the Norwegian pipeline infrastructure and processing facilities. Gassco AS is 100% owned by the Norwegian state. The operator role includes the safe operation of the 7975 km long network of gas pipelines. Gassco AS is responsible for system operation and capacity administration. To facilitate these tasks, a control system of the whole infrastructure is modelled in real time using process monitoring signals as input. The pipe flow is modelled as a 1D system. A wide arrangement of pipeline transport aspects are subject to control with this online model. This includes arrival estimation of gas quality batches, avoidance of over pressurization and leak detection. The individual pipeline and network models are also used offline. An example of this is to determine available transport capacity. Another example is the design of solutions for enlarging the network through tie-in of e.g. new fields.

A typical transport pipeline on the NCS has a compressor station at the inlet. Measurement of gas transport properties like pressure, temperature, and flow rate is conducted primarily at the pipeline inlet and outlet. The hydraulic flow properties in between these points can only be estimated by calculation. During the winter months, the pipelines are often utilized to maximum capacity. Capacity increase offers a potential for increased sale of gas from shippers to end customers. For operation and control of the network, accurate calculation of pressure and temperature profiles are, amongst others, important for real time leak detection. Another important aspect is that inventory control and knowing at what time a batch with a specific gas quality will arrive at the receiving terminal. This all depends on accurate calculations of pressures and temperatures, as these determine the volume taken by a mass quantity of gas.

Experience shows that under transient conditions the model calculations are less accurate than desired. Flow transients are the changes in flow, pressure, and temperature resulting in packing and unpacking of the gas inventory in the network. The transients originate from fluctuations in demand. Understanding the causes of deviations during transient flow is highly significant because the gas is more likely to be in a transient state, steady state rather being the exception. The transients are occurring on a time scale of minutes, and the period of interest to follow a single transient to the system ranges from several hours to several days.

This thesis discusses the effect of the ambient heat transfer model upon the accuracy of pipe flow calculation. The focus is on buried pipelines. For a long gas pipeline, the ambient heat transfer problem is a 3D temporal problem. The thermal gradients in the soil along the flow direction are several orders of magnitude smaller than in the cross-sectional plane. A succession of two-dimensional, alternatively 1D domains, each representative for a section of the pipeline, may therefore represent the ambient heat transfer domain. As the pipelines are long, and the networks extensive, there is a pressure to keep the ambient models as simple as possible. This often results in the use of a steady state 1D conduction model for real-time calculations. For off-line calculations, a 1D radial unsteady heat conduction model may be used. Only for short pipeline sections, it is practical to use a two-dimensional (2D) model. Heat conduction is normally the only mode of heat transfer that is modelled. In special cases, the effect of soil moisture is included, often in connection with the phase transition of freezing/thawing of the soil layers around the pipe.

Minimum two thermal boundary conditions need to be employed; the soil surface temperature and pipe wall temperature. When defining the buried pipeline and ambient as a two dimensional problem, the thermal boundary conditions at lower and side edges of the domain need to be defined as well. Pipe inner wall temperatures are depending on the heat transfer between the turbulent gas stream and the inner wall; this needs to be described as part of the inner boundary condition. The soil surface temperature is normally not known and approximated from the air temperature. This is either measured or based upon meteorological statistics. The effects of the soil surface radiation balance, including soil moisture migration (evaporation, condensation, and precipitation), are usually ignored. The soil surface temperature has two distinct cycles in time, diurnal and annual. The diurnal cycle attenuates to practically constant temperatures a few decimetres into the soil. The effect of the annual cycle is noticed with a time delay up to several meters into the soil. Gas temperature transients attenuate at varying distances into the soil depending on their rate of change.

2.2 Modelling of 1D pipe flow of natural gas

Pipe flow of natural gas is governed by the Navier Stokes equations. The governing equations for 1D compressible flow are found by averaging the 3D equations across the pipe cross section. The basic equations and methods of solution can be found in Thorley and Tiley [11]. Langelandsvik [8], Helgaker [10] and Chaczykowsky [12] provides the equations in a more elaborate fashion. The derivation of the one dimensional equations to the from shown here is included in Appendix B. The equations that are used have the following form:

Conservation of mass:

$$\frac{\partial \rho}{\partial t} + \frac{\partial (\rho u)}{\partial x} = 0 \quad (2.1)$$

Conservation of momentum:

$$\frac{\partial(\rho u)}{\partial t} + \frac{\partial(\rho u^2 + p)}{\partial x} = -\frac{f \rho u |u|}{2D} - \rho g \sin \theta \quad (2.2)$$

Energy:

$$\rho c_v \left(\frac{\partial T}{\partial t} + u \frac{\partial T}{\partial x} \right) + T \left(\frac{\partial p}{\partial T} \right)_p \frac{\partial u}{\partial x} = \frac{f \rho u^3}{2D} - \frac{4q_w}{D} \quad (2.3)$$

The energy equation (Equation (2.3)) is expressed in the non-conserved, internal energy form. The second term on the left hand side is related to the Joule-Thomson effect, which is the change in temperature due to the pressure change of the gas. The second term on the right hand side is the dissipation term, which is the breakdown of mechanical energy to thermal energy. The last term represents the heat exchange between the gas and the surrounding environment. When using a steady state external heat transfer model, combining the thermal resistances of the pipe wall and soil layers in an overall heat transfer coefficient U , we can use:

$$q_w = U (T_{gas} - T_{amb}) \quad (2.4)$$

In the momentum and energy equation, f , is the friction factor which can be determined from the Colebrook-White friction formula, Colebrook [13].

$$\frac{1}{\sqrt{f}} = -2 \log \left(\frac{\epsilon}{3.7D} + \frac{2.51}{Re \sqrt{f}} \right) \quad (2.5)$$

The governing Equations (2.1) to (2.3) form a system of hyperbolic partial differential equations that have to be solved numerically. This can be done by implicit finite difference method, as shown in Abbaspour and Chapman [7]. The governing equations are transformed into algebraic expressions in discrete time and space and solved for the mass flow rate \dot{m} , pressure P and temperature T .

2.3 Fluid properties of natural gas

The values of the compressibility factor Z are obtained using the Benedict-Webb-Rubin-Starling (BWRS) equation of state (EOS). This viral equation of state is described in Starling [14]. The derivatives of Z , as used in the discretized modified Navier Stokes equations are also obtained from this equation of state. Fluid viscosity is calculated by the Lee Gonzales Eakin correlation as describe by Lee et al. [15] but using the extended coefficients of Whitson and Brule [16]. This provides the most accurate predictions of viscosity from a range of selected viscosity models when evaluated against measurements of Kårstø gas, as reported in Langelandsvik [8]:

Problem Description and State of the Art review

$$\mu = \frac{9.4 + 0.02M}{209 + 19M} \left(\frac{(9T/5)^{1.5}}{(9T/5)^{1.5} + 0.01M} \right) e^{\left(\frac{3.5 + \frac{986}{9T/5} + 0.01M}{1000} \right)^{(2.4 - 0.2X)}} \quad (2.6)$$

Here M is the molar mass of the fluid. Both the isobaric and isochoric heat capacity of the gas is used in the models. The isobaric heat capacity of the gas is taken from Katz et al. ([17]) and used in the calculation of the inner wall heat transfer coefficient:

$$(2.7) \quad c_p = 1.432 \cdot 10^4 - 1.045 \cdot 10^4 \cdot SG + \\ (5.859 + 18.018 \cdot SG) \cdot T + \frac{15.69 \cdot 10^{-2} \cdot p^{1.106} \cdot e^{-6.203 \cdot 10^{-3} \cdot T}}{SG}$$

Here SG is the specific gravity of the gas.

The isochoric heat capacity, used in the energy equation, is approximated as:

$$c_v = -3.1 \times 10^{(-16)} * p^2 + 1.46 \times 10^{(-8)} * p + 1.6826 \times 1000 \quad (2.8)$$

2.4 Gas to ambient heat transfer-models

For pipeline systems, we have typical four different thermal configurations, as shown in Figure 2.1. These configurations represent full and partial burial on land and offshore.

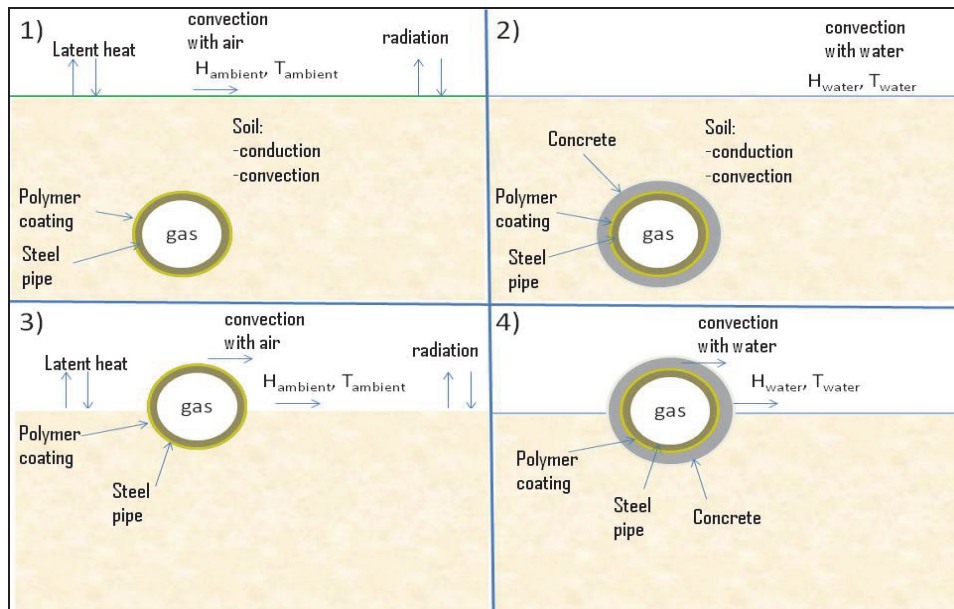


Figure 2.1: Configurations for heat transfer between the gas inside a pipeline and the ambient.

Problem Description and State of the Art review

The heat transfer between the turbulent gas flow and the pipeline inner wall is predominantly convective. Radiative heat transfer plays a negligible role due to the low temperatures involved (<330 K).

To define the heat transfer at the inner wall, a film coefficient is used, defined through the Nusselt number. The Nusselt number is the ratio between convective and conductive heat transfer inside the fluid as it occurs at the boundary, and is defined as:

$$Nu = \frac{q_w D}{\lambda_{gas} (T_{wall} - T_{gas})} = \frac{h_i D}{\lambda_{gas}} \quad (2.9)$$

Where h_i is the film coefficient:

$$h_i = \frac{q_w}{T_{wall} - T_{gas}} \quad (2.10)$$

The correlation used by Gassco is the well-known Dittus-Boelter correlation (Dittus and Boelter [18]) with the coefficient value as introduced by McAdams [19] (Winterton [20]). The correlation expresses the Nusselt number Nu in the Reynolds (Re) and Prandtl (Pr) numbers of the internal flow.

$$h_i = Nu \frac{\lambda_{gas}}{2r_i} = 0.023 Re^{0.8} Pr^n \frac{\lambda_{gas}}{2r_i} \quad (2.11)$$

The power n is set to 0.4 in case the fluid is heated through the wall and at 0.3 in case the fluid is cooled. λ_{gas} is the thermal conductivity of the gas. The normal flow condition for natural gas inside a pipeline is the rough turbulent flow regime, occurring at high Reynolds numbers (10^7). The resulting high Nusselt number implies that convective heat transfer in the gas is dominating, and that gas temperature over the pipeline cross-section may be considered constant.

The heat transfer through the pipe wall layers is conductive and governed by the Fourier heat conduction equation:

$$\frac{\partial T}{\partial t} = \alpha \nabla^2 T \quad (2.12)$$

The heat transfer problem in the soil domain can both have a conductive and convective component. The conductive component is described through the heat conduction equation (Equation 2.12).

In the steady state, the heat transfer configuration of a fully buried pipe can be reduced to a single overall heat transfer coefficient U . This overall heat transfer coefficient combines the inner wall film coefficient, h_i , derived from the Nusselt number (Equation

Problem Description and State of the Art review

(2.11)), the thermal resistance of the pipe wall layers, and the thermal resistance of the soil domain.

For a non-buried pipeline, convective heat transfer will occur between the pipe outer wall layer and the ambient fluid (air or seawater). The outer film coefficient, h_o , is derived from the Nusselt number of the heat transfer to the seawater:

$$Nu = \frac{h_o d_o}{\lambda_{seawater}} = 0.26 Re^{0.6} Pr^{0.3} \quad (2.13)$$

The slightly modified form as presented in Zukauskas and Ziugzda [21] is used. The correlation is under the assumption that the pipe is subjected to a cross flow current.

Convective heat transfer can play a role in case ground water is present in the soil pores. Three additional elements to the heat transfer problem may play a role:

- Forced convection.
- Natural convection; the thermal gradient induced liquid mass flux in a porous media.
- Vapour mass flux inside the pores of a porous media.

The Darcy law governs forced convection in saturated porous media. We can consider the soil as a porous media, containing packed grains. In between the grains are interstitial spaces. The ratio of interstitial space volume in relation to the total volume of a porous media is the porosity, ϕ . For a hydraulic gradient dp/dL the Darcy law gives a Darcy flow Q (Bejan [22]):

$$Q = v_d A_d = \frac{-\kappa}{\mu} \frac{dp}{dL} \cdot A = -K \frac{dh}{dL} \cdot A \quad (2.14)$$

In this correlation, v_d is the Darcy velocity, κ is the intrinsic permeability, μ the fluid dynamic viscosity, K is the hydraulic conductivity, ρ is the fluid density, A is the cross-sectional area, A_d is the pore area, h is the hydraulic head and g is the gravitational acceleration.

In the case of convective heat transfer, the heat conduction equation is extended to (Nield and Bejan [22]) :

$$\rho c_p \frac{\partial T}{\partial t} + \rho_w c_{pw} \overline{v_d} \cdot \nabla T = \lambda \nabla^2 T \quad (2.15)$$

Where c_p is the combined heat capacity, ρ the combined density and λ the combined thermal conductivity of the porous media and the fluid, c_{pw} and ρ_w are the heat capacity and the density of the fluid, respectively.

Problem Description and State of the Art review

With unsaturated, moist soil, phase changes of water and vapor transport will contribute to the heat transfer. The flow through the porous media is now a two-phase problem.

Two phase flow and heat transfer in porous media is described in Kaviany [23] and is briefly reviewed below. The fluid medium can be considered to containing a wetting (liquid) phase and a gaseous phase. The ratio between the wetting and gaseous phase is the saturation s , defined as (Kaviany [23]):

$$s = \frac{\phi_L}{\phi} \quad (2.16)$$

Here ϕ_L is the pore space taken up by the fluid phase, and ϕ is the total pore space of the porous medium.

The dynamics of the flow are influenced by:

Surface tension: the magnitudes of the gas-liquid interfacial tension and the liquid-solid interfacial tension.

Wettability: the extent the liquid phase spreads over the solid surface. This is governed by the contact angle and influenced by surface roughness, adsorption, and surfactants.

Matrix of the porous medium: topology of the matrix and the size, shape and distribution of the pores influence the distribution of the phases.

Viscosity ratio: the viscosity difference between the fluid and gas phase influences the flow patterns. Both through the interfacial shear stress and the displacement front behavior.

Density ratio: influences the buoyancy, body, and inertial forces affecting the flow.

Saturation: the extent the liquid phase fills the pores. At low saturation rates, the liquid phase becomes immobile, vice versa for the gas phase.

Temperature and concentration gradients: these result in interfacial tension gradients influencing the flow rates and phase distributions.

The two-phase flow through the porous media can be described in idealized terms as a funicular flow regime. The gaseous and fluid phase move simultaneously, the gaseous phase on the inside and liquid phase on the outside. In a disordered porous media, like soil, the flow pattern will mostly be unlike that. Observations indicate that each phase moves through its own separate network inside the matrix. With decreasing saturation, the gaseous phase flows through a larger part of the matrix at the expense of the liquid phase resulting in a so-called channel flow regime. Porous medium flow is thus inherently complex; within the context of this thesis, only saturated flow is considered.

Problem Description and State of the Art review

The heat exchange between the soil surface and the atmosphere is dependent on the full description of the surface energy balance. In Willams [24], the surface energy balance is defined as :

$$q^* = q_H + q_{LE} + q_G \quad (2.17)$$

Here q^* is the net exchange of radiation between the atmosphere and the soil surface. The transfer of sensible heat between soil surface and the air is denominated as q_H , while q_{LE} is the transfer of latent heat between the soil surface and the air is q_{LE} and q_G is the conduction of heat into the ground. The energy balance is such that during the day more radiation energy is absorbed than reflected/ emitted. Heat is conducted into the ground and at the surface transferred away through convection and evaporation. During the night, there is a net loss due to long wave radiation from the surface, and a net transfer from the sum of q_H , q_{LE} , and q_G . Proper estimation of the term q_{LE} depends on accurate measurement of moisture loss due to evaporation at the surface during dry periods and moisture transfer to the surface during conditions of high air humidity and precipitation. This implies measurement of the moisture profile in the air boundary layer right above the soil. Alternatively, the term q_{LE} can be determined from the air temperature profile just above the surface. The sensible heat depends upon estimating a convective heat transfer coefficient.

An approach to estimate q_H is discussed in Mihalakakou et al. [25]. The boundary condition for the heat conduction equation at the ground surface can be defined as:

$$-\lambda \frac{dT}{dz} \Big|_{z=0} = q^* - q_{LE} - q_H \quad (2.18)$$

The sensible heat q_H is expressed through a convection heat transfer coefficient between air and soil temperature:

$$q_H = h_s (T_s - T_a) \quad (2.19)$$

This heat transfer coefficient h_s at the soil surface consists of a natural and a forced convection term. The first is defined through the soil top layer humidity; the latter is a function of the wind velocity at the surface. Herb et al. [26] gives the following correlations:

$$h_s = \rho_{air} c_{p,water} (C_{fc} u_s + C_{nc} \Delta T_v^{1/3}) \quad (2.20)$$

Constants C_{fc} and C_{nc} scale the forced and natural convection contributions. Herb et al. [26] suggest a value of 0.0015 for both. The difference between virtual air temperature and soil surface temperature is ΔT_v . The wind velocity at ground level is u_s . The form of the equations shown here are for bare soil surfaces. In Herb et al. [26], these correlations are scaled to vegetation coverage conditions by employing a scaling factor less than one. This scaling factor can include both the extent and type of vegetation cover.

Problem Description and State of the Art review

In the same work, the correlation provided for the latent heat Q_{LH} is:

$$q_{LE} = \rho_{air} C_{p,water} (C_{fc} u_s + C_{nc} \Delta T_v^{1/3}) * (r_{sat} - r_a) \quad (2.21)$$

Here, r_{sat} and r_a are saturation and ambient specific humidity [kg_{water}/kg_{air}].

Other, similar type of correlations as shown in Equations 2.20 and 2.21 can be found in the literature.

The combined effects of convection, latent heat, and radiation heat transfer at the soil surface results in a time varying temperature of the soil surface. At the soil surface, both daily and annual temperature cycles can be distinguished. These temperature cycles attenuate downwards into the soil. It is well known from the literature how the amplitude of these temperature cycles decay and phase delay with depth. This is described in for example Williams [24]. Langelandsvik [8] discusses the delayed soil surface temperature change at burial depth for subsea pipelines and notes that this effect is not accounted for in the commonly used external heat transfer models based upon steady state heat transfer.

In transient heat conduction, the dimensionless Biot and Fourier number are often used to compare thermal system behaviour. The Fourier number is the dimensionless time for a temperature change to propagate through a system. The Biot number is the ratio between the heat transfer at the surface boundary (convection) and the internal heat conduction. The convection heat transfer between the turbulent gas flow and the pipe inner wall during flow is described with the film heat transfer coefficient from Equation (2.11). This inner film coefficient has typical values from 1000-2000 W/m²K in natural gas transmission. For a cylindrical heat transfer system, the Biot number is defined as:

$$Bi_{cylinder} = \frac{R_{conduction}}{R_{convection}} = \frac{h_f L}{\lambda_s} = \frac{h_f r_i}{\lambda_s} \quad (2.22)$$

The Fourier number shows if the heat transfer of a system in response to a change in thermal boundary conditions is dominated by heat conduction or heat storage. It is also the dimensionless time of a temperature change of a system.

$$Fo = \frac{\alpha \tau}{L_e^2} \quad (2.23)$$

Here α is thermal diffusivity, τ is the time scale, and L_e is the characteristic length of a system, for example the external radius in case of a cylinder. According to [27], the Fourier number can be interpreted in each of the following manners. A larger Fourier number indicates that more heat is conducted in the system than stored. Over a given period, the heat penetration is deeper with a larger Fourier number, as well as the rate of the temperature change at a certain distance from the boundary.

2.5 Review of relevant literature

This literature review on the thermal modelling of pipe flow is divided in four sections:

- Steady state conduction heat transfer models.
- Unsteady heat transfer conduction models and effect on transient flow.
- Including convective heat transfer.
- Modelling of heat transfer related to the annual ambient cycle.

2.5.1 Steady state conduction heat transfer models

Models for steady conduction heat transfer of a buried pipe are based on defining the overall heat transfer coefficient of the thermal domain. In the literature, some variations how to calculate the overall heat transfer coefficient can be found. In Bau [28], transformation into bi-cylindrical coordinates is used to derive the shape factor for the case of laminar pipe flow. With laminar pipe flow, the assumption of a uniform heat transfer coefficient at the pipe inner wall is not valid. For the resulting conduction shape factor, the differences are shown to stay within 10% between the laminar and turbulent case for a range of fluid-soil thermal conductivity ratios. The conclusion is that the following expression for shape factor is within 2% accurate for turbulent pipe flow and within 10% for laminar pipe flow:

$$S = \frac{Bi}{\sqrt{1 + Bi^2 \alpha_0^2 + 2 * Bi * \alpha_0 * \coth \alpha_0}} \quad (2.24)$$

In the equation, the Biot number Bi is containing the inner wall heat transfer coefficient, the pipe inner radius, and the soil thermal conductivity. For the pipe surface α_0 follows:

$$\sigma = \cosh \alpha_0 \Rightarrow \alpha_0 = \ln \left(\sigma + \sqrt{(\sigma)^2 - 1} \right) \quad (2.25)$$

In Ovworide [29], bipolar transformation is carried out for the cases of both partial and fully buried pipelines. Assumed are convective boundary conditions at the pipe wall and the soil surface. The shape factor equations are based on an isothermal soil surface boundary condition. These become inaccurate if the pipe is buried close to the surface. To improve upon this, two Biot numbers are introduced: B_g for the atmosphere to soil and B_p from the pipe to soil. The corresponding shape factor for the buried pipe configuration becomes:

$$S = \frac{B_p a_{bur}}{\sqrt{\left(\cosh \alpha_0 - B_p a_{bur} \alpha_0 + \frac{B_p}{B_g} \right)^2 - \left(1 + \frac{B_p}{B_g} \right)^2}} \quad (2.26)$$

Problem Description and State of the Art review

The coefficient a_{bur} is:

$$a_{bur} = \sqrt{(\sigma^2 - 1)} \quad (2.27)$$

Similar correlations are provided for the case the pipe is touching the ground and for the case of partial buried pipes. The basic derivation for these correlations for partial buried pipes are also provided in Morud and Simonsen [30]. The reported accuracy of prediction is in such case within 10%.

In Archer and O'Sullivan [31] the soil domain is considered as a homogeneous annular layer around the pipe. This is extended to the case of a trenched pipeline with backfilled material of different thermal conductivity. The equivalent cylinder radius is determined in order to match the resulting steady heat transfer rate with that of the bipolar transformed domain. For a pipe with a convective heat transfer condition at the inner surface the equivalent cylinder radius is:

$$r_e = \frac{r_i}{e^{(1/S - 1/Bi)}} \quad (2.28)$$

For the non-uniform thermal domain, an equation for an effective thermal conductivity is introduced.

An alternative way to calculate the equivalent cylinder radius is given in OLGA [32]:

$$re = r_i(\sigma + \sqrt{\sigma^2 - 1}) \quad (2.29)$$

In Ramsen et al. [33] the effect of heat transfer modelling on the calculated gas temperatures is described for offshore gas export pipeline cases. The conclusions from this work are that for exposed and partially buried pipelines the flow velocity plays an important role during steady flow. At low flow rates, the gas temperature will quickly approach the ambient (seawater) temperature and is thus more dependent on ambient temperature than the U values. For short pipelines, this effect is more pronounced, as well as with overall low U values (high degree of burial). In this work, the importance of correct estimation of gas temperature is discussed. The density of the gas will decrease with increasing temperature. This will in turn decrease the maximum possible flow rate.

In Langelandsvik [8], the sensitivity for the overall heat transfer coefficient U is determined for an gas export pipeline case. The offshore pipeline is fully exposed to seawater over its entire length, with resulting high U values. Steady state flow simulation showed low sensitivity of flow rate and gas outlet temperature for the U values along the pipeline route. Instead, the sensitivity was found to be high for the seawater temperature and current velocity.

In Modisette [34] an overview of strategies for modelling of the ambient in pipe flow calculation is provided. A distinction is made between steady state and transient conditions. This publication notes that the temperature conditions at the outside of the thermal domain ‘are relatively unimportant’ compared to the correct setting of thermal conductivities of pipe wall and soil layers for steady state calculations.

2.5.2 Unsteady heat transfer models and effect on transient flow

In Modisette [34] it is noted that for transient simulations the time scale of the thermal diffusion in the soil is much larger than that of the fluid inside the pipe. In case a 1D radial unsteady model is used, the grid size near the pipe wall needs to be small. Grid size and details of the outermost cells have relatively minor effect on the calculation.

In Chaczykowski [12], an unsteady heat transfer model for gas pipe flow is introduced. Fourier heat conduction through the pipe wall and soil domain is modelled for each pipe calculation element. For this purpose the wall and soil is modelled as a circular domain over which the 1D radial unsteady heat conduction equation is discretized. The heat exchange between the gas inside the pipeline and the ambient is calculated at the pipe inner wall and the resulting heat transfer rate used in the energy equation when calculating the pipe hydraulic flow. As the ambient model is unsteady, the effect of heat storage in the pipe wall and soil during transient flow is included in this model, but its consequences on the flow are not investigated in this work.

In Chaczykowski [35], the effect of the thermal model on flow parameters during transient flow is studied. The 1D radial unsteady model from Chaczykowski [12] is used. A stepwise inlet temperature and outlet flow transient is employed in the study. A noticeable difference of the inlet flow rate between steady and unsteady heat transfer model occurred as a result. A real pipeline case was used, showing that a steady state heat transfer model gives large deviations in gas temperatures in response to outlet flow transients (inlet temperature and pressure kept constant). The inlet flow rate and outlet pressure showed much smaller behavioural difference.

In Nicholas [36] the effect of the thermal model on the flow parameters during transient flow is investigated. Only fully buried pipelines are considered. Both inlet temperature and inlet pressure ramp up scenarios are studied. The ambient soil was modelled as a circular domain over which the 1D radial unsteady heat conduction equation is discretized. The results show significant differences in the response of the pipe flow to the inlet transients when comparing ambient heat exchange models with (unsteady) and without (steady) the ground heat storage term. It takes several days for the temperature transient to dissipate through the soil domain until a new steady state is reached. Initially the temperature difference between the steady and unsteady model is highest at the pipeline entrance, reducing in the downstream direction of the pipeline with time. For the pressure transient it is noted that the initial response leads to a sudden temperature increase in the first part of the pipeline. This increase is larger for the steady heat transfer model. The effect on packing rates is discussed: for the temperature ramp up scenario the packing rate, using a steady state heat transfer model is

overestimated by almost 1% for several hours after the temperature ramp up. For the pressure transient a similar pipeline packing error is found. Initially the differences in packing rate between the two models are very large. Nicholas [36] concludes that the transient thermal behaviour of the ground should be included for transient flow calculation. The use of an overall heat transfer coefficient is inadequate for such purpose. The heat transfer through the pipe wall can be ignored for transient time scales over 30 seconds, but not the heat capacity of the pipe wall. Thermal time scales of the soil are noted to be several weeks to months.

In Helgaker et al. [37], the steady heat transfer model as used at Gassco is compared to the 1D radial unsteady heat transfer model of Chaczykowski [12]. The results are compared with real pipeline data. The findings of this work are that the steady state heat transfer model over-predicts the amplitude of the temperature response in the flow calculation. Using an unsteady thermal model, the accuracy of modeled inlet pressure and outlet mass flow rate increased. The calculated outlet temperature is also improved but there are still discrepancies with actual measurements. The work underlines the importance of the thermal properties of the pipe wall layers and soil for calculating the outlet gas temperature. Lack of accurate data for soil thermal conductivity is emphasized as a significant factor of uncertainty. It is realized that while the heat transfer models used are 1D, the configuration of a buried pipe is at least a 2D problem. It is uncertain how this simplification affects the accuracy of the flow calculation. For the configuration of a partially buried pipe that is exposed to ambient air or seawater, it remains unclear how heat storage can be included in a 1D model.

In Barletta et al. [38], 2D unsteady heat transfer from completely buried pipelines is studied numerically. Both step-rise (rapid transient) and smooth rising fluid temperature cases (slow transient) are studied and compared to an unsteady 1D radial model. In the model, only the soil heat transfer is modelled, not the flow of the gas inside the pipe. The problem investigated is that of pipeline start-up; i.e. initially, the flow is at standstill and the thermal domain at equilibrium. The start-up of the flow through the pipeline is modelled by changing the pipe inner wall temperature accordingly for a single 2D-plane (soil slice). The response of the soil domain upon the temperature change at the pipe inner wall is evaluated through the dimensionless thermal power exchange at the wall per unit length. The conclusion from Barletta et al. [38] is that for engineering purposes the 1D radial unsteady model is accurate enough to follow the transients.

2.5.3 Analytical solutions

Exact solutions for unsteady heat transfer from a buried pipe can be found in the literature for 1D radial configuration. In Lu [39] an exact solution is provided for a 1D multilayered hollow cylinder with a general formulation for the boundary conditions at the inner and outer surface as Fourier series of temperatures. The time-varying temperature is coupled to the wall by a constant heat transfer coefficient. The method uses Laplace transformation to obtain the approximated analytical solution. Comparisons to numerical simulations demonstrate high accuracy of the analytical

solution. The accuracy is dependent on how well the boundary conditions can be matched with Fourier series.

Exact solutions of the two dimensional transient problem of heat transfer from a buried pipe are limited in the literature. In Martin and Sadhal [40] upper and lower bounds for the temperature distribution surrounding a cylinder are given.

2.5.4 Including convective heat transfer

Soil is commonly considered a porous media and the presence of moisture between soil grains can play a role in the overall heat transfer.

The effect of ground water convection upon the heat transfer from a hot buried pipe is investigated in Bau [41]. An analytical solution is provided for the steady state configuration with both (moisture) impermeable and permeable soil surfaces. The solution considers low Reynolds number convection in saturated soil. The Darcy-Oberbeck-Boussinesq equation is formulated using bi-cylindrical coordinates. The additional heat transfer rate from natural convection is established by the Nusselt number, obtained through perturbation expansion of the Raleigh-Darcy number Ra (Bau [41]):

$$Nu = \sum_{i=0}^{\infty} (\sinh(\alpha_0) Ra)^3 N_i, \quad (2.30)$$

where N_i are expansion coefficients, provided in Bau [41]. The configuration of a buried hot pipe shows different convection and temperature patterns for permeable and impermeable top surfaces. Ra is defined as (Bau [41]):

$$Ra = \frac{\beta g k r}{\alpha_{eq} v} (T_1 - T_2) \quad (2.31)$$

In Himasekhar and Bau [42], the theoretical approach of Bau [41] is further developed. The Biot number of the pipe is included in the expression for the Nusselt number. The developed formulas allow estimation of the conductive and convective contributions to the heat transfer rate at the pipe wall for a larger range of Ra and Bi numbers.

2.5.5 Annual ambient temperature cycle

Published work in which a 2D approach to soil conduction is used are mostly limited to the steady state case. In Barletta et al. [43], steady periodic heat transfer for buried offshore pipelines is studied in 2D. The case considered is that of the annual temperature variation in the seabed in shallow water. In this work, the periodical unsteady heat 2D heat conduction problem is transformed and solved numerically as a

steady problem. The analytical solution yields the following expression for the heat transfer across the pipe outer wall per unit length (Barletta et al. [43]), in rewritten form:

$$\dot{Q}_m = (T_{\text{gas}} - T_m) * \frac{2\pi\lambda_{\text{soil}}}{\text{arccosh}(\sigma)} + \frac{2\pi\lambda_{\text{soil}}\Delta T}{\text{arccosh}(\sigma)} * (A \sin(\omega t) + B \cos(\omega t)) \quad (2.32)$$

ΔT and T_m are the amplitude and average of the ambient fluid. The constants A and B are functions of σ , α , ω and R . The constants A and B can be obtained by numerically solving a set of two Poisson equations for the boundary conditions given in the paper. From the equation, it is clear that the phase delay of the ambient temperature profile penetrating down in the soil is captured in the final term to the right. For scenarios with significant transient behavior of the gas temperature, it is questionable if this approach will be applicable, as a basic assumption of the derived correlation is that T_{gas} is constant.

2.6 Discussion and summary

Using a 1D steady state ambient heat transfer model in flow modelling of natural gas pipelines is common practice and well understood. From both the literature and the experience at Gassco AS, it is clear that a steady state formulation of the ambient heat transfer can be a source of error in the calculation of flow parameters. Uncertainties are related to both the transient development of ambient temperature cycles in the soil and the propagation of the gas temperature fluctuations in the pipe wall and surrounding soil (Nicolas [36], Chaczykowski [35], Helgaker et al [37], Barletta et al [43] [38]).

The heat transfer between the gas inside a buried pipeline and the ambient is in essence a 3D problem. The soil thermal gradients in the direction of the pipe axis are small compared to those in the perpendicular plane. Therefore, this 3D heat transfer problem can be simplified as heat transfer in a succession of 2D planes. For the pipe flow calculations, the pipe is divided into sequential pipe elements. On the nodes, or grid points, of these pipe elements, the one dimensional flow equations are discretized. Each pipe element has a corresponding 2D external heat transfer model, with the plane perpendicular to the pipe element axis. For large pipeline networks, such an approach would still be computationally expensive. This is particularly the case when the flow parameters have to be calculated in ‘real-time’ for control purposes of a pipeline network. A more common formulation of unsteady ambient heat transfer is through a 1D unsteady radial heat conduction model. This provides a cylindrical representation of the pipe wall and surrounding soil layers. Although this presents a correct geometry for the pipe wall layers and the surrounding soil close to the pipe wall, the boundary condition at the outer edge of the domain is less correct. A common solution to this is to dimension the radius of the soil layer surrounding the pipe in order for the steady state shape factor of the circular domain to be equal to that of the 2D shape factor of the buried pipe (OLGA [32]).

Problem Description and State of the Art review

Neither of these approaches allows for the two-dimensionality of the heat transfer problem of a buried pipe; this problem has essentially three main boundary conditions:

1. Pipe wall temperature.
2. Soil top layer temperature.
3. The temperature deep down in the soil.

The first boundary condition can be correctly represented in the 1D unsteady radial heat conduction models at the inner boundary. It is not straightforward to set the outer boundary condition if soil surface temperatures are not actually measured. A common assumption is that the soil surface temperature follows the bulk temperature of the surrounding fluid, air for land-based, and seawater for offshore pipelines. Due to the high convective heat transfer coefficient with seawater, the assumption is reasonable for an offshore-buried pipeline. For a land-based buried pipeline, this is more uncertain, because effects of solar radiation and latent heat transfer play a significant role in the temporal development of the soil surface temperature. The third boundary condition is ignored in the 1D radial unsteady heat conduction models. It is unclear what effect omitting this boundary condition present in terms of transient heat transfer calculation. The models do not capture the effects of convective heat transfer due to moisture movement in porous soil either. Particularly for pipelines that are trenched and buried in the seabed, ignoring convective heat transfer could be a source of error. Another common assumption is that the soil thermal properties are constant in time. With soil moisture content changing over time this may not always be the case. To what extent this variation is a source of error is also a viable question.

3 Experimental setup

This Chapter describes the experimental installation used to study the heat transfer between the gas inside a buried pipeline and the ambient

3.1 Description of pipeline case-Europipe 2

The case study used the first 12 km of Europipe 2. The same pipeline has been previously investigated by Langelandsvik [8] and Helgaker [10]. Europipe 2 is a 642 km long gas export pipeline from Kårstø in Norway to Dornum in Germany. The pipeline inner diameter is 0.508 m and the transport capacity is 24.000 Msm³/yr. The ‘onshore’ pipeline route from Kårstø to the landfall at Trøsnavåg on Vestre Bokn is shown in Figure 3.1.



Figure 3.1: Pipeline route from Kårstø to the offshore landfall at Vestre Bokn (courtesy Gassco AS).

Experimental setup

Onshore the pipeline is buried to a depth varying between 1.5 m to 2.5 m t.o.p. (top of pipe). In the first 12 km, the pipeline passes through two short sea-sections where it alternatingly lies on the seabed, is covered with silt or rock dump material, or trenched.

The instrumentation at the pipeline inlet consists of gas pressure, gas temperature, gas volumetric flow rate, density, and compositional measurement of the gas. This equipment is described in detail in Langelandsvik [8]. At the end of the route over Vestre Bokn, there is a landfall valve station (Trosnavåg) where gas pressure and pipeline skin temperature (outer wall surface temperature) are measured. Figure 3.2 shows the pipeline elevation profile and measurement equipment for the first 12 km of the route.

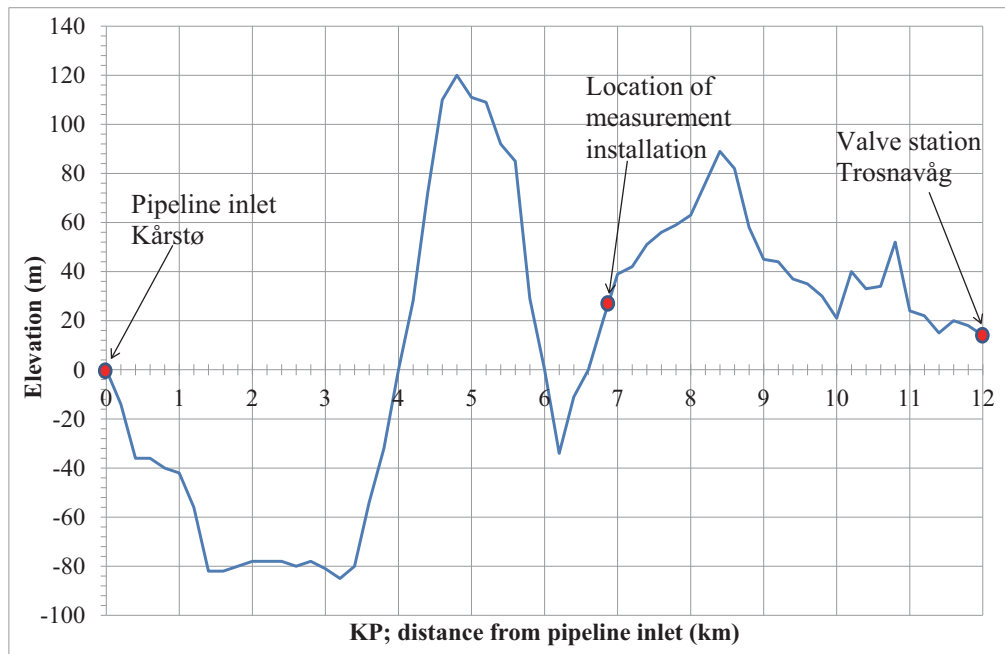


Figure 3.2: Pipeline elevation profile 'onshore' (Kårstø to Trosnavåg).

3.2 Measurement site at Bokn-experimental installation

The experimental installation is approximately 7 km from the pipeline inlet. Here the pipeline and soil were instrumented. Figure 3.3 shows a detailed satellite image of the measurement site in relation to the position of the buried pipeline. Figure 3.4. shows how the pipeline is installed.

Experimental setup



Figure 3.3: Google Earth picture of the measurement location. The red line indicates the approximate route of the pipeline.

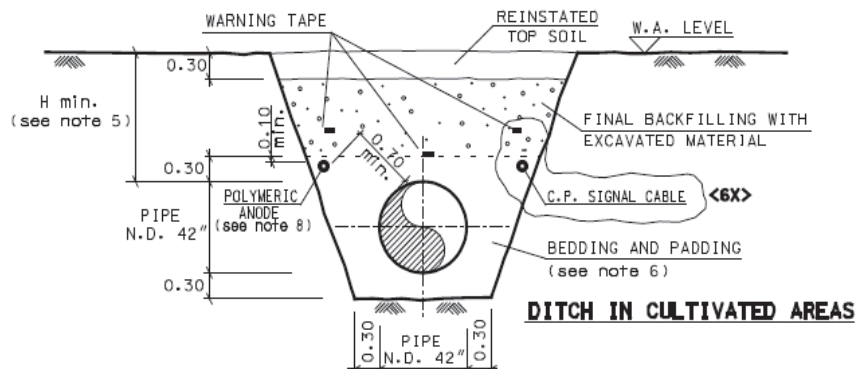


Figure 3.4: Ditch design from original design documentation (Snamprogetti [44]).

Figure 3.5 shows the experimental installation. To install the sensors around the pipe, the backfill consisting of medium grain fill sand was excavated with a suction excavator. With the pipe fully excavated, the sensors near and around the pipe were installed. On the pipeline outer wall, film type PT100 temperature sensors were mounted (top, side and bottom position). The sensors were fitted using a pipeline epoxy repair compound and secured with elastic rubber tape around the entire circumference

Experimental setup

of the pipe. This is in accordance with a normal repair solution for the coating of this type of pipeline.

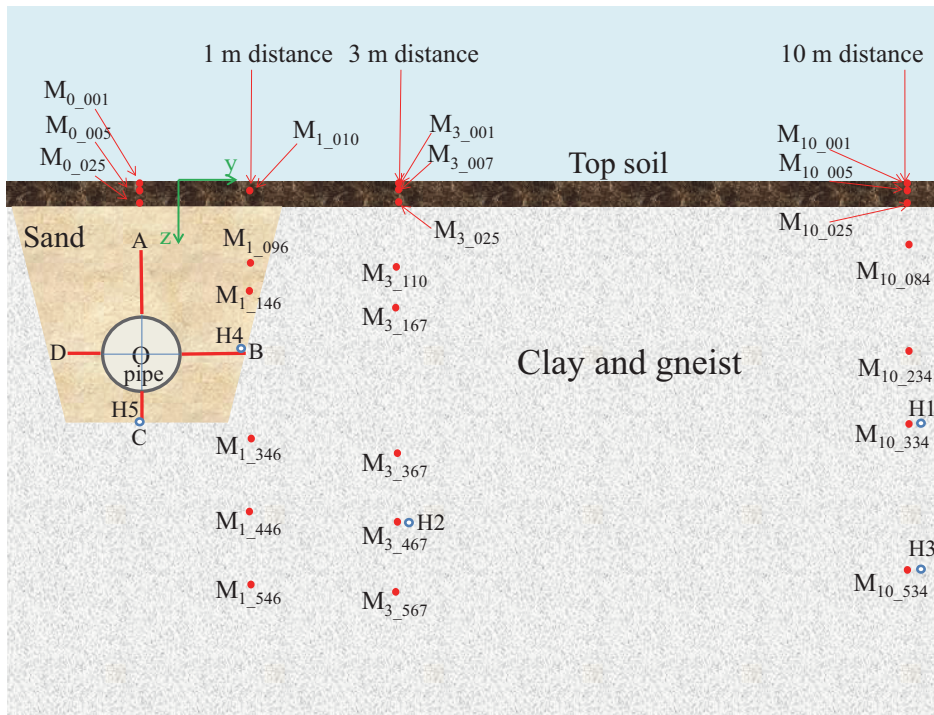


Figure 3.5: Location of measurement sensors around the pipe and in the soil. The direction of view is the same as the flow direction of the gas inside the pipeline.



Figure 3.6: Sensor boom shown during its installation at right hand side of the pipe.

Experimental setup

In the soil around the pipe, temperature sensors were distributed in a radial array at regular distances along the lines O-A, O-B, O-C, and O-D. The sensors were mounted collectively on booms at a distance of 2, 5, 10, 20, 50, and 100 mm from the pipe wall, as shown in Figure 3.6. At the top, one extra temperature sensor is included measuring at 2 mm distance from the pipe wall. First, the measurement boom (O-C) was installed below the pipe. Subsequently the ditch was refilled with sand until pipe axis level. The horizontal measurement booms (O-B and O-D) were put in place and the ditch filled with sand until the top of the pipe just remained visible. The top measurement boom was subsequently secured in position. Care was taken that the sensor boom maintained at right angles in relation to the pipe surface during refilling of the remainder of the ditch. The exposed pipe and some of the installed wall sensors are shown in Figure 3.7.



Figure 3.7: Excavated pipeline. The thin film sensors are beneath the black tape. The epoxy compound is there to keep the wiring in place during installation (Oosterkamp [45]). The thin film sensors at the left and right hands side failed in their function after a short time of operation.

Experimental setup

The soil temperature depth profiles were measured with similar PT100 sensors. To install these sensors, a drill rig made 10 cm diameter holes at 1m, 3 m, and 10 m lateral distance from the pipe outer wall, shown in Figure 3.8. For each hole, the sensors were mounted together on a PVC pipe in order to secure their relative distance during and after installation.



Figure 3.8: Drill rig used for installation of vertical soil temperature sensors.

A total station theodolite was used to map the relative pipeline position, sensor boom positions, and contour of the terrain after refilling the ditch. This allowed the determination of all sensors positions in relation to each other, the soil surface, and the pipeline axis. The accuracy of this equipment is approximately ± 1.5 mm.

The temperature sensors (PT100) are mounted in a 4 mm diameter stainless steel sheath. They were connected to the data-logger (ALMEMO 5690-1M with UA10 cards) in a full bridge configuration with four 20 m long leads. The resolution of the system is 0.01 K (using the ALMEMO ZA9030-FS2 connectors).

For each measurement point, the sensor, leads, measurement bridge and data-logger channel are calibrated as an integrated system. The calibration procedure comprised of a series of multiple comparative measurements in the temperature interval from 0-30 °C. The sensors were tested in a hot bath calibrator (Hart 7103 Microbath) against a calibrated reference PT100 temperature measurement probe (ASL250 MK2).

The measurement system further contains a four component net radiometer, ambient temperature, and humidity measurement. Ambient temperature and air humidity instruments are located in a Stevenson box. Wind velocity was measured for a significant part of the duration of the measurement campaign (premature breakage

Experimental setup

during a storm). At five locations, soil volumetric water content sensors are installed (tagged as H1-H5 in Figure 3.5. These are of type EC-5 from Decagon and measure dielectric permittivity (Campbell [46]) and connected to a Decagon data logger with factory calibration and settings. Calibration curves were made using soil samples, taken at the site during installation.

At two locations, TP01 thermal property sensors from Hukseflux were installed (H2 and H4 in Figure 3.5) (Huskeflux [47]). The TP01 is a thin film sensor containing a central heating wire with two sets of thermopiles parallel (one at each side) to the heating wire. At both sides the thermocouple hot junctions are one millimetre from the heating wire and the hot cold junctions 5 mm at the other side. Both sets of thermopiles are connected in series. The differential voltage over the thermopiles is closely related to the radial temperature gradient around the heating wire. By heating the central wire for a known period with a known voltage, and subsequently measuring the temperature decay, the soil heat storage term can be determined.

The method is explained in detail in Huskeflux [47]. After an initial transient heating period, the soil around the wire assumes a more or less steady state and the temperature rise depends only on the thermal conductivity. Thermal diffusivity can be determined if the current to the heating wire is interrupted; the decay time of the radial temperature profile to the level prior to heating is used to determine the thermal diffusivity (this is valid in case the thermal mass of the sensor is negligible).

The net radiometer Huskeflux NR01 is described in Huskeflux [48]. It measures incoming hemispherical solar radiation and reflected solar radiation, incoming long wave radiation and upward long wave radiation. Twin pyrgeometers measure the incoming atmospheric and returning soil radiation in the 4500 to 50000 nm range. The meters are mounted back to back, containing a black coated thermopile sensor.

This sensor potentially absorbs all LW and SW radiation in a flat spectrum in the 300 to 50000 nanometer range. The sensor is covered by a silicon window: This window has a solar blocking and limits the spectral response from 4500 to 50000 nanometers (cutting off the part below 4500 nm). The field of view is 150 degrees. The black coating on the sensor transforms the long wave radiation into heat, resulting into a signal from the thermopile proportional to the LW radiation. The sensor emits also some LW radiation; the amount of this can be calculated by additional measurement of the sensor temperature with an incorporated PT100 sensor.

A pair of pyranometers measures the incoming atmospheric and returning soil short wave radiation in the spectrum from 300 to 2800 nm. The sensors are similar thermopiles with a black coating. The domed housing cuts off incoming radiation above 2800 nm.

Figure 3.9 shows the experimental site. The yellow sign in the right hand corner indicates the location of the buried gas pipeline. The left hand side shows the container housing the data-loggers, power supply, and environmental instrumentation.

Experimental setup



Figure 3.9: Picture of the experimental site at Bokn. The yellow sign indicates the location of the buried pipeline. The direction of view is opposite to the gas flow.

3.3 Measurement of soil properties at the experimental location

The measurement data collected at the experimental site is used to verify the validity of the assumptions of the external heat transfer models under study. In these models, the values of the soil thermal properties are a source of uncertainty. A more detailed knowledge about the thermal properties of the different soil layers at the experimental site reduces this uncertainty. This is also of key importance for interpreting the temperature measurements, the estimation of gas temperature, and the pipe wall heat flux at the experimental location. The latter can only be estimated using the soil temperature profiles around the pipe. The accuracy of these estimations is highly dependent upon accurate knowledge of the local soil thermal properties. Gas temperature and pipe wall heat flux are needed for the verification of the different heat transfer models and to assess the validity of the underlying assumptions.

3.3.1 Modelling of soil thermal properties

The literature provides correlations that relate soil thermal properties to their basic mineral constituents, and as a function of water content. One method to determine thermal conductivity is the De Vries method [49]. The soil is considered to consist of

Experimental setup

water, air, and solid fractions. Thermal conductivity λ is considered a function of volume fraction ϕ_n , using the soil constituent thermal conductivity λ_n :

$$\lambda = \frac{\sum_n f_n \phi_n \lambda_n}{\sum_n f_n \phi_n} \quad (3.1)$$

In Equation (3.1), f_n is a weight factor for constituent n determined by:

$$f_n = \left[1 + \frac{1}{3} \left(\frac{\lambda_{h,n}}{\lambda_{h,air} + \beta_{aw} (\lambda_{h,water} - \lambda_{h,air})} - 1 \right) \right]^{-1} \quad (3.2)$$

The parameter β_{aw} is a transition parameter (Campbell [50], Westermann [51]):

$$\beta_{aw} = \left[1 + \left(\frac{\phi_w}{\phi_{wc}} \right)^{-s} \right]^{-1} \quad (3.3)$$

The cut-off value ϕ_{wc} for the transition of dominance of the water phase in the pore space is set to 0.15. The smoothing factor s is set to 4 in a possible range of 2-6 as proposed by Campbell [50].

The soil heat capacity can be expressed as the volume fraction weighed average of each constituent leading to this expression for thermal diffusivity (Huang et al. [52]):

$$\alpha = \frac{\lambda}{\sum_n \phi_n \rho_n C_{pn}} \quad (3.4)$$

The basic thermal properties of the constituents used in the calculation of the soil thermal properties are shown in Table 1.

Table 1: Thermal properties of soil constituents (Campbell [50]).

Constituent	Density (kg/m ³)	Heat capacity (J/kg·K)	Thermal conductivity (W/m·K)	Thermal diffusivity (m ² /s)
Quartz	2660	750	8.8	$4.4 \cdot 10^{-6}$
Clay	2650	755	2.9	$1.44 \cdot 10^{-6}$
Organic	1300	1925	0.25	$1 \cdot 10^{-7}$
Water	1000	4200	0.57	$1.36 \cdot 10^{-7}$
Air	1.25	1000	0.025	$2 \cdot 10^{-5}$

Experimental setup

3.3.2 Measurement of soil thermal properties

The collected soil samples were analyzed for their thermal and porous flow properties. The KD-2 thermal properties analyzer from Decagon was used for measurement of thermal diffusivity, heat capacity, and thermal conductivity. This instrument uses the line heat source method. The instrument has a specified accuracy of ± 5 to $\pm 10\%$ on thermal conductivity, $\pm 10\%$ on specific heat and $\pm 10\%$ on thermal diffusivity. For the measurements, a dual probe is used. This probe has two parallel needles, one for heating, and one for measuring temperature. The measurement method is as follows (Decagon [53]): an electric current is applied to the heating needle for a set period of time. During the heating and subsequent cooling time, the temperature is continuously measured in the parallel needle (at 6 mm radial distance). The measured temperature data is regression fitted to two correlations in order to obtain thermal conductivity and diffusivity as shown in (Decagon [53]).

Samples were collected from three different locations during installation of the measurement equipment at Bokn:

- 1- sample from fill sand around the exposed pipe
- 2- mass excavated with drilling rig 10 meter from the pipe
- 3- top soil

The measurement procedure contains the following steps:

- The soil samples were dried overnight in a drying cupboard at 60 °C and left to cool to room temperature. The volumetric water content was measured with two EC-5 probes to verify that the soil samples were suitably dry.
- A total of 500 ml of each dry soil sample was compacted and weighed to determine the dry density.
- The KD-2 thermal needle was lubricated with arctic silver thermal conduction paste before placement into the dry soil sample. Thermal measurements were conducted using the default settings of the KD2 pro and the SH-1 dual probe thermal needle. Three or more parallel readings were conducted with relocation of the probe in between measurements. Thermal conductivity, diffusivity, and volumetric heat capacity were recorded.
- The soil sample was weighed again, and 50 grams of water added. After thorough mixing and compacting, the volumetric water content and thermal property measurements were repeated.
- These measurement cycles, each time with incremental addition of 50 grams of water were repeated until the sample was water saturated.

The volumetric water content is calculated in the following way (Ward and Trimble [54]):

$$\phi = \frac{V_w}{V_w + V_s + V_a} \quad (3.5)$$

Experimental setup

Here V_w is the volume of water, V_a the volume of enclosed air and V_s the volume of soil. These assumptions are made:

- The resulting volume of water, V_w is the same as the water added (measured by weight: division obtains the volume with the density of water).
- The sum of V_a and V_s remain constant after adding and mixing water.

To ensure that conditions are close to that in the field, the soil/water mixture was re-compacted on a shaking tray during each measurement cycle (each time for the same duration). This ensures that the grains settle with a minimum amount of trapped air. A possible error introduced in this way is water absorbed or taken up by soil compounds as crystalline water leading to a lower V_w value. The samples collected in the field had high volumetric water content and were dried at a relative low temperature. It is fair to assume that most of the absorbed water would not have been released during the drying process. Therefore, the introduced error can be expected to be minimal.

3.3.3 Determination of thermal diffusivity from temperature profiles

Thermal diffusivity can be derived from the soil vertical temperature profile using the propagation and attenuation of diurnal temperature cycles in the upper soil layer, assuming that thermal conduction is the prevailing mode of soil heat transfer. To estimate the bulk thermal diffusivity of the clay soil outside the pipeline installation ditch, the propagation and attenuation of the annual temperature cycles may be used. The temperature measurements at 10 m distance from the pipe are most suitable for this purpose. This distance is sufficiently far for the thermal influence from the pipeline to be small. 1D heat conduction in vertical direction is assumed. The ambient temperature can be considered as a sinus signal with two distinct periods, the diurnal, and the annual. The exact solution for the 1D heat equation with a temperature wave as boundary condition at one end can be used to find the soil thermal diffusivity (Carslaw & Jaeger [55]). Both the amplitude damping and phase shift between temperature responses at different depths are valid approaches. For a sine shaped temperature at the soil surface propagating deeper into the soil, the resulting temperature profile at time t and distance z from the soil surface follows from an elementary separated variable solution of Equation (2.12) in one dimension:

$$T(z, t) = \Delta T e^{-\sqrt{(\omega / 2\alpha)} z} \cos(\omega t - \sqrt{(\omega / 2\alpha)} z) \quad (3.6)$$

Here ΔT is the amplitude of the oscillating surface temperature and ω is the angular velocity.

With two temperature measurements, having amplitude ΔT_1 at depth y_1 and ΔT_2 at depth y_2 , the thermal diffusivity can be calculated from the amplitude dampening (P is length of wave period (Williams [24])):

Experimental setup

$$\alpha = \frac{\pi}{P} \left(\frac{(z_2 - z_1)}{\ln(\Delta T_1 / \Delta T_2)} \right)^2 \quad (3.7)$$

The progressive phase lag with depth can also be used. With two temperature measurements, having phase delay t_1 at depth y_1 and t_2 at depth y_2 , the thermal diffusivity can be calculated from the amplitude dampening (Williams [24]):

$$\alpha = \frac{(z_2 - z_1)^2}{(t_2 - t_1)^2} \frac{P}{4\pi} \quad (3.8)$$

These two methods are applied to the four measurement locations in the clay layer. These are located at 10 m lateral distance from the pipe.

3.3.4 Use of TP01 sensors to measure soil thermal properties

The analysis of thermal properties with the Hukseflux TP01 sensor is described in Huskeflux, [56]. The TP01 is a sensor for measuring soil thermal conductivity, thermal diffusivity, and heat capacity. The sensor contains a differential temperature sensor, consisting of two thermopiles measuring the radial temperature difference around a heating wire. The thermopiles consist of 20 copper-constantan series connected thermocouples each. The hot junctions are at 1 mm lateral distance from the heating wire, the cold junctions at 5 mm lateral distance. The total thermal diffusivity of the sensor is low as it is foil printed system. To perform a measurement, the following cycle is followed: the heating wire is first given a low, fixed supply voltage, of 180-second duration. During these 180 seconds, the supply voltage to the heating wire is logged as well as the resulting voltage signal given by the thermopile. Measurement of the thermopile signal is continued for another 180 seconds after the heating wire voltage is switched off. As the resistance of the heating wire is known, the logged heating wire voltage can be used to calculate the thermal energy input into the soil during the first 180 seconds of the measurement cycle. The measuring principles are described in Huskeflux, [56].

3.3.5 Grain size measurement and porous media parameters

In the literature, several correlations are provided to link hydraulic conductivity, K to porosity ϕ and soil grain parameters. The grain parameters can be obtained from the grain size distribution of the soil samples. The grain size distribution can be measured with a sieve analysis (ASTM [57]). In sieve analysis, the granular soil sample is passed through a column of sieves mounted on a shaker. The dry sample is placed in the top sieve. The top sieve has the largest mesh with mesh sizes progressively being finer for the lower sieves. The arrangement is left to shake for a predetermined amount of time; after this, the mass collected in each individual sieve is measured.

Experimental setup

An often used empirical correlation for hydraulic conductivity is that of Carman-Kozeny (Carman [58]). This correlation may be used successfully when the soil does not contain clay-like fine particles, the particles are not excessively coarse, the particles are close to round shape, the particle distribution is such that there is no bias towards the finer grain sizes, and anisotropy is absent (Carrier [59]).

The form of the Carman-Kozeny equation used here is the one that includes the specific surface area of the particles ($a_s=6/D_m$), shown for example in Nield and Bejan [22]:

$$K = \frac{\rho g}{\mu} \frac{\phi_e^3}{180(1-\phi_e)^2} D_m^2 \quad (3.9)$$

In Uromović [60], the choice of the mean particle diameter D_m is discussed. It is suggested to use the geometric particle size diameter D_{ing} instead of the mean particle D_m . The following correlation may be used (Uromović [60]):

$$D_{ing} = e^{0.01 \sum_i P_i \ln(d_{i,g})} \quad (3.10)$$

Here P_i represents the fraction of sieve residue i .

The correlation uses the effective porosity ϕ_e of the sample. This is the porosity of the soil available for the flow of water. This value is always smaller than the volumetric water content ϕ obtained with Equation (3.5). This excludes the water bound by adsorption to grain surfaces and water trapped in un-connected pores within the matrix. The effective porosity can be obtained by comparing the density of the water-saturated sample to that of the fully drained.

The permeability value obtained with the Carman-Kozeny correlation is highly influenced by the choice of geometric particle size. In Yadzhi et al. [61], creeping flow through a porous medium has been investigated numerically. The conclusion is that the Carman-Kozeny correlation does not capture the permeability accurately as a function of porosity. This is especially the case with low porosity levels (<0.4). The tortuosity needs to be included, which is shown to be achievable with a correction coefficient. This correction coefficient is defined as a function of the flow path tortuosity and the shape factor of the pores.

The accuracy of the Carman-Kozeny correlation is also discussed in Chapuis and Aubertin [62]. The accuracy was evaluated against laboratory tests. Their conclusion is that vertical hydraulic conductivity can be predicted within experimental uncertainty using the Carman-Kozeny correlation. This is within 1/3 to 3 times the measured value for sandy soils.

A comparative study of often used correlations for intrinsic permeability is shown in Aquilar [63]. The study shows that the Carman-Kozeny is one of the better performing

Experimental setup

correlations along the larger range of sediment conditions, indicating similar spread against measurement data as found by Chapuis and Aubertin [62].

3.4 Estimation of gas temperature and wall heat flux

It was not possible to measure the gas temperature directly at the experimental site. The only possibility is to make an estimate based on the temperature measurements at the outer wall and in the surrounding soil layers. A draw-back of this approach is that the heating/cooling of the steel pipe wall will mask some of the quick gas temperature fluctuation when measuring beyond the pipe outer wall. Information is lost by measuring the temperatures beyond the outer wall.

By choosing the measurement interval longer than the thermal time constant of the pipe wall this problem can to some extent be overcome, leading to a smoothed estimate of the gas temperature over time. Within a measurement interval, there can be additional gas temperature fluctuations that remain undetected by the measurements. Similarly, the heat flux can only be assessed from the soil temperature measurements.

The thermal energy that is stored or released in the pipe-wall in response to the gas temperature fluctuations occurring at smaller time scale than the measurement interval cannot be estimated in this manner. Over a sufficiently long period, these differences will average out. The time scales of the flow boundary transients are expected to be sufficiently long for this not to be a major issue.

To estimate the gas temperature and inner pipe-wall heat flux, the convective heat transfer coefficient between gas and pipe wall also need to be estimated. The gas inside the pipeline is subject to turbulent flow conditions with high Reynolds numbers (10^6 - 10^7). A consequence of the high turbulence is that the cross-sectional thermal gradient of the gas inside the pipeline is very small. We may assume gas temperatures constant throughout the cross-section. Due to the high turbulence level, heat transfer from the gas and the pipe inner wall will be mainly convection driven. Due to the low temperatures of the gas, radiation heat transfer will not play a significant role. The convective heat transfer coefficient can be estimated by the Dittus-Boelter correlation (Equation (2.14)).

To approximate the gas temperature, the soil measurements close to the pipe wall are used. A coarse estimate of the gas temperature can be made from the measurements at 2 and 5 cm from the pipe wall. The radius of curvature of the pipe wall is large compared to the distance from the pipe inner wall to the soil measurement sensor at 5 cm distance from the pipe outer wall (9.7 cm). Therefore, the 1D heat conduction equation can be employed with minimal error instead of the 1D radial variant. To approximate the gas temperature from the measurements, the thermal energy balance of a linear 1D-calculation cell surrounding these measurement points was used, as shown in Figure 3.10.

Experimental setup

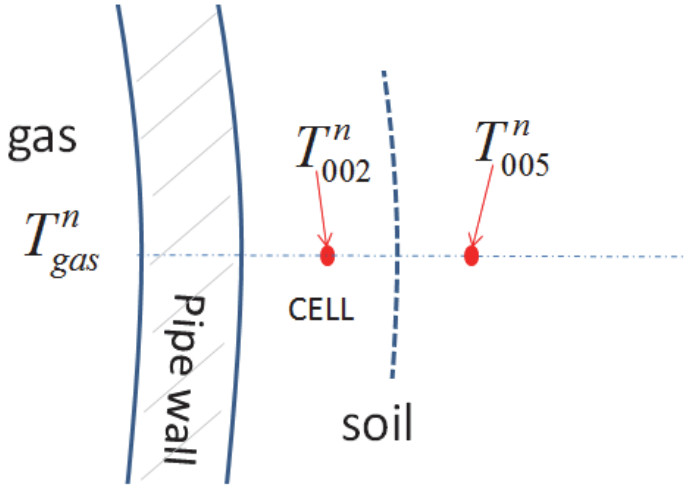


Figure 3.10: Schematic of the system used for calculating gas temperatures from the soil measurements close to the pipe wall.

The calculation cell stretches 3 cm in radial direction from the pipe wall, with the temperature measurement point in the centre. The change in thermal energy from time step $n-1$ to n ($\Delta t=300$ s) is balanced with the energy flux over the cell boundaries in time step n . Thermal energy storage in the pipe wall is neglected so that the thermal energy flux over the inner cell boundary can be expressed as:

$$q = U(T_{gas}^t - T_{002}^t) \quad (3.11)$$

Here U is the overall heat transfer coefficient combining the thermal resistances of the inner wall film coefficient obtained with Equation (2.11), the pipe wall layer and the first 2 cm of soil. T_{gas}^n is the unknown gas temperature and T_{002}^n the measurement at the cell centre at time step t . By using the temperature measurement T_{005}^n at 5 cm distance from the pipe wall, the thermal energy flux over the outer cell boundary can be calculated. T_{gas}^n will follow from:

$$T_{gas}^n = T_{002}^n + \frac{0.03\rho C_p}{U\Delta t} (T_{002}^n - T_{002}^{n-1}) - \frac{\lambda}{0.03U} (T_{005}^n - T_{002}^n) \quad (3.12)$$

A more systematic way to approximate the gas temperature is by using a discretization of the unsteady heat conduction equation in cylindrical coordinates. At the top location, we have measurements at 2 mm, 20 mm, 50 mm, and 100 mm from the pipe wall.

Experimental setup

The following assumptions are made:

- The thermal properties of the soil around the pipe are known and constant in time.
- The thermal gradient in the pipe wall achieves steady state within each measurement interval.
- Radial heat conduction is the only form of heat transfer present.

A numerical domain according to Figure 3.11 may be used.

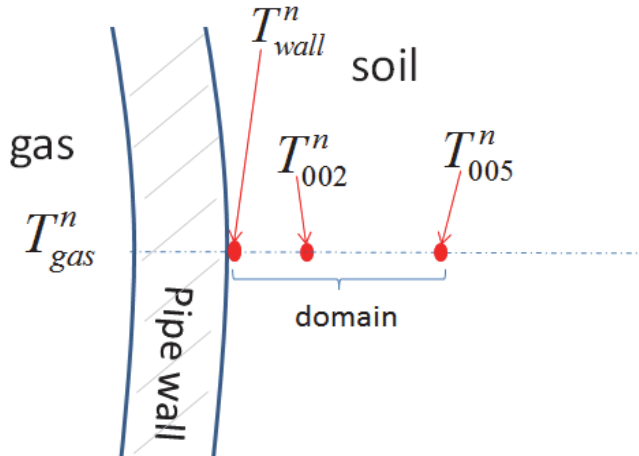


Figure 3.11: Domain for finite difference scheme used to estimate gas temperatures.

On the domain, the radial heat conduction equation is discretized using an implicit finite difference scheme.

The measurement points at 2 mm, 20 mm, and 50 mm from the pipe wall are used. The domain boundaries are provided with Dirichlet boundary conditions using the measured temperature at 2 mm and 50 mm distance from the pipe wall. A set of equations of the general form is obtained when backward differencing in time as shown in for example Gutierrez-Miravette [64]:

$$T_i^n = -c_1 T_{i-1}^{n+1} + (1 + c_1 + c_2) T_i^{n+1} - c_2 T_{i+1}^{n+1} \quad (3.13)$$

The definitions of c_1 and c_2 are:

$$c_1 = \frac{\alpha_i r_{i-1/2} \Delta t}{r_i \Delta r^2} \quad c_2 = \frac{\alpha_i r_{i+1/2} \Delta t}{r_i \Delta r^2} \quad (3.14)$$

The heat transfer rate into the soil domain from the pipe wall (per unit length) is evaluated as:

Experimental setup

$$\dot{Q}^{n+1} = -2\pi\lambda_{soil} \frac{T_3^{n+1} - T_2^{n+1}}{\ln(r_3 / r_2)} \quad (3.15)$$

The problem is subsequently set up in matrix form as:

$$\begin{bmatrix} 1 & & & \\ -c_1 & 1 + c_1 + c_2 & -c_2 & \\ & \ddots & \ddots & \\ & & \ddots & \\ & & & -c_1 & 1 + c_1 + c_2 & -c_2 \\ & & & & 1 & \end{bmatrix} \begin{bmatrix} T_1^{n+1} \\ T_2^{n+1} \\ \vdots \\ \vdots \\ T_i^{n+1} \end{bmatrix} = \begin{bmatrix} T_1^n \\ T_2^n \\ \vdots \\ \vdots \\ T_i^n \end{bmatrix} \quad (3.16)$$

This set of equations is solved using the left array division function in MATLAB, inverting the matrix. The boundary temperatures T_1^n and T_i^n are set to the measured value of the new time step $n+1$, as well as the node corresponding to T_{002} . To estimate the heat transfer rate between gas and the pipe, the following relationship holds (based on correlations provided in Incropera and DeWitt [65]):

$$\dot{Q}^{n+1} = -\frac{T_{gas}^{n+1} - T_1^{n+1}}{\frac{1}{2\pi r_{pipe_in} h_f} + \frac{\ln(r_{pipe_out} / r_{pipe_in})}{2\pi\lambda_{steel}} + \frac{\ln(r_{plastic_out} / r_{pipe_out})}{2\pi\lambda_{plastic}} + \frac{\ln(r_1 / r_{plastic_out})}{2\pi\lambda_{sand}}} \quad (3.17)$$

The unknown gas temperature follows from equalizing Equation (3.15) and (3.17).

3.5 Seawater temperatures-model values and measurements

The seawater temperatures used in the numerical models of the pipeline case are obtained with the Norkyst 800 model. As described in Albretsen [66], the Norkyst 800 model is a numerical model of the coastal areas in Norway. It can reproduce sea level, temperature, salinity, and sea currents for the coastal waters of Norway. The model is a so-called ROMS model (Regional Ocean Modelling System) as described in Shchepetkin and McWilliams [67]. The model has a 2600×900 grid cell size. Each cell has a size of 800×800 m. In vertical direction there can be up to 35 cells. The model uses local bathymetry data and boundary condition inputs from the operational model ROMS model (Regional Ocean Modelling System) Nordic-4 (Norwegian Meteorological Institute [68]). Nordic-4 covers the surrounding sea areas (North Sea,

Experimental setup

Nordic seas, part of the Barents Sea and the Arctic Ocean). The grid size of ROMS is 4×4 km. The seawater temperature boundary conditions are obtained from satellite data. Atmospheric forcing is supplied from the HIRLAM12km weather prediction model described in Haugen et al. [69]. The Norkyst 800 model includes tidal forcing and river run-off. The model can simulate the entire Norwegian coastal waters in one simulation. Normally smaller areas are defined due to the calculation effort that is involved. For the actual pipeline case, there is only one Norkyst 800 grid point coinciding with the subsea section. The actual grid point is at 75 m depth. Figure 3.12 shows the modelled seabed temperature data retrieved for this point during the period from the 1st of January 2012 until the 1st of November 2014. The time resolution of the data was 24 hours. Ole Henrik Segtnan from Uni-Research Polytec in Haugesund provided the data.

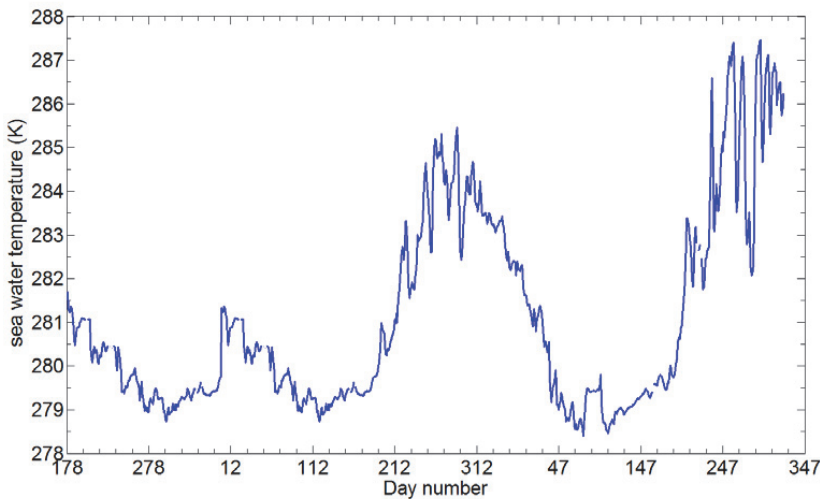


Figure 3.12: Development of daily seawater temperature representative for subsea parts of Europipe 2 pipeline case. The data has been generated with the Norkyst 800 model for the period from June 2012 to November 2014

To increase confidence in the use of the Norkyst 800 data for our models, seabed water temperatures along the pipeline route were measured. For this purpose, a measurement system was constructed to measure and record the seawater temperature on the seabed. The measurement system consists of a thermocouple mounted in a stainless steel sheet connected to a singular channel data-logger. The data-logger is a LASCAR EL-USB-1. The thermocouple and data-logger were calibrated in a hot bath calibrator (Hart 7103 Microbath). The resolution of the measurement was 0.25 °C. The data-logger and thermocouple are mounted in a waterproof polymer container leaving only the tip of the thermocouple protruding and in contact with the seawater. The bottle is filled with vegetable oil in order to protect the electronics from direct contact with seawater and to even out the hydrostatic pressure. Six of these measurement systems were deployed along the pipeline route. Prior to deployment, the USM-coordinates of the measurement locations were determined from the pipeline as laid route. Deployment commenced on the 22nd of June 2014. With the vessel S/Y Sirene, the deployment locations were visited using GPS-navigation and the measurement devices lowered to the sea bottom.

Experimental setup

Each measurement device was connected to a drop anchor with sufficient length of mooring cable, ending in a visible floating mooring buoy. Deployment locations are shown in Figure 3.13. The coordinates and deployment depths of the six measurement points are given in Table 3.

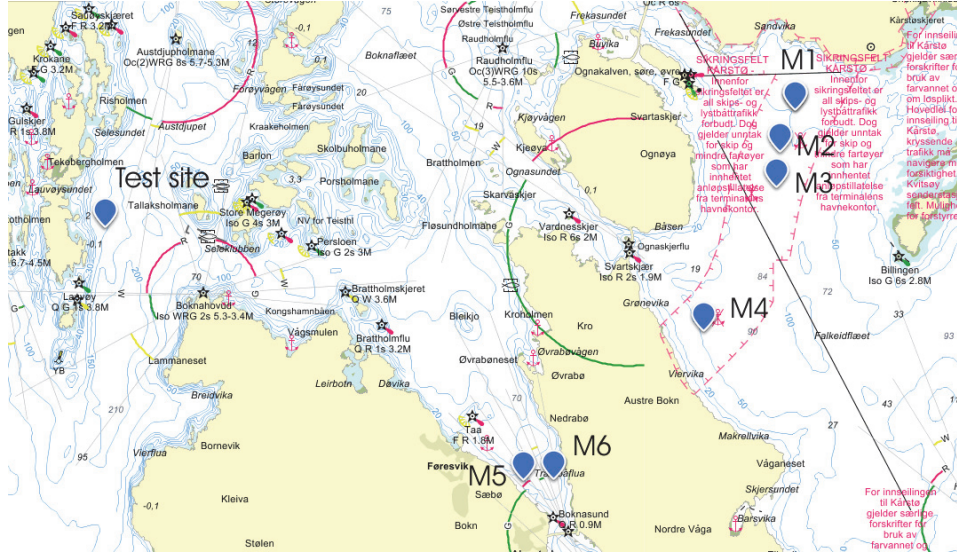


Figure 3.13: Location of sea bottom temperature measurement devices along the pipeline route (M1-M6) (Lothe and Oosterkamp [70]).

Table 2: Locations sea bottom temperature measurements (Lothe and Oosterkamp) [70].

Location	Latitude	longitude	depth
M1	N59°15.9'	E5°30.32'	40
M2	N59°15.63'	E5°30.07'	80
M3	N59°15.47'	E5°29.95'	76
M4	N59°14.62'	E5°29.32'	80
M5	N59°13.67'	E5°27.6'	25
M6	N59°13.7'	E5°27.5'	40

On September 7, 2014, a retrieval expedition was undertaken with S/Y Sirene. Measurement devices M2, M4, and M5 could be relocated and successfully retrieved. All three mooring buoys showed extensive signs of contact with ship hulls and ship propeller damage. This is according to expectation as the equipment was deployed in areas of intensive ship traffic. M1, M3, and M6 could not be relocated and are considered lost at sea.

3.6 Experimental uncertainty

Care was taken to limit the measurement uncertainty in the experimental set up. The uncertainty levels of the different measurements is discussed in this sub chapter

3.6.1 Assessment of uncertainty with soil temperature sensors

The following sources of errors are identified for the soil temperature measurements:

- calibration accuracy
- drift
- scale resolution
- positional accuracy

Each PT100 temperature sensor was calibrated. The sensors and data loggers installed below the soil surface layer were calibrated in a hot bath calibrator against a calibrated reference probe. The temperature sensors in the soil surface layer were installed on a later date. These eight sensors have a factory calibration. The assessment of the measurement error for these sensors is therefore different compared to that of the initially installed set.

The calibration procedure of the PT100 sensors resulted in the determination of a third degree polynomial calibration curve, fitted for the combination of each sensor, cable, bridge and data-logger channel (ALMEMO 5690-1M with U-A10 modules, ZA-FS9030 plugs and 1/5 DIN PT100 with double 20 m leads). The calibration curves and the accuracy of the fit are documented in Appendix C. The scale resolution error during both calibration and measurement is ± 0.005 K. The thermal drift of the data logger channel (U-A10) and measurement bridge (ZA9030FS2) is at most 0.003%/K, according to the manufacturer. The linearization accuracy of the bridge electronics and the DAC (data acquisition system) is quoted ± 0.05 K. Each probe and channel is calibrated against the same calibrated PT100 reference probe (ASL F250 MK 2) with a read out accuracy of 0.001 K and the measured value corrected with a third order polynomial correction curve. The linearization error is assumed to be compensated when adjusting the measured values with the correction curve following from the calibration procedure. The temperature measurement error is therefore composed of the accuracy of the calibration curve, the drift, and the scale resolution. The accuracy of the calibration curve is depending on the scale resolution of the measurement system (± 0.005 K), the scale resolution of the reference probe (± 0.0005 K) and the thermal gradients in the oil bath of the bath calibrator (Hart Microbath 7102). The uniformity of the bath temperature is specified by the manufacturer as ± 0.02 K. For the soil measurements, accurate values for the thermal gradients in the soil are desired.

The relative differences between the measurements are therefore more important than the absolute values. The reference probe has been calibrated both prior to and after calibration at Scalibra AS. It is thus possible to express the temperature measurement error for each measurement point in relative and absolute values. The deviation of the

Experimental setup

reference probe in both calibrations at Scalibra AS was found to be within 0.02 K from the measured values within a measurement uncertainty of ± 0.1 K.

List of error sources:

- | | |
|---|--|
| • temperature drift ALMEMO: | 0.003%/K ->0.009 K @30 °C |
| • scale resolution ALMEMO: | ± 0.005 K |
| • calibrator bath uniformity (HART): | ± 0.02 K |
| • scale resolution (ASL): | ± 0.0005 K |
| • temperature drift (ASL): | 0.0005 K/K temperature change |
| • repeatability (ASL). | ± 0.002 K |
| • accuracy of fit of calibration curve:
sensor | $\pm 0.01-0.03$ K, different for each sensor |
| • absolute accuracy of reference probe: | ± 0.1 K |

The errors are estimated according to the methods presented in Wheeler and Ganji [71]. The measurement errors are grouped in systematic and random errors. First, the errors are assessed for the calibration process. At each calibration point, 40 temperature measurements were made at 10 s intervals. The mean value of these 40 measurements is used in the calibration procedure. The random errors affecting this measurement are:

- temperature drift ALMEMO
- scale resolution ALMEMO
- calibrator bath uniformity (HART)
- scale resolution (ASL)
- temperature drift (ASL):
- repeatability (ASL).

With these values the sum of random errors $S_x = 0.02$ K. Using a student distribution and a 95% confidence interval, the random uncertainty $P_x = tS_x/\sqrt{M} = 0.007$ K with $t=1.96$ and $M=40$.

The following systematic uncertainties were identified:

- accuracy of fit of calibration curve
- absolute accuracy of reference probe

The sum of the systematic errors, $B_x = 0.104$ K in absolute terms. For the purpose of comparative measurements, the sum of the systematic errors, $B_x = 0.03$ K.

The overall uncertainty from the calibration in absolute terms is $\sqrt{(B_x^2 + S_x^2)} = 0.1$ K. In relative terms, the overall uncertainty reduces to ± 0.03 K.

Experimental setup

For a single measurement of the installed system, the random uncertainty is composed of the temperature drift and scale resolution of the data-logger. The overall uncertainty of the calibration is considered as a systematic error. The random uncertainty is $P_x=tS_x=0.02$ K ($t=1.96$). The absolute uncertainty of a single measurement is then estimated to be $\sqrt{(0.02^2+0.104^2)}=\pm \mathbf{0.105}$ K and the relative uncertainty between the individual measurement points is $\sqrt{(0.02^2+0.03^2)}=\pm \mathbf{0.04}$ K.

3.6.2 Assessment of uncertainty with the soil surface temperature sensors.

The measurement error in this case includes the temperature drift, thermal resolution, linearization error, and calibration error. The calibration was carried out at the Deutscher Kalibrierdienst. The claimed uncertainty of this calibration is ± 0.1 K.

The following error sources were identified:

- | | |
|----------------------|---|
| • temperature drift: | 0.009 K (with 30 K temperature variation) |
| • scale resolution: | 0.005 K |
| • calibration | 0.1 K |

The random uncertainty for a single measurement is the same as previously calculated: $P_x=tS_x=0.02$ K. With the systematic error being the calibration inaccuracy of 0.1 K, the overall uncertainty of these measurements in relation to each other, and the other measurement points is $\pm \mathbf{0.105}$ K.

3.6.3 Positional accuracy of the sensors

The sensors surrounding the pipe are mounted on a pvc sensor boom. Mounting holes of 4.3 mm diameter were drilled at predetermined distances in the boom in the following manner: first, the positions were marked using a millimetre graded steel ruler and pilot holes drilled using a 1 mm diameter drill bit. The drilling was carried out in a bench drill with the boom fixed in a screw clamp, ensuring a ninety degrees angle between drill bit and pipe surface. Subsequently, the pilot holes were used to guide a 4.3 mm drill bit. The PT100 is fit tight in the holes, resulting in a permanent interference fit between the outer protective sheath of the PT100 and the hole. Using the clamp, the angular position of the centre-lines of the drilled holes could be kept uniform, resulting in the same angular deviation for each hole. The estimated accuracy of the drilling operation is ± 0.5 mm, giving a maximum distance variation between two neighbouring sensor tips of ± 1 mm. Prior to installation, the sensor tips for all sensors were checked to verify that they are all within 1 mm of the specified distance. The booms and sensors risk bending during or after installation and refilling of the sand. The risk of bending for the horizontally placed sensor booms and top sensor boom is minimal; these sensors have not been under strain during refilling of the sand inside the ditch. The error in the thermal gradient dT/dx between two consecutive sensor positions is the largest for the sensors with the smallest (30 mm) spacing interval. Using the calculated value of the

Experimental setup

relative uncertainty for each measurement points of 0.04 K, the maximum error in the gradient is $\pm 0.003 \text{ K/mm}$.

The vertical sensors at 1m, 3m and 10 m from the pipe were installed on booms to maintain their vertical position in relation to each other after installation. The positional error of the vertical sensors is estimated at $\pm 5 \text{ mm}$ for those installed at depths exceeding 0.5 meter. The positional accuracy of the sensors in the soil surface layer (at 0.01, .05 and 0.25 depth) is $\pm 1 \text{ mm}$. The position in relation to the central axis is calculated from the measurements done with the total station theodolite. This results in a total vertical positional error of $\pm 8 \text{ mm}$. The horizontal position of the sensors is determined by the accuracy of the position and angle of the drilled installation hole. The positional accuracy in horizontal direction cannot be better than the diameter of the installation hole. The horizontal positioning and vertical alignment of the drill hole is controlled by a satellite navigation based control system. The horizontal estimated accuracy is $\pm 10 \text{ cm}$ for the centreline of the hole.

3.6.4 Dual wave length radiometer

The dual wavelength radiometers contain a double set of pyrano and pyrgeo meters. For the incoming radiation, the measurement errors are caused by the directional change of the sun and the imperfect optical properties of the protective dome of the instrument. According to Huskeflux [48], the errors and uncertainties for the pyrano- and pyrgeo meters are:

- drift: $1\% \text{ per year}$
- non-linearity: $\pm 2.5\%$
- spectral selectivity: $\pm 5\%$
- expected overall accuracy on a daily basis: $\pm 10\%$

The scale error, drift and inaccuracy of the instrumentation (ALMEMO 5690-1M with U-A10 modules, ZA-FS9030 plugs) logging the voltage outputs of the radiometer is very small compared to the quoted instrument accuracy. The measurement error of the dual wavelength radiometer is therefore assumed $\pm 10\%$.

3.6.5 Soil volumetric water content measurements

The soil volumetric water content probes use the factory calibration and factory settings in the data-logger. The accuracy is specified by the manufacturer as $\pm 3\% \text{ VWC}$. The scale resolution is 0.1%. For a maximum measurement level of 0.5 VWC, the measurement uncertainty is $\pm 0.015 \text{ VWC}$. The collected measurement values are adjusted using the calibration values obtained with the soil samples.

Experimental setup

3.6.6 Uncertainty in ambient weather data measurements.

The air temperature measurements are done with a PT100 sensor that is calibrated together with the soil surface temperature sensors. The measurement uncertainty is thus the same, at ± 0.104 K.

The seawater temperature measurements have a scale resolution of 0.2 K. They are calibrated, using in the Hart Microbath 7102. Without the use of a reference probe, the calibration accuracy of the Hart Microbath 7102, ± 0.1 K, is a systematic error. The drift of the Lascar data-loggers is not specified. The overall measurement uncertainty is at least ± 0.22 K.

3.6.7 Collected SCADA data for the Kårstø-Trosnavåg pipeline section

The uncertainty of the process measurements at the Kårstø-Trosnavåg pipeline section is discussed, and estimates provided in Langelandsvik [8]. The provided uncertainties are verified using the available documentation of the installed measuring equipment.

The inlet temperature measurement at Kårstø (Fisher Rosemount PT100) has the following error sources:

Random

- scale resolution: 0.005 K
- repeatability: 0.03 K
- accuracy: 0.21 K

Systematic

- calibration: 0.1 K

The resulting uncertainty is ± 0.43 K (95% confidence interval). This is slightly less accurate than the estimate provided by Langelandsvik [8].

The pressure measurements at the inlet and outlet are described in Langelandsvik [8]. The maximum uncertainty is estimated as ± 52 mbar in a 0-200 bara range.

Flow metering is done at the inlet. It consists of two independent metering stations, at the end of the two process trains at Kårstø supplying the gas into the pipeline. Each station has two parallel metering lines. In addition, a small amount of gas is taken out just downstream the pipeline inlet into the Rogass local gas distribution network.

According to Langelandsvik [8] this flow metering equipment has an uncertainty in both mass and volume flow of $\pm 0.6\%$. If statistic uncertainty of these five meters is assumed, the maximum uncertainty is $\pm 1.3\%$. The inlet flow is subject to fiscal metering agreements and therefore regularly checked.

3.6.8 Effect of gas composition

The model studies were all conducted using a nominal gas composition. The actual gas composition in the real pipeline case studies vary around this nominal composition. This has an effect on the flow model calculations. Primarily the composition affects the calculations performed by the BWRS equation of state. The equation of state provides the compressibility factor Z, used in the density calculation, and its derivatives are used in the numerical discretization scheme. The three major constituents in the gas composition are Methane, Ethane, and Propane. In the period from the 1st of January 2013 to the 31st of December 2014, these components had the following mean and standard deviation (in mole fraction).

-CH₄: mean=0.88 stdev.=0.0055
-C₂H₆: mean=0.07 stdev.=0.0041
-C₃H₈: mean=0.007 stdev.=0.002

The chosen nominal composition for these gas components is within one standard deviation from the mean values for the two-year period analysed (2013-2014).

4 Pipe flow and heat transfer models

This chapter describes the pipe flow and heat transfer models that are used in the numerical investigations.

4.1 Pipe flow model

The pipe flow model is the one made by Jan Fredrik Helgaker, documented in Helgaker [10]. The model is a finite difference discretization of the one dimensional Navier Stokes equations. The basic form of these equations is shown in Chapter 2.2 (Equations (2.1) to (2.3)). The equations are modified to better suit the problem of unsteady compressible pipe flow. The gas density ρ is exchanged for the pressure p by using a real gas equation of state and considering the mass flow rate as $u=\dot{m}/\rho A_p$, as described by Chaczykowski [12]. The gas density ρ in the equations is replaced by the state parameters p , T and Z through:

$$\rho = \frac{p}{ZRT} \quad (4.1)$$

This is done out of convenience, as p and \dot{m} are predominantly the measured variables in pipeline transportation. In Equation (4.1), Z , is the compressibility factor determined by an equation of state. The equation of state expresses the compressibility factor as a function of pressure and temperature. The velocity u is subsequently expressed in the state parameters using logarithmic differentiation. The derivation and modification of the equations is shown in Appendix B.

The resulting equations, used in the flow model, are:

Conservation of mass:

$$\frac{\partial p}{\partial t} = \left[\frac{1}{T} + \frac{1}{Z} \left(\frac{\partial Z}{\partial T} \right)_p \right] \left[\frac{1}{p} - \frac{1}{Z} \left(\frac{\partial Z}{\partial p} \right)_T \right]^{-1} \frac{\partial T}{\partial t} - \frac{ZRT}{pA} \left[\frac{1}{p} - \frac{1}{Z} \left(\frac{\partial Z}{\partial p} \right)_T \right]^{-1} \frac{\partial \dot{m}}{\partial x} \quad (4.2)$$

Conservation of momentum:

$$\begin{aligned} \frac{\partial \dot{m}}{\partial t} &= \frac{\dot{m}ZRT}{pA} \left(-2 \frac{\partial \dot{m}}{\partial x} + \dot{m} \left[\frac{1}{p} - \frac{1}{Z} \left(\frac{\partial Z}{\partial p} \right)_T \right] \frac{\partial p}{\partial x} - \dot{m} \left[\frac{1}{T} + \frac{1}{Z} \left(\frac{\partial Z}{\partial T} \right)_p \right] \frac{\partial T}{\partial x} \right) \\ &- A \frac{\partial p}{\partial x} - \frac{fZRT\dot{m}}{2DAp} - \frac{pA}{ZRT} g \sin \theta \end{aligned} \quad (4.3)$$

Conservation of energy:

$$\begin{aligned} \frac{\partial T}{\partial t} = & -\frac{\dot{m}ZRT}{pA}\frac{\partial T}{\partial x} - \frac{\dot{m}(ZRT)^2}{pA_p c_v}T\left[\frac{1}{T} + \frac{1}{Z}\left(\frac{\partial Z}{\partial T}\right)_p\right] \\ & \times \left(\frac{1}{\dot{m}}\frac{\partial \dot{m}}{\partial x} - \left[\frac{1}{p} - \frac{1}{Z}\left(\frac{\partial Z}{\partial p}\right)_T \right]\frac{\partial p}{\partial x} + \left[\frac{1}{T} + \frac{1}{Z}\left(\frac{\partial Z}{\partial T}\right)_p \right]\frac{\partial T}{\partial x} \right) \\ & + \frac{f}{2c_v D}\left(\frac{ZRT|\dot{m}|}{pA}\right)^3 - \frac{4q_w}{D}\frac{ZRT}{pc_v} \end{aligned} \quad (4.4)$$

When an overall heat transfer coefficient U is used as a steady state external heat transfer model, the energy equation has the following form:

$$\begin{aligned} \frac{\partial T}{\partial t} = & -\frac{\dot{m}ZRT}{pA}\frac{\partial T}{\partial x} - \frac{\dot{m}(ZRT)^2}{pA c_v}T\left[\frac{1}{T} + \frac{1}{Z}\left(\frac{\partial Z}{\partial T}\right)_p\right] \\ & \times \left(\frac{1}{\dot{m}}\frac{\partial \dot{m}}{\partial x} - \left[\frac{1}{p} - \frac{1}{Z}\left(\frac{\partial Z}{\partial p}\right)_T \right]\frac{\partial p}{\partial x} + \left[\frac{1}{T} + \frac{1}{Z}\left(\frac{\partial Z}{\partial T}\right)_p \right]\frac{\partial T}{\partial x} \right) \\ & + \frac{f}{2c_v D}\left(\frac{ZRT|\dot{m}|}{pA}\right)^3 - \frac{ZRT}{pc_v}\frac{4U}{D}(T_{gas} - T_{amb}) \end{aligned} \quad (4.5)$$

In the last term of Equation (4.5), the thermal energy exchange with the environment is defined through the overall heat transfer coefficient U and the difference between the gas and ambient temperature.

The continuity, momentum, and energy equations (Equations (4.2), (4.3) and (4.4)) are discretized using a finite difference scheme. The cell centered method is used in the discretization, as used in Abbaspour and Chapman [7]. This method is first order correct in time and second order correct in space. The partial derivatives are determined for each pipe section, rather than at the grid points. For a pipe section I , Helgaker [10] defines derivatives of quantity Y (P , T , and \dot{m}) in pipe section I as follows:

$$\frac{\partial Y(x_I, t_{n+1})}{\partial t} = \frac{Y_{i+1}^{n+1} + Y_i^{n+1} - Y_{i+1}^n - Y_i^n}{2\Delta t} + \mathcal{O}(\Delta t) \quad (4.6)$$

And:

$$\frac{\partial Y(x_I, t_{n+1})}{\partial x} = \frac{Y_{i+1}^{n+1} - Y_i^{n+1}}{\Delta x} + \mathcal{O}(\Delta x^2) \quad (4.7)$$

The quantity Y for section I is thus averaged from the two bordering grid points i and $i+1$:

$$Y(x_i, t_{n+1}) = \frac{Y_{i+1}^{n+1} + Y_i^{n+1}}{2} + \mathcal{O}(\Delta x^2) \quad (4.8)$$

The advantage of the cell-centered method is that the boundary conditions are easier to handle. The non-linear terms in the continuity, momentum, and energy equation are linearized using Taylor expansion. The resulting discretized equations form a system of linear equations that can be written in matrix form as:

$$Ax = b \quad (4.9)$$

The vector x contains the unknown grid values for pressure, temperature, and mass flow rate of the new time step, t_{n+1} . The vector b contains the known grid values of the previous time step t_n . The flow model is implemented in MATLAB and the set of linear equations solved by using the left array division function.

In the flow model, the gas properties are calculated for each time step using the BWRS equation of state, and the viscosity correlation according to Equation (2.6). The gas isochoric specific heat capacity is calculated according to Equation (2.8).

As part of this work, the MATLAB code of the pipe flow model has been adapted to interact with heat transfers models in ANSYS Fluent during transient simulations. The 1D radial unsteady heat transfer model, already implemented in the code, was modified to include additional soil calculation elements. The possibility to calculate the flow and external thermal models at different time step lengths was also implemented. This version of the 1D radial unsteady model was also verified against a 1D radial unsteady heat transfer model using a finite difference discretization.

4.2 External Heat Transfer Models

Three different external models of the thermal domain are compared. Underlying assumption for the models is that soil heat transfer in axial direction can be neglected; radial heat transfer is dominant.

4.2.1 1D steady model

The 1D steady model is similar to the model described in Langelandsvik [2]. This model is commonly used for modelling the ambient in gas pipe flow. The heat flux from the gas in the pipeline to the ambient and vice versa is represented as a single heat transfer coefficient, U . The equations used to calculate U are summarized in Langelandsvik [8] and Sund et al.[9]. Their derivations can be found in standard literature, e.g. [65]. The overall heat transfer coefficient U entails the combined thermal resistance of the inner film coefficient, the pipe wall layers and the soil domain.

$$U = \left[\frac{r_o}{r_i} \frac{1}{h_i} + \sum_n^N \left(\frac{r_o}{\lambda_n} \ln \left(\frac{r_{n+1}}{r_n} \right) \right) + \frac{1}{h_o} \right]^{-1} \quad (4.10)$$

here, r_i is the pipe inner wall radius, and r_o is the outer radius of the outermost pipe wall layer. For pipe wall layer n , the inner and outer radius are given by r_n and r_{n+1} and the thermal conductivity by λ_n . The heat transfer from the turbulent gas flow to the pipe inner wall is given by the inner film coefficient h_i . The outer film coefficient h_o represents the thermal resistance of the 2D soil domain. The correlation used is derived from bi polar coordinate transformation of a buried pipe in an infinite 2D domain as given in for example Bau [28]:

$$h_o = \frac{\lambda_{soil}}{r_o \cosh^{-1} \left(\frac{H}{r_o} \right)} \quad (4.11)$$

with H the burial depth of the pipe and λ_{soil} being the thermal conductivity of the soil.

Equations (4.10) and (4.11) are used to define the 1D steady state model. When the pipe is buried, Equation (4.11) is used to define the pipe outer wall heat transfer coefficient h_o . For shallow burial cases, Equations (2.26) and (2.27) as presented in Ovwurorie [72] are used. The reason is that for shallow burial, the boundary condition at the top of the soil can no longer be assumed isothermal. When the pipe is exposed to seawater, Equation (2.13) is used for h_o . The Dittus Boelter correlation shown in Incropera and DeWitt [6] is used for the inner film coefficient h_i , shown in Equation (2.11). With the correlations used for the gas specific heat and conductivity, the inner film coefficient in the pipe flow scheme has been calculated as follows (for all three external heat transfer models):

$$h_f = \left(\frac{0.002 p}{1000000} + 0.024 \right) * 0.023 * \left(\frac{\rho v D}{\mu} \right)^{0.8} * \left(\frac{C_p \mu}{\frac{0.002 p}{1000000} + 0.024} \right)^{0.4} \quad (4.12)$$

It should be noted here that in Equation (4.12) the isobaric heat capacity is used to obtain the Prandtl number, while the flow scheme uses the isochoric heat capacity in the energy equation (Equation (2.3)). According to Incropera and DeWitt [65], the uncertainty of the derived film coefficient can be as large as 25%. The results presented in [8] indicate that for steady state flow the heat transfer rates are not very sensitive for the value of the film coefficient; gas to ambient heat transfer is governed by the thermal resistance of the pipe wall layers and the soil.

4.2.2 1D radial unsteady model

The 1D radial unsteady model is an elemental model of transient heat conduction in one dimensional radial coordinates. An extensive description of this model and its coupling with the flow model is provided in Chaczykowsky [12] and Helgaker [10]. In this work,

an adapted version of the model included in the original pipe flow code from Helgaker is used. The model consists of coaxial cylindrical layers surrounding the pipe as shown in Figure 4.1.

The gas temperature is coupled through the film heat transfer coefficient at the inner wall of the innermost layer (the pipe wall), and the ambient temperature is imposed as surface temperature on the outermost layer. The temperature field varies both in time and in the radial spatial dimension, but not angularly. The flow parameters and the external heat transfer model are calculated separately during each time step.

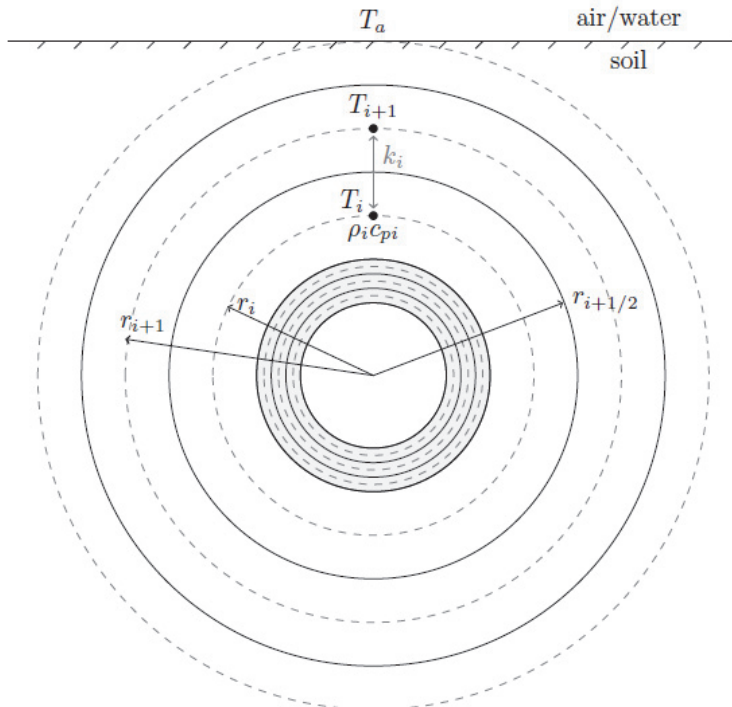


Figure 4.1: Discretization scheme of the 1D radial unsteady model (Helgaker [10]).

Each simulation is started by setting up a steady state flow condition and corresponding thermal gradient in the pipe wall and soil layers. The steady state is achieved by running the transient model with constant boundary conditions over a sufficient number of time steps. Within each new time step, first the thermal model is solved, using the gas temperature, gas density, Reynolds, and Prandtl number to obtain the pipe inner wall heat flux resulting from solving the flow model in the preceding time step. Subsequently, the flow model is solved, using the heat flux from the heat transfer calculation in the current time step as input. This is schematically shown in Figure 4.2.

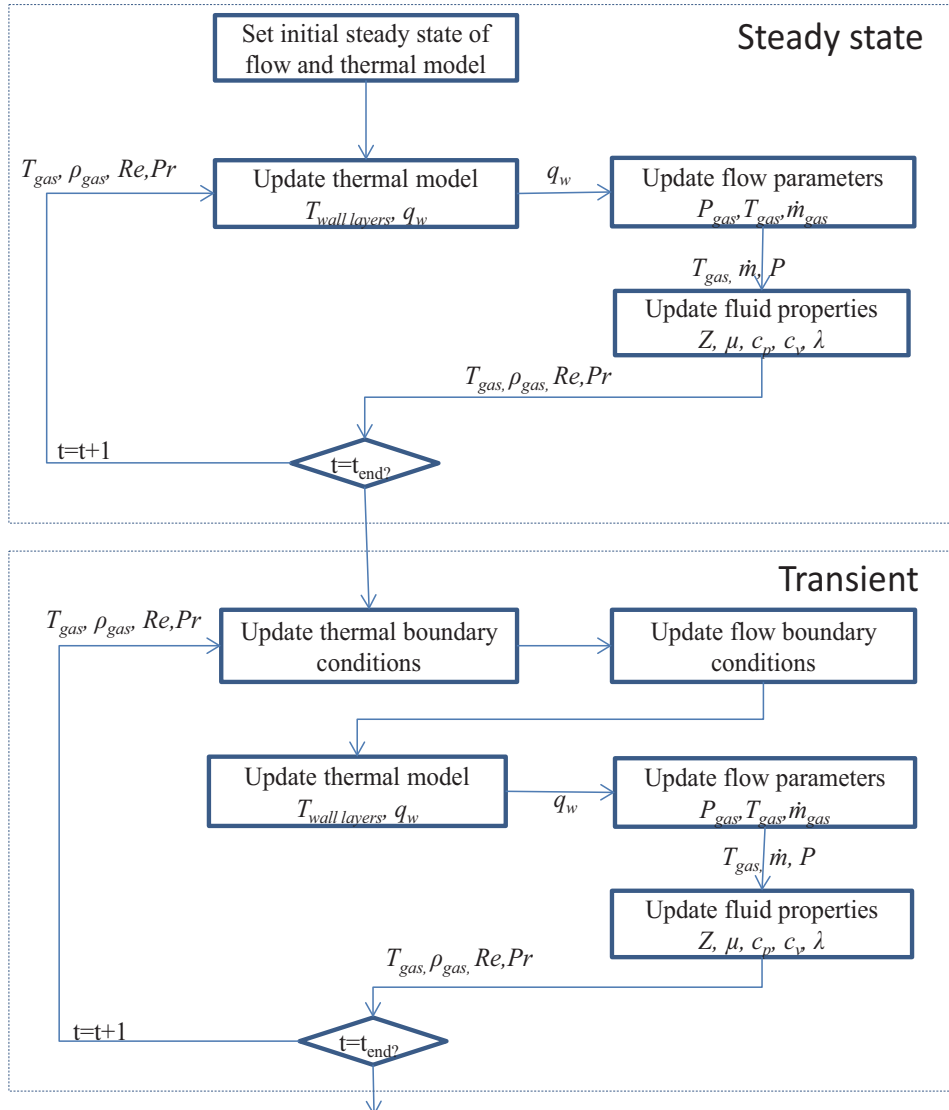


Figure 4.2: Coupling between flow model and unsteady external heat transfer models.

For a model with n elements, representing the heat conduction and storage through the pipe wall layers and the soil as concentric rings, the 1D radial heat exchange is represented by the following equations (Chaczykowski, [12]), Helgaker, [10]):

$$q_w = -k_0 (T_{gas}^{n+1} - T_1^{n+1}) \quad (4.13)$$

$$\rho_i C_i \frac{T_i^{n+1} - T_i^n}{\Delta t} = \frac{k_i}{A_i} (T_{i+1}^{n+1} - T_i^{n+1}) - \frac{k_0}{A_i} (T_1^{n+1} - T_{\text{gas}}^{n+1}) \quad (4.14)$$

$$\rho_i C_i \frac{T_i^{n+1} - T_i^n}{\Delta t} = \frac{k_i}{A_i} (T_{i+1}^{n+1} - T_i^{n+1}) - \frac{k_{i-1}}{A_i} (T_i^{n+1} - T_{i-1}^{n+1}) \quad (4.15)$$

$$\rho_N C_N \frac{T_N^{n+1} - T_N^n}{\Delta t} = \frac{k_N}{A_N} (T_{\text{amb}}^{n+1} - T_N^{n+1}) - \frac{k_{N-1}}{A_N} (T_N^{n+1} - T_{N-1}^{n+1}) \quad (4.16)$$

$$k_{01} = \frac{\lambda_{\text{gas}}^{n+1} \times 0.023 \text{Re}_{\text{gas}}^{n+1} \text{Pr}_{\text{gas}}^{n+1}}{2\pi r_1} \quad (4.17)$$

$$k_0 = \frac{1}{\frac{1}{2\pi r_1 k_{01}} + \frac{\ln(r_2/r_1)}{2\pi \lambda_1}} \quad (4.18)$$

$$k_i = \frac{2\pi \lambda_i}{\ln\left(\frac{r_{i+1}}{r_i}\right)} \quad (4.19)$$

Here, ρ_i , C_i , λ_i and A_i are respectively the density, specific heat capacity, thermal conductivity, and the area of ring i .

The scheme is solved implicitly using the Backward Euler method for the time discretisation. Central differences are used for the space derivatives. The scheme is thus first order accurate in time and second order in space. In the coupling between the pipe flow and thermal domain, the 1D flow equations are solved using the heat flux q_w calculated on the ambient thermal domain.

One problem arising is how to define the total radial thickness, r_s , of the soil domain. An initial approach is to set r_s equal to the depth of burial from the top of the soil to the pipe most outer layer. As discussed in Helgaker et al. [37], this approach gives a smaller thermal domain compared to the 2D case and a too short steady state conduction path. The energy exchange between gas inside the pipe and the ambience in steady state is in those cases overestimated. As discussed in Chapter 2, a suggested way to improve upon the latter is to use a so-called equivalent, or effective soil layer radius. This is for example applied in the multiphase flow simulation software OLGA. The equivalent soil

layer radius, based upon isothermal boundary conditions is given in Equation (2.29) (OLGA documentation [32]). This calculation of the equivalent wall layer has been used for the dimensioning of the 1D radial unsteady model.

The model studies with the 1D radial unsteady heat transfer model have all been conducted with a ten-layer model (ten grid cells). In each model, the pipe wall and plastic outer coating both contain one grid cell each. To cover the extent of the equivalent soil domain, eight grid cells are available. These have been distributed according to the advice given in Modisette [34]. The grid cells closest to the pipe wall have thus small radial thicknesses and are chosen progressively larger towards the outer boundary. Typically, a grid size thickness of 5 cm is applied at the inner soil boundary. This is similar to the grid sizes applied in the 2D unsteady model.

The sensitivity of the 1D radial unsteady model for grid cell size was tested by increasing the number of cells in the soil and reducing the size to 2.5 cm. The resulting differences in gas temperature and pressure response to the mass inlet rate transients is 0.025 K and 70 Pa. Refining the grid and increasing the number of cells does therefore not significantly change the response compared to the actual 1D unsteady radial model used in the investigations.

The choice of having only one grid cell representing the steel pipe wall is motivated by the need for stability in coupling the flow to the thermal calculation. The von Neumann number is the ratio of the distance the diffused quantity (in this case heat) travels in one time step compared to grid size, given as $VNN = \alpha \Delta t / x^2$. With a grid cell size $x = 44$ mm, $\Delta t = 60$ s and $\alpha = 1.27 \times 10^{-5}$ m²/s, $VNN = 0.4$. For both the 1D radial unsteady and the 2D unsteady model, it was found that the coupling between the flow and heat transfer is stable with this grid size in the pipe wall. Only some minor fluctuation of pipe wall heat flux around mean values does sometimes occur: this does not result in a noticeable effect upon the gas temperature. When using two grid cells across the pipe wall ($VNN = 4.88$), the results show some instability; heat transfer rate and gas temperature start to chase each other in subsequent time steps. This 1D radial unsteady model was compared with a version based upon a finite difference discretization of the 1D radial unsteady heat conduction equation. No significant difference in heat transfer rates were found between the discretizations.

4.2.3 2D unsteady model

The 2D unsteady model couples the thermal soil domain to the energy equation of the flow model similar to the 1D radial unsteady model, using the gas temperature and resulting pipe wall heat flux. For buried sections, each pipe flow calculation element has a corresponding 2D thermal model of the pipe wall and soil through the plane perpendicular to the pipe axis. The system is shown schematically in Figure 4.3. The 2D thermal domains form 2D ‘slices’ of the soil, discretized using a Finite Volume grid with the commercially available software FLUENT (ANSYS [73]). The physical dimensions of these 2D soil domains are 50×25 meters and the pipe wall layer is modelled with perfect thermal contact to the soil. The size of the domain is chosen

sufficiently large for the thermal gradients to be near zero at the vertical and lower borders.

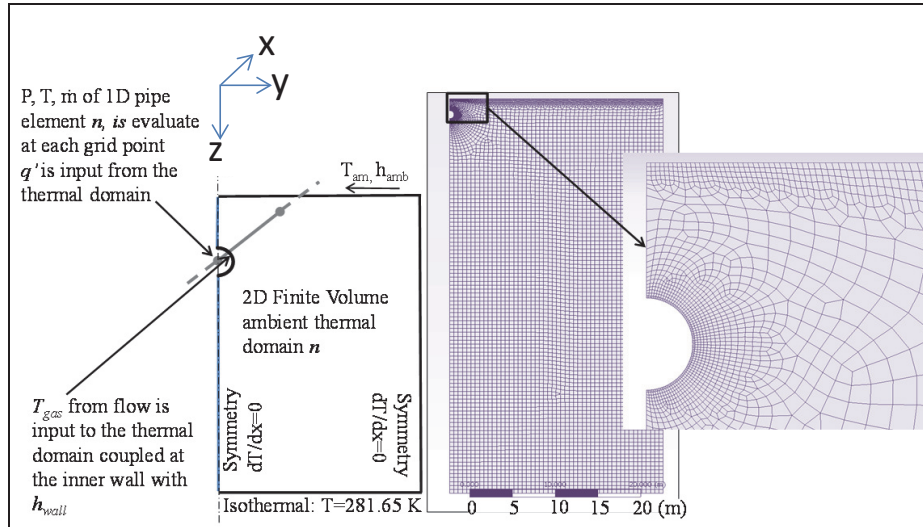


Figure 4.3: 2D model description and detail of finite volume grid of each soil slice (Oosterkamp [74]).

The symmetry along the y-axis is utilized to reduce the size of the model. On the lower and right hand side border of the domain, Neumann boundary conditions are employed with zero heat flux. Ambient temperature is coupled to the top border of the domain through a convective boundary condition employing heat transfer coefficient of 50 W/m²K. As discussed in Chapter 2.4, the soil surface energy balance is in reality much more complicated. The simplification of a convective boundary condition is suggested in [29]. The assumed value of 50 W/m²K has been taken as an intermediate value of forced convection of air over a horizontal surface (10-100 W/m²K).

The model grid was refined until the steady state heat transfer rate at the inner wall for $T_{gas}=303.15$ K and $T_{ambient}=278.15$ K did not change more than 1% with further refinement. This was evaluated after letting the solution converge to a residual of the energy equation of $1 \cdot 10^{-9}$. Only the energy equation for the solid domains is solved. In FLUENT, the discretization scheme for the energy equation is second order upwind in space and first order implicit in time. The under relaxation factor for the energy equation is set to one, and the V cycle multigrid solver is used. At the pipeline inner wall, a convective heat transfer boundary condition is used. The gas temperature is coupled to the pipe inner wall through a fixed heat transfer coefficient. The value of the heat transfer coefficient is representative for the film coefficient as described in Chapter 3.4. Radiative heat transfer is ignored, as gas temperatures are low. The resulting heat transfer through the boundary is calculated in FLUENT (ANSYS [73]) by summation of the net heat exchanged at each element on the boundary.

In the solid domain ANSYS FLUENT uses the following energy transport equation (ANSYS [73]):

$$\frac{\partial}{\partial t} \left(\rho \int_{T_{ref}}^T C_p dT \right) + \nabla (\vec{v} \rho h) = \nabla (\lambda \nabla T) + S_h \quad (4.20)$$

The second term on the right represents the convective energy transfer due to rotation or translational motion of the solids. In our model, all solids are stationary and source terms are absent therefore the energy transport equation reduces to the heat conduction equation. With absence of a fluid domain in the model, only the energy equation for the solid domains is solved. FLUENT uses a control-volume-based technique consisting of:

- Division of the domain into discrete control volumes on a computational grid.
- Integration of the governing equations on the individual control volumes to construct algebraic equations for the discrete dependent variables (“unknowns”) such as velocities, pressure, temperature, and conserved scalars.
- Linearization of the discretized equations, and solution of the resulting linear equation system to obtain updated values of the dependent variables.

The discretization scheme for the energy equation is second order upwind in space and first order implicit in time. In FLUENT the general scheme for implicit time integration for a scalar ϕ is (ANSYS [73]):

$$\frac{\partial Y}{\partial t} = F(Y) \quad \frac{Y^{n+1} - Y^n}{\Delta t} = F(Y^{n+1}) \quad (4.21)$$

The under relaxation factor for the energy equation is set to one, and the V cycle multigrid solver is used. At the pipeline inner wall, a convective heat transfer boundary condition is used. The heat flux at the boundary is defined by FLUENT as:

$$q_b = h_{boundary} (T_{fluid} - T_{boundary}) \quad (4.22)$$

4.3 Europipe 2 flow model – Kårstø-Trosnavåg

The first section of Europipe 2, from the inlet at Kårstø to the valve station at Trosnavåg is modelled. The flow model is using the height profile as shown in Figure 3.2. The pipe flow calculation elements have a length of 200 m each. The pipeline wall thicknesses and burial depths for the onshore parts are taken from the pipeline alignment sheets (Snamprogetti and Statoil [75]). The burial depths for the offshore part of the pipeline are derived from survey data (Statoil [76]).

A nominal, constant, gas composition is assumed as shown in Table 3.

Table 3: nominal gas composition

Component	Mole fraction
Methane	0.891524
Ethane	0.073513
Propane	0.005104
iso-Butane	0.000251
n-Butane	0.000311
iso-Pentane	0.00009
n-Pentane	0.000024
Nitrogen	0.006980
Carbon Dioxide	0.022209

The thermal properties of the soil are the values from the measurements as discussed in Chapter 3.4. The U-values for the steady state heat transfer model are calculated using the pipe wall layers and x-parameter according to the Equations (4.10 and (4.11). The equivalent soil radius for the 1D unsteady model is calculated using Equation (2.29). The gas temperature is coupled to the pipe wall through use of a film coefficient using Equation (2.11). Onshore, the ambient temperature is directly coupled to the soil surface. The values used are those measured at the experimental site on Bokn. For the onshore part of the pipeline, the seawater temperature is coupled to the pipeline soil domain (buried) or the pipeline outer concrete layer. The seawater temperatures have been generated with the Norkyst 800 model. Only one data point along the route, at 75 m water depth, is available. For the steady model, the soil conductivity is subsequently tuned so that the calculated pipe outer wall temperature at the Bokn test site location matches the measurement of the upper pipeline outer wall as closely as possible. For the 1D unsteady model, both thermal conductivity and thermal capacitance are tuned in order to match the pipe wall measured temperature at Bokn as closely as possible. The thermal conductivity is tuned to achieve an overall temperature match while the thermal capacitance is tuned to match the dynamic response. An overview of pipe wall layers, elevation, and burial depth used in the model is given in Appendix D.

4.4 Porous media models

The porous media model available in ANSYS was used to estimate the effects of groundwater convection on the heat transfer rate between gas and ambient. The models were built in ANSYS FLUENT and ANSYS CFX. In essence, the porous model is generated by adding a sink to the momentum equation. A relevant limitation in this approach relates to the fact that the pores are not physically present in the model. By default, the velocity of the flow field is the superficial velocity the fluid would have in the presence of the pores (ANSYS [73]):

$$u_s = \phi v \quad (4.23)$$

It is possible to have the true physical velocity calculated in the porous zones. In that case, the physical velocity is included in the differential terms of the equations. In FLUENT the assumption is isotropic porosity.

The additional momentum sink is modelled as a source term including a viscous (Darcy) and inertial part. The momentum sink leads to a pressure gradient in the porous calculation element, which in turn creates a pressure drop proportional to the fluid velocity. For simple homogeneous porous media the source term is (ANSYS [73]):

$$S_i = -\left(\frac{\mu}{\kappa} v + C_{inert} \frac{1}{2} \rho |v| v \right) \quad (4.24)$$

With μ as dynamic viscosity and κ as intrinsic permeability, the first term is the pressure drop according to Darcy's law. The constant C_{inert} represents the inertial losses occurring at high flow velocities.

The thermal part of the porous model provides two options. The first is the equilibrium thermal model. Assumed is that the fluid and the pore material are at all times in thermal equilibrium. The thermal conductivity in the porous solid is computed as the volume average of fluid and solid conductivity (ANSYS [73]).

$$\lambda_{eff} = \phi \lambda_f + (1-\phi) \lambda_s \quad (4.25)$$

The energy equation gets the following form (ANSYS [73]):

$$\frac{\partial}{\partial t} (\phi \rho_f E_f + (1-\phi) \rho_s E_s) + \nabla \cdot \left(\vec{v} (\rho_f E_f + p) \right) = S_f^h + \nabla \cdot \left[\lambda_{eff} \nabla T - \left(\sum_i h_i J_i \right) + (\bar{\tau} \cdot \vec{v}) \right] \quad (4.26)$$

The other option is the non-equilibrium thermal model. In this model, at each location, two spatially coinciding cells are used, one for the solid zone and one for the porous fluid zone. The solid zone interacts only thermally with the porous fluid zone. The energy equation is solved separately for both zones. The porous fluid energy equation is (ANSYS [73]):

$$\frac{\partial}{\partial t} (\phi \rho_f E_f) + \nabla \cdot \left(\vec{v} (\rho_f E_f + p) \right) = + \nabla \cdot \left[\phi \lambda_f \nabla T_f - \left(\sum_i h_i J_i \right) + (\bar{\tau} \cdot \vec{v}) \right] + S_f^h + h_{fs} A_{fs} (T_s - T_f) \quad (4.27)$$

The energy equation for the solid is (ANSYS [73]):

$$\frac{\partial}{\partial t} ((1-\phi) \rho_s E_s) = \nabla \cdot ((1-\phi) \lambda_s \nabla T_s) + S_s^h + h_{fs} A_{fs} (T_f - T_s) \quad (4.28)$$

In the porous media models, the permeability κ needs to be provided. The grain size distribution measurements of the sand samples have been used with literature correlations to estimate the hydraulic conductivity value K . For Darcy flow, the permeability is related to hydraulic conductivity as (ANSYS [73]):

$$\kappa = K \frac{\mu}{\rho g} \quad (4.29)$$

The ground water can contribute to the heat transfer in three different ways:

1. Forced convection due to a hydraulic gradient
2. Natural convection with water as a single phase
3. Differences in vapour pressure leading to evaporation and migration of water vapour from areas with higher pore water content to lower pore water content

The ANSYS porous media model was used to model the first and second phenomena.

4.5 Forced convection model

Figure 4.4 shows the meshed ANSYS CFX forced convection model. The model is a 3D section of the soil and pipeline with a vertical symmetry plan coinciding with the pipe-axis. The bulk soil (clay), top soil layer, ditch and pipe wall layers are modelled as separate solids with different thermal properties. The solid domains are coupled thermally. The gas flow is not modelled directly but represented by the gas temperature coupled to the pipeline inner wall through a fixed film coefficient. The pipeline section has a length of 100 m. The cross-sectional domain is similar to that of the 2D-model of Chapter 4.1.3. The ditch domain is split horizontally at the height of the pipeline axis. This is the assumed height of the local ground water level. Initially the water phase is chosen as an incompressible liquid with constant density.

To include convection phenomena, the water density is made temperature dependent according to the Boussinesq approach of buoyancy driven flow. Both the thermal equilibrium and non-equilibrium models are used. The non-equilibrium model needs the specific surface area and heat transfer coefficient of the porous media. The specific surface area can be calculated if we assume the sand to be a spherically packed bed. A rough estimate of the specific surface area $S = 6/d_{50} = 8570 \text{ m}^{-1}$ is used.

At the measurement location, the driving force for ground water flow is a hydraulic gradient of 474 Pa/m. This is used to calculate the Darcy velocity with the range of established K values obtained from the sand grain size distribution.

In the model the lower soil boundary has a fixed temperature boundary condition (281.65 K). The front and back faces perpendicular to the pipeline axis are symmetry conditions as well as the faces lying on the symmetry plane coinciding with the pipeline axis and the faces on the opposite parallel plane. The top (soil) surface is given a fixed temperature corresponding to measured soil surface temperature. The front and back faces of the lower ditch porous domain are subject to a fluid inlet and outlet with prescribed flow rate. The simulation is run in steady state with the gas temperature and surface soil temperature from a period with near constant gas flow conditions.

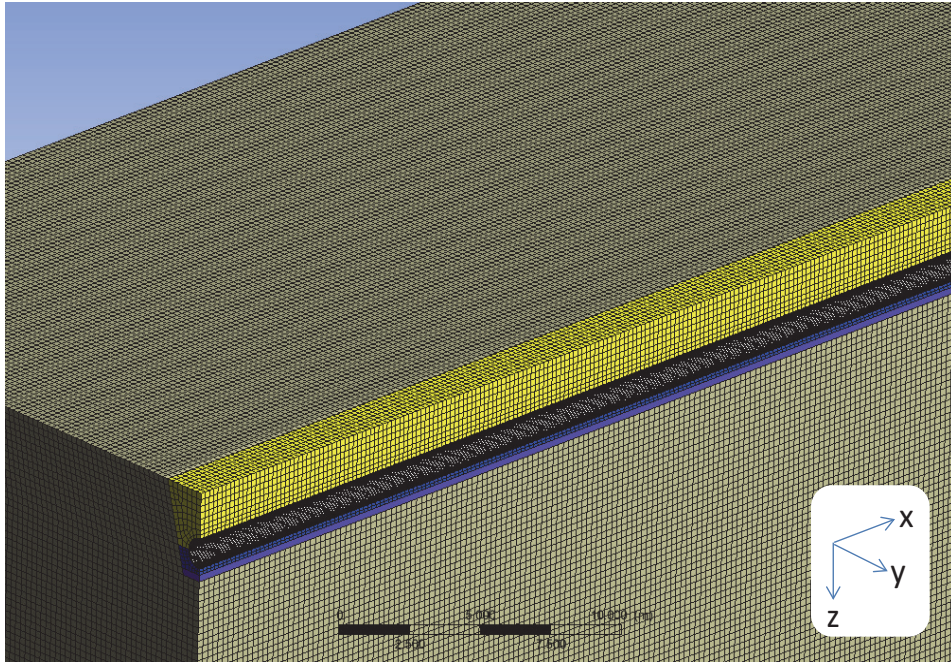


Figure 4.4: Part of the forced convection numerical model showing the calculation grid. Gray part is the bulk clay soil. The black mesh part is the pipeline. The yellow, blue and purple meshed parts are the fill sand in the ditch surrounding the pipe. The ground water is allowed to flow through the blue and purple lower parts.

4.6 Natural convection model

The natural convection model is set up as a 2D slice from the pipe and soil at Bokn. As with the 3D model, the bulk soil (clay), top soil layer, ditch and pipe wall layers are modelled as separate surface solids with different thermal properties. The solid domains are coupled thermally.

The porous media domain is modelled both with water as an incompressible liquid using the Boussinesq approach for thermally driven convection. The grid size used in the model is shown in Figure 4.5. The convection driven heat transfer is assumed to occur only in the sand inside the ditch; this part of the model has a refined grid.

The vertical boundaries of the soil domain have a symmetry boundary condition. At the lower edge of the soil domain, a constant temperature of 281.65 K is applied. The top of the soil domain has a constant temperature of 280.15 K applied. The inner wall of the pipe has a convective heat transfer boundary condition with a gas temperature of 302 K and a heat transfer coefficient of 1650 W/m²K. To solve the equations, the SIMPLE scheme (ANSYS [73]) is used with second order upwind discretization for both momentum and energy equations.

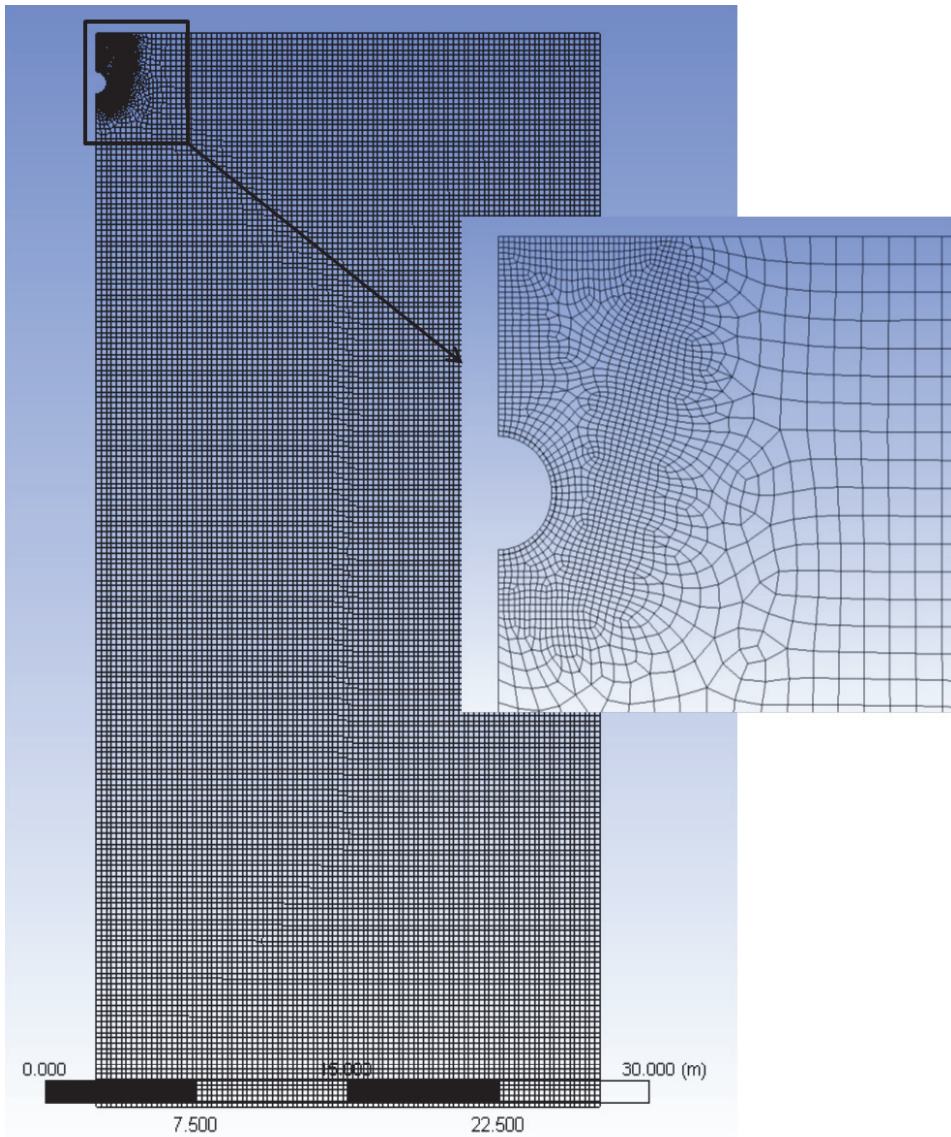


Figure 4.5: Mesh of the natural convection model.

4.7 Bokn experimental site model

The Bokn experimental site model is a simplified representation of the soil and pipe wall layers at the actual measurement site. The model has the same domain dimensions as the natural convection model, but with a finer mesh around the pipe. Detail of the meshed model is shown in Figure 4.6.

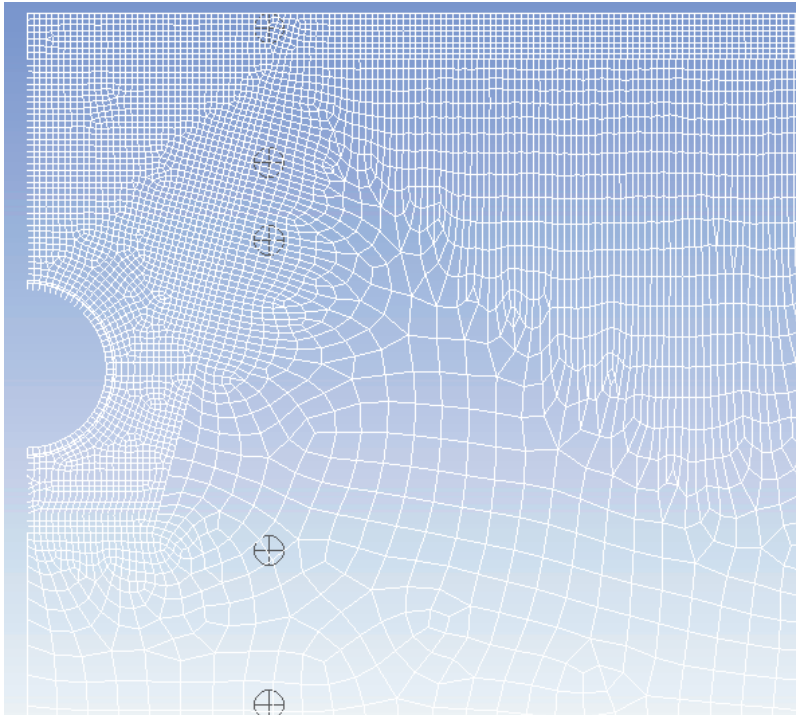


Figure 4.6: Detail of mesh of Bokn experimental site model

The model is using the FLUENT as a server option. This allows a third part application to take control of FLUENT by executing commands in the text console. Purposely written MATLAB code is used to control the FLUENT case. The MATLAB code reads the measurement data of the top soil layer temperature and pipe gas temperature. These are used as boundary conditions in the FLUENT case and refreshed at the beginning of each 5 min transient time step. At the end of each time step, the resulting temperature values at each measurement location are collected by MATLAB. The transient FLUENT case is given an initial temperature field by running the model with one-hour time steps. In this initial run, the ambient air temperature of the preceding eight years is used as upper soil boundary condition. In this period, the gas temperature stays constant at 301 K. At the lower edge of the domain, the temperature is set constant 281.65 K. Thermal soil properties are initially set to the values obtained from the measurements done on soil samples collected at the site. The model run starts at the 28th of April 2013 at midnight and is continued for over a year. The fit between the measured and calculated values at each measurement location in the soil and around the pipe are assessed using the Normal Root Mean Square Error. The heat exchange rate over the pipe wall is also collected for assessment. The model can be run with pure heat conduction or include natural convection with the porous media formulation. The effect of forced convection can be emulated by including an energy source term on parts of the solid domain. The effect of simplification of the upper soil boundary condition upon the gas to ambient heat exchange rate can also be studied.

Results

5 Results

This chapter provides the results of the investigations. In this chapter, the heat transfer rate over the pipe wall is always per meter pipeline length. The sign convention is such that when the gas transfers heat to the environment, the heat transfer rate is negative.

5.1 Analysis of transient flow conditions in Europipe 2

Data from the SCADA system at Gassco AS were analysed to understand the type and nature of the inlet flow conditions present in Europipe 2 from April 2013 until September 2014. The data are interpolations from the real time measurements resulting in 60 seconds intervals between consecutive samples. Volume flow rates are converted to mass rates using the gas density measurements available in the SCADA system. The inlet flow, pressure, and temperature data are treated in the following way: first, the missing data points are replaced by interpolation between the neighbouring points. Rates of change are obtained through time differentiation of the data:

$$f'(t) = \frac{f_{t+1} - f_{t-1}}{2\Delta t} \quad (5.1)$$

Figure 5.1 to Figure 5.3 show the mass flow rate, pressure and temperature, and their rate of change.

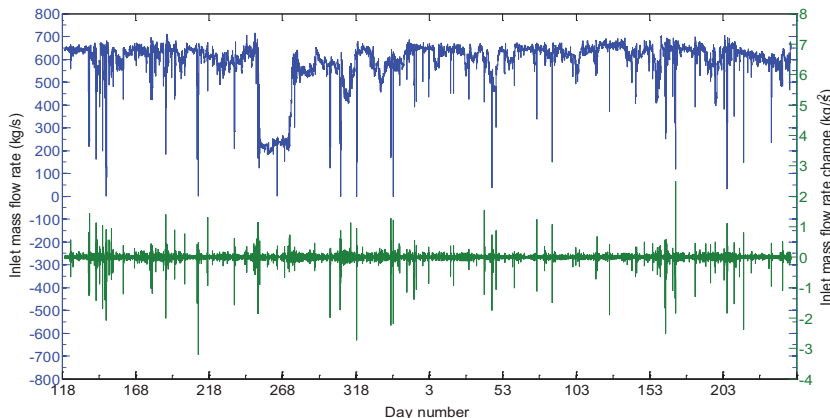


Figure 5.1: Inlet mass flow rate (blue curve) and rate of change (green curve).

Figure 5.1 shows that the inlet mass flow rate has an average level of roughly 650 kg/s with occasional drops to levels below 200 kg/s, followed by a recovery back to the median. The largest dips in the inlet flow rate occur at the highest rate of change. Predominantly, the rate of change falls in a band from -1 to 1 kg/s² and is continuous fluctuating. The highest rates of change (2-3.5 kg/s²) occur during the largest overall changes in mass flow rate. There are seven complete stops in the inlet flow. Figure 5.2 shows the inlet pressure data. The average level is approximately 180 barg, with sudden

Results

drops of 30 to 50 barg, followed by a rise back to the median pressure level. The pressure drops and rises generally coincide with the inlet mass flow rate changes, but occur over a longer period (less steep drops). The rate of change falls predominantly within a band of -0.005 to 0.005 barg/s, with peak rates of change (0.02- 0.06 barg/s) coinciding with the larger pressure changes. Typically, the drop in pressure occurs at a higher rate than the following rise in pressure. The correlation between mass flow rate and pressure can clearly be seen when comparing Figure 5.1 and Figure 5.2.

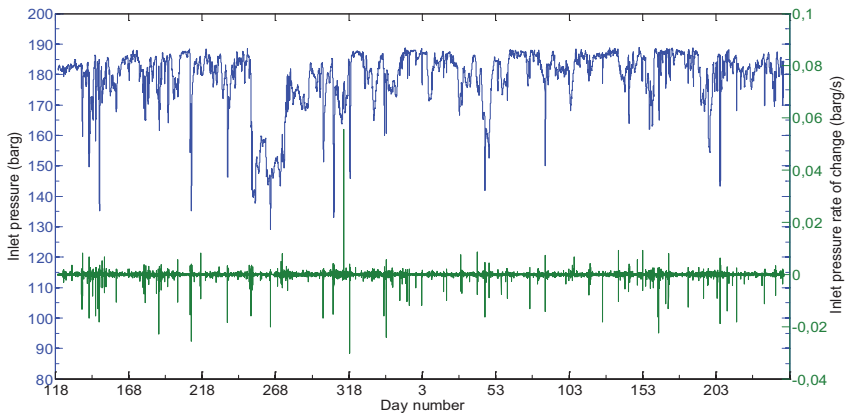


Figure 5.2: Inlet pressure (blue curve) and rate of change (green curve).

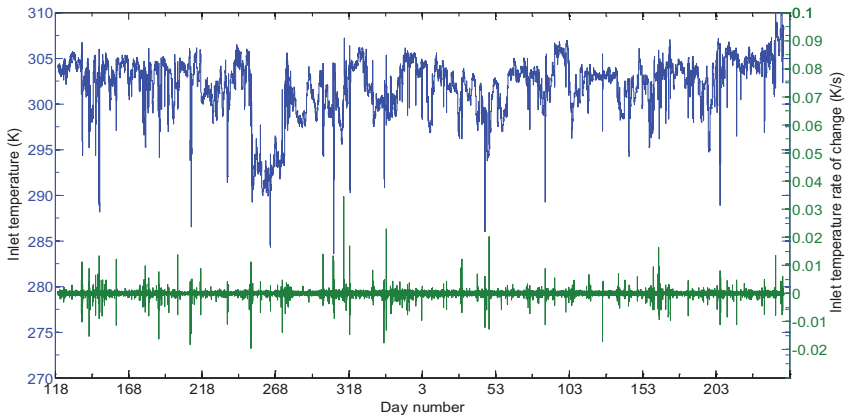


Figure 5.3: Inlet temperature (blue curve) and rate of change (green curve).

Figure 5.3 shows inlet temperature data. The average level is roughly 305 K, with sharp drops of 5-15 K, followed by a rise back to the average level. The inlet temperature follows the overall trend of the inlet flow rate. The overall values of the rate of change are in a band from -0.005 to 0.005 K/s with peaks in the range of 0.02-0.04 K/s. Figure 5.4 shows a more detailed time development of a typical inlet flow transient. The inlet mass flow rate transient has a characteristic ‘saw tooth’ shape, consisting of a quick

Results

ramp down from the median flow rate at a rate of change of $1-2 \text{ kg/s}^2$, followed by a slower ramp up back to the median level. The inlet gas temperature and pressure follow the same development as the mass rate but at slower rates: the local minimum is reached later in time compared to the mass rate.

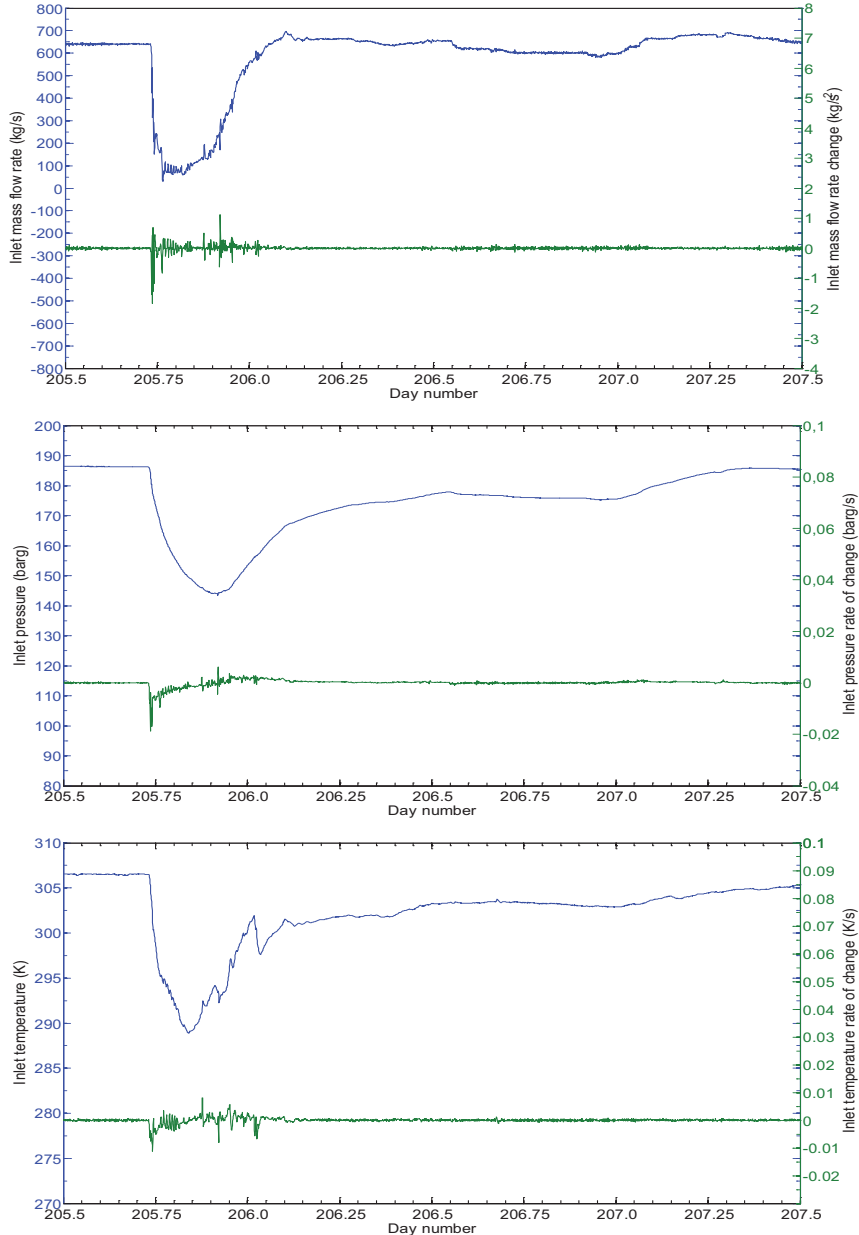


Figure 5.4: Detail of inlet transient (24th of July to 26th of July 2013).

Results

Fast Fourier transformation was performed on the full set of inlet measurement data to identify dominating frequencies in the inlet flow changes. The results show no distinguishable frequencies on a minute, hour, day, week, or monthly time scale. A minor annual cycle can be distinguished (gas demand is higher in winter compared to the summer).

5.2 Parametric model studies

Parametric model studies were conducted using the pipe flow model described in Chapter 4.1 together with the heat transfer models described Chapter 4.2. For this study, a 100 km long generic pipeline case was defined. This pipeline is buried onshore for the first and final 10 km. The 80 km long offshore section is exposed to seawater. The pipeline has an inner diameter of 1.016 m and a 44 mm thick steel wall with a 3 mm thick polymer coating. The pipe flow calculation domain is divided in 100 elements. Figure 5.5 shows the pipeline schematically.



Figure 5.5: Schematic representation of the generic pipeline case used in the parametric studies.

5.2.1 Rapid Transients: effect of choice of ambient model

The results described in this chapter have been partly published in Oosterkamp et al. [74]. The aim was to determine the basic influence of the external heat transfer model on transient flow calculation. A likely operational scenario is to set a flow rate at the inlet together with an outlet pressure, calculating inlet pressure. Other inlet and outlet boundary conditions are possible: for example pre-described inlet pressure, -flow and -temperature with calculation of the outlet pressure. In most cases, the pressure and flow rate changes closely follow each other, and the principles of transient flow behaviour are expected to be similar. Figure 5.6 shows the two generic inlet transients used in the study. These are defined to for maximum response to the choice of the external heat transfer model. Transient A is a step change in mass flow rate at the pipeline entrance, at constant inlet gas temperature. Both the ramp-up and ramp down occur within one minute, followed by several days of steady mass flow rate levels. The same transient is studied in Helgaker et al. [37]. Transient B is a one-minute step change of the inlet temperature, keeping the inlet mass flow rate constant. The magnitude of the step change and the rates of change are comparable with that of the fastest inlet transients. Table 4 shows the boundary conditions for the flow. In the external heat transfer models, soil thermal conductivity (λ_{soil}) is set to three W/mK and thermal diffusivity

Results

(α_{soil}) to $1.2 \cdot 10^{-6} \text{ m}^2/\text{s}$. These values are at the high end of the range. Where the pipeline is exposed to seawater, a fixed outer film coefficient is used (Equation (2.13)).

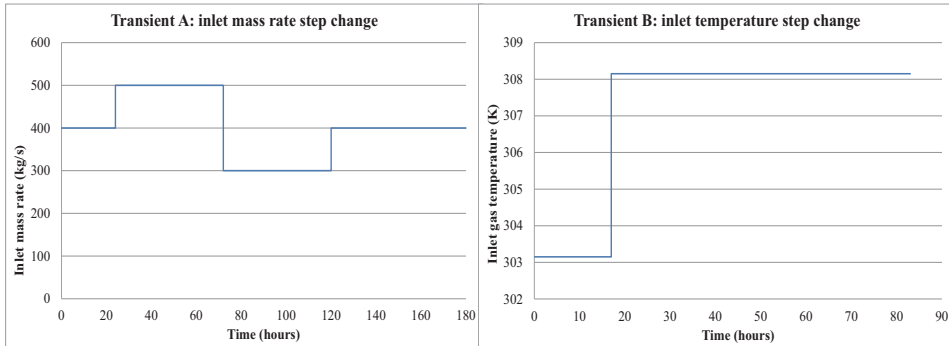


Figure 5.6: Inlet mass flow rate (transient A) and temperature (transient B) transients used in the numerical study (Oosterkamp et al. [74]).

Table 4: Boundary conditions parametric case studies

Boundary condition	A	B
Inlet gas pressure	calculated	calculated
Inlet mass flow rate	Transient A	400 kg/s
Inlet gas temperature	303.15 K	Transient B
Outlet gas pressure (barg)	90 MPa	90 MPa
Outlet mass flow rate	calculated	calculated
Outlet gas temperature	calculated	calculated
Ambient air temperature	278.15 K	278.15 K
Sea water temperature	277.15 K	277.15 K
Sea water current velocity	0.5 m/s	0.5 m/s

Four different external heat transfer models were used:

1. Adiabatic model: to understand the basic flow response to the transients.
2. 1D steady model: commonly used for control purposes at Gassco AS
3. 1D radial unsteady model: to understand the effect of the heat storage term in the heat transfer formulation. This is the transient heat transfer model of choice for pipeline modelling.
4. 2D unsteady model: to understand the effect of the 2D geometry of the heat transfer problem of a buried pipe.

Table 5 shows the combinations of onshore burial depth:

Table 5: Definition of burial cases.

Case	Burial depth (m)	$\sigma = (H/r_o)$
Base case	2	3.58
1	1	1.8
2	0.565	0.02
3	-0.555	-1.1

Results

5.2.1.1 Flow response with the adiabatic model

The adiabatic model does not allow for heat exchange with the environment. To achieve this, the overall heat transfer coefficient U , used with Equation (4.5) is set to zero. Figure 5.7 shows the time development of the pipeline gas temperature and pressure profiles along the pipeline route in response to the first inlet mass rate transient. The sudden mass rate increase results in a higher velocity of the gas entering the pipe compared to the gas in front of it inside the pipeline. In response to this, the downstream gas molecules inside the pipeline are pressed closer together. This results in a temperature increase of the gas (increase of internal energy) flowing through the pipeline.

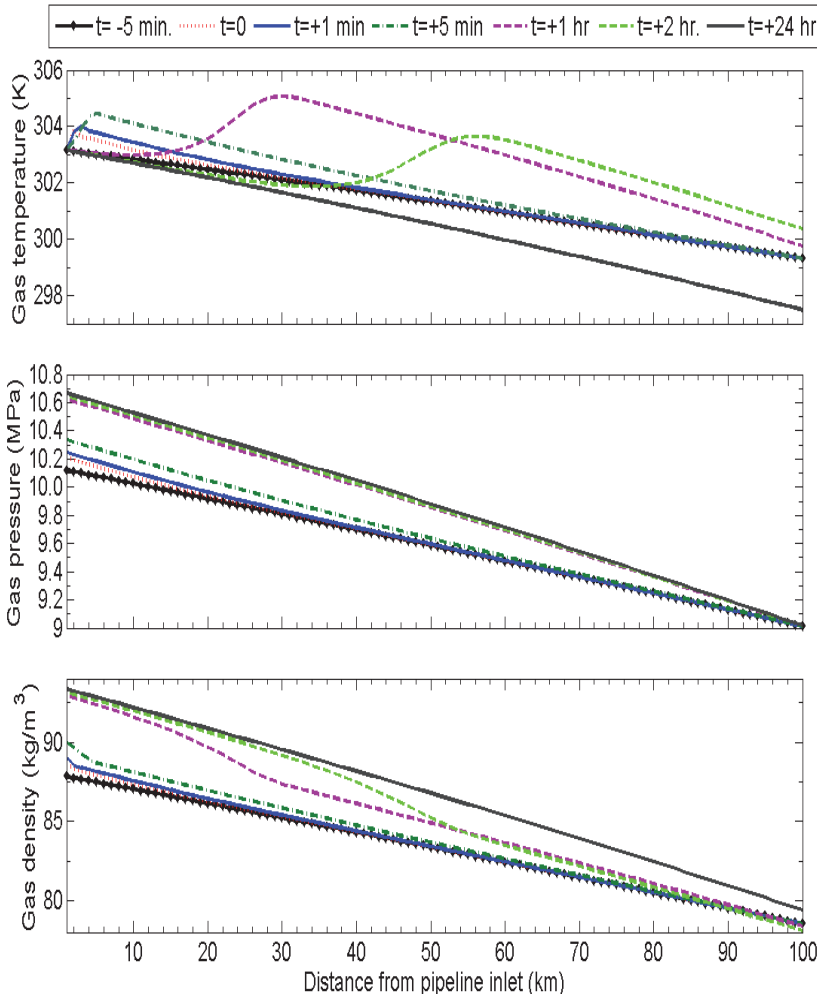


Figure 5.7: Transient A: time development of the pipeline profile for gas pressure, gas temperature and gas density in response to the first inlet mass rate transient.

Results

The compression is highest for gas that entered the pipeline just prior to the mass rate increase. This results in a temperature peak of 305.4 K, occurring circa half an hour after the inlet mass rate change, at 20 km from the inlet. In the wake of this, a through compression heated batch of gas, with higher pressure, density, and velocity, follows. This gas, flowing at the increased mass rate level has a correspondingly larger pressure drop per km. This results also in a larger temperature drop per km (due to Joule Thomson expansion). The flow establishes a new steady state temperature profile in the pipeline after 5 to 6 hours with a lower gas temperature at the exit. It takes much less time for the pressure to settle between the successive steady states compared to the gas temperature. This is as expected, the information of the pressure change travels with the speed of sound of the gas through pipeline, while the gas temperature rise travels through the pipeline with the gas velocity.

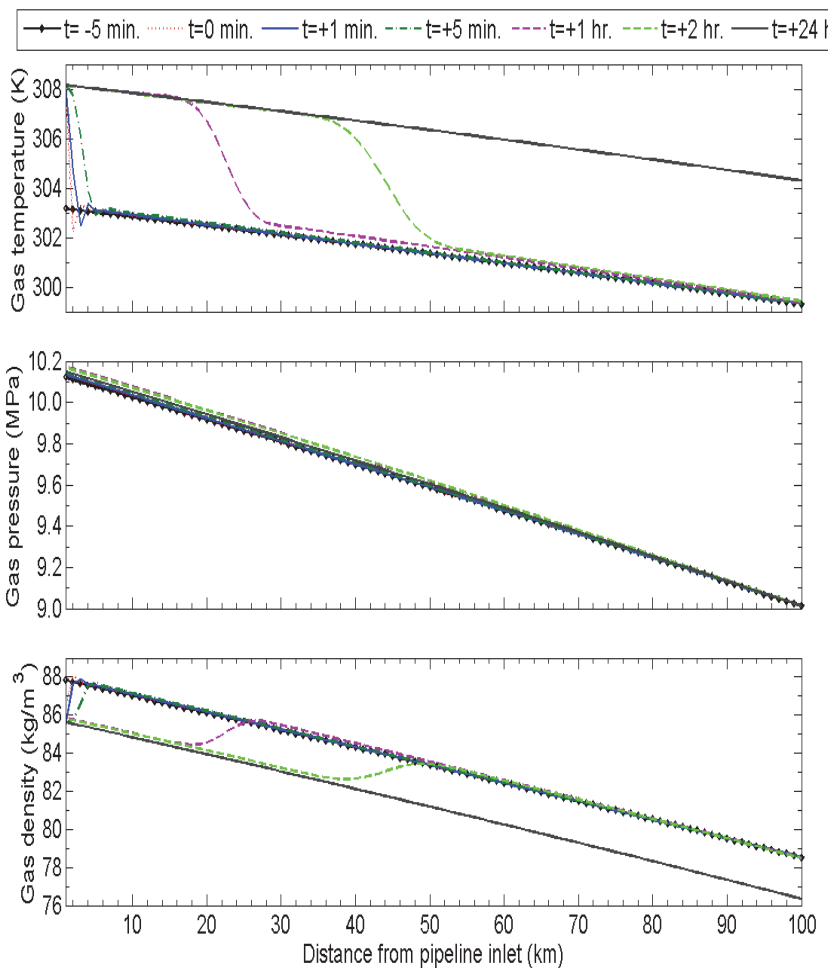


Figure 5.8: Transient B: time development of the gas pressure, gas temperature and gas density profile in response to the inlet temperature transient.

Results

Figure 5.8 shows the time development of the gas temperature and pressure profiles in response to the temperature transient (B). The hotter gas entering the pipeline has a lower density and thus a higher gas velocity (constant inlet mass rate). This initially compresses the colder and denser gas just downstream in the pipe, resulting in an initial, small temperature increase. This gas subsequently undergoes a small temperature drop when it expands towards the less dense gas following it upstream inside the pipeline (as can be seen from the red and blue line in the gas temperature and density profiles of Figure 5.8). Over time, the pipeline is filled with gas at the new condition (warmer and less dense). This further compresses the colder gas in front of it, slightly increasing its temperature as it travels further downstream the pipeline. Eventually, after five to six hours, all gas inside the pipeline is replaced by gas at the new condition, establishing a new steady state flow condition.

Figure 5.7 and Figure 5.8 show that the isothermal response of the gas inside the pipeline is depending on the type of transient. The inlet mass rate transient (A) results in a significantly larger response in the inlet pressure compared to the inlet temperature transient (B). The resulting gas temperature response is also different: the inlet mass rate transient (A) leads to significant, immediate, transient temperature rise of the gas downstream the pipeline, this is not the case with the inlet temperature transient (B).

5.2.1.2 Flow response with the different heat transfer models.

The effect of the three thermal models is studied for the generic pipeline case. The onshore sections are fully buried (soil surface to centre line of pipe is 2 m). Using Equations (2.11), (4.10), and (4.11), the calculated overall heat transfer coefficient of the buried parts U is $2.9 \text{ W/m}^2\text{K}$. The equivalent soil layer radius of the 1D radial unsteady model, with Equation (2.29) is 4.2 m.

For this pipeline scenario, there are three distinct heat transfer regimes along the pipeline (as discussed in Ramsen et al [33]). To evaluate the response of the gas flow parameters upon the transients, the locations at the end of each of these three distinctive regimes are chosen: at the end of the first buried part of the pipeline, the end of the offshore part and the pipeline exit. This is further explained in Oosterkamp et al.[74].

The following figures are also shown in Oosterkamp et al.[74], and a short version of the explanation is repeated here to illustrate the results. Figure 5.9 show that there is a significant difference in gas temperature response to the inlet mass rate transient, but *not* regarding gas pressure. In the first buried section, the differences in gas temperatures between the three heat transfer models are the largest. The difference in gas temperature response to the rise in flow rate is 1.5 K at the end of the first buried section. For the second, larger, mass rate transient (drop in flow rate), the difference between the steady and unsteady models is as large as 4 K. At the end of the offshore section, the differences in gas temperature response are significantly smaller due to the high heat transfer rate to the seawater. There is no time dependent storage of heat in the sea domain with the unsteady models. The gas temperatures are governed by the balance between heating through external heat transfer and expansive cooling; the difference

Results

between the models becomes negligible. Flowing through the final buried section, the differences in gas temperature response become apparent again. The exit temperature difference between the steady and unsteady models is 0.4 K for the mass rate increase and 0.6 K for the mass rate decrease. The differences in gas pressure response inside the pipeline are much smaller (<0.1 bar) and are negligible closer to the exit because the exit pressure is set as a fixed boundary condition.

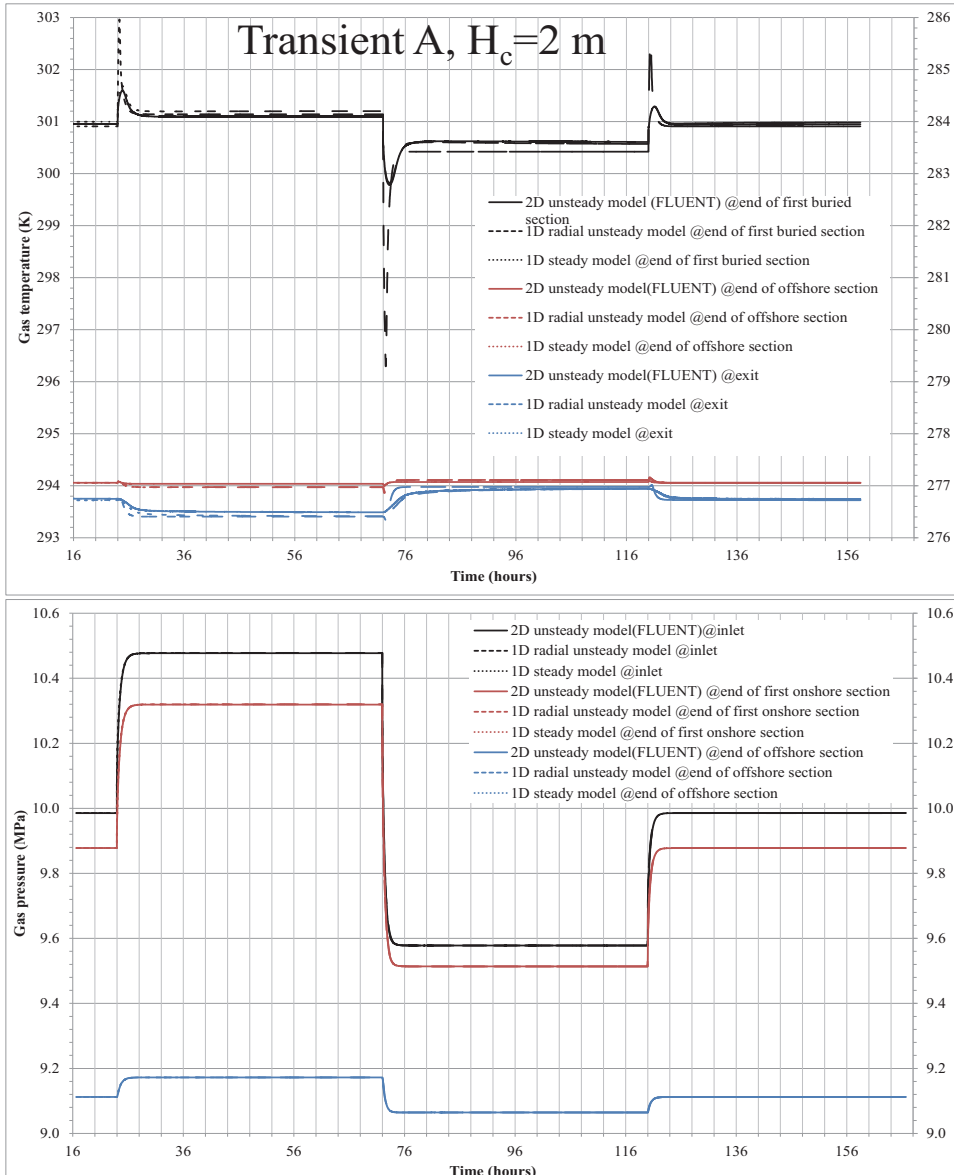


Figure 5.9: Base case (2 m burial depth). Gas response to inlet mass rate transient at different pipeline route locations (above gas temperatures, below gas pressures).

Results

Figure 5.10 shows the development of the gas temperature in the first, buried, part of the pipeline. The differences in the temporal development of the gas temperature profile obtained with the steady and unsteady models are clearly visible.

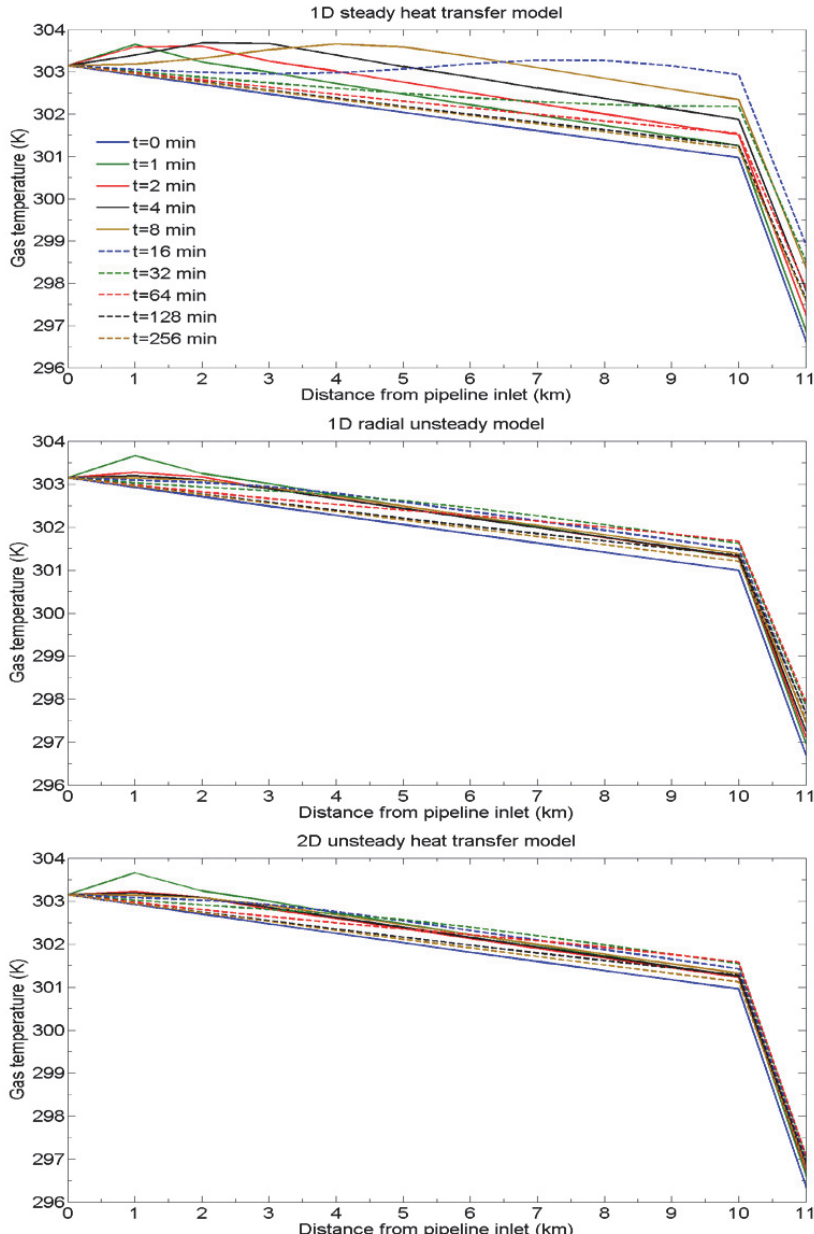


Figure 5.10: Temperature development in the first part of the pipeline in response to the first inlet mass rate transient, shown for each heat transfer model.

Results

Comparing to Figure 5.7, the temporal development of the gas temperature profile, using the 1D steady heat transfer model, is very similar to the adiabatic case.

The qualitative and quantitative differences in calculated gas temperature between the 1D radial unsteady and the 2D unsteady model are small compared to those obtained with the 1D steady model. The response is much more damped than with either the adiabatic or 1D steady model. The explanation of the difference between the steady and unsteady heat transfer models follows from the absence of temporal heat storage in the steady model.

Figure 5.11 illustrates the differences in heat transfer response. The heat transfer response to the mass rate transient using the steady model is at least an order of magnitude smaller compared to the responses of both unsteady heat transfer models. For the steady state model, the overall heat transfer coefficient U remains constant in time. The contribution to the internal energy budget of the gas follows from the heat exchange to the environment over the pipe wall, $q_w = U \times (T_{gas} - T_{amb})$, in the energy equation (Equation (4.5)).

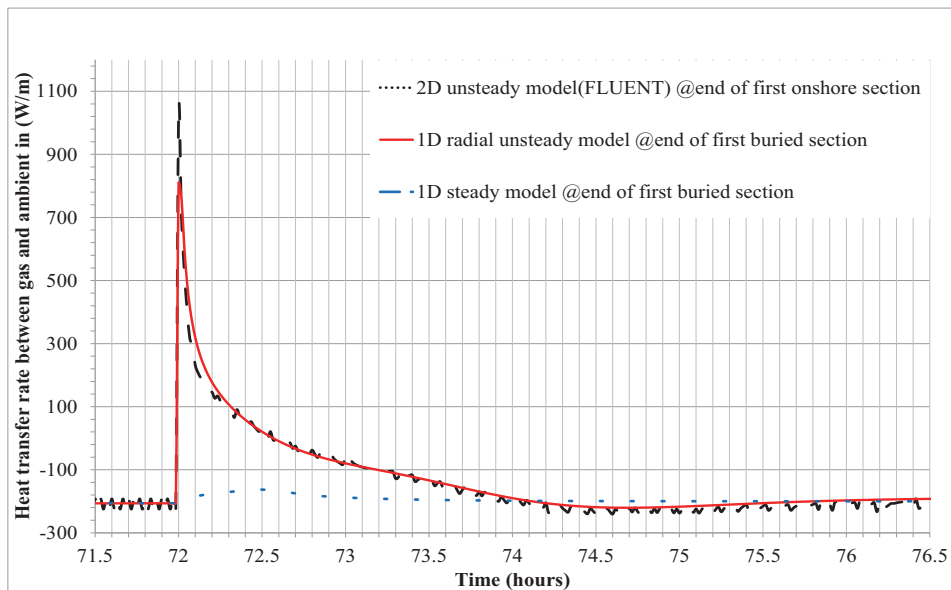


Figure 5.11: Base case (2 m burial depth). Energy exchange between gas and ambient at the end of first buried section in response to a drop in mass rate.

A sudden increase in gas temperature can only result in a modest increase in the heat transfer rate, as this depends on the thermal gradient over the entire heat transfer domain. For the unsteady thermal models, the instant thermal response of the pipe wall and surrounding soil layers is to store the thermal energy before conducting it further out through the soil domain. The resulting inner wall heat flux follows from the *local* thermal gradient at the inner wall, being much higher during transient heat conduction compared to the steady state.

Results

The second type of transient is a change in inlet temperature (Transient B). Figure 5.12 shows the resulting pressure and temperature responses of the gas inside the pipeline. Again, the results for both unsteady heat transfer models show a similar pressure and temperature response that differs significantly from that obtained with the 1D steady model.

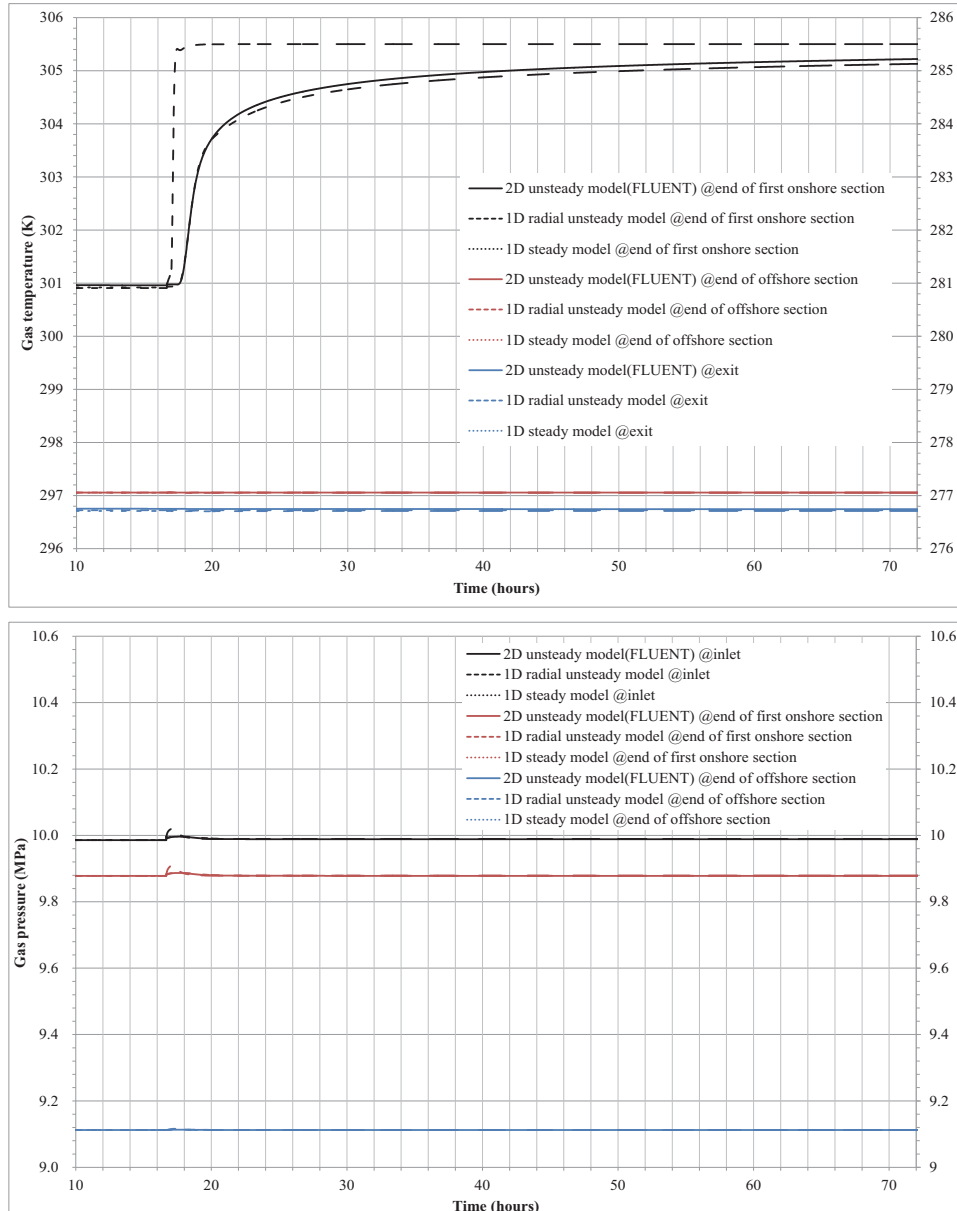


Figure 5.12: Base case (2 m burial depth). Above, gas temperatures, and below gas pressures, in response to the inlet temperature transient.

Results

In the first buried section, the new thermal steady state is reached much sooner with the 1D steady model. At the end of the first buried section, the maximum gas temperature difference between the steady and unsteady models is 4.5 K. The difference in gas temperature response between the models is minimal at the other two locations.

In contrast to the mass rate change, the gas pressure response now shows a minor difference between the steady and unsteady heat transfer models. At the end of the first buried section, the gas response to the inlet temperature rise, results in 0.3 barg higher pressure when using the 1D steady model, compared to both unsteady models. The explanation for this different response follows from the difference in heat transfer rate at the pipe inner wall. Figure 5.13 shows the pipe inner wall heat transfer at the end of the first onshore section. Compared to the 1D steady model, the energy exchange between the gas and the environment is also for this type of transient an order of magnitude higher when using the unsteady heat transfer models. The higher heat transfer rates resulting from heat storage in the pipe wall and soil delays the gas temperature increase inside the pipe. With the 1D steady heat transfer model, the cooling of the hotter gas at the colder pipe wall is much less compared to the unsteady models. This hotter gas has a lower density than the colder gas just in front of it. In order to maintain the same mass rate, the flow velocity of the gas into the pipe increases. This results in some compression due to the inertia of the slower, colder gas in front, leading to a small, temporary pressure increase of this gas. This is clearly seen at the first two locations in Figure 5.12. This initial compression of the gas downstream of the hotter gas entering the pipeline also explains the initial increase in heat transfer rate with both unsteady models (the initial dip from -200 to -300 W/m in Figure 5.13).

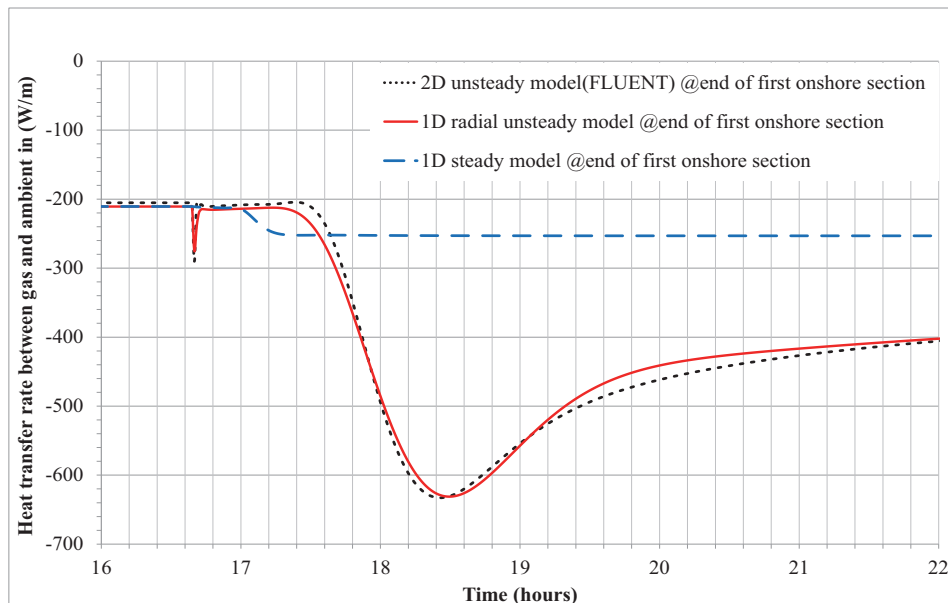


Figure 5.13: Base case, 2 m burial depth. Energy exchange between gas and ambient in response to the inlet temperature transient at end of first buried section

Results

Figure 5.14 shows the development of the gas temperature profile along the pipeline route in response to the inlet temperature rise.

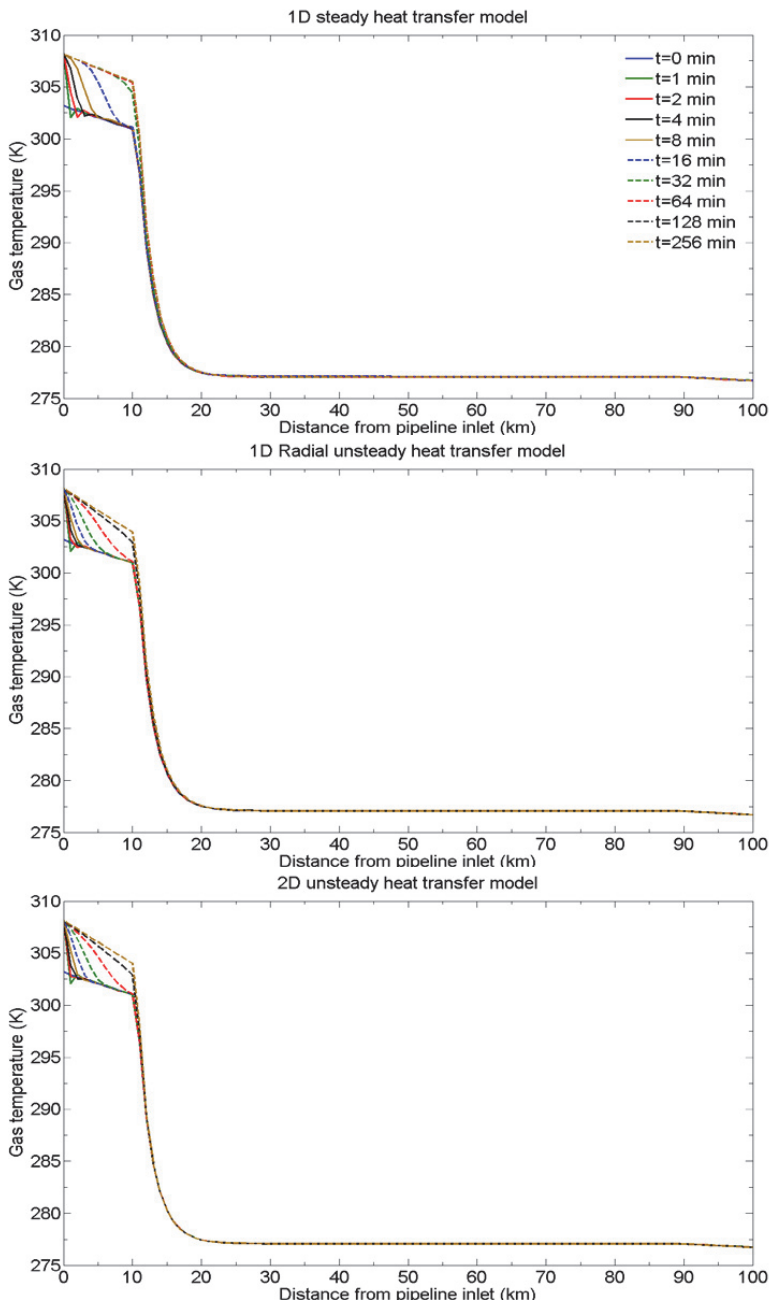


Figure 5.14: Temperature development in the first part of the pipeline in response to the temperature inlet transient, shown for each heat transfer models.

Results

In the first buried section, the time development of the pipeline temperature profiles is similar for both unsteady models. The pipeline temperature profile with the steady model is closer to the isothermal case shown in Figure 5.8, reaching the new steady state level much sooner. For the remainder of the pipeline route, the temperature response is almost identical for the three models. This can be attributed to the high heat transfer rate to the seawater and the absence of soil heat storage in the offshore section of the pipeline.

5.2.1.3 Effect of heat storage in the pipe wall

Figure 5.15 shows the contribution of the pipe steel wall to the damping of the gas temperature response for the mass rate transient (A). Compared is the gas temperature response of the 1D steady and 1D radial unsteady heat transfer models. In the first case, the 1D radial unsteady model has a significant thermal capacitance in both the pipe wall and the surrounding soil. In the second case, only the thermal capacitance in the steel wall is included; the surrounding soil is only allowed to conduct heat (thermal capacitance is set to one J/m^3K). The results show that the heat storage in the pipe wall accounts for approximately 20% of the difference in the peak gas temperature response between the steady and unsteady model.

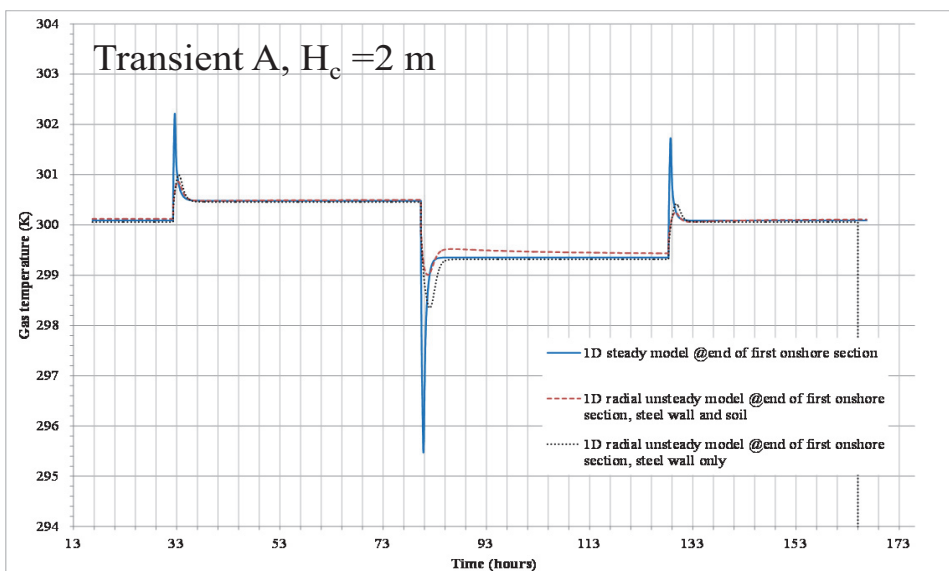


Figure 5.15: Effect of wall heat storage on the gas temperature response to the inlet mass rate transients (transient A).

Figure 5.16 shows the results for the same cases with the gas temperature transient (B). The results show that heat storage in the wall accounts for the first 2K of the gas temperature increase. Beyond this, the behavior of the 1D radial unsteady model is similar to that of the 1D steady model. Note that the heat transfer response with the 1D radial unsteady model has two stages. Initially the thermal energy of the hotter gas is

Results

stored in the pipe wall; due to the limited capacity of the wall, the gas temperature rises quickly along the pipeline route. The conduction and storage of heat through the soil layers occurs at a slower rate, but the soil has a larger thermal capacity. The pipe wall itself thus quickly heats up and assumes a new steady state temperature profile. Heat transfer is then restricted by the longer and slower heat transfer process of storing and conducting thermal energy outward into the soil domain. This will continue until a new thermal steady state is reached in the entire thermal domain of the external heat transfer model. The results show that including heat storage in the pipe wall is important for the prediction of the gas temperatures during transient flow. These results are very similar to those obtained by Nicholas [36].

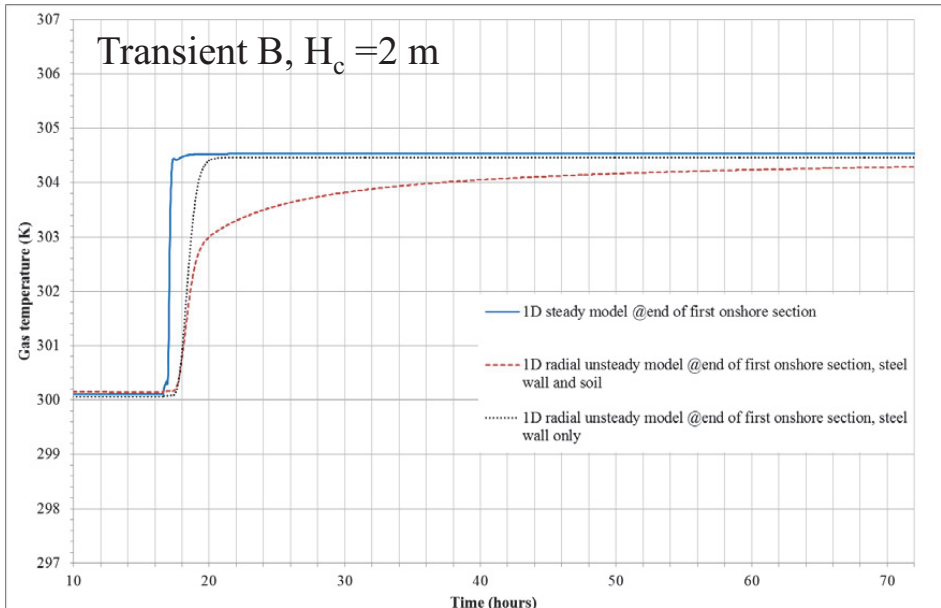


Figure 5.16: Effect of wall heat storage on the gas temperature response to the inlet temperature transient (transient B).

5.2.1.4 Effect of soil thermal properties

The same flow model was used to determine the effect of the soil thermal properties on the transient flow response. For both inlet transients, cases with decreased and increased thermal conductivity values were run. The resulting pressure and gas temperature responses, obtained with three external heat transfer models are shown in Appendix E.

In the first case, the thermal conductivity of the soil is reduced to one W/m²K, while thermal capacitance is kept the same; this effectively reduces the thermal diffusivity from 1.2×10^{-6} m²/s to 0.4×10^{-7} m²/s. The results show that the gas response in the pipeline is similar to the base case shown in Figure 5.9. Decreasing the thermal

Results

conductivity and thermal diffusivity does not alter the relative heat transfer response between the three models.

In the second case, the thermal conductivity is increased to six W/m²K. Keeping the same thermal capacitance gives a thermal diffusivity of $3 \times 6 \cdot 10^{-6}$ m²/s. The difference in response between the steady and unsteady heat transfer models remains qualitatively and quantitatively similar. There is a somewhat larger difference in response with the 1D unsteady radial compared to using the 2D unsteady model. This difference is still an order of magnitude smaller compared to the response with the 1D steady model. Increasing thermal conductivity to values above typical soil values (1-3 W/mK) results in a minor increase of the difference between the unsteady models. In case of pipelines installed in rock, this could be of significance.

5.2.1.5 Effect of burial depth

The effect of the burial depth was assessed for three cases. In the first two cases, the onshore parts of the pipeline are buried to a depth of one m and one cm respectively (from top of pipe to the soil surfaces). The third case is a partially buried pipe with the half of the pipe exposed to the air. Appendix E shows the resulting flow responses.

To make a useful comparison between the three heat transfer models, the steady state gas temperatures and heat transfer rates should be the same for all three models. To satisfy this for both the shallow burial and partially buried cases, the 2D model is run in steady state. The resulting inner pipe wall heat transfer rate is used to determine the overall heat transfer coefficient U . This value for U is used for the 1D steady model and to calculate the equivalent wall thickness of the 1D radial unsteady model, and is somewhat lower than that obtained with Equation (2.29). For the partial burial case, the overall heat transfer coefficient, determined with the 2D model is higher than those obtained with the correlations provided in Morud and Simonsen [30], indicating that the steady state heat transfer is dominated by the heat transfer of the exposed part of the pipe to the air ($h_{air}=50$ W/m²K). The cases are summarized in Table 6.

Table 6: Data from burial cases

Burial Case	Burial depth H	U from 2D model	Equivalent Soil layer thickness
Base case	2 m	2.9 W/mK	4.20 m
1	1 m	4.2 W/mK	2.23 m
2	0.565 m	11.2 W/mK	0.93 m
3	-0.555	18.1 W/mK	0.12 m

For burial case 1, the differences in gas temperature and pressure response obtained with the three external heat transfer models are similar to the base case. This is true for both transients. Some differences in the gas temperature response are apparent for the shallow burial case (case 2). Apart from a large difference between the steady and unsteady models, a minor difference in the gas temperature response to the inlet mass

Results

rate transient is now visible between the 1D radial unsteady and 2D unsteady heat transfer model.

Figure 5.17 shows the response to the mass rate transient (A) for the partial buried case. There is still a significant difference in gas temperature response between the steady and unsteady models, but now there is also a significant discrepancy between the 1D radial unsteady and 2D unsteady model. With the 2D unsteady model, the pipeline temperature profile takes a longer time to reach new steady state levels. The main reason is that the mass of the effective thermal domain of the 1D radial unsteady model is much smaller than that of the 2D model, even when the thermal conduction path has the same length. The differences in gas temperature at the end of the first section between the steady and unsteady models are smaller compared to the base case. As expected, heat storage thus plays a smaller role in the partial buried case.

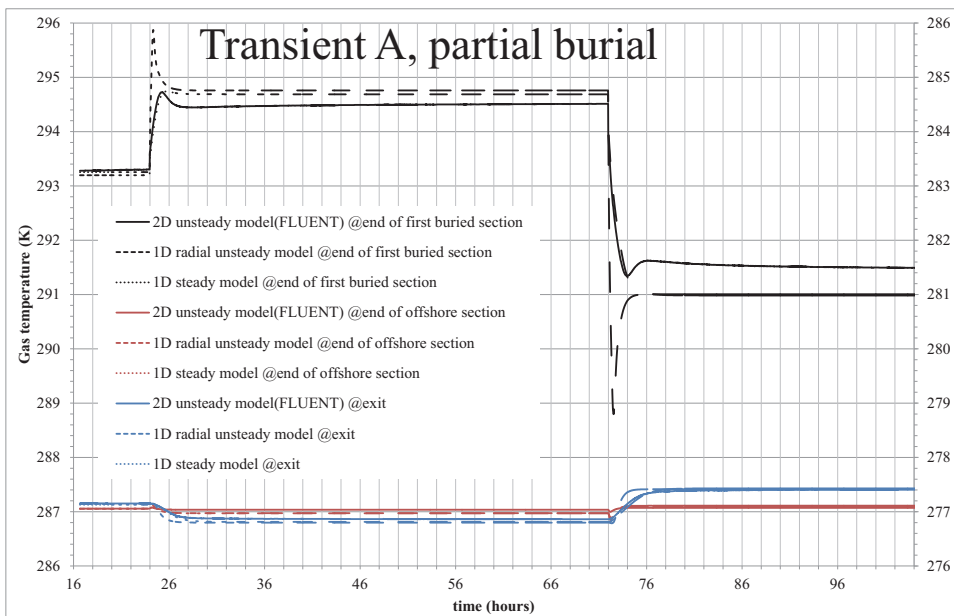


Figure 5.17: Partial burial case: Gas temperatures in response to the inlet mass rate transient are shown at different locations along the pipeline route.

In Figure 5.18 the results with the gas temperature transient (B) are shown.

The gas temperature response for the inlet temperature transient is, as with the other cases, almost similar for the two unsteady models, compared to the faster response of the 1D steady model. The 2D unsteady model takes longer time to obtain a new thermal steady state as it has a larger thermal domain compared to the 1D radial unsteady model. Again, the differences in gas temperature at the end of the first section between the steady and unsteady models are smaller compared to the base case. Also for the inlet temperature transient, heat storage plays a smaller role in the partial buried case.

Results

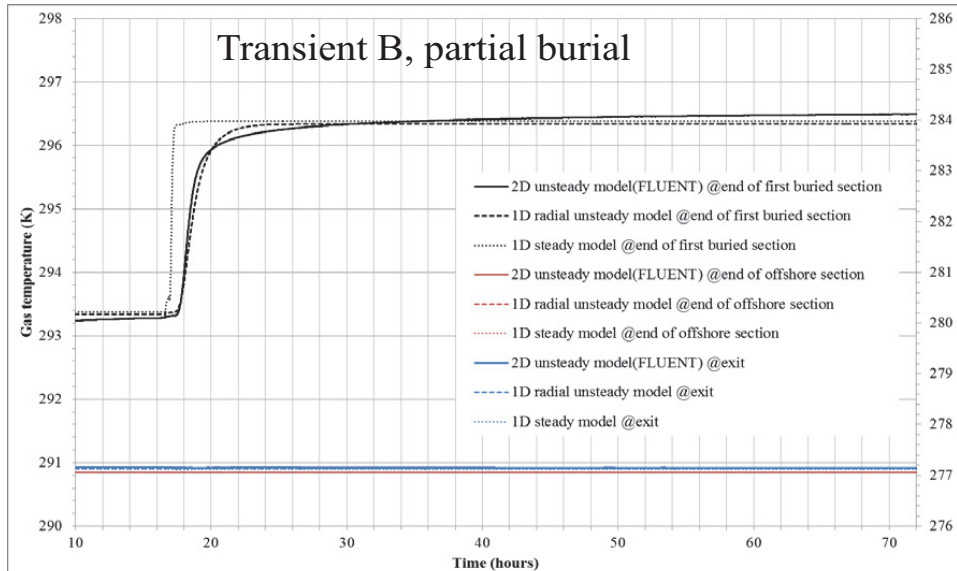


Figure 5.18: Partial burial case. Gas temperatures in response to the inlet temperature transient are shown at different locations along the pipeline route.

5.2.1.6 Effect of ramp time of the transient

The transients described in Chapter 4.1.1 have a one-minute ramp time and can be considered worst case (expected to give the largest gas response). As discussed in Chapter 5.1, the real life ramp times for changes in both mass rate and temperature are often longer. The effect of the ramp time on the flow response was studied for both inlet mass rate and temperature transients. For the inlet mass rate transient, the inlet mass rate follows steady state conditions at a mass flow rate of 600 kg/s and is then dropped to a new steady state of 300 kg/s. The inlet temperature transient is a drop in inlet gas temperature from 303.15 K down to 298.15. For each transient, four different cases of ramp-down duration are compared: 1, 10, 60, and 360 minute, as shown in Figure 5.19.

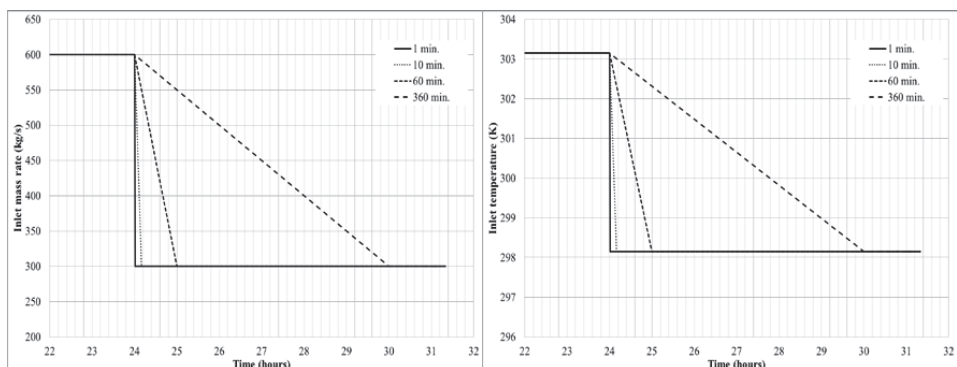


Figure 5.19: Inlet transients used in the study of the effect of ramp time.

Results

The resulting gas temperature responses for each of the transient cases are shown in Appendix E. For the inlet mass flow rate transient these results show that with increasing ramp time, the difference in gas temperature response between the steady and unsteady models diminishes. The small difference in gas temperature response between the 1D radial unsteady and 2D unsteady models does not show a distinct sensitivity for ramp time. For the inlet temperature transient, both unsteady models result in a similar gas temperature response for all four ramp down times. With increasing ramp time, the gas temperature development with the 1D steady model is still different compared to the two unsteady models. The results show that sensitivity for the ramp time of the temperature transient on time scales of less than one hour is not large. The results also show that only at the first location the gas temperature is sensitive to both the choice of heat transfer model and the ramp down time of the inlet transients.

These results can be explained from the heat stored in the pipe wall and surrounding soil delaying the drop in gas temperature for quite some time after the colder gas starts arriving at the end of the first buried section. Only increasing the ramp time to several hours changes the gas temperature development with the 1D steady model significantly, and brings it closer to that obtained with the two unsteady models. The temperature development is approximately similar for both unsteady heat transfer models. It is further worth noting that increase of the ramp time changes the gas temperature development only to a minor extent for the unsteady models.

Figure 5.20 and Figure 5.21 show the effect of inlet transient ramp time on the gas temperature *difference* between the 1 D steady and 2D unsteady model at the end of the first buried part of the pipeline.

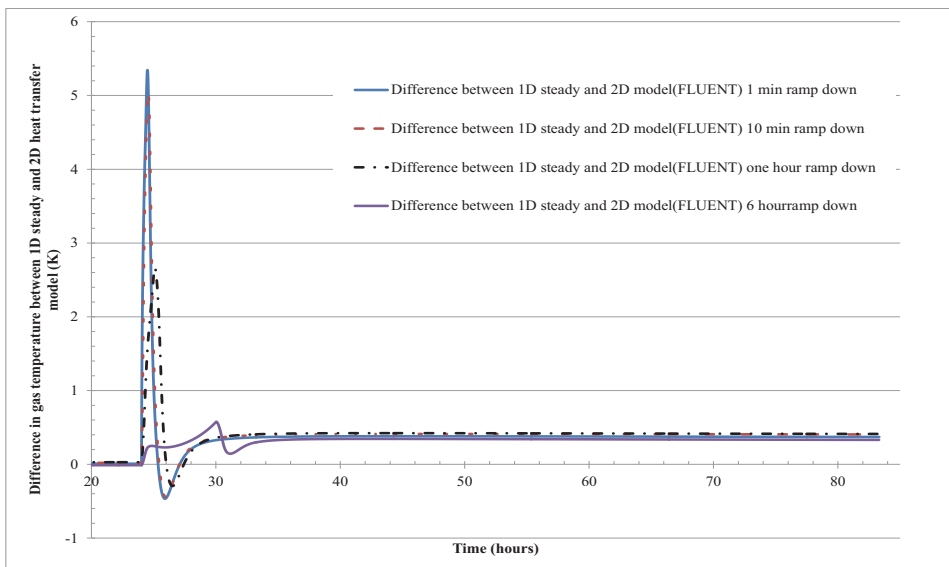


Figure 5.20: Gas temperature response to inlet mass rate transient. Shown is the relative difference between 1D steady and 2D unsteady model at the end of the first onshore location.

Results

For both the mass rate and the temperature transient, the increase in ramp time from one to ten minutes does not reduce this difference noticeably. Increasing the ramp time to one and six hours reduces the maximum difference from 4.6 K to 3.7 K and 1.7 K respectively.

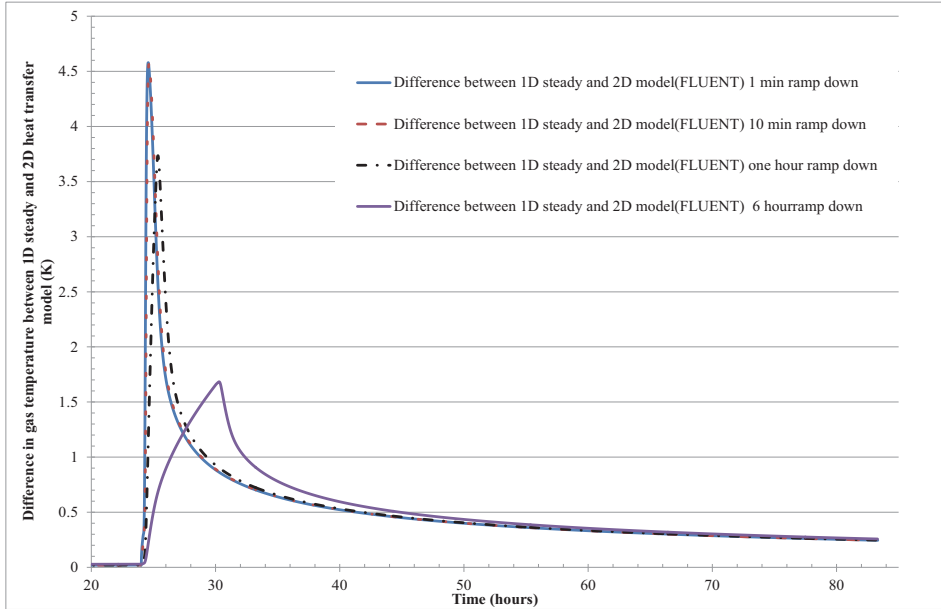


Figure 5.21: Gas temperature response to inlet temperature transient. The relative difference between 1D steady and 2D unsteady model at the end of the first onshore location is shown.

5.2.1.7 ‘Saw tooth’ inlet mass flow rate transient

Figure 5.22 shows the gas response to a ‘saw tooth shape’ inlet mass flow rate transient, comparable to those shown in Figure 5.4. The ‘saw tooth’ consists of a drop from 600 kg/s to 300 kg/s over a one hour period, followed by a two hour long steady rise to a new constant level of 500 kg/s. Again, the gas temperature response with the 1D steady model is different (by up to 2.6 K) from that obtained with both unsteady external heat transfer models, showing the characteristic large undershoot and over shoot in gas temperature in response to a rise or fall in mass flow rate.

Both unsteady models lead to a similar gas temperature response to the mass flow rate transient, but the 2D unsteady model gives a larger overshoot (by 0.3 K) when the flow rate levels off to the new steady state level. Also with the ‘saw tooth’ mass flow rate transient, the differences between the pressure profiles obtained with the different models are negligible.

Results

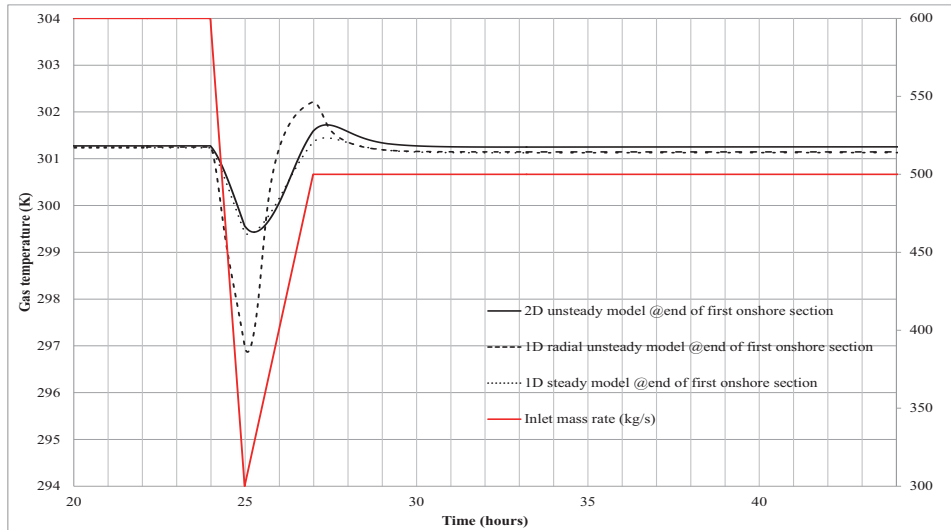


Figure 5.22: Temperature response at end of first onshore section in response to 'saw tooth shape' inlet mass transient.

5.2.1.8 Fourier number and transient time scale

In transient heat conduction, the dimensionless Fourier number is often used to compare thermal system behaviour. An explanation for the differences in gas temperature response between the 1D steady and the 1D radial unsteady model, using the Fourier number is provided prior by the author in Helgaker et al [77]. With higher Fourier numbers, heat conduction dominates the heat transfer response to a thermal change at the boundary. At low Fourier numbers (<1), heat storage dominates, explaining the difference in heat transfer response to a sudden gas temperature change. In the unsteady model, heat storage will dictate the heat transfer rate, while in the steady model the heat transfer rate will remain proportional to the product of the temperature difference ($T_{gas} - T_{amb}$) and the overall heat transfer coefficient U .

For the case shown in Helgaker et al [77], the Fourier number is 0.1 for an inlet mass rate transient of 50 hours duration. For transients of shorter duration, the Fourier number will be even smaller.

For the cases studied here, with the transients occurring within one minute, the Fourier numbers are shown in Table 7. The length L_e has been defined as the distance from the pipe wall to the soil ambient boundary when transforming the 2 D system of a buried pipe into a bipolar cylindrical coordinate system. This transformation is in detail described in (C.Ovworrie [29]). The expression obtained for the conduction length is $L_e = \cosh^{-1}(\sigma)$. The equivalent length L_e for the pipe wall is chosen to be the wall thickness. The Fourier number of the pipe wall is below one, thus heat storage in the steel wall plays also role (as the results from Chapter 5.2.1.2 show), even though the thermal conductivity is relatively high.

Results

Table 7: Fourier numbers for cases ($\tau = 60$ seconds)

Case	r_i (m)	r_o (m)	Fo pipe	$\sigma=H/r_o$ soil	L_e soil (m)	Fo soil
$H=2$ m	0.508	0.552	0.4	3.58	1.95	$1.9*10^{-5}$
$H=1$ m	0.508	0.552	0.4	1.79	1.18	$5.2*10^{-5}$
$H=0.01$ m	0.508	0.552	0.4	0.02	0.2	$1.8*10^{-3}$

For the soil, in all burial cases, the Fourier number is much lower than one, and even a one cm thin layer soil of has a Fourier number smaller than one in response to the step change in flow boundary conditions. This a result of the combination of high thermal diffusivity and heat capacity of the pipe wall combined with the low thermal diffusivity of the soil. In case of rapid fluctuations in the gas temperature, the gas to ambient heat transfer is mainly governed by the flow of thermal energy through the pipe wall and the heat storage in the pipe wall and a surrounding thin soil layer. These are the main reasons that the 1D radial unsteady model shows such similarity in behaviour to the 2D unsteady model. With heat transfer response to a transient dominated by heat storage in the pipe wall and small layer of surrounding soil, the geometry of the part of the 2D domain active in the initial heat transfer response is essentially cylindrical.

Considering the time scale of the slower transients of Chapter 5.2.1.5, even a six hours ramp time will still result in soil Fo numbers smaller than one. The time needed to achieve steady state over the distance L_e in the soil after a temperature change at the boundary of the system is approximately l_e^2/α . For the case, with $\tau=60$ s, the conductive length $l_e < 8$ mm to reach the new steady state with 60 s, and $l_e < 16$ cm for $\tau=6$ hr. Over the entire domain, the time to the new steady state is exceeding 740 hours for the deepest burial case ($H=2$) and still 7.4 hours for the shallow burial case.

The implication of this is that for a thermal transient in the pipe flow, with a thermal time scale of the ambient in hours or even days, soil heat transfer cannot be represented accurately with a steady state conduction model. Even the case where the surface of the pipe is almost exposed and with a value of σ being very close to one, it takes several hours before a new steady thermal state in the soil is fully reached. Thus, for flow transients resulting in gas temperature fluctuations with a short time characteristic time, it is only the steel pipe wall, the outer pipe wall layers and the soil close to the pipe outer wall that play a role in the initial response to a flow transient.

The time to steady state of the pipe wall (44 mm) in this case is 161 s. In response to a temperature change of the gas, the pipe wall will quickly be able to conduct the thermal energy through it compared to the soil (thermal diffusivity is an order of magnitude higher). In addition, the heat storage term of steel is 3/2 times that of the soil. The initial response on a transient is therefore governed by the pipe wall thermal properties. At the measurement site, the logging interval is 5 minutes. With a time to steady state of ≈ 2.5 min it is therefore reasonable to assume that the pipe wall is predominantly subject to steady state conduction within the duration of the measurement interval.

Results

5.2.2 Influence of the annual ambient temperature cycle

The soil surface temperature has a distinct cycle on an annual timescale. This boundary condition can be approximated as a sinusoidal surface temperature variation with a one year period, as discussed in for example Williams and Smith [24]. The problem of one-dimensional heat conduction in an infinite medium with a sinusoidal temperature variation as boundary condition has a classical, exact, solution (Equation (3.6)). This is shown in for example Williams and Smith [24] and Carslaw and Jaeger [55]. The solution implies an attenuation and phase lag of the surface temperature cycle deeper into the soil. The extent of both the attenuation and phase lag increases with depth, and is a function of both thermal diffusivity and period length. The steady periodic solution provided in Barletta et al.[43] (Equation (2.32)) shows that the pipeline heat transfer has a similar response, demonstrating a phase shift and amplitude attenuation of the pipe inner wall heat transfer rates. The ability of the external heat transfer models to predict these effects was studied. The aim was to understand the effect on the inner wall heat transfer rate and resulting gas temperatures. The underlying assumption is that the 2D unsteady model (FLUENT) can accurately reproduce the two dimensional temperature profiles in the soil under transient conditions and accordingly provide the most accurate inner wall heat transfer rate. The performance of three other models, 1D steady, 1D radial unsteady and Barletta's model are evaluated against the 2D unsteady model. The result of the investigations are shown in detail in Oosterkamp [78]. The results show that the Barletta model provides heat transfer rates very close to those obtained with the 2D unsteady model. The steady state heat transfer model does not account for the effect of amplitude attenuation and phase shift of the annual ambient temperature cycle, and the deviations in the heat transfer rates are the highest with this model. When using the 1D radial unsteady model, the time dependent two-dimensional temperature profile is not reproduced. When dimensioning the soil domain to obtain similar steady state heat transfer rates, the cyclic heat transfer rates are also not accurately reproduced. The phase shift, average level, and amplitude are different from the 2D case, as seen in the example of Figure 5.23. For the 1D radial unsteady heat transfer model, several concepts to dimension the domain extent were evaluated. Ideally, the model should reproduce the level of the heat transfer values as well as the fluctuations due to the gas transients and the annual ambient temperature cycle. The derivation of Barletta [43] demonstrates that for a situation with a constant gas temperature, it is possible to express the steady state overall heat transfer coefficient as a time varying function of the dimensional burial depth and the average difference between the gas and ambient temperature. The fact that the time varying heat transfer coefficient U is also a function of this temperature difference provides us with a challenge to dimension the domain of the 1D radial unsteady model to provide the correct heat transfer behavior in response to the annual ambient temperature cycle. The radial unsteady model can be set up to give the same steady state behavior as the 2D unsteady model when the soil domain is dimensioned according to Equation (2.29). Effectively the steady state shape factors of both the 1D radial and a buried pipe in 2D are equalized in Equation (2.29) by adjusting the radius of the 1D radial model. The steady state heat transfer of both models is the same, but not the unsteady heat transfer response to ambient temperature. The 1D radial unsteady model can be manipulated to some extent to give the same heat transfer response to the ambient temperature as the 2D unsteady model. One can adjust the

Results

equivalent soil radius in order to obtain the correct phase shift in heat transfer response. Thermal conductivity and capacitance can subsequently be changed to match the average heat transfer rate, while keeping the same thermal diffusivity. Unfortunately, such a tuning only works for a specific set of temperature conditions; as soon as the gas temperature, mean ambient temperature, or amplitude of the ambient temperature is changed, the model will show different heat transfer behavior compared to the 2D unsteady model (Oosterkamp [78]).

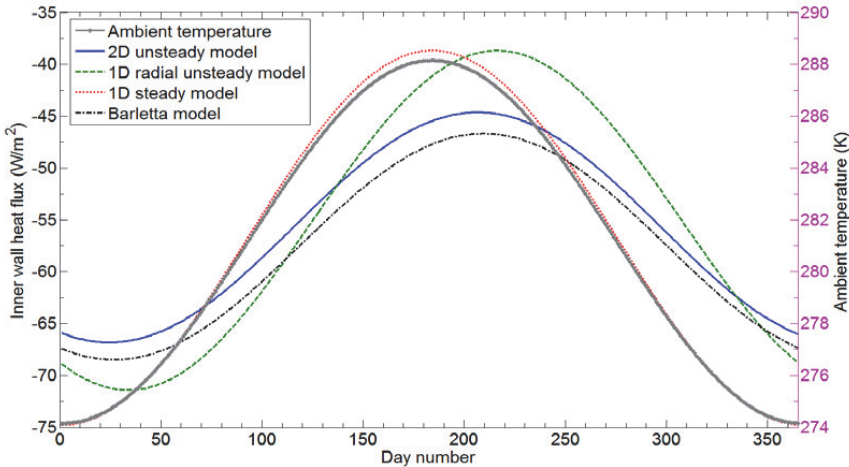


Figure 5.23: Pipe wall heat transfer in response to ambient temperature cycle for a pipeline with diameter 1.0 m and 2.5 m burial depth (Oosterkamp [78]).

In Oosterkamp [78], the results of a parameter sensitivity study are presented. The results show that for the range of governing parameters of the heat transfer model (pipeline diameter, burial depth, temperature difference between gas and ambient, soil thermal conductivity and diffusivity, amplitude of the annual temperature cycle); the resulting maximum error is the largest with the 1D steady model, followed by the 1D radial unsteady model. For almost all the cases, the heat transfer obtained with the Barletta model is almost similar to that with the 2D unsteady model. Of the parameters considered, reducing pipe diameter, increasing thermal conductivity and increasing the amplitude of the ambient temperature cycle result in the largest increase of the heat transfer error compared to the base case. Figure 5.24 shows the effect of the parameter change in terms of the change in maximum heat transfer deviation in relation to that of the 2D unsteady model. This is shown for each of the other three external heat transfer models. The base case is a pipeline with a diameter of 1.0 m buried at 2.5 m depth. Soil thermal conductivity is three W/mK and the thermal capacitance is 2×10^6 J/Km³. The gas temperature is 303.15 K and the soil surface temperature cycle has a mean temperature of 281.15 K and 7 K amplitude. The inner wall heat flux is expressed as Watt per cubic meter gas inventory per meter length of the pipe. This makes it easier to assess the effect on the gas temperature. The gas heat capacity and density are a function of pressure and temperature, but if the pressure and temperature do not vary much along a pipeline, a good correlation with the additional heating/cooling of the gas due to the heat flux deviation can be expected. The Barletta external heat transfer model

Results

results for most cases in heat transfer rates close to those obtained with the 2D unsteady model. The phase delay in the pipe wall heat transfer is correctly predicted and the heat transfer error is mostly between 1-10 W/m, except for the reduced thermal conductivity case and the shallow burial case. The heat transfer errors are the largest when using the 1D steady model. The errors with the 1D radial unsteady model are $\frac{1}{4}$ - $\frac{1}{3}$ smaller.

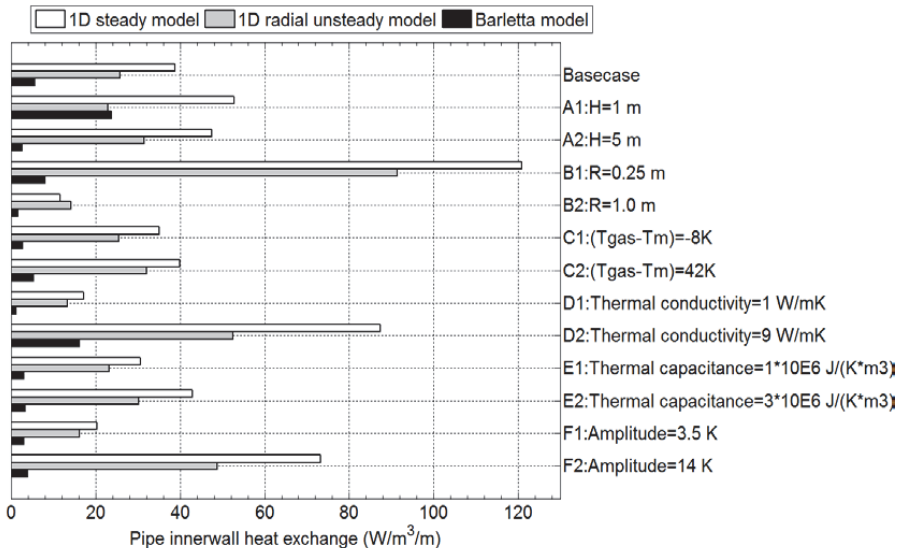


Figure 5.24: Effect of parameter variation on heat flux error.

5.2.2.1 Effect on gas temperature and pressure

Two cases using the generic pipeline were run to understand the effect of the choice of heat transfer model on the gas temperatures due to the annual ambient cycle. The first case is representative for an export gas pipeline. The pipeline has a diameter of 1.0 m buried at 2.5 m depth. Soil thermal conductivity is three W/mK, and the thermal capacitance is 2×10^6 J/Km³. The ambient temperature cycle has a mean temperature of 281.15 K and 7 K amplitude. The seawater temperature is kept constant at 277.15 K. In the second case, the pipeline diameter is reduced to 0.5 m, thermal conductivity increased to 6 W/mK and the amplitude of the annual temperature cycle is 14 K. The gas outlet pressure is 90 MPa, the gas inlet temperature is 303.15 K, and the gas inlet mass rate is 400 kg/s (100 kg/s for the second case). For the first case, the resulting gas temperatures at three locations along the pipeline route are shown in Figure 5.25. The results show small differences in the gas temperatures at both the end of the initial and final buried sections; the results with both the 1D steady model and 1D radial unsteady model deviate up to 0.25 K from the results obtained with the 2D unsteady model. At the end of the offshore section, the gas temperatures are fully dominated by the heat exchange with the constant temperature seawater. The differences between the models here are insignificant. At the pipeline exit, the temperature development with the three models shows the same development and differences as in the first onshore part.

Results

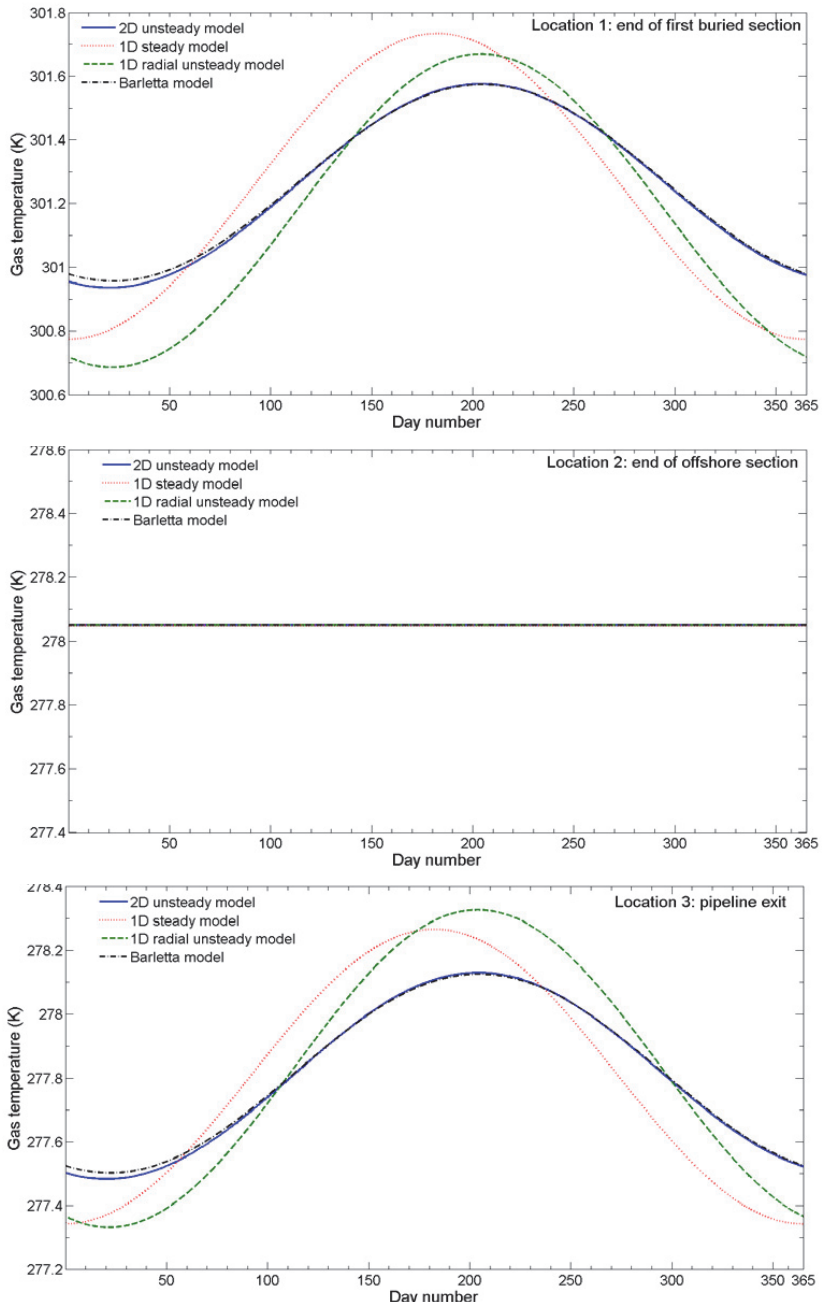


Figure 5.25: Effect of heat transfer model on gas temperatures with annual ambient air temperature cycle and constant seawater temperature. Gas temperatures obtained with the 2D unsteady, 1D radial unsteady, 1D steady and Barletta model are compared.

Results

The results of the second case, shown in Oosterkamp [78], display significantly larger gas temperature differences between the models. For the 1D radial unsteady model, the temperature difference at the end of both buried pipeline sections is maximum 1.2 K. The differences in inlet pressure is small for both cases (<0.1 bar), as shown in Oosterkamp [78]. It should be noted that for the cases presented here the length of the buried section is only 10 km. For some pipelines, the length of the buried sections can be significantly longer. This will give a corresponding increase in the gas temperature errors due to the incorrect heat transfer response to the ambient temperature cycle with use of the 1D steady or 1D radial unsteady models.

5.3 Soil properties and boundary conditions of the verification models

Accurate estimation of the soil intrinsic permeability, soil thermal properties and boundary conditions (inner film coefficient, gas temperature, ambient temperatures) were needed to obtain reliable results from the verification models

5.3.1 Soil grain size distribution and intrinsic permeability estimation

The standard sieve test (ASTM[57]) was used to investigate samples of the filling sand and clay for grain size distribution. These tests were conducted at the Norwegian Geotechnical Institute. Figure 5.26 on the next page shows the resulting grain size distributions. For the clay sample, the mud percentage (percentage of grains smaller than 0.075 mm) is 35%. This is a high mud content; therefore, the soil is in this context considered impervious for ground water movement. Resulting sand grains sizes are:

d_{10}	d_{16}	d_{25}	$d_{50}=d_m$	d_{60}	d_{75}	d_{84}
0.16 mm	0.22 mm	0.32 mm	0.66 mm	0.85 mm	1.44 mm	1.94 mm

The sorting $S_o=[d_{25}/d_{75}]^{1/2} =0.47$, which means that the sample is well sorted. The skewness, $S_k=[d_{25}\cdot d_{75}/d_{50}]^{1/2}=0.84$. The majority of the grains are in the medium range. The mud percentage (percentage of grains smaller than 0.075 mm) was measured to 2%. The sample contains grains in the range from very fine sand to fine gravel on the ISO 14688-1 scale. Using Equation (3.10) the total geometrical particle diameter d_{ing} is calculated to 0.25 mm. The porosity ϕ is calculated from the volume of water added to achieve saturation, resulting in $\phi=0.35$. Assuming $\phi_e=\phi=0.35$, the intrinsic permeability is calculated with Equation (3.9) to be $0.35\cdot 10^{-10} \text{ m}^2$. When using the arithmetic of mean grains sizes ($D_a=0.4 \text{ mm}$) the intrinsic permeability becomes $0.9\cdot 10^{-10} \text{ m}^2$. When using the mean grain size d_{50} , the intrinsic permeability is $2.46\cdot 10^{-10} \text{ m}^2$. There is thus quite a span in the obtained permeability values, depending on choice of representative grain size. A final note on the choice of the effective porosity ϕ_e : in Urmović [60] results for calculated effective porosity of sand as function of D_{ing} are provided. For the uniformity $d_{60}/d_{10}=5.34$, the effective porosity is expected to be between 0.32-0.34. This potentially reduces the intrinsic permeability by 25%.

Results

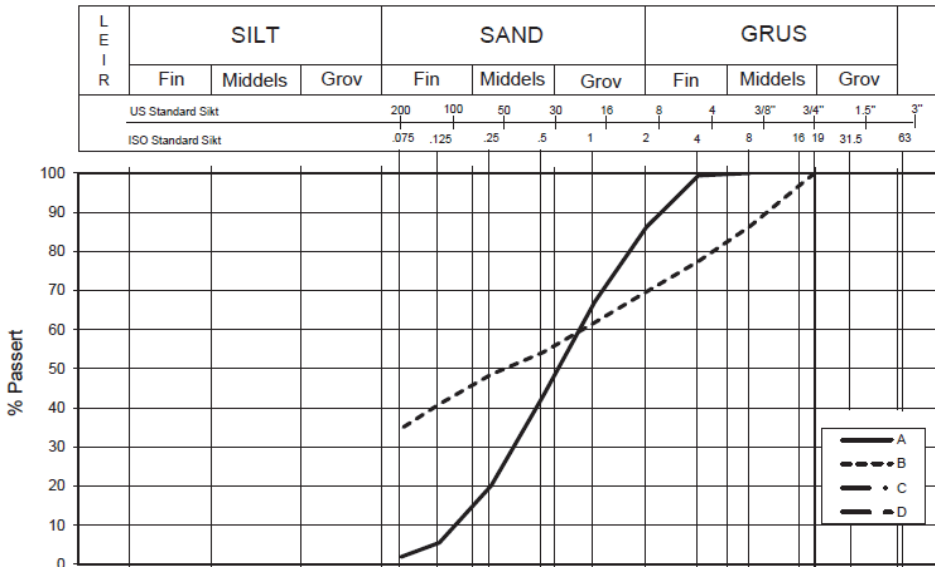


Figure 5.26: Grain size distribution of clay (dotted line) and sand (continuous line) (Oosterkamp [45]).

5.3.2 Measurements of the thermal properties of the soil

The soil thermal properties were evaluated with different methods. These included measurements on the soil samples, application of the De Vries model, through the temporal development of the ambient temperature cycle in the soil, and through predictive numerical modelling. The first three methods have also been reported in (Oosterkamp [45]) and are reproduced here partly in verbatim.

5.3.2.1 Thermal needle probe measurements and De Vries model

The following soil samples were collected during installation:

- 1- Samples from the filler sand in the pipeline installation ditch.
- 2- Samples of clay excavated with digger and drilling rig.
- 3- Samples of the top soil.

For the De Vries model, the bulk thermal properties of soil constituent of Chapter 3.3 are used. The thermal needle probe technique was used to measure the thermal properties of the soil samples (top soil, sand, and clay) at different water content using the thermal needle probe technique as described in Chapter 3.3. The instrument has a specified accuracy of $\pm 5\%$ to $\pm 10\%$ for thermal conductivity, $\pm 10\%$ for specific heat, and $\pm 10\%$ for thermal diffusivity (Decagon [53]). A total of 500 ml of the dry soil sample was compacted and weighed to determine the dry density. Thermal

Results

measurements were conducted with the Decagon KD2 pro with SH-1 dual probe thermal needle at incremental water content levels. At each water content level, minimum three parallels were conducted. The probe was repositioned in the sample for each measurement. The default instrument settings were used (Decagon Devices [53]). The measurements give values of thermal conductivity, thermal diffusivity, and volumetric heat capacity. The resulting values for thermal conductivity and diffusivity are shown in Figure 5.27. In the figure, the calculated measurement errors have been included as error bars.

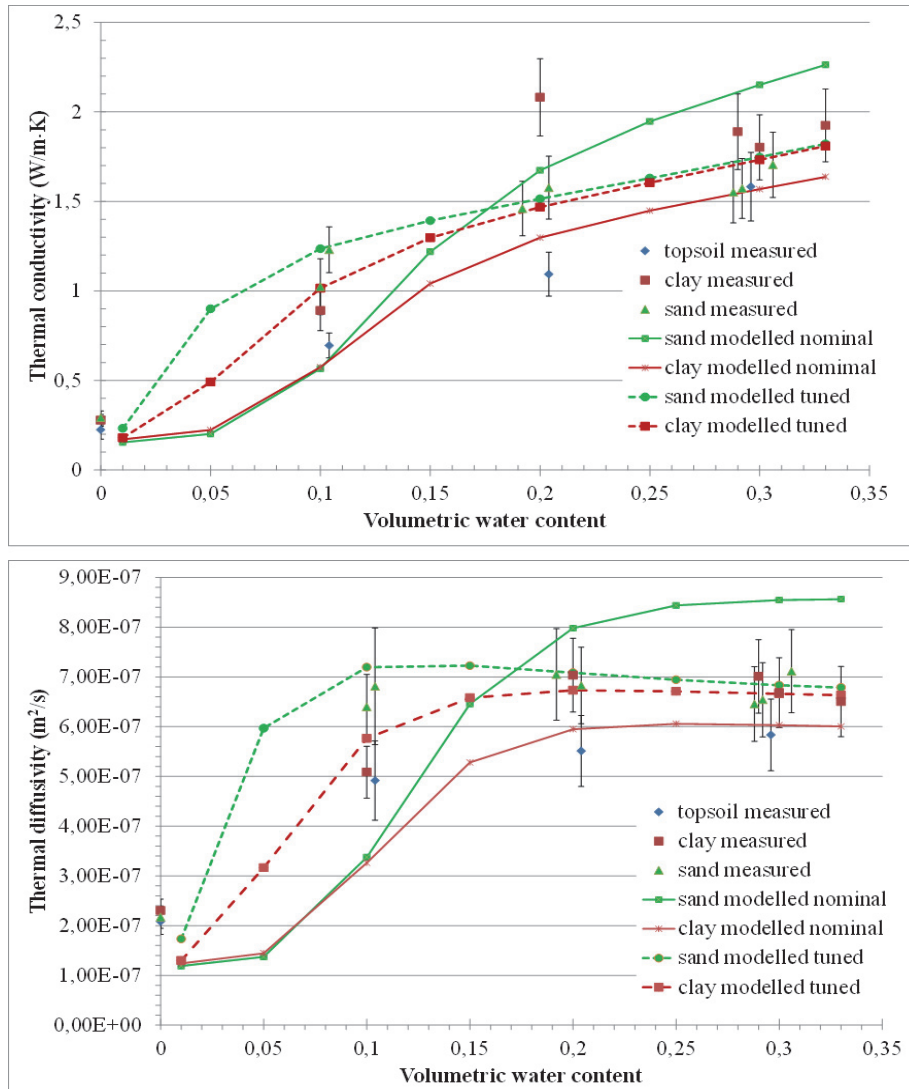


Figure 5.27: Measured and modelled (De Vries) thermal conductivity (above) and thermal diffusivity (below) values of soil samples (Oosterkamp [45]).

Results

The measurements were tested with the modified Thompson technique in order to identify and reject outlier measurements. The measurement errors were evaluated as follows: the systematic uncertainty B_x of the measurement is $\pm 10\%$. The random uncertainty is calculated by using the sample standard deviation of each parallel after rejection of all the outliers. A 95% confidence interval is chosen. The random uncertainty is defined similar as in Chapter 3.6.1 as $P_x=tS_x/\sqrt{M}$. Where t is the student distribution and S_x is the sample standard deviation. The total measurement error is evaluated as $w_x=\sqrt{(B_x^2+S_x^2)}$

The modelled soil properties are shown with nominal cut-off value $\phi_{wc} = 0.15$ and smoothing factor $s=4$. For both the clay and sand, this does not give a satisfactory match between the measured and modelled values. Therefore, for both soils, the nominal cut-off value and smoothing factor are tuned until the shape of the curves matches the thermal conductivity and diffusivity measurements. For both soils, the thermal conductivity and diffusivity values become too large. A match was obtained by reducing the bulk thermal conductivity of the sand and clay constituent. For the sand soil, a good match between modelled and measured properties as function of volumetric water contents is achieved using $\lambda_{sand}=4$ W/mK, $\phi_{wc} = 0.05$ and $s=2$. For the clay, the values are $\lambda_{clay}=3.5$ W/mK, $\phi_{wc} = 0.1$ and $s=2.5$.

5.3.2.2 Derivation using the surface soil temperature cycle

Chapter 3.3.3 describes how to use the development of the annual temperature cycle into the soil to estimate thermal diffusivity. The underlying assumptions are that 1D heat conduction is the prevailing mode of heat transfer and that the annual soil surface temperature cycle is a sine function of time. This assumption is reasonable for the clay soil measurements at 10 m lateral distance from the pipe wall. The intrinsic permeability of the clay soil is very low, and convection heat transfer is negligible. The distance to the pipeline is expected to be sufficiently far for its thermal influence to be minimal. For each pair of soil temperature profiles, the calculated values of the thermal diffusivity α are shown in Table 8 (using Equation (3.7) and Equation (3.8)).

Table 8: calculated values for thermal diffusivity and standard deviation std(X).

Pairs (depth in m)	α (10^{-6} m ² /s) amplitude attenuation	α (10^{-6} m ² /s) phase shift
0.84-2.34	0.83, std(X)=0.4	1.35, std(X)=0.5
0.84-3.34	0.93, std(X)=0.34	1.10, std(X)=0.24
0.84-5.34	0.85	1.09, std(X)=0.16
2.34-3.34	1.22, std(X)=0.18	1.16, std(X)=0.5
2.34-5.34	0.83	1.08, std(X)=0.15
3.34-5.34	0.81, std(X)=0.11	1.30, std(X)=0.47

There is a relatively large spread in the results between the different pairs and the two methods. The values derived with Equation (3.8), based on the phase shift, are larger than those with Equation (3.7), based on the amplitude attenuation.

Results

5.3.3 Thermal properties measurement at the experimental site

The soil thermal conductivity and thermal diffusivity at the measurement site were measured on a continuous basis. Two TP01 thermal property sensors took measurements at six-hour intervals. The sensor locations are shown in Figure 3.5. One sensor is located in the clay at 3.7 m depth, three meters from the pipe outer wall. The other location is in the sand, one meter from the pipe wall at 2.3 m depth. Figure 5.28 shows the measured thermal conductivity and thermal diffusivity in the clay.

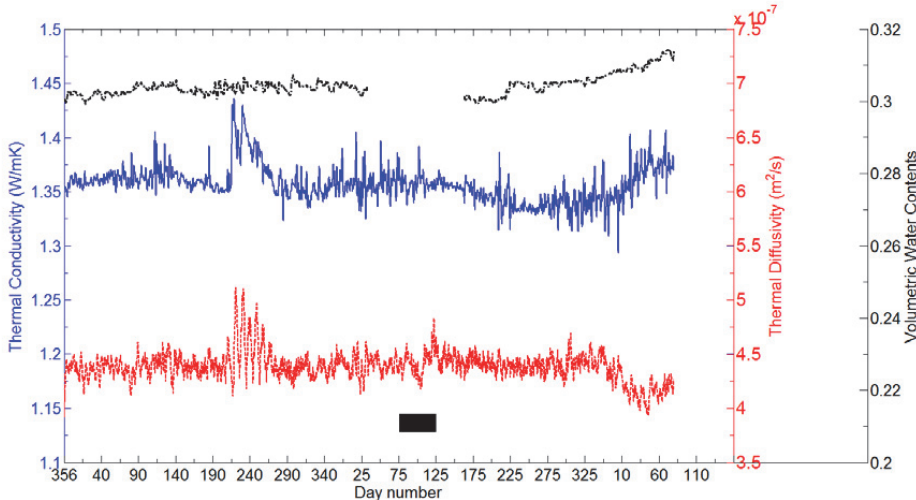


Figure 5.28: Thermal properties and soil humidity measured at the experimental site. The location is 3.7 m depth in the clay, at three meter lateral distance from the pipe. The blue line shows the thermal conductivity, the red line shows thermal diffusivity, the black line soil moisture content (the 21th of December 2012 until the 31st of March 2015).

Notice that the thermal properties are 20-25% lower than those measured on the soil samples and are closer to the modelled values. The differences can partly be attributed to the experimental uncertainty of each method (at least 10%) and differences in soil composition.

The thermal properties show a small variation in time: thermal conductivity varies by ± 0.05 W/m²K while thermal diffusivity varies by $\pm 1 \cdot 10^{-7}$ m²/s. The soil moisture measurement at the same location shows a clear correlation to the thermal properties. Increasing water content increases thermal conductivity and decreases thermal diffusivity.

Figure 5.29 shows the thermal conductivity and thermal diffusivity in the sand at the left hand side of the pipe. In this case, the onsite measured thermal conductivity is in good agreement with the soil sample measurements, while the thermal diffusivity values are 20% lower.

Results

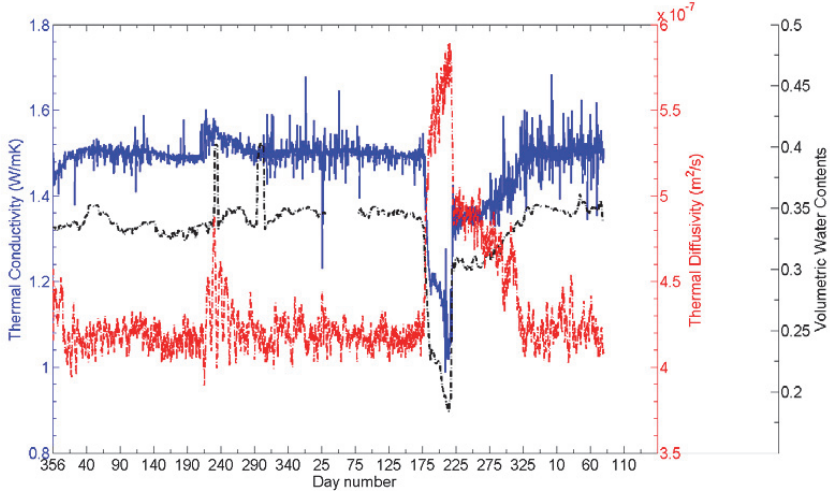


Figure 5.29: Thermal properties and soil humidity measured at the experimental site. The blue line shows the thermal conductivity, the red line shows thermal diffusivity, the black line soil moisture content. Measurements in the sand, at one meter lateral distance from the pipe (the 21th of December 2012 until the 31st of March 2015).

Notice that the thermal properties vary much more over time compared to the measurements in the clay; during the summer months of 2014, from the 21st of June (day 172) to the 6th of August (day 218), there is a drop in thermal conductivity and increase in thermal diffusivity. This coincides with a drop in soil humidity. This behaviour correlates well with the results of the soil sample measurements. The precipitation data available from the e-Klima database (e-Klima [79]) for the nearest weather stations (Kvitøy and Hydro Karmøy) do not show a particularly dry period. The air temperatures during June and July are higher. On June 6th (day 157), the field was mowed. A possibility is thus that the sand has dried out during this period and is regaining moisture during the following period with increased precipitation from day 187 onward.

5.3.4 Lower boundary condition

Prior to installation of the measurement equipment, the assumption, based upon calculation of the steady state soil isotherms, is that the warmer pipe does not significantly influence the soil temperature profile at 10 m lateral distance. The development of the temperature profile into the soil at this location can therefore be used to determine the thermal boundary condition at the lower edge of the models. The temperature profiles in the soil can be approximated as sine functions with a one year period (Williams and Smith [24]). The statistical mean of the measurements at different depths over periods exceeding one year (one yearly temperature cycle) are used to obtain a ‘quasi steady state’ soil temperature profile. The collected measurement data of

Results

M_{10_001} , M_{10_005} , M_{10_025} , M_{10_084} , M_{10_234} , M_{10_334} and M_{10_543} (see Figure 3.5) for the period 16th of May 2013 until 3rd September 2014 are used. For each measurement series, the statistical mean is calculated and plotted against the depth below the soil surface, as shown in Figure 5.30. The resulting trend of the mean soil temperatures versus depth is a gradual reduction to a constant temperature level deeper down into the soil. With the MATLAB curve fitting toolbox, the power curve: $T(z) = -1.906 \cdot z^{0.226} + 285.2$ results in a fit with a $R^2 = 0.98$. Extrapolating this curve deeper down in the soil gives a soil temperature of 281.3 K at 25 m depth or 280.6 K at 50 m depth. These values are taken as reasonable initial estimates to be used as boundary conditions at the lower edge of the 2D soil models. Investigations with 1D soil models described in Oosterkamp, Ytrehus, and Galtung [80] confirm the validity of using these values for the lower boundary condition of the soil thermal domain (setting this temperature at the lower boundary results in zero thermal gradient).

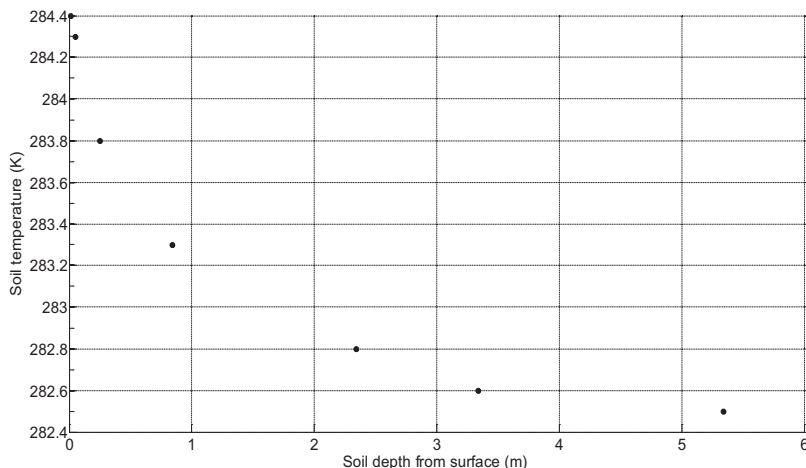


Figure 5.30: Mean of soil temperature measurements at 10 m distance from the pipe during period 16th of May 2013 until 3rd of September 2014.

5.3.5 Inner pipe wall boundary conditions-estimation of inner film coefficient and gas temperature

The measurement set up does not allow for direct measurement of gas temperatures inside the pipe. For verification of the results obtained with the numerical models, accurate estimation of gas temperatures was needed. To approximate the gas temperature, the soil measurements close to the pipe wall are used. The resulting heat transfer rate and gas temperature were estimated with the two methods described in Chapter 3.4. For both methods, the thermal properties of the soil and the value of the inner film coefficient need to be known. For the former, the measured values presented in Chapter 5.3.3 are used. The time dependent inner film coefficient is obtained by running the Europipe 2 flow model with 1D radial external heat transfer model with SCADA data as boundary condition for the period of interest. The resulting values for

Results

the inner film coefficient are shown in Appendix F. Both methods for calculating gas temperatures are in reasonable agreement with each other, as seen in Figure 5.31. The first method discussed in Chapter 3.3 is less sensitive for the changes in gas temperature. This is according to expectation; the evaluation of the energy balance is done further from the pipe wall; the additional heat storage will dampen the response at this position compared to the second method. The gas temperatures and wall heat fluxes derived with the second method are therefore used for the verification analysis.

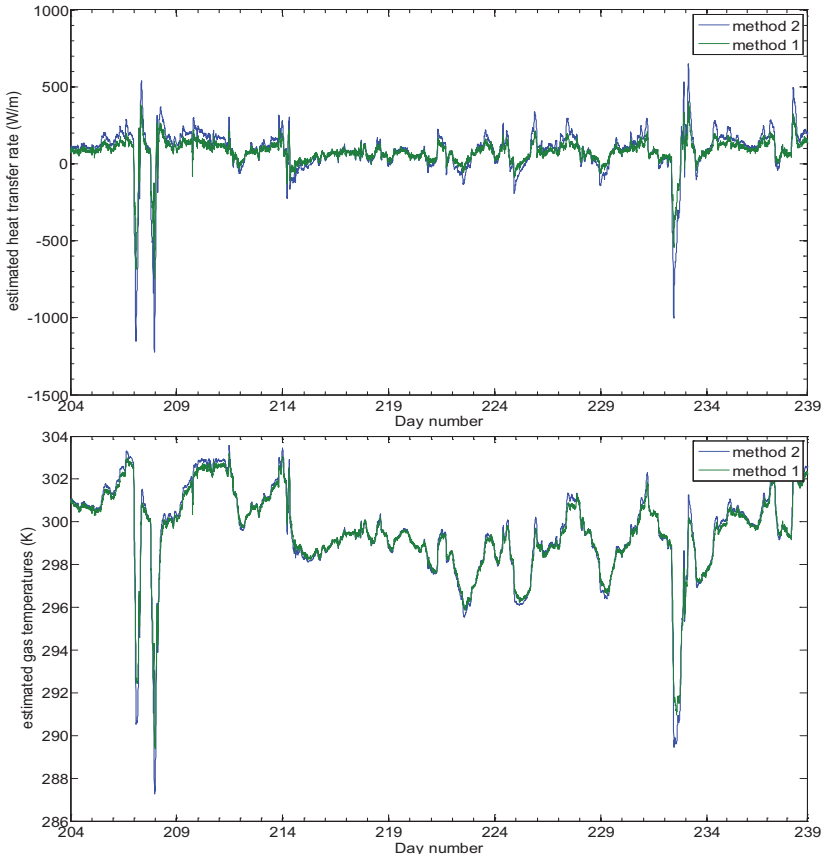


Figure 5.31: Estimated heat transfer rate and gas temperatures, using both methods (23 July 2013-27 August 2013).

5.3.6 Norkyst 800 data- Accuracy Seawater temperature values used in the verification model

From Kårstø to Austre Bokn and from Austre Bokn to Vestre Bokn the pipeline goes through two short sea-sections before becoming offshore. In our pipeline model, we use water temperatures at sea bottom level that are generated with the Norkyst 800 model.

Results

The measurement locations are shown in the pipeline depth profile of Figure 5.32. Figure 5.33 shows the comparison between the measurements and the Norkyst800 data.

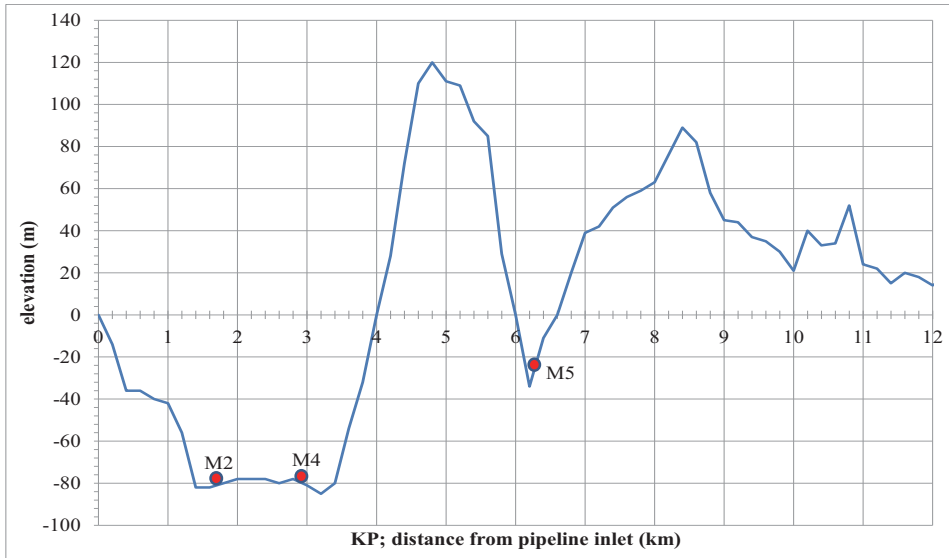


Figure 5.32: Location of measurement devices along the pipeline route and elevation profile.

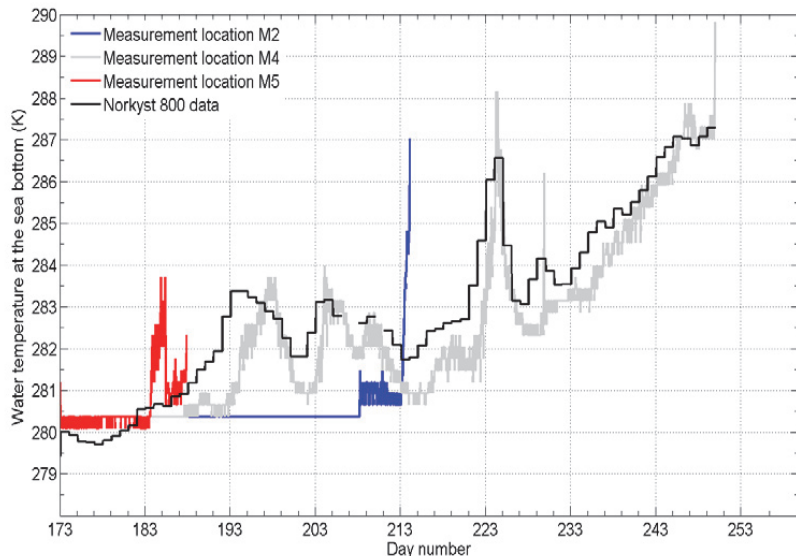


Figure 5.33: Sea bottom temperature measurements versus Norkyst 800 model data. Dark blue line is the Norkyst 800 data.

Results

The results show that the measurements at location M4 are in very good agreement with the Norkyst 800 data. The temperature rise at location M4 occurs a few days later compared to M5. The temperature rise can be attributed to the mixing of the warmed up surface water with remaining cold-water layer from winter on the sea bottom. M5 is in a different sound and in more shallow water, possibly explaining why the effect of surface water warming occurs earlier.

5.4 Soil Measurement series Bokn-observations

Analysis of the measurement data collected at the experimental site led to a number of observations. These are shown here together with a brief interpretation.

5.4.1 Difference between soil surface temperature and air temperature

At three different lateral positions from the pipe, the soil surface temperature was measured one cm below the soil surface. The soil surface temperature is influenced by the net radiation balance, convective heat transfer to the overlying air layer, latent heat from evaporation/condensation and heat conduction into the soil below. In addition, there are the effects of precipitation and moisture transport into the soil. The measurements in Figure 5.34 show the influence of the pipe on the soil surface temperature and the relation between the soil surface temperature and the air temperature.

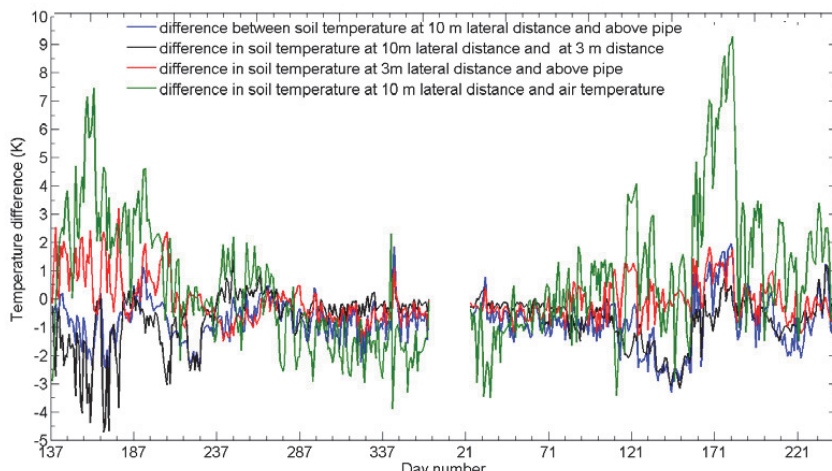


Figure 5.34: Measured air and soil surface temperatures, comparative differences. The period is from the 17th of May 2013 until the 3rd of September 2014. The daily averaged values are used.

Results

The measurements lead to the following observations relevant for the upper thermal boundary condition of the external heat transfer model.

1. The surface temperature during the summer can be up to 10 K higher than the air temperature. During the winter this difference is less, the air temperatures can be 2-5 K higher than the soil surface temperature. In light of these differences, the choice of soil surface boundary condition is not necessarily trivial. It can be expected that choosing either surface temperature or air temperature as one of the boundary conditions for the heat transfer model will lead to differences in heat transfer rates at the pipe inner wall.
2. The variation in the measured soil surface temperatures at the three locations is much smaller than between the soil surface and air temperature measurements. Choosing a measured soil surface temperature instead of measured air temperature should therefore result in more accurate heat transfer calculations.
3. Soil surface temperatures above the pipe are not significantly higher than those at three or at ten meter lateral distance. This supports the assumption of an isothermal surface. It should also be noted that the soil surface measurements have several sources of variability. The local vegetation coverage, the effects of soil erosion, and cattle movement can all influence the measurements. There is no distinguishable trend in the deviations between the measurements.
4. There is a much larger surface temperature fluctuation during the summer of 2013 compared to the summer of 2014. The sensors in the soil surface were installed on 15th of May 2013. During installation the grass coverage was removed locally, leaving exposed black top soil. This is a possible explanation for the initially large surface temperature fluctuations; these fluctuations are reduced when the soil grass cover is regrown.

5.4.2 Soil temperature profiles

Soil-temperature profiles during the period from the 1st of January 2013 until the 10th of April 2013 are shown in Appendix G. Figure 5.35 and Figure 5.36 show an example of the development of soil temperatures around the pipe in response to gas transients (during a five-day period, from the 23rd of May 2013 until the 27th of May 2013). During this period two large inlet mass rate transients occur. The second mass rate transient drops the flow rate to zero. The figures illustrate the temperature response of the soil around the pipe to the transients. As expected, the soil closest to the pipe wall has the largest and fastest temperature drop in response to the drop in gas temperature. In response to the drop in gas temperature, the radial thermal gradient in the soil around the pipe changes direction, and thus the direction of heat transfer, initially from the gas to the soil, reverses. During the following gas temperature rise, the thermal gradient and heat transfer change direction again. The rate of attenuation of the gas temperature fluctuations in radial direction away from the pipe wall is clearly frequency dependent. Temperature fluctuations occurring at quick rates of change attenuate faster compared to the slower changes. The increasing phase lag of the temperature fluctuation with radial distance can clearly be seen in the figures.

Results

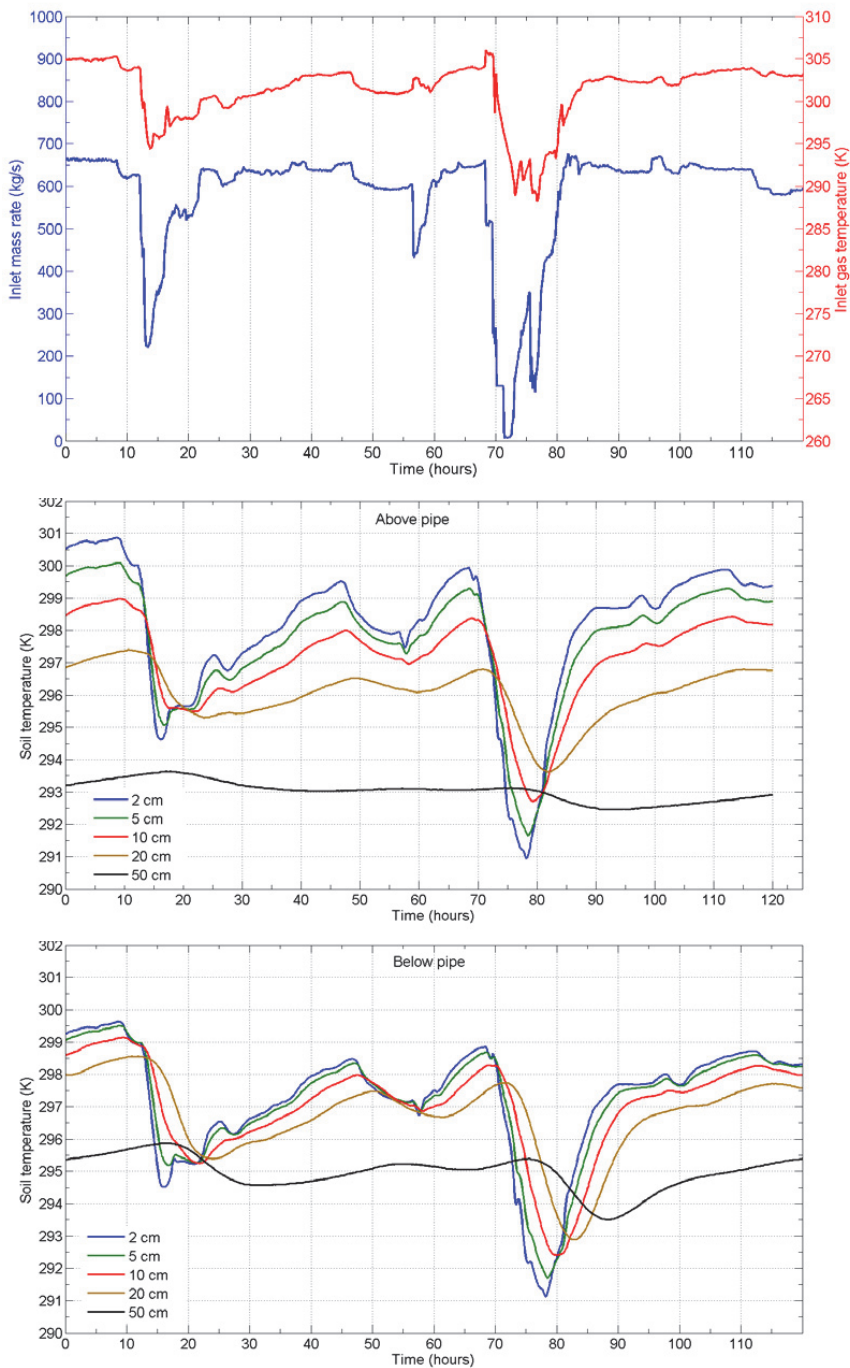


Figure 5.35: Time development of measured soil temperatures around the pipe (above and under) in response to gas temperature transients.

Results

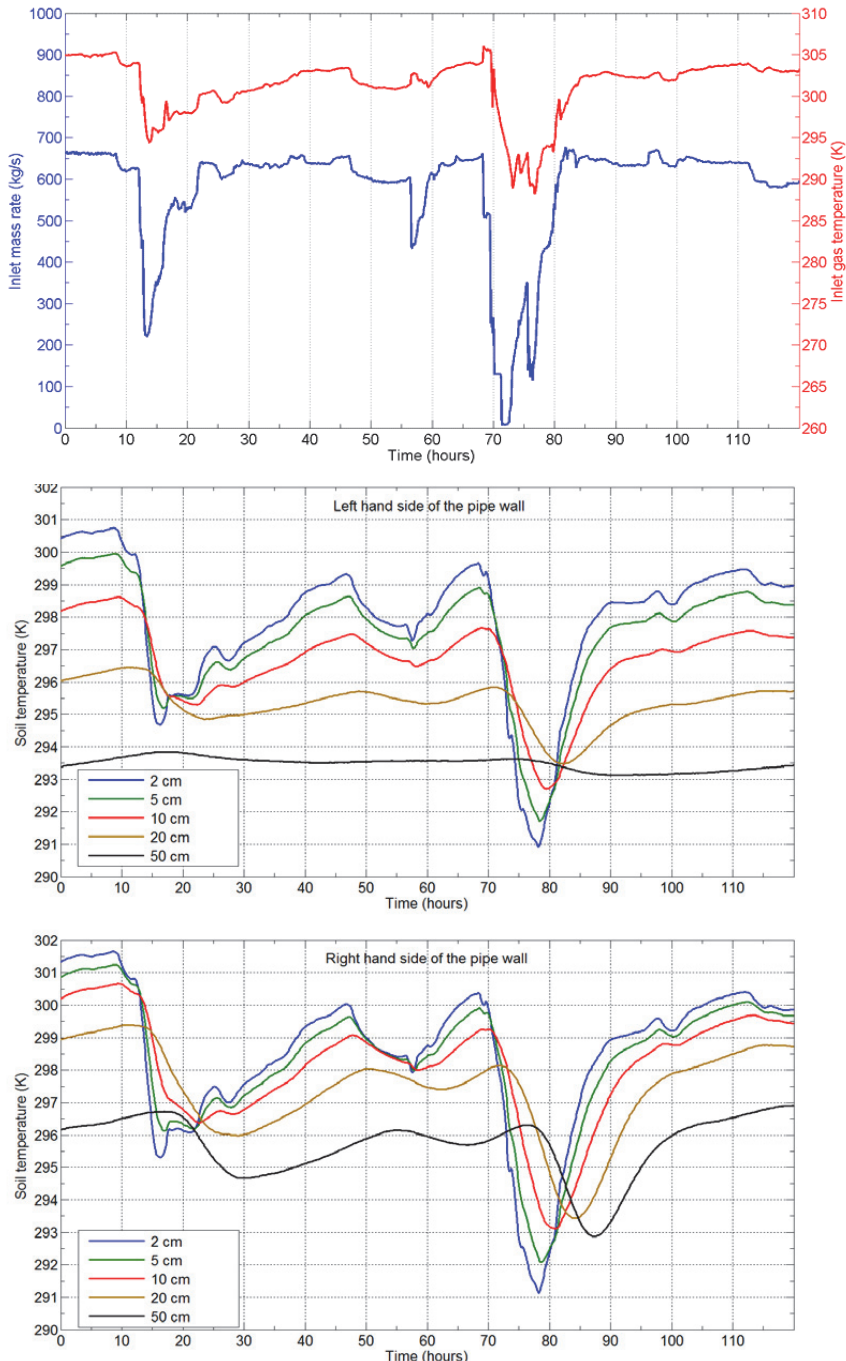


Figure 5.36: Time development of measured soil temperatures around the pipe (right and left hand side) in response to gas temperature transients.

Results

The measured soil temperatures clearly show that the thermal response of the soil to a gas temperature change occurs primarily in the first twenty centimeters from the pipe wall. The attenuation of temperature fluctuations in the first ten centimeters is almost similar in the different radial directions around the pipe (top, bottom, and left, right). This supports the results from the model studies that a 1D radial unsteady heat transfer model can capture accurately the heat transfer response with rapid gas transients; the heat transfer response is mainly occurring in the soil close to the pipe. In the soil layer close to the pipe wall, the resulting temperature profiles are almost axi-symmetric.

The first ten centimeters of soil around the pipe has an approximate time to steady state of three hours. Temperature fluctuations with a shorter time scale will almost entirely attenuate over this distance, as the measurements indeed do show. These observations are in line with the theoretically anticipated behavior of the heat conduction equation, which describes heat conduction as a diffusion process. Thermal diffusion effectively functions as a low pass filter allowing the slower transients to be noticeable over a longer distance. An exact solution of an infinite one-dimensional domain with a sine shaped temperature input at the boundary is shown in Equation (3.6). In this equation we may consider the thermal relaxation distance d as: (amplitude reduced to its 1/e fraction), Salazar [81]:

$$d = \sqrt{\frac{2\alpha}{\omega}} = \sqrt{\frac{\alpha}{\pi f}} \quad (5.2)$$

Here f is the frequency of the temperature sine and α is the thermal diffusivity of the medium. From Equation (5.4) it is clear that both higher frequency and lower thermal diffusivity result in quicker spatial attenuation of temperature fluctuations into the medium. In an infinite one-dimensional domain with thermal diffusivity $\alpha=0.6\times10^{-6}$ m²/s (sand value), for the two transient in Figure 5.35, the thermal relaxation distance ≈ 0.17 m (assuming a 40 hr. period). This is quite close to the attenuation seen in the measurements.

There are however noticeable differences in the attenuation of the temperature fluctuations in the different radial directions at larger distance from the pipe wall. At larger radial distance from the pipe wall, the temperature fluctuations have larger attenuation in the vertical and horizontal direction in the soil above and to the right of the pipe, compared to the attenuation in radial direction below and to the left of the pipe. The measurements thus indicate that the assumption of 1D radial heat transfer is at best valid within the first 10-20 cm from the pipe wall. The two dimensional aspect of the heat transfer in the soil is apparent with vertical distance above and below the pipe, showing both increasing temperature differences and rate of attenuation at equal radial distance from the wall. Differences in heat transfer behavior in vertical direction above and below the pipe are to be expected due to the 2D nature of the heat transfer problem of a buried pipe; the difference in amplitude attenuation in the left and right horizontal direction is more unexpected. In addition, the attenuation of the temperature fluctuations is significantly larger at the left hand side of the pipe compared to the right hand side. This can be an indication that the thermal diffusivity of the sand at the left hand side of

Results

the pipe is smaller than at the right hand side. Another possible explanation is asymmetric convective heat conduction due to ground water movement around the pipe.

Appendix G shows the measured soil temperature profiles. At one-meter lateral distance from the pipe outer wall, the measurements show that the fluctuations in the gas temperature propagate sideways and influence the measurements at 1.46 and 2.30 m depth noticeable. Deeper down, the influence becomes less and is barely noticeable at 5.46 m depth. At three meters lateral distance from the pipe outer wall, the temperature fluctuations at the pipe outer wall are only noticeable at the shallow measurement locations. At ten meters lateral distance from the pipe outer wall, the temperature fluctuations at the pipe outer wall are not noticeable at all.

Measurements with thin film sensors mounted directly on the pipe outer wall show that the top of the pipe wall is consistently hotter than the lower end. Figure 5.37 shows a detail of the skin temperature measurement. The difference reduces when the temperature approaches ambient temperature.

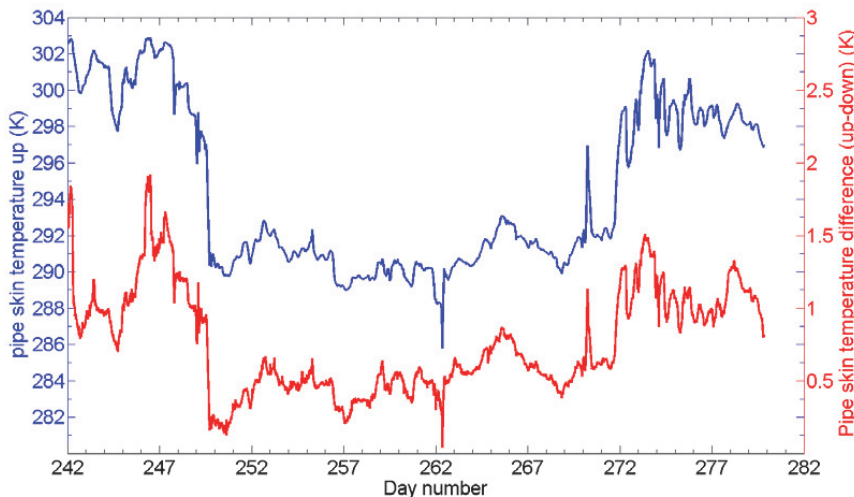


Figure 5.37: Detail of upper pipe skin measurement (blue). Difference between upper and lower measurements (green).

5.4.3 Soil moisture measurements

Measurement of soil volumetric water content is conducted at five locations in the soil around the pipeline. The measurement values are adjusted with the calibration values derived from the measurements on the soil samples as described in Chapter 3. Figure 5.38 shows the measurements in the period 12th of June 2012 until 28th of March 2015. In the clay soil, after an initial period of settling, the measurements show near constant values within the measurement accuracy ($\pm 2\%$ VWC). From the measurements, follows

Results

that deeper down, the clay soil is fully water saturated. Towards the surface, the water content is slightly less.

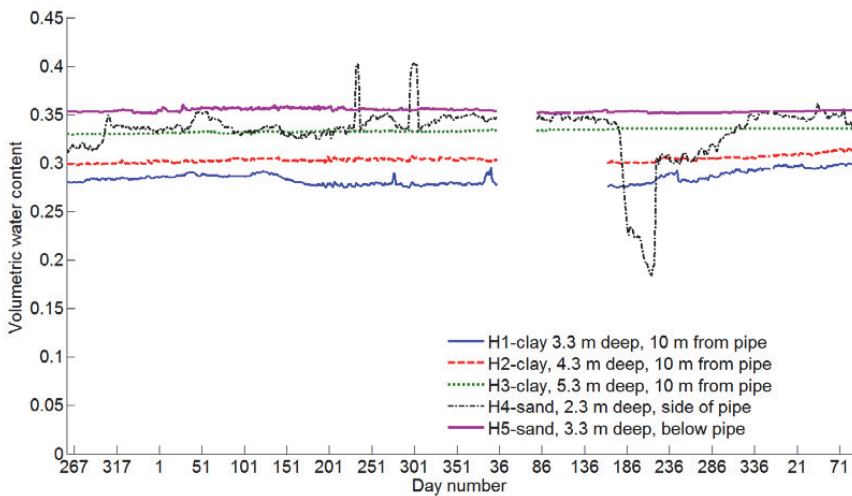


Figure 5.38: Daily soil moisture measurements in the clay from 12th of June 2012 until 28th of March 2015 (gaps in the data are due to data logger malfunction).

The measurements in the sand below the pipe indicate water saturation at all times. The measurements in the sand at the pipe center level show variations that at times are significantly below saturation. There are also two peaks in the measurement in the sand beside the pipe indicating occasional water values above saturation. The sand at both locations is filled at the same time from the same source and is expected to have similar porosity values. Vapor transport through the pores from the water-saturated sand below the pipe to higher, unsaturated layers is therefore a distinct possibility. This is even more likely because there is a thermal gradient around the pipe that can facilitate the convective transport of water vapor through the sand pore matrix.

5.5 Reproducing measured soil temperature profiles with a 2D heat conduction model of the experimental site

One of the research questions was to what extent a heat conduction model can reproduce the actual soil temperature profiles. For this purpose, the 2D heat transfer model of the experimental site, as described in Chapter 4.6 is used. With this model is also the effect of ground water convection and the effect of soil surface boundary conditions were determined. To obtain an as accurate as possible model, the soil thermal properties were tuned to achieve the best agreement between measured and modelled soil temperatures. The 2D heat conduction model ran thereafter with the following boundary conditions:

- Lower edge of soil domain: fixed temperature of 281.65 K.

Results

- Top of soil domain: using the average of the three soil surface temperature measurements to set the soil surface temperature during each time step.
- Inner pipe wall: convective heat transfer with gas temperatures calculated from the temperature measurements as described in Chapter 3.3.

To give the soil domain an as realistic as possible initial temperature distribution, the model was first run with an one hour time step and constant gas temperature for an eight year period. During this run, the historic air temperature data of the preceding eight years were applied at the soil surface boundary condition. Starting with the thus obtained initial temperature distribution, the model was run at five-minute time steps, using the boundary conditions as described above. The model run covers the period the 16th of May 2013 until the 29th of August 2014. The temperatures from the model simulation are compared to the actual soil measurements. The ability of the model to reproduce the measurements was assessed using the deviation between the calculated and measured temperature profiles and the NRMSE (Normal Root Mean Square Error) of the fit between calculations and measurements.

The thermal properties of the different soil constituents were initially chosen on basis of the measurement results reported in Chapter 5.3.2. The soil thermal properties can be tuned to improve the fit between model results and measurements. In case the amplitude attenuation of the soil temperature fluctuations around the pipe or the annual ambient air temperature cycle are larger than the model predicts, the thermal diffusivity α_{soil} of the soil should be reduced and vice versa. Higher thermal diffusivity results in less damping of the temperature fluctuations, lower thermal diffusivity increases damping of the temperature fluctuations over distance. Thermal conductivity λ_{soil} can be tuned to match the average levels of the soil temperatures. Too high soil temperature levels indicate that λ_{soil} is too low and conversely, if the level of the soil temperature is too low, λ_{soil} is overestimated. The tuned soil thermal properties providing the best fit are:

$$\begin{array}{ll} \text{Sand: } \lambda_{soil}=1.6 \text{ W/m}^2\text{K} & \alpha_{soil}=0.65 \times 10^{-6} \text{ m}^2/\text{s} \\ \text{Clay: } \lambda_{soil}=1.8 \text{ W/m}^2\text{K} & \alpha_{soil}=0.82 \times 10^{-6} \text{ m}^2/\text{s} \end{array}$$

Table 9 shows the resulting fit of the calculations to the measurements. Appendix H shows the calculated and measured temperature profiles. These results are also presented in Oosterkamp [45].

The NRMSE of the fit is calculated with the MATLAB routine using the following general scheme:

$$NRMSE = 1 - \frac{\|x(1:N) - x_{ref}(1:N)\|}{\|x(1:N) - mean(x_{ref}(1:N))\|} \quad (5.3)$$

If the NRMSE is one, the fit is perfect. A NRMSE of zero implies that the fit is no better than that obtained with fitting a straight line. Larger negative values of NRMSE occur with worse fit.

Results

Table 9: NRMSE values of fit between numerical model calculations and soil measurements (including mean and standard deviation).

10 m from pipe		3 m from pipe		1 m from pipe	
Depth (cm)	NRMSE/ \bar{x}/σ	Depth (cm)	NRMSE/ \bar{x}/σ	Depth (cm)	NRMSE/ \bar{x}/σ
005	0.9/0/0.6	007	0.8/0/1.1	010	0.8/0.3/1
025	0.9/0.2/0.6	025	0.8/-0.6/0.8	096	0.8/0.3/0.6
084	0.8/0.4/0.7	110	0.7/0.5/0.7	146	0.6/-0.5/0.8
234	0.8/0.3/0.3	167	0.7/0.8/0.3	346	0.4/0.5/0.6
334	0.8/0.3/0.2	367	0.1/1.2/0.2	446	-0.2/0.9/0.3
534	0.6/0.4/0.2	467	-0.4/1.3/0.1	546	-3.7/ 3/0.3
		567	-1/1.2/0.1		
A: top of pipe		B: right hand side of pipe		C: below pipe	
Radial (cm)	NRMSE/ \bar{x}/σ	Radial (cm)	NRMSE/ \bar{x}/σ	Radial (cm)	NRMSE/ \bar{x}/σ
002	0.8/0.4/0.2	002	0.9/0-1/0.2	002	0.5/1.2/0.5
005	09/0.3/0.2	005	0.9/-0.1/0.3	005	0.6/1/0.4
010	0.9/0.1/0.3	010	0.7-0.6/05	010	0.6/0.7/0.3
020	0.8/-0.1/0.5	020	0.5/-1.1/0.7	020	0.8/0.2/0.4
050	0.7/-0.2/0.7	050	-0.2/-2.3/1.2	050	0.7/0.4/0.5
100	0.8/0.5/0.6	100	0.3/-1.5/1		

Summarized, the model results compared to the measurements show the following:

- The model does not reproduce the measured temperature differences in radial direction above and below the pipe close to the pipe wall.
- In vertical radial direction above the pipe, the difference increases with radial distance. At larger distance from the pipe wall, the difference shows a more pronounced seasonal dependency with the maximum during the winter. This difference changes sign between 0.5 and 1m radial distance from the pipe wall; closer to the pipe the calculated values are colder, further from the pipe they are warmer than the measurements.
- In horizontal radial direction, the difference increases with distance to the pipe wall. Between 0.5 m and 1 m, distance the reproduction with the model is poor, showing a high variation in the difference between calculated and measured values.
- In vertical direction below the pipe, the calculated temperatures closest to the pipe wall are between 1 and 2 K too high compared to the measurements. Further away from the pipe wall the difference reduces. In addition, here is a seasonal dependency of the difference.
- Deeper down in the soil, the numerical model reproduces the measured vertical soil temperature profiles at 10 m lateral distance from the pipe with an accuracy of 0.5-1.0 K. In the upper layer (circa one metre) there is a clear seasonal dependency of the difference between measured and calculated temperatures. During the summer time, the calculated upper soil temperatures are as much as 3K higher compared to the measurements. This difference reduces with depth and reduces to 0.5-1.0 K during the winter. This seasonally dependent difference can be explained from the absence of surface evaporation and moisture transport

Results

from the upper soil layers deeper down into the soil. The conduction heat transfer model does not include these effects in the soil surface boundary condition. This results in the energy balance at the soil surface being balanced towards more heat conduction into the ground, potentially explaining the higher temperatures in the soil layers immediately below during the summer. The relative importance of the soil surface boundary condition is further investigated Chapter 5.6.

- The same trend is present at three metres lateral distance from the pipe, but not so pronounced for the upper most measurement. Deeper down into the soil, the difference between calculated and measured temperatures gets progressively larger.
- At one meter lateral distance the difference between calculated and measured temperatures is larger. Deeper in the soil, below the installation depth of the pipe, the model increasingly over-predicts the temperatures.
- For the measurement point M_{1_546} at one metres lateral distance, and at 546 cm depth, the calculations are 3.5 K higher than the measurements. For the measurement point at the same depth as the centreline of the pipe (M₁₋₂₃₀), the model is giving overall too low temperatures and too large damping of the temperature fluctuations. This could be an indication that in the model, the thermal diffusivity in horizontal radial direction from the pipe is set too low. The measurement locations M_{1_115} and M_{1_167} show the same trend with respect to damping but overall temperature levels are in good agreement.
- In the radial direction immediately above the pipe, there is a good fit between model and measurement but also here the damping of the temperature fluctuations with the model is too large.
- The damping of the temperature fluctuations in vertical radial direction below the pipe show good agreement with the measurements. In horizontal direction, the model shows a more damped response.
- Analysis of the first time derivative of the temperature data closest to the pipe wall shows it to follows closely that of the measurements, but exceeds slightly the local maxima and minima. At further distance of the pipe wall, this becomes opposite, the further from the pipe wall the difference increases. This possibly indicates that the thermal diffusivity in radial direction is not constant and assumed too low at larger distance from the pipe wall.
- Comparison between the model calculated inner wall heat transfer rate of the model and the measurements based calculation of the inner wall heat transfer rate from Chapter 5.3.5 shows a good overall agreement. The agreement diminishes during large fluctuations in gas temperature, when heat transfer rates are high. The model results show significantly higher peak heat transfer rates. This is to be expected, the cell method used to calculate the heat transfer rates from the measurements uses a large thermal mass, resulting in significant damping of these peaks. The average difference over the entire period is seven W/m (<10 % of the average value).

Results

5.6 Effect of upper soil boundary conditions

This Chapter describes the results obtained with 1D and 2D heat transfer models of the measurement location. The effect of different assumptions for the soil surface boundary condition upon the soil thermal profiles and the pipe inner wall heat transfer are studied.

5.6.1 Soil-atmosphere boundary

The results described in this chapter are also reported in Oosterkamp et al. [80]. The external heat transfer models used in modelling gas pipe flow have simplified boundary conditions. The full energy balance at the soil surface is not considered; it is not practical to measure this everywhere along the land-based sections of a pipeline route. Usually, detail knowledge of the soil surface temperatures along a buried pipeline is not available either. For the pipe flow heat transfer models it is common practice that the soil surface temperature is forced either directly with the air temperature or through a convective boundary condition. Air temperatures along the pipeline route are usually not measured directly. They are obtained either from a nearby meteorological station or from historical weather data. Oosterkamp et al. [80] studied the effect of different types of soil surface boundary conditions on the prediction of the thermal regime in the ground. This was subsequently expanded to the effect of the boundary conditions on the heat transfer between the pipeline fluid and the surrounding soil. The results were verified using the measured soil temperature profiles around the pipe.

The sensitivity of the soil thermal profile for the soil surface boundary conditions were first investigated with a 1D heat conduction model of the soil at ten meter lateral distance from the pipe wall. The results were compared to the measured soil temperature at different depths. The full surface energy balance was estimated from correlations using measured weather data and net radiation measurements. The effect of the choice of the soil surface boundary condition on the heat transfer between pipe and soil was thereafter determined, using the 2D model described in Chapter 4.6. A specific objective of the study was to quantify the effect of using measured air temperature for the soil surface boundary condition in terms of the heat transfer between the gas inside the pipeline and the ambient.

The 1D numerical model is a finite difference discretization of the 1D heat conduction equation with 0.05 m spatial steps and 500 calculation elements (25 m depth). The discretization was according to the explicit Euler scheme:

$$\frac{1}{\alpha} \frac{T_m^{n+1} - T_m^n}{\Delta t} = \frac{T_{m+1}^n - 2T_m^n + T_{m-1}^n}{(\Delta z)^2} \quad (5.4)$$

Care was taken that the time step size led to fulfilment of the CFL stability criterion $\alpha\Delta t/\Delta z^2 \leq 1/2$. The thermal properties were tuned to obtain the best fit to the measurements using the base case boundary condition: $T(\mathbf{0}, t) = \mathbf{M}_{001}(t)$. The best fit

Results

was obtained using: top soil (0-0.30 m), $\alpha=0.60 \times 10^{-6} \text{ m}^2/\text{s}$, lower soil layers (0.30-25.00 m): $\alpha=0.90 \times 10^{-6} \text{ m}^2/\text{s}$. The thermal conductivity in the top soil layer is set to 1.5 W/m·K. These values are within the range of the measured thermal diffusivity of the soil samples.

Different boundary condition cases were applied to the upper node of the model ($z=0$). This node represents the soil surface. Table 10 shows the different boundary condition cases for the upper node. The lowest node at $z=25$ m is set at 281.55 K.

Table 10: Boundary condition cases (Oosterkamp et al. [80].

Boundary condition	Expression	Description
1:Basecase	$T(0,t) = M_{001}(t)$	Dirichlet, top node follows soil surface temperature
2:Air temperature	$T(0,t) = T_a(t)$	Dirichlet, top node follows air temperature
3:Convection	$-\lambda \frac{\partial T}{\partial z} \Big _{z=0} = -h(T(0,t) - T_a(t))$ h=100 W/m ² K	Neumann, heat conduction rate into the soil surface equal to the heat transfer between soil surface and air
4:Convection plus radiation	$-\lambda \frac{\partial T}{\partial z} \Big _{z=0} = -h(T(0,t) - T_a(t)) + q^*$ h=100 W/m ² K	Neumann, heat conduction rate into the soil surface is equal to the sum of the heat transfer between soil surface and air and the soil surface radiation balance
5: full surface energy balance	$-\lambda \frac{\partial T}{\partial z} \Big _{z=0} = -h(T(0,t) - T_a(t)) + q^* - q_{le}$	Neumann, heat conduction rate into the soil surface is equal to the full soil surface energy balance
6: daily average air temperatures	$T(0,t) = T_a(\text{daily averages})$	Dirichlet, top node follows daily averaged air temperature measurements
7: monthly average air temperatures	$T(0,t) = T_a(\text{monthly averages})$	Dirichlet, top node follows monthly averaged air temperature measurements
8: monthly normal air temperatures	$T(0,t) = T_a(\text{monthly normal values})$	Dirichlet, top node follows monthly normal air temperature from the Kvitsøy station statistics (Eklima) [82].

The third boundary condition, BC3, has the following discretization in the explicit models:

$$-\lambda \left(\frac{T_2^n - T_1^n}{dz} \right) = h(T_1^n - T_a^n) \quad (5.5)$$

For BC3 and BC4, a heat transfer coefficient of 100 W/m²K was used. For the fourth and fifth boundary cases, the right hand term of Equation (5.7) is extended with the respective contributions of q^* , q_h and, q_{le} . The values of q^* , q_h and, q_{le} are updated in each time step. The net radiation q^* are measurement values taken at the experimental

Results

site. The values for q_h and, q_{le} are calculated using measured weather data according to Equation (2.28) and Equation (2.2) from Herb et al. [26]. These values were qualified by comparing the resulting ground heat conduction. Subtracting the ground conductive energy flux from the measured nett solar radiation provides the sum of the ground surface latent and sensible heat. This is compared to those calculated with the base case 1D model, as described in Oosterkamp et al [80]. The two methods show a good overall agreement, but the correlation from Herb et al. results in somewhat lower values.

Prior to each run, the calculation domain is given an initial temperature profile. This initial temperature profile is obtained by running the model using the day normal air temperatures for a 25 year period. When the initial temperature profile is set, the hourly ambient temperatures (Kvitsøy station, NMI [82]) from 16-May-2005 until 16-May-2013 are applied as upper boundary condition. The resulting temperature profile is used as initial condition for each model case. For each of the boundary condition cases from Table 10, a transient simulation was run with the one-dimensional model. The accuracy of fit of the calculated temperature depth profiles to the measured values is used for evaluation. The used criteria are the Normal Root Mean Square Error (NRMSE) of the fit (Equation (5.6), the maximum difference, and the mean and standard deviation of the difference, as shown in Figure 5.39 for each boundary condition case.

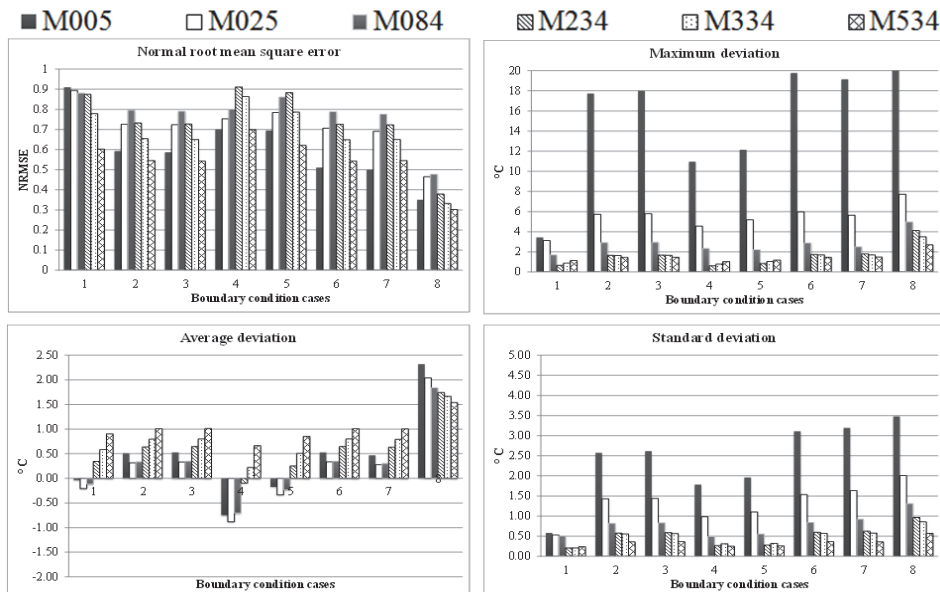


Figure 5.39: Results from the boundary case studies with the one-dimensional model. The deviation is defined as measured value minus calculated value, from Oosterkamp et al.[80].

For the base case (using the measured soil surface temperature as boundary condition), there is a good match between calculated and measured soil temperatures. The maximum deviations are low, and the average difference is less than one degree. Deeper down in the soil the accuracy is less, the deepest measurement M₅₃₄ shows on average

Results

one degree higher measured temperatures compared to the calculation. Note that the calculated temperature in the soil surface layers is higher than the measurements. Using the air temperature to set the soil surface temperature (CASE 2) results in a significantly reduced accuracy of the fit, but still gives almost as accurate results in the lower soil layers compared to the base case. For the upper measurement positions (top soil layer), the resulting accuracy is significantly lower, with a high maximum temperature deviation close to the surface. This is to be expected, the effect of solar radiative heating of the soil surface during summer daytime is not captured with this boundary condition.

Using a convective boundary condition (CASE 3) with air temperature results in almost identical calculated temperature profiles as those obtained when using the air temperature as a Dirichlet boundary condition.

Adding net radiation to the convective boundary condition (CASE4) gives a large improvement in fit lower down in the soil compared to the air temperature boundary condition (CASE 3). The extra energy added to the soil surface from the net radiation boosts the soil temperatures during the summer months. The fit of the two lowest measurement positions improves compared to CASE2, except in the soil surface layer. The surface temperatures are overestimated in this case. Using the full surface energy balance (CASE 5) has a similar effect on the temperatures lower down in the soil as with CASE 4. In this case, the additional heating of the soil surface is less, because the latent heat is included (cooling effect). When using daily averaged air temperature measurements (CASE 6) instead of the measurements at five-minute resolution (CASE 2), no significant loss of accuracy is seen. This is also the case with using monthly averages of measured temperatures (CASE 7). The effect of using statistical weather data instead of real-time measurements is shown in CASE 8. Using the monthly normal values result in a worse fit, with larger average and maximum deviation.

The 2D Ansys model from Chapter 4.7 was used to evaluate the effect of different soil surface boundary conditions on the heat transfer over the pipe wall. When modelling pipe flow, often only the daily average air temperatures are available to use for the boundary condition (CASE 6). The resulting heat transfer over the pipe wall was compared to the base case boundary condition (CASE 1 measured soil surface temperatures as Dirichlet boundary condition). For each analysis the gas temperatures obtained from the measurements, as described in Chapter 5.3.5, were used in the convective boundary condition at the pipe inner wall. The last case, CASE 8, uses monthly normal air temperatures (obtained from weather statistics). For the three cases, the pipe wall heat transfer was compared to that of the base case. Figure 5.40 shows the resulting deviations ($q_{case} - q_{basecase}$). The results show that during the summer months, using the air temperature as boundary condition increases the heat transfer between gas and the ambient by six W/m². During the winter months, the resulting heat transfer is 0.5-3 W/m² less. The deviations are larger when using the monthly averaged air temperatures. Using the measured air temperatures, updated in each time step, (BC2) does not improve accuracy compared to the use of daily averaged values.

With an average heat flux from gas to ambience of 30 W/m², using air temperature as the soil surface boundary condition instead of measured soil surface temperatures leads

Results

in the summer months to a 15% too high heat flux with both BC2 and BC6 and a 20% too high heat flux with BC8. This is consistent with the air temperature during the summer being on average lower than the soil surface temperature. During the winter months, this is the opposite, with a higher resultant heat flux when using air temperatures as soil surface boundary condition. This will have a long term effect on the gas temperatures. The measured differences are small compared to the high rates occurring during transient flow conditions. They are significant in relation to the average (near steady state state) heat transfer and will therefore predominantly effect the gas temperature over longer time scales (months to years).

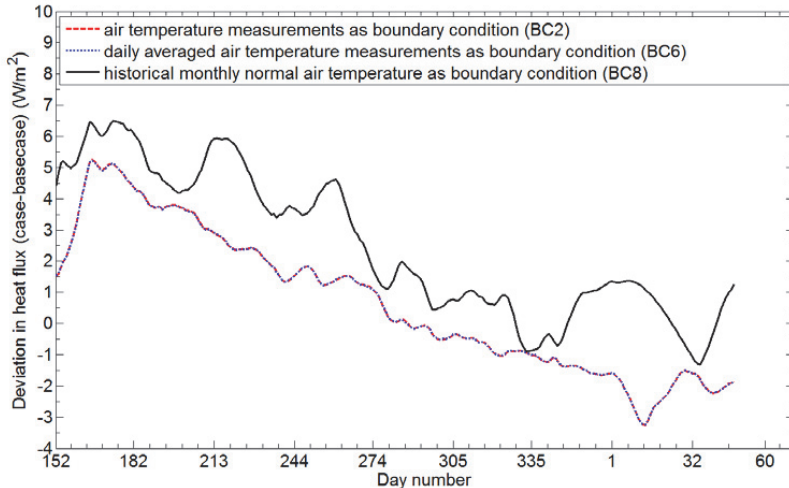


Figure 5.40: Pipe wall heat transfer: deviation from base case (BC1) when using available air temperature data as boundary conditions. The black line is for monthly normal, and the gray line for daily averaged air temperature data. The start date is the 1st of June 2013 (Oosterkamp et al. [80])

5.6.2 Soil surface moisture migration

For a short time period, the moisture content in the top soil layer was measured. Two EC-5 sensors were buried at respectively five and ten cm depth in the top soil at ten meter lateral distance from the pipe. The soil moisture content was measured during the period from the 3rd of May 2014 until the 6th of June 2104. The results are shown in Figure 5.41. The results show that there is considerable moisture migration in the top soil layer. A small daily cycle is present in the measurement data. This is more pronounced close to the surface. There is also a large variation over periods spanning more than one week. The rises in soil humidity coincide with rainfall, occurring at the 6th, 7th, 8th, 16th, and the 22th of May. The delayed response of the lower measurement during the decline of the moisture content following rainfall, together with the presence of a daily cycle indicates that the reduction in upper soil moisture content during the dry period is partly due to soil surface evaporation.

Results

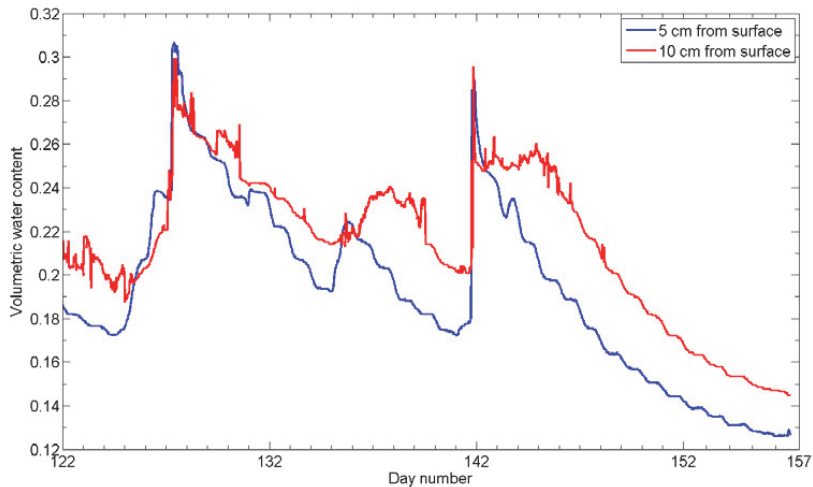


Figure 5.41: Soil surface layer moisture measurements, the 3rd of May 2014 until the 6th of June 2014.

There is also evidence of moisture migration lower into the soil; the values of the lower measurement being consistently higher compared to the upper measurement. The deeper soil measurements (Figure 5.38) also show a moisture content gradient to saturation deeper down in the soil. These results show that a heat conduction model does not physically describe all heat transfer mechanisms active in the soil surface layer. The results with the heat conduction model using measured soil surface temperature as boundary condition (**CASE 1**) support this. During the summer, the calculated temperatures in the top soil layer are slightly too high, while during the winter they are too low. This is an indication that moisture transport in the upper soil layer plays a minor role in the soil heat transfer. The good overall match deeper down in the soil between calculation and measurement is a strong indication that the contribution of moisture migration into the soil does not play a large role on the overall heat transfer. Further study is necessary to gain a complete understanding of the contribution of these heat transfer mechanisms.

5.7 Effect of groundwater convection

The burial configuration of the pipeline at the experimental location makes it susceptible for convective heat transfer from ground water. The pipeline is lying in a ditch refilled with sand that is pervious to water. In the pipeline elevation profile shown in Figure 3.2, there is a local crest at KP8.17. Downstream this point, the general direction of the pipeline is downhill. Here the pipeline crosses bog and wet land areas. From KP8.17 to KP12.2 there are several water plugs installed to avoid the pipeline ditch draining the surrounding bog areas and wet lands. A water plug is also present at KP8.2. Between KP7.7 and KP7.9, the pipeline crosses a small lake (Boknabergvatnet). At both sides of the lake, the pipeline is laying higher in the terrain. It is thus unlikely

Results

that there is ground water flow from this lake through the pipeline ditch towards the sea. Between KP6.5 to KP 7.7, the general direction of the pipeline is uphill. According to design drawings, no water plugs are installed at this part of the route. The elevation difference is 58 m for this part of the route. The installation ditch can potentially serve as a drainage channel for surface water, as the underlying clay soil is relatively impervious. The ground water flow would be in this case be in the opposite direction of the gas flow inside the pipe.

5.7.1.1 Forced convection

The pipeline and ditch are under a slight incline resulting in an overall pressure gradient of 470 Pa/m. As reported in Chapter 5.3.1, the calculated intrinsic permeability of the fill sand is estimated between $0.35 \times 10^{-10} \text{ m}^2$ to $2.5 \times 10^{-10} \text{ m}^2$, dependent on choice of representative grain size. Using Darcy's equation, the resulting ground water Darcian velocity was estimated. For the range of calculated intrinsic permeability this estimate spans from $1.7 \cdot 10^{-5}$ to $1.2 \cdot 10^{-4} \text{ m/s}$. An initial assessment of the advective contribution of ground water flow to the heat transfer is possible by using the Peclet number. Heat diffusion is considered to dominate when the Peclet number exceeds unity (Huysmans [83]). For heat transfer on the particle size scale, the particle Reynolds number may be chosen, leading to the following correlation for the Peclet number:

$$Pe_d = \frac{v_d d}{\alpha_{fluid}} \quad (5.6)$$

With $d=d_{ing}=0.25 \text{ mm}$, the Darcian velocity (not pore velocity) $v_d=1.7 \cdot 10^{-5} \text{ m/s}$ gives $Pe_d=0.03$. Using $d=d_{50}=0.66 \text{ mm}$ and $v_d=1.12 \cdot 10^{-4} \text{ m/s}$, gives $Pe_d=0.5$. This would indicate that for the low permeability value, conduction is dominating compared to advective heat transfer in the direction of the pipe axis. For the high value, the Peclet number is still below unity, but could be large enough for advective heat transfer to play a (minor) role.

It is questionable if the particle Reynolds number leads to a proper representation of the heat transfer problem for the case of a horizontal buried pipe in porous media with ground water flow in the axial direction. In Nield and Bojan [22] the problem of convective heat transfer from a heated plate in contact with a porous media flow is given. This is one of the closest analogous problems found in the literature. Using similarity variables, Nield and Bojan [22] provide an exact solution of the energy equation governing this 1D problem. This result in an expression of the Nusselt number in the direction of the flow along the plate (x-direction), given as:

$$Nu_x \approx \frac{q''}{\Delta T} \frac{x}{\lambda_m} = 0.564 \sqrt{Pe_x} = 0.564 \sqrt{\frac{vx}{\alpha_{fluid}}} \quad (5.7)$$

Results

Here λ_m is the averaged thermal conductivity of the solid and fluid phase and ΔT is the temperature difference between the bulk fluid and the wall at distance x from the starting point. Again, the assumption is used that the ground water runs along the pipe for a distance $x = 1200$ m downhill to the measurement location. With the upper value of the Darcian flow ($v=1.12 \times 10^{-4}$ m/s), the Nusselt number according to Eq. (4.38) is approximately 550. The resulting heat flux due to forced convection, q'' is one W/m² per degree temperature difference between the wall and bulk fluid. This is at least an order of magnitude smaller than the conduction heat transfer over the pipe wall. This is however only a rough estimate; the buried pipeline problem could be better estimated with a 3D representation.

Oosterkamp [45], presents results obtained with the 3D computational model from Chapter 4.6. This model was used to estimate the effect of forced convection due to Darcy flow of the ground water in the ditch. Three steady state simulation cases were run: $v=0$ m/s, $v=4.3 \times 10^{-5}$ m/s, and $v=1.16 \times 10^{-4}$ m/s. In the open ditch, during installation, the ground water level in the ditch did not raise beyond the centre line of the pipe. Figure 5.42 shows the ground water level during installation. Below the blue line, the pipe wall shows signs of moisture and associated surface corrosion.

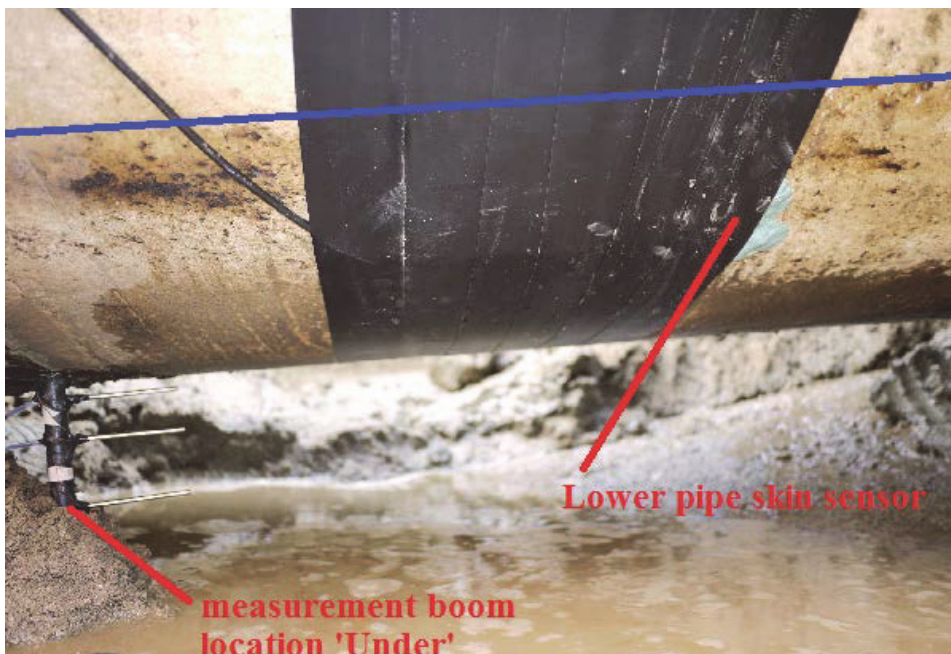


Figure 5.42: Detail of pipeline during sensor installation. Shown is the ground water level. Below the blue line, the pipeline wall shows signs of wetting and surface corrosion.

Based upon these observations, in the simulations, the ground water flow is assumed to flow only below the centre-line of the pipe. The water temperature entering the porous domain is considered to be at the lowest possible value, 273.15 K, to provoke the

Results

maximum effect of forced convection on the pipe inner wall heat transfer. The pipe inner wall film coefficient and gas temperatures are set at 1500 W/m²K and 302 K. The results show that within 100 m flow distance along the pipe, the water has already warmed to the temperature of the surrounding sand matrix. Downstream along the pipe, the temperature profiles and pipe-wall heat flux rapidly approach similarity for all three cases. The results are thus in agreement with the theoretical consideration that forced convection in horizontal direction does not play a significant role in this case.

5.7.1.2 Natural convection

The thermal gradient around the pipe can lead to natural convection heat transfer. The contribution of natural convection on the overall pipe to ambient heat transfer was studied using the 2D steady state ANSYS FLUENT model from Chapter 4.6. These results are also presented in Oosterkamp [45], and partly represented her ad verbatim. The Fluent porous model case uses the same thermal properties as those used for the measurement site model, and the following boundary conditions:

- Soil surface temperature: 280 K.
- Gas temperature 302 K: uniform along the pipe length.
- Inner film coefficient: 1500 W/m²K.
- Porosity: 0.35.
- Boussinesq fluid density model for water.

To evaluate the pipe wall heat transfer, the pipe wall is divided in three arc segments; the upper segment from the 12 to the 2 o'clock position, the second, side segment is from the 2 to 4 o'clock position and the third, lower segment from the 4 to the 6 o'clock position. For the base case (conduction only), the resulting heat flow rate through the upper segment is almost double compared to that at the lower segment. The model was thereafter run using a range of intrinsic permeability values. Figure 5.43 shows the resulting Nusselt numbers of the pipe wall heat-transfer and the approximated exact solution from Himasekhar and Bau [42]. The simulation results show that natural convective heat transfer does not play a role for permeabilities below 1.5×10^{-10} m². Increase of permeability by a factor 10 results in $Nu \approx 1$ with a doubled total heat transfer rate. The low value for intrinsic permeability $\kappa = 1.44 \times 10^{-11}$ m² results in a heat transfer rate of 42 W/m² and the Nusselt number remaining close to zero. At $\kappa = 1.5 \times 10^{-10}$ m², the overall heat transfer has increased to 45 W/m² and $Nu \approx 0.1$, indicating a small contribution of convective heat transfer. The heat flow rate through the upper and lower pipe segment is now roughly equal.

The exact solution from Himasekhar and Bau [42] predicts a higher contribution of convective heat transfer at all permeability values, but with the same trend as the simulation. The resulting Nusselt number is roughly 0.25 higher. The differences could originate from the simulation considering only the sand in the ditch around the pipe to be a porous medium, where the exact solution considers the entire transformed domain as uniformly porous. The latter provides greater freedom for the movement of the ground water.

Results

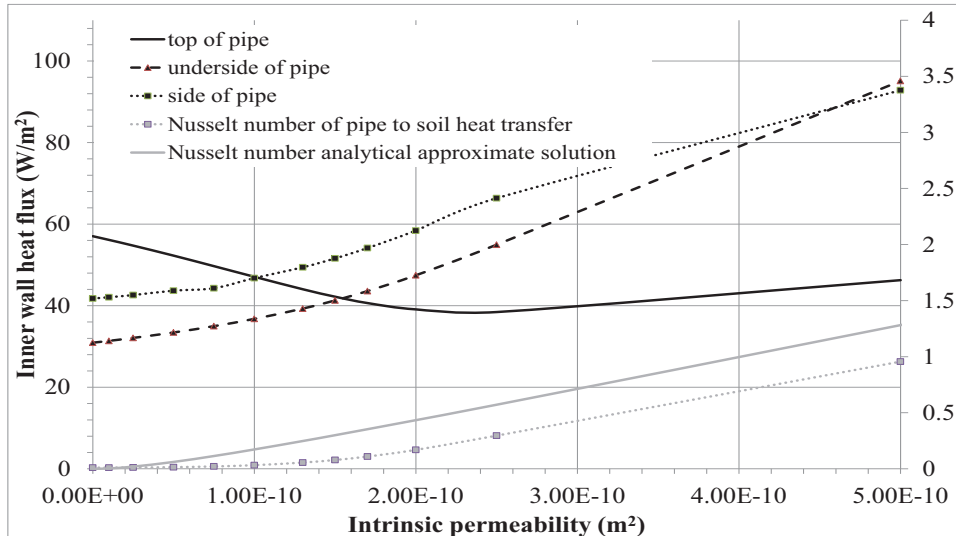


Figure 5.43: Pipe inner wall heat flux and Nusselt number for different intrinsic permeability values. Heat flux is shown for different orientations of the pipe wall.

The 2D Ansys Fluent model from Chapter 4.6 was run for 100 days at the following intrinsic permeability values:

- none ($\kappa=0 m^2$).
- medium ($\kappa=1.3 \times 10^{-10} m^2$).
- high permeability values ($\kappa=1.3 \times 10^{10} m^2$).

The purpose was to see if a better match with the measured values could be achieved when including natural convection heat transfer. Figure 5.44 shows the difference between measured and calculated temperatures in vertical direction above and below the pipe. For the transient case, increased natural convection gives higher heat transfer rates through the lower part of the pipe, while simultaneously reducing the heat transfer rate through the top of the pipe. This results in a minor improvement of the fit to the measured temperatures in the soil below the pipe with convective heat transfer. The same, but opposite trend is seen for the soil temperatures above the pipe close to the wall. The natural convection can explain only to some extent the difference between the model and measurements. The higher intrinsic permeability does decreases further the temperature deviations at the top and bottom measurement locations near the pipe wall. The additional convective heat transfer also results in calculated soil temperatures significantly lower than the measurements closer to the soil surface. The results also show a reducing trend in the temperature deviations with time. It could be interesting to extend the simulations for a longer duration in to see if this trend continues. Other possible causes may contribute to the noted soil temperature asymmetry between the four radial directions. Alternative explanations are that the actual permeability of the sand surrounding the pipe is much higher than the estimated value or that forced convection plays a more significant role than estimated. Higher water flow rates close to

Results

the wall due to channelling (porosity of the sand in contact with the pipe wall can be larger than the bulk value) can also play a role. Erosion along the pipe wall, wash out of fine particles and reduced packing of sand below the pipe can all be contributors to local higher porosity underneath the pipe.

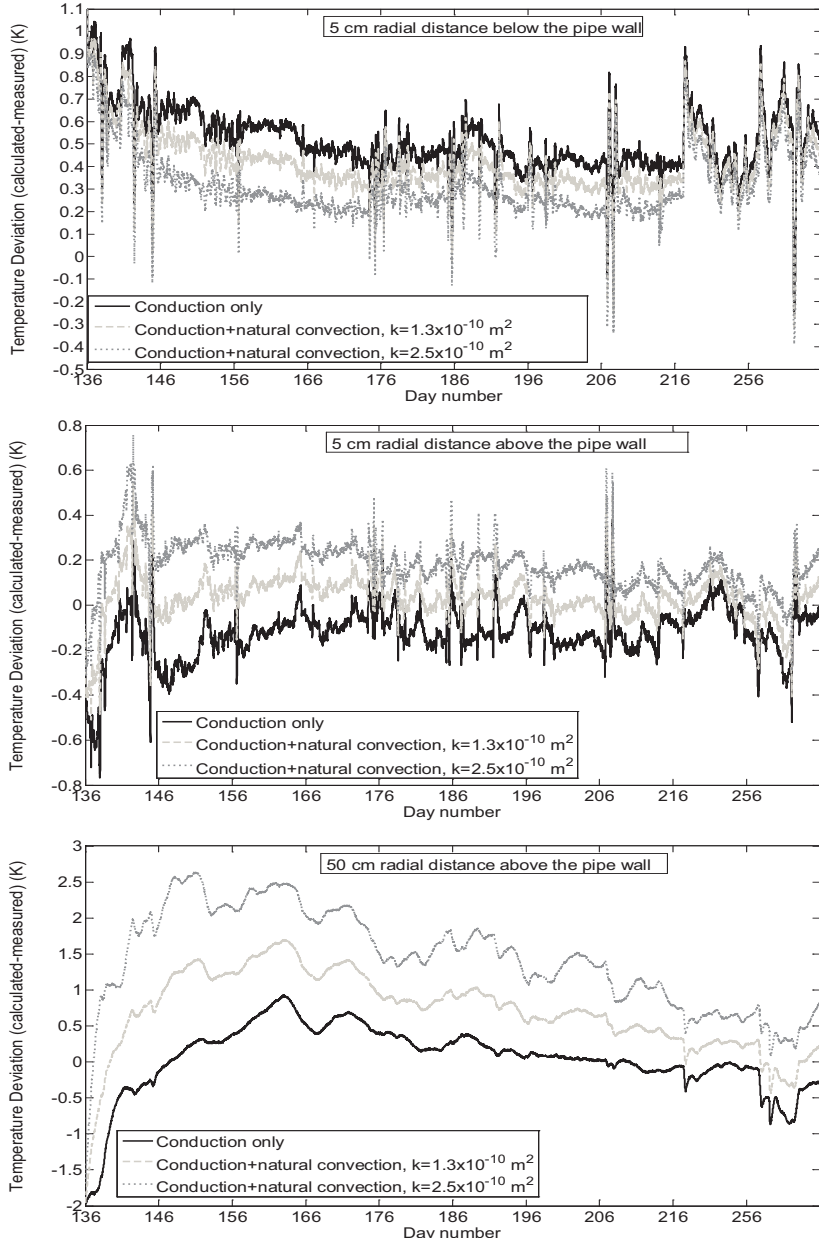


Figure 5.44: Temperature differences between model calculation and measurement for three cases of convection heat transfer in the sand [45].

Results

5.8 Verification: long term comparison of heat transfer model performance

The flow model of the first 12 km of Europipe 2, as shown in Chapter 4.3 was run with the external heat transfer models from the parametric studies. The reason for choosing this particular part of the pipeline is that the pipeline section has a large burial section, overall high gas temperatures, and large gas temperature fluctuations. As seen in the parametric model studies, the pipe flow is most sensitive to the heat transfer model at the first buried part. For the steady state heat transfer model, the initial U values are based on the burial depths of the pipeline as derived from survey data. The U values have been adjusted to obtain the best overall match between calculated and measured pressures and temperatures. For the 1D radial unsteady model, the initial U values have been used to determine the equivalent soil radius for each pipe flow calculation element, based upon the actual burial depth (using Equation (2.19)). Subsequently, the soil thermal diffusivity and thermal conductivity were fine-tuned to obtain the best match between calculated and measured values. The models are run using SCADA based real inlet gas temperature and mass flow rates as inlet boundary conditions. The gas pressure at the valve station at KP12 is used for the outlet boundary conditions, shown in Figure 5.45. The one-minute resolution SCADA data was treated for missing records and outliers, and subsequently smoothed using a Savitsky-Golay filter, applying a linear fit over a span of five consecutive data points. In this way, the temporal resolution of the input data is similar to that of the measurements (logged at five-minute time step). The data starts at the 28th of April 2013 and ends on the 28th of April 2014. At the ambient boundary condition, the measured air temperature at Bokn and the seawater temperature from the Norkyst 800 model were used.

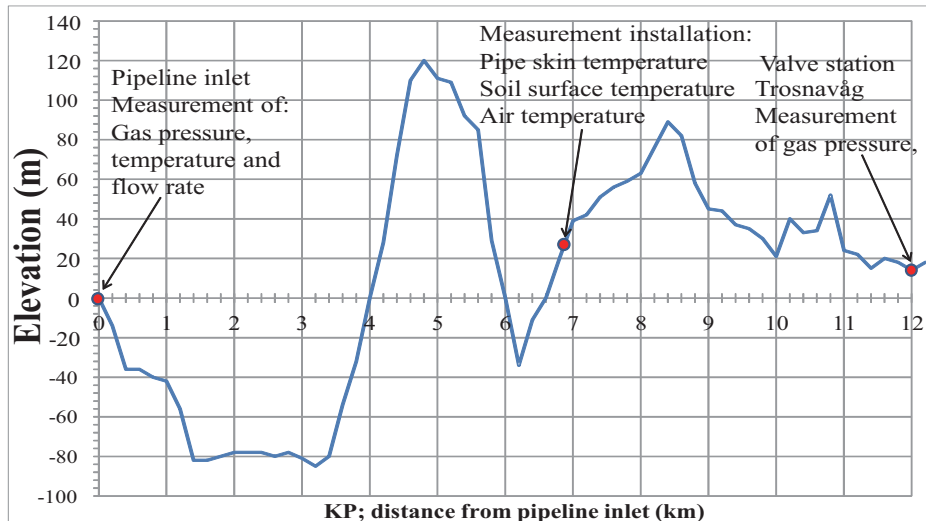


Figure 5.45: Pipeline model, boundary conditions and measurement locations.

Results

5.8.1 Comparison of 1D steady and 1D radial unsteady heat transfer model

Using the 1D steady and 1D radial unsteady heat transfer models, the calculated inlet pressure and pipe skin temperature at Bokn (KP6.8) are compared to the measurements. Figure 5.46 shows the inlet pressure deviations for both heat transfer models.

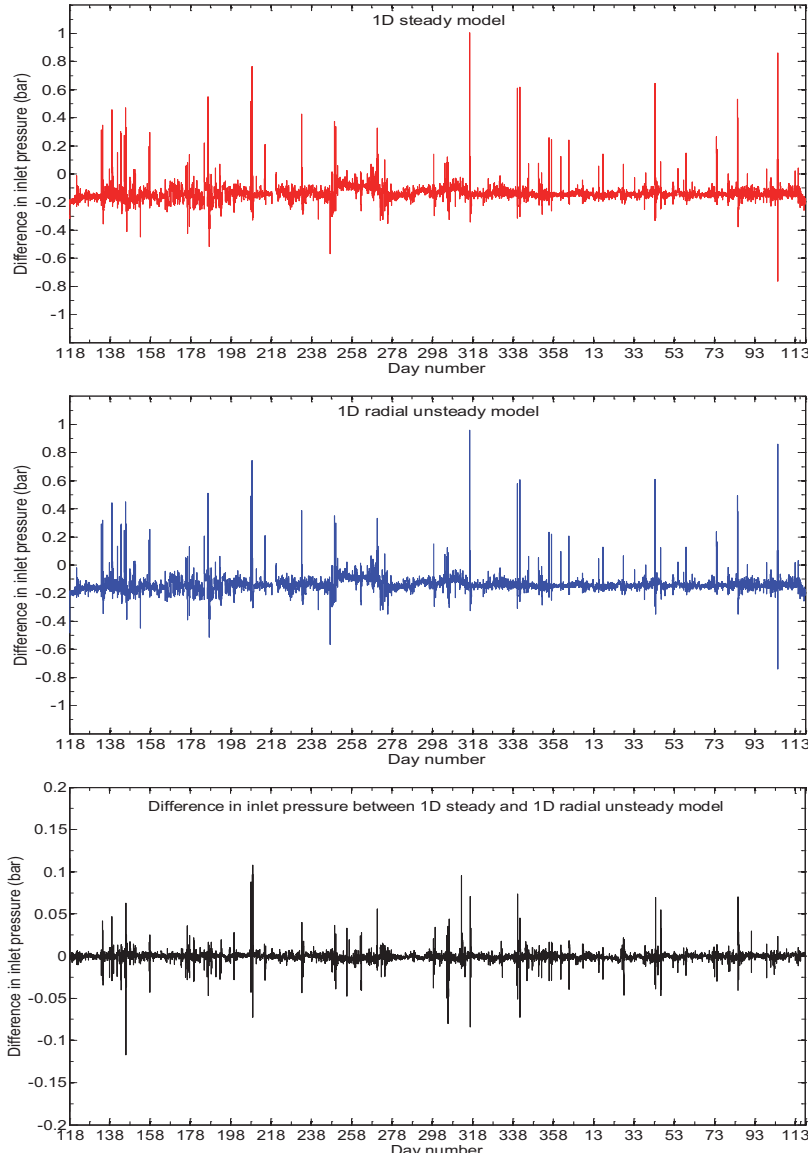


Figure 5.46: Inlet pressure deviations (calculated minus measured) using the 1D steady (top), and 1D radial unsteady (middle) heat transfer models. The relative difference in inlet pressure between the two models is also shown (below).

Results

A systematic inlet pressure deviation of 0.15-0.2 bar is seen with both models. This systematic deviation can be removed by tuning the model; a well-known way to do this is by tuning the pipe roughness, as discussed in Langelandsvik [8]. Occasional larger deviations occur. The peak values in the difference between calculated and measured pressure occur at the same time with both models and are of similar magnitude.

Figure 5.47 shows the inlet pressure development during four large inlet transients.

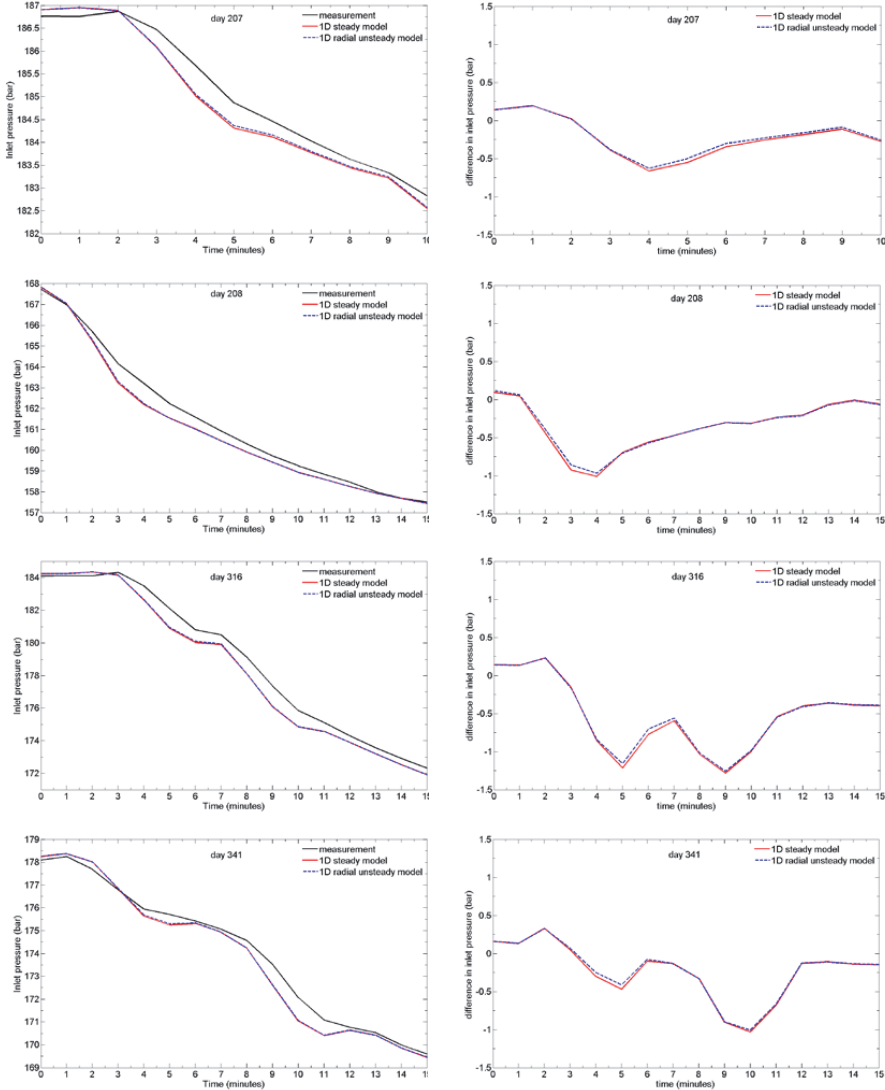


Figure 5.47: Peak differences in inlet pressure (days 207, 208, 316 and 341).

The peak differences in inlet pressure occur during quick drops in inlet pressure and are due to different rate of change between the measured and calculated inlet pressure. The

Results

peak variations in inlet pressure are of short duration, typically between five to ten minutes. During a pressure drop event there are two distinct periods noticeable; in the first period the calculated inlet pressure drops at a faster rate compared to the calculated pressure, in the second period the rate of change reduces to below that of the measurement until the measured and calculated pressures match again at the end of the pressure drop. It is not clear what causes this difference in pressure response; likely candidates are hysteresis in the pressure measurement instruments, the collection and treatment of the measurement data (timing mismatches, interpolation, and averaging of the SCADA data) or a limitation of the flow model. The results however do show that the differences in inlet pressure response between the two heat transfer models are not significant. A similar pressure difference can be seen in the verification of flow model for the entire 650 km long pipeline in Helgaker, Oosterkamp and Ytrehus [37]. In this work, a similar deviation between measured and modelled inlet pressure is seen with both heat transfer models, and, the pressure differences are somewhat smaller with the 1D radial unsteady model. Further investigation into the cause of these pressure differences were considered beyond the scope of this work.

Figure 5.48 shows the deviations between calculated and measured outer pipe wall temperature (pipe skin temperature) at the measurement location. In contrast to the pressures, the 1D steady heat transfer model results in much larger temperature errors compared to using the 1D radial unsteady model (14 K versus 2 K). The results support the findings from the model study of Chapter 5.2.1; correct calculation of the gas temperature during transient flow is much more sensitive to the choice of the heat transfer model than the gas pressure. This is also in accordance with the results shown in Chaczykowski[35] and Helgaker et al [37]. Omitting heat storage in the heat transfer model leads to large gas temperature deviations during transient flow characterized by quick gas temperature fluctuations. The gas temperatures at the model exit (KP12.2) show a similar difference between the two heat transfer models. The results further show that the peak gas temperature errors occurring with the 1D steady heat transfer model correlate strongly with the inlet mass rate and temperature extent and rate of change. The quicker and larger the inlet flow changes are, the larger the deviations between the calculated and measured pressures and temperatures.

The choice of the heat transfer model has thus a significant effect on the accuracy of the gas temperature calculations during transient flow boundary conditions. Figure 5.49 shows the calculated gas temperature at the measurement location and the end of the pipeline. Compared is the gas temperature response at both the measurement location (KP6.8) and the model outlet (KP12) with both heat transfer models. The gas temperature response to an inlet mass rate transient occurs much faster when using the 1D steady model, compared to the 1D radial model. This is in good agreement with the results of the model studies in Chapter 5.2.1. A more gradual gas temperature response to a sudden drop in inlet mass rate is seen with the 1D radial unsteady model, resulting from transfer of stored heat in the pipe wall and surrounding soil to the gas at high rates.

Results

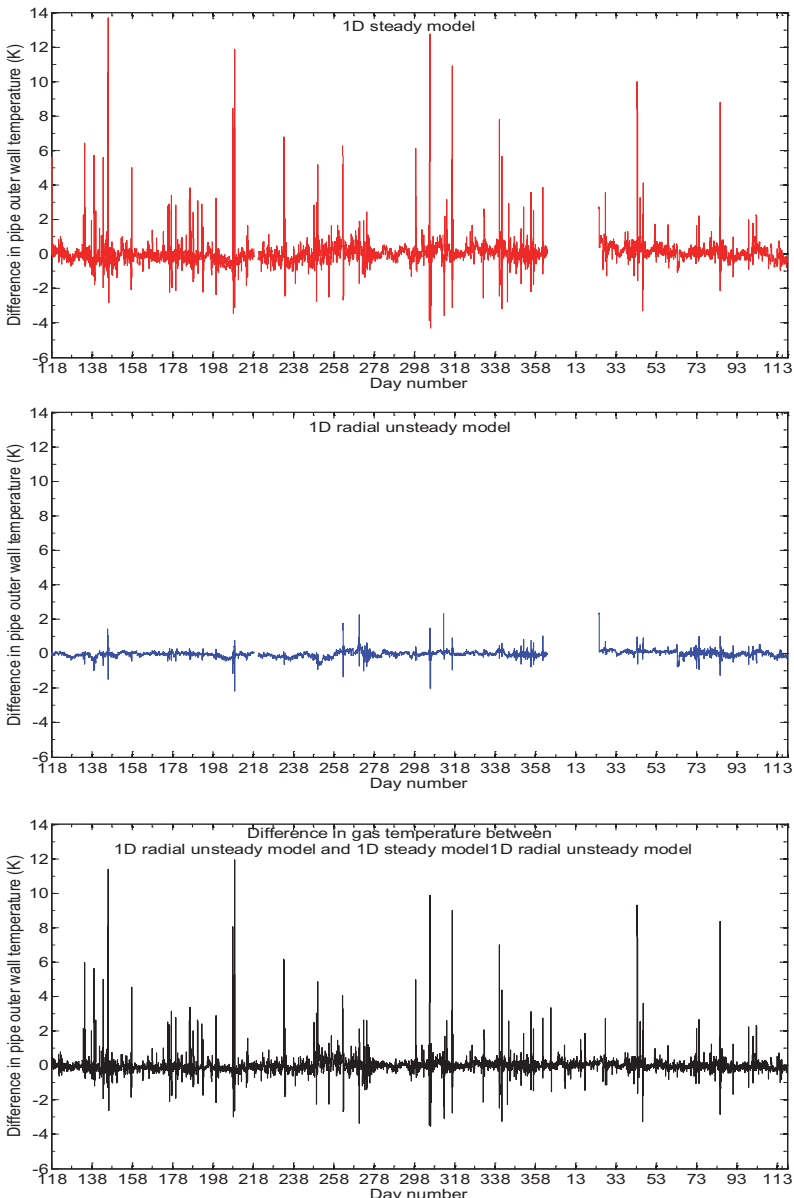


Figure 5.48: Pipe outer wall temperature deviations (measured minus calculated) using the 1D steady (top) and 1D radial unsteady (middle) heat transfer models. The relative difference in pipe outer wall temperature between the two models is also shown (below).

Results

The heat transfer response to the inlet transients is shown in detail in Figure 5.49.

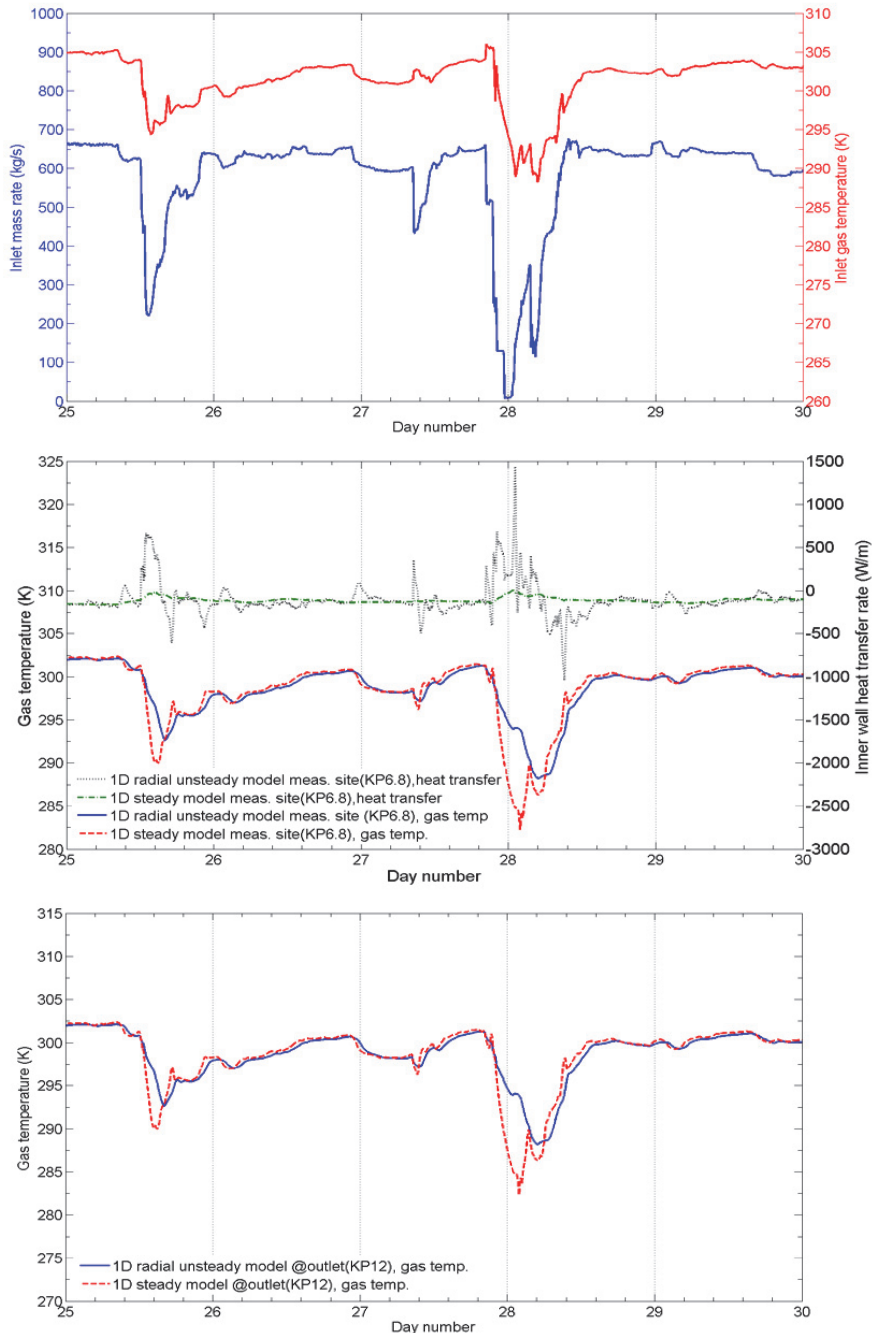


Figure 5.49: Detail of gas temperature development in response to rapid inlet transients.

Results

In response to the inlet transient, the gas temperature drops. Using the 1D radial unsteady model, the thermal energy stored in the pipe wall and surrounding soil results in higher instantaneous heat transfer rates over the pipe inner wall to the gas. This reduces the rate of the gas temperature drop compared to the 1D steady model. As seen in the parametric model studies, the heat transfer rates in response to a gas temperature change are an order of magnitude smaller when using the 1D steady model. Figure 5.50 further illustrates the difference in heat transfer rate over the pipe wall at the measurement site for the two external heat transfer models. The first 100 days of the one-year simulation are shown. For comparison, the estimated heat transfer rates using the measurement data (as described in Chapter 3.4) are included. The results clearly show the underestimation of the heat transfer rates during transient flow conditions using the 1D steady model, and that the 1D unsteady radial model results in heat transfer behaviour similar to the experimental results

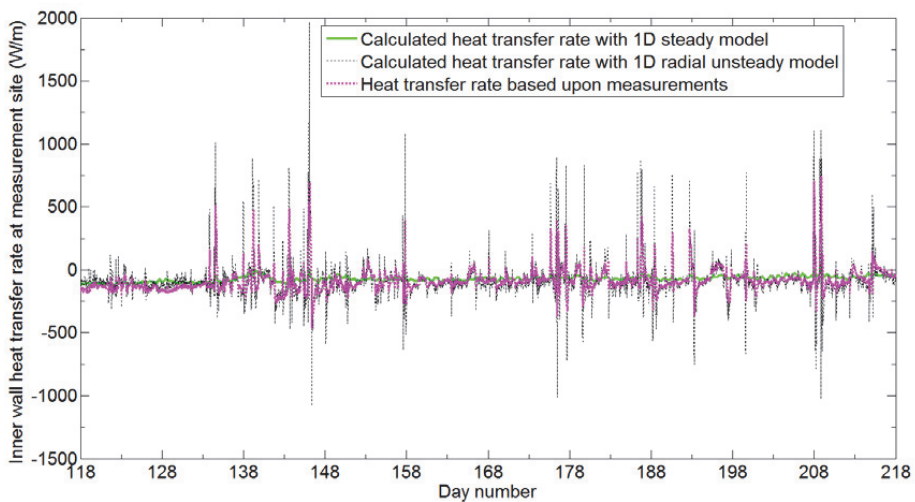


Figure 5.50: Inner pipe wall heat transfer rate obtained with both models at the measurement location. The calculated values from the measurements from Chapter 5.3.5 have been included.

The performance of the 1D radial model is further demonstrated in Figure 5.51, showing the gas temperatures obtained with the model during the first 100 days of the simulation. Figure 5.51 also shows the experimentally determined gas temperatures, obtained from the soil temperature measurements as shown in Chapter 3.4. It can be noted that there is a general good agreement between the two temperatures, also during the quicker and larger fluctuations. Only at the local minima of the larger drops in gas temperature there is a noticeable difference. A part of the difference may be explained from the method of estimating real gas temperatures. An underlying assumption is that there is a thermal steady state in the pipe wall in between every measurement, resulting in small differences when the heat transfer changes direction. The temperature differences at the end of the temperature drops are of the same magnitude as shown in Figure 5.48, showing calculated and measured pipe wall temperature. This is a good indication that the gas temperature estimation with the second method (Chapter 3.4) is

Results

reliable. This bolsters the observation that the use of the 1D radial unsteady model still results in a noticeable gas temperature error during large and quick gas temperature fluctuations.

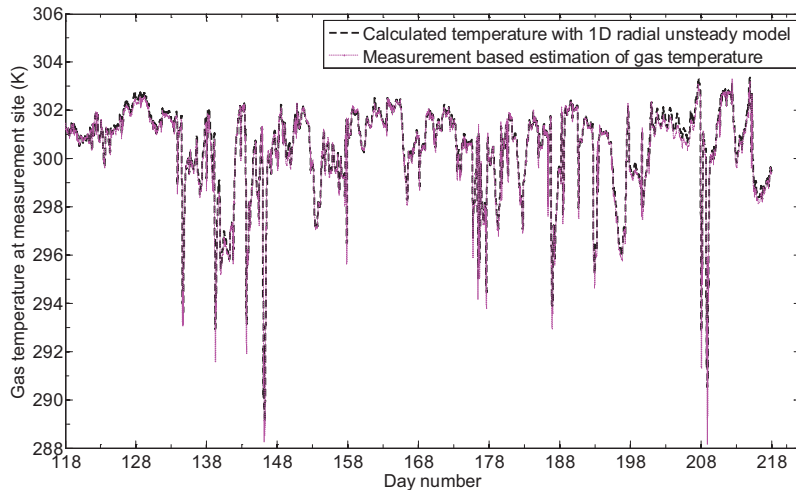


Figure 5.51: Comparison between the measurement estimation and the calculated gas temperatures using the 1D radial unsteady model.

The soil property measurements, shown in Figure 5.28 and Figure 5.29, have occasional changes in soil thermal properties. There can be identified two major property changes in the sand surrounding the pipe (summer 2013 and summer 2014). The simulation with the 1D radial unsteady model was extended to the autumn of 2014 to check the correlation between the thermal properties and the gas temperature error. The results did not show a marked effect of the variation of the soil thermal properties on the gas temperature deviation.

5.8.2 2D unsteady ambient model

The final assessment was to verify the result from the model studies that a 2D unsteady model results in similar heat transfer behaviour as the 1D radial unsteady model. For this purpose, the pipe calculation element (further to be referred to as pipe element 35) representing the measurement location at Bokn is coupled to a 2D FLUENT thermal domain (as described in Chapter 4.2.3) replacing the equivalent one dimensional radial domain. Upstream and downstream of the measurement location, the coupled pipe flow and thermal model are further exactly the same as the 1D radial unsteady model. In the 2D heat transfer model, the thermal properties according to Table 11 are used. These values are the same as used in the 1D radial unsteady model and provide the same steady state U value for the 2D unsteady and 1D radial model ‘slice’ at the measurement location.

Results

Table 11: Thermal properties used in the 2D model of the measurement location.

	Thermal conductivity (W/m ² K)	Thermal diffusivity (m ² s)
Pipe steel	45	$1.3 \cdot 10^{-5}$
Outer coating	0.38	$0.3 \cdot 10^{-6}$
Soil	1.6	$0.66 \cdot 10^{-6}$

The lower edge of the 2D domain has a Dirichlet boundary condition (280.6 K). The left and right vertical boundaries have Neumann boundary conditions ($dT/dx=0$). The top of the soil domain is forced to follow the air temperature (as is the case with the 1D radial model). The model is run with one-minute time steps.

Figure 5.52 shows the calculated heat transfer rates versus the measurement derived values at the measurement location. The use of a 2D unsteady heat transfer model at pipe element 35 does not significantly change the inner pipe wall heat transfer rate. The effect upon the gas temperature at this pipe element (and further downstream) is negligible (<0.05 K). This is also the case with the inlet pressure and pressure at pipe element 35. There is an overall good match between the experimental and calculated heat transfer rate in response to the smaller flow transients. The results do show an increasing difference in heat transfer response with the larger gas temperature changes. The experimental values are time-delayed and do not reach the same peak values during the larger drops/increases of the gas temperatures.

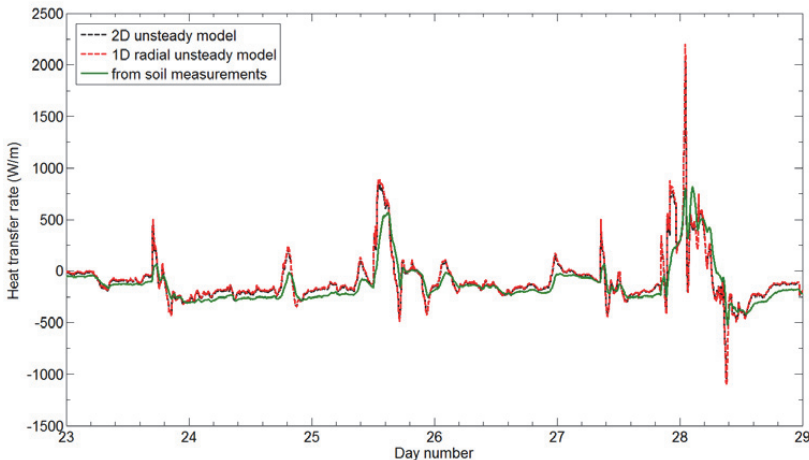


Figure 5.52: Inner pipe wall heat transfer rate shown during three day time period. Comparison between 2D unsteady, 1D radial unsteady heat transfer model and estimated rates using soil measurements and method 2 from Chapter 3.3.

Figure 5.53 shows the development of the measured and calculated soil temperature profiles at different radial distances and directions from the pipe wall. For both models, the general trends in the calculated soil temperature profiles are qualitatively similar to each other and the measurements. For the measurements close to the pipe wall (2 cm) at the three principal locations (top-12 o'clock, right hand side-3 o'clock, and below-6

Results

o'clock), there is a distinct difference in temperature level between top and bottom. This temperature difference is not reproduced by the simulations. Close to the pipe wall (2 cm distance) the difference in the calculated values are small and overall higher than the measurements. Below the pipe, this can be as much as 1.5 K. These differences between measured and calculated temperatures are reduced at the local minima of the gas temperature.

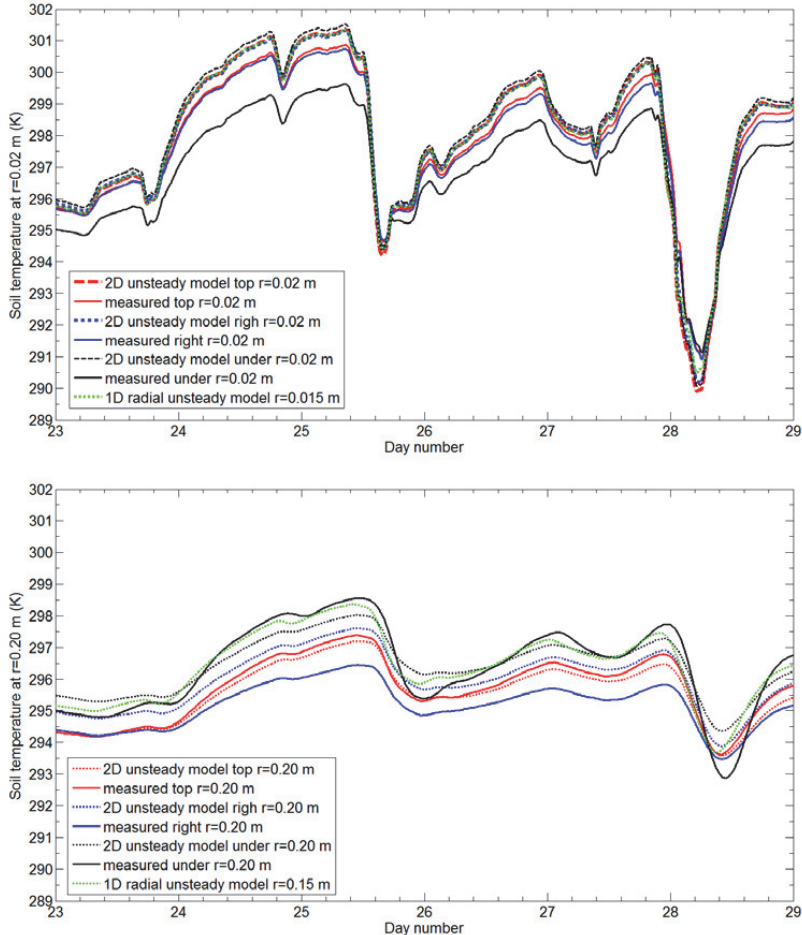


Figure 5.53: Development of soil temperature profiles at radial distance from the pipe. The actual measured values are also shown.

The measurements at 20 cm radial distance from the pipe wall show a better match with the calculations with using the 2D unsteady model. The measured temperature below the pipe is at this radial distance higher than above the pipe. This is in accordance with expectation. The fit between the 2D model and the measurements is worst at the right hand side of the pipe. The measurements also show that damping of the temperature fluctuations in the radial direction above and to the right of the pipe is larger than in the

Results

radial direction below the pipe. This is to a lesser extent the case for the 2D unsteady model. The 1D radial unsteady model provides a single value for the pipe wall heat transfer rate. In reality, the measurements show that the heat transfer rate varies along the perimeter of the wall. The 2D unsteady model more accurately captures this. The calculation results show that there are differences in the heat transfer rates through the upper and lower part of the pipe wall. These differences are not increasing during the rapid gas temperature changes. This is shown in Figure 5.54.

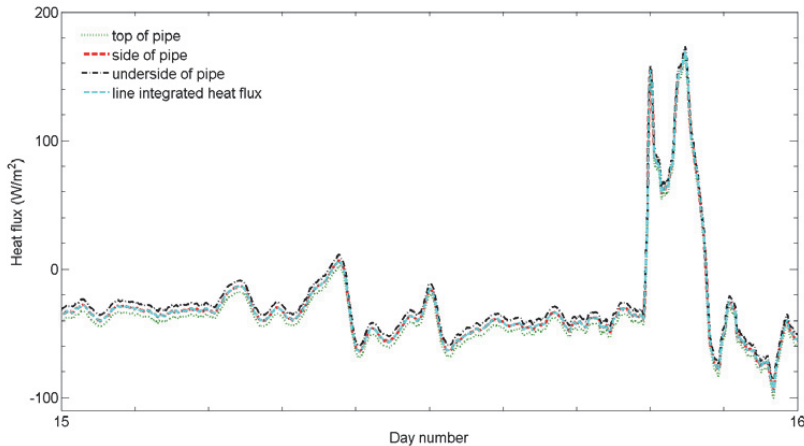


Figure 5.54: two dimensional inner pipe heat transfer: heat flux through top, side and below locations compared to line integrated heat flux at pipe inner wall (using 2D unsteady FLUENT model).

The 2D nature of the temperature profiles thus does not influence the line integrated pipe inner wall heat transfer rate significantly. The resulting heat transfer response of the 1D radial unsteady model can in such a case be expected to be very similar to that obtained with the 2D unsteady model, providing the heat transfer is dominated by heat storage in the pipe wall and the soil over a short radial distance from the pipe wall.

5.8.3 Sensitivity for thermal properties and boundary conditions

The flow model of Europipe 2 with the 1D radial unsteady heat transfer model was used to study the parameter sensitivities. The purpose was to gain an understanding of the importance of the other governing parameters of the heat transfer model. The 100 day duration simulations used a one-minute time step. The collected SCADA- and measured ambient temperature data were used as boundary conditions. For the seawater temperature, the values from the Norkyst 800 model were used. The main parameters are varied within bounds representative for the uncertainty levels they can have with the industrial models as used at Gassco AS. The parameter variation cases are shown in Table 12 and the results evaluated with respect to change in inlet pressure, the heat exchange rate at the experimental location (measurement site at Bokn), and the gas temperature and pressure at the experimental location and KP12.

Results

Table 12: Parameter variations

Ambient temperature (T_{amb})	
<u>1</u>	Measured air temperatures offset by + 2 K
<u>2</u>	Measured air temperatures offset by - 2 K
<u>3</u>	Use of daily normal air temperatures instead of real time air temperatures
<u>4</u>	Use of measured soil surface temperature instead of air temperature
Sea water temperature (T_{sea})	
<u>5</u>	Norkyst 800 model temperatures offset by + 2 K
<u>6</u>	Norkyst 800 model temperatures offset by - 2 K
<u>7</u>	Constant temperature of 280.15 K instead of Norkyst 800 temperatures
Heat transfer model equivalent soil radius (r_e)	
<u>8</u>	75% equivalent soil radius
<u>9</u>	125% equivalent soil radius
Soil thermal conductivity (λ_{soil})	
<u>10</u>	75 % of nominal value
<u>11</u>	50 % of nominal value
<u>12</u>	200 % of nominal value
Soil thermal capacitance (ρC_p)	
<u>13</u>	75 % of nominal value
<u>14</u>	50 % of nominal value
<u>15</u>	200 % of nominal value
Inner film coefficient (h_i)	
<u>16</u>	75 % of nominal value
<u>17</u>	50 % of nominal value
<u>18</u>	200 % of nominal value

Each of the output parameters were evaluated for the entire simulation period. For each case, the difference with the base case was calculated for the flow parameters. The statistical mean and maximum deviation of this difference were calculated. The results show that the gas pressure profile is not sensitive for the changes in the studied parameters (the differences are less than 0.04 bar at both the inlet and the experimental location). For each parameter change, the difference with the base case for gas temperatures, pressures and heat exchange rates all show identical trends.

Observed are two different time scales for which each parameter change affects pressure, temperature, and heat exchange rate. There is a long-term effect of a change for each parameter. This shows as a gradual change in the overall level of the difference to the base case. Superimposed upon this are larger fluctuations of short duration, coinciding with the larger changes in inlet mass flow rate and inlet temperature. For each parameter change, these fluctuations occur at the same moments in time, and are in most cases of similar shape, although overall levels and sign differ. In Figure 5.55, the pipeline gas conditions at the inlet are shown together with the effect on the gas temperature at KP12 for a selection of the most sensitive parameters. The results show a noticeable effect of all the parameters during the larger changes of the inlet mass flow rates and inlet temperature.

Results

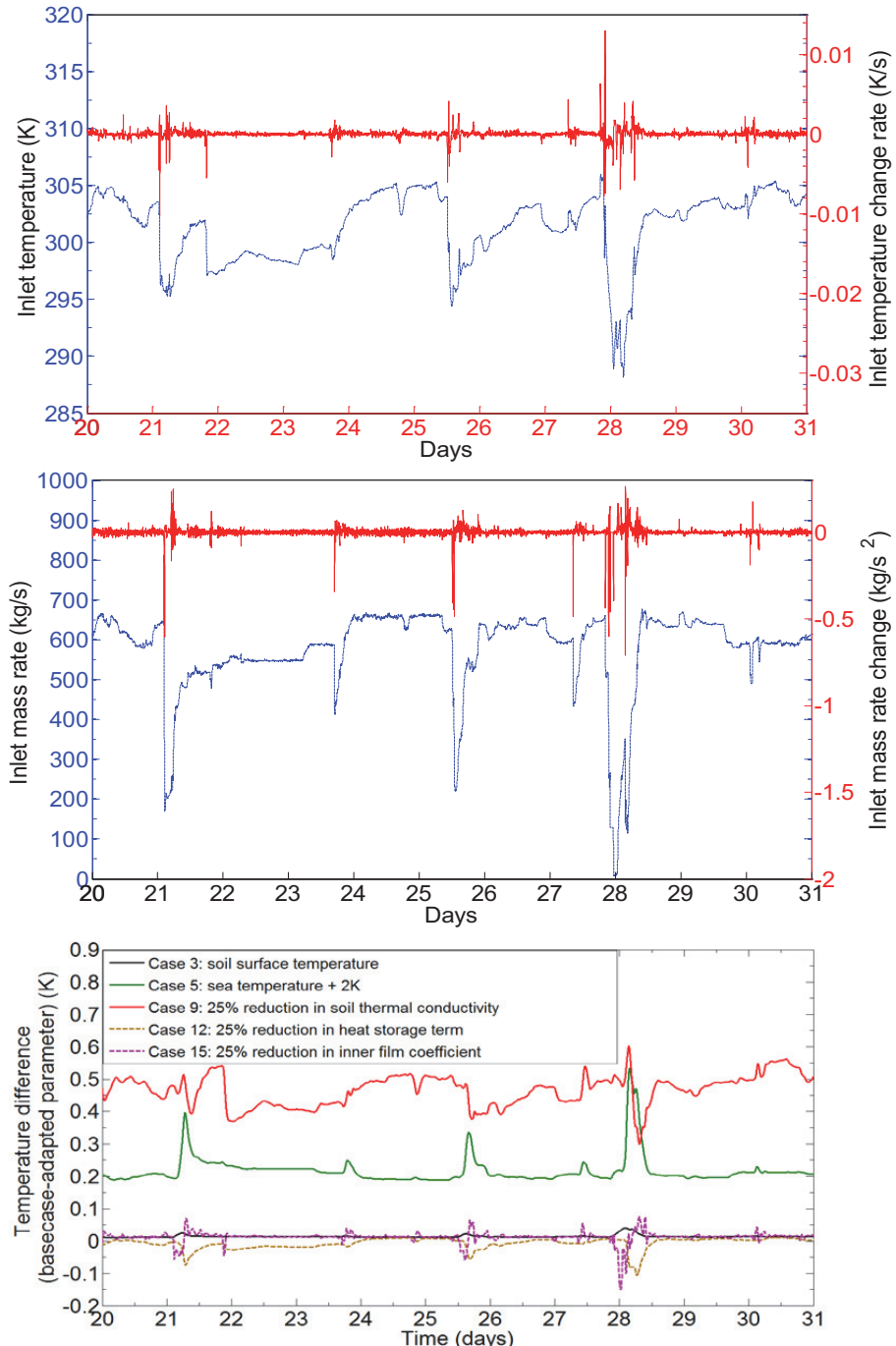


Figure 5.55: Above, inlet conditions of the pipeline. Below:difference in gas temperature at KP12 with selected changes of parameters.

Results

Appendix I shows the inner wall heat transfer and gas temperature responses for each case. The maximum difference in gas temperature for the five largest peaks were determined as well as the average difference during the 100 day period. Figure 5.56 shows the average and peak differences in gas temperature at the experimental site for each case. The results show a similar trend at KP12 (Appendix I). The average values of the gas temperature differences (both at the experimental location and the exit) between each case and the base case reflect the effect each parameter has on the levels of heat transfer and gas temperatures at a longer timescale (several months). The most significant parameter here is the soil thermal conductivity followed by the seawater temperature. The other parameters do not influence the gas temperatures nearly as much. The reason the seawater temperature has a high influence is that the subsea sections at some locations are exposed, resulting in high overall heat transfer rates. When considering the peak differences, the soil thermal conductivity and seawater temperatures are still the most important parameters. Now also the thermal capacitance and the value of the inner film coefficient become significant. The parameter sensitivity also shows that the heat transfer during quick gas temperature changes is more sensitive to the value of the soil thermal conductivity than to the soil thermal capacitance.

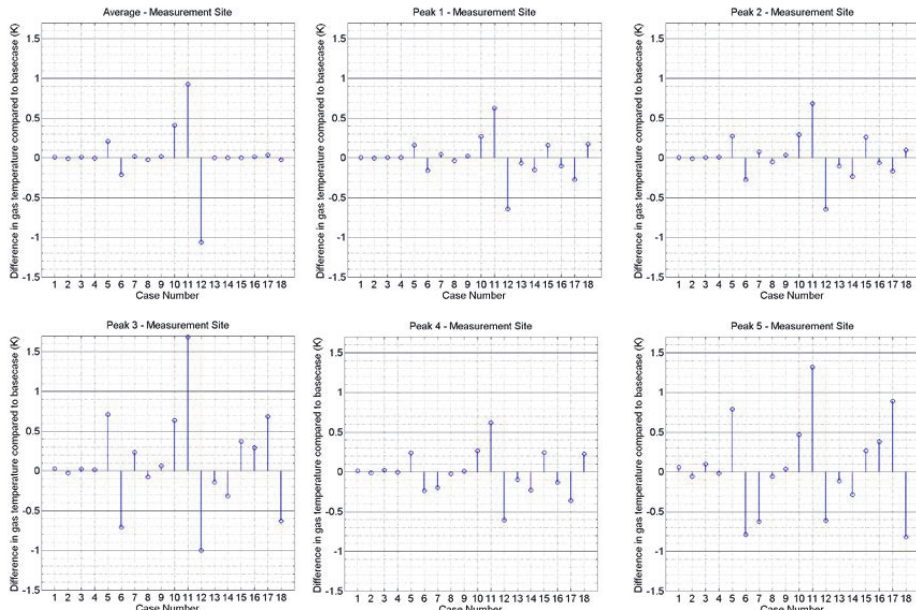


Figure 5.56: Average gas temperature difference and peak gas temperature difference between each case and the base case (at the measurement site).

At the measurement site, the effect of applying a 2K offset to the air temperature, or using soil surface temperatures as boundary condition on the heat transfer rate and gas temperature is smaller. These results are in line with expectation; the measurement site is right after an exposed subsea section. Gas temperature here is dominated by the seawater temperature. In addition, the burial depth does not have a significant effect upon heat transfer rates during transient flow. This is in line with the observation that a

Results

thin layer of soil around the pipe predominantly governs the heat transfer response to a quick gas temperature change. At the second location, KP12.2, five kilometres downstream of the measurement site, the residual effect of the seawater temperature on the gas temperature is much less. Soil thermal conductivity, seawater temperature level, and inner film coefficient values are still the dominating parameters for the peak differences. The sensitivity of the average gas temperature level for the ambient temperature level and the choice of soil surface thermal boundary condition is doubled at this location compared to the measurement location. For a significant longer section of buried pipeline, the effect the ambient temperature boundary condition on the gas temperature can be expected to be larger. A comparison with the sensitivity cases of Chapter 5.6.1 give very similar results, as shown in Figure 5.57. During the summer, a progressively increasing error in heat transfer rate is introduced by using the daily average of the measured air temperatures as boundary condition (compared to using measured soil surface temperatures). The effect on the calculated gas temperature downstream of the measurement site (KP12) in a periodic long term difference in calculated gas temperature of 0.05 K after 5 km of buried pipeline.

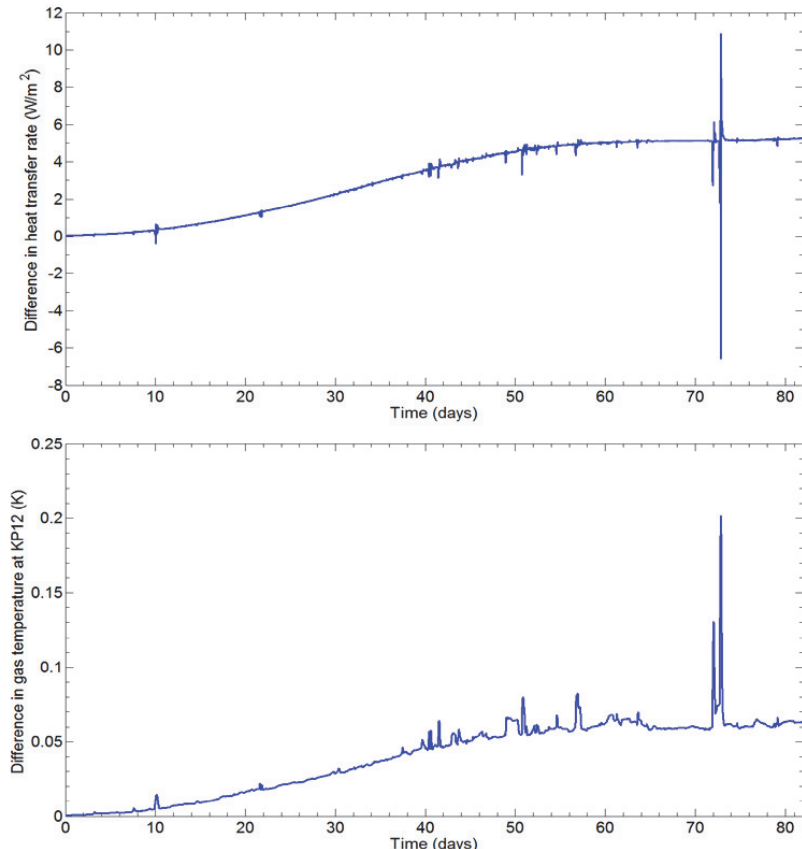


Figure 5.57: Difference in pipe wall heat transfer at experimental location and gas temperature at KP12 using the 1D radial unsteady model with air temperature.

6 Discussion

The results are discussed in this chapter. The relation with relevant results published in preceding literature will be evaluated and the implications discussed.

6.1 The characteristics of rapid flow transients

The analysis of SCADA data of the experimental pipeline case shows that a typical mass rate transient at the inlet consists of a quick drop in flow rate, followed by a slow rise to a new steady mass flow rate level (saw tooth shape). In the majority of cases a change in mass flow rate is followed by an equivalent change in gas temperature, with some exceptions where the inlet gas temperature changes independently of the inlet mass flow rate; either following the mass flow rate staying constant or showing an opposite trend. The parametric model studies were conducted with simplified step-wise approximations of both inlet mass rate and temperature transients. Studying only one transient parameter at a time allows to separate the effects and to study the pipe flow response. The results show that for both types of transients the gas temperature is affected by the choice of heat transfer model rather than the pressure. The extent and rates of change of the model transients are in the high end of the range observed with the real experimental case pipeline. The parametric model transients from Chapter 5.2 are therefore representative for the faster gas flow transients occurring in the system.

Fourier analysis of the inlet flow parameters does not show any significant periodic fluctuations. The viability to express the time varying inlet mass rate and temperature as a Fourier series is thus limited. This reduces the possibility to use exact solutions for the heat transfer problem with time dependent boundary conditions, as these are often limited to Fourier series of boundary temperatures.

6.2 The influence of the external thermal model on the accuracy of calculate gas pressure and temperature during transient flow

The results show that with transient flow conditions the choice of the external heat transfer model is far from trivial. The models that are compared are all based on the Fourier heat conduction equation. The 1D steady model is based on the one-dimensional steady form. The 1D radial unsteady model is based on heat conduction in cylindrical coordinates. The 2D unsteady model (FLUENT) is in essence a discretization of the 2D unsteady heat conduction equation.

The heat transfer response is significantly different with the 1D steady heat transfer model compared to the two unsteady heat transfer models. This is the case for both mass rate and gas temperature transients. The largest difference is in the temperature response of the gas inside the pipe. Using the 1D steady model, the gas temperature can deviate by over 10 K in response to a transient. Compared to the 1D steady model, the differences in temperature response between the 2D unsteady and the 1D radial unsteady heat transfer models are small. This is the case for both mass and temperature transients. The heat transfer behaviour of these two models was found to be similar

Discussion

independent of burial depth. The results show that only in case of a partial exposed pipe some differences in gas temperatures between the two unsteady models can be seen. Compared to the 1D steady model, these differences are still relatively minor.

Increasing the ramp time (rate of change) of the inlet transients reduces the relative difference in gas temperature response between the steady and unsteady models. The gas temperature response shows a higher sensitivity to the ramp time for a mass inlet change compared to an inlet temperature change. This is consistent with the gas temperature response to an inlet mass rate transient being rate of change dependent: the change in inlet pressure and the associated compression/decompression of the gas already inside the pipeline is much smaller with smaller rate of change of inlet mass rate. This effect of ramp time for both type of transients is as expected; the slower the rate of change, the closer the 1D steady model heat transfer behaviour is to that of the two unsteady models. The time scale of the transient needs to be close to the time the soil domain takes to go from one thermal steady state to another. Even for a shallow buried pipeline, this time scale is much larger than that of the gas temperature changes in response to the inlet transient conditions.

From the literature and the results shown in Chapter 5.2.1 and 5.8.1 it is clear that using the 1D steady heat transfer model can only provide accurate results when the pipe flow is very close to steady conditions. When the characteristics of the pipe flow become more transient, the accuracy of calculating gas temperatures and pressures reduces. In the work of Chaczykowski [35] the effect of the 1D steady versus 1D radial unsteady heat transfer model upon the calculated pipe flow parameters is demonstrated for a buried natural gas pipeline case. This pipeline case ($D=1.38\text{ m}$, $H=1.5$) is roughly comparable to the base case of the parametric studies from Chapter 5.2.1. This pipeline case is subject to rapid flow rate transients at the outlet. The results from the base case are comparable to those obtained by Chaczykowski [35]; the major difference between the two heat transfer models shows as a difference in the calculated gas temperature rather than in the gas pressures or flow rates inside the pipe. Nicholas [36] has done a similar comparison study of the 1D steady versus the 1D unsteady heat transfer model for several buried pipeline cases. Both inlet temperature and inlet pressure transients are studied. Primarily the development of the gas temperatures inside the pipe is considered and the effect on pipeline inventory. The pipeline diameter and burial depths are comparable to the base case and one-metre burial depth case of the parametric model studies. Again, the results presented are in good agreement. In both Helgaker [10] and Helgaker, Oosterkamp and Ytrehus [37], the effect of the heat transfer model is studied for the case of an exposed offshore pipeline with initial and final onshore buried sections. The effect of the 1D steady and 1D unsteady heat transfer models are compared for the same mass rate inlet transient as transient A in Chapter 5.2.1. The results are evaluated for the exit gas temperature. The gas temperature differences at the exit are similar to those obtained here (shown in Chapter 5.2.1). These results are verified in Helgaker [10] using a model of Europipe 2. The verification is done for the complete 650 km long pipeline, and during a limited period (four days). SCADA data is used and the effect of the heat transfer models is evaluated against operational gas temperature measurement at the pipeline exit. The findings of Chapter 5.6.1 are in good agreement with these results, both showing that the outlet gas temperature is sensitive

Discussion

for the choice of heat transfer model, but not the inlet pressure. During this four day period the mass rate transients are much smaller than some of these observed during the longer period of the model verification discussed in Chapter 5.1. In Helgaker [10] and Helgaker, Oosterkamp and Ytrehus [37], the evaluation of gas temperatures is at the pipeline exit after a long exposed offshore section. In this work, it is also evaluated at the end of the buried sections. The high heat transfer rate with the seawater masks much of the effect of the heat transfer model upon gas temperatures at the exit. For this reason, with the 1D steady model, the extent of the gas temperature deviations occurring during transient flow is underestimated when evaluated at the pipeline exit. All four publications do underline the necessity to include heat storage in the heat transfer model to accurately calculate gas temperatures during transient flow and the improvement that is obtained with the 1D radial unsteady model compared to the 1D steady model.

The sensitivity for the heat transfer model parameters were studied with the 1D radial unsteady model. The results show no significant sensitivity of the gas pressure to a change in the parameters of the heat transfer model. The gas temperature responds in two distinct ways to parameter changes. Firstly, there is a modest change in overall gas temperature level. This is occurring on a longer timescale (months to years). Secondly, there is a large temporary gas temperature deviation during rapid changes in gas temperature. These are occurring with the major inlet transients. The parameter sensitivity is highest for the soil thermal conductivity. A change in overall seawater temperature levels also has a significant effect. Changes in equivalent soil layer, thermal diffusivity and inner film coefficient all have smaller effect on gas temperatures. The deviation of the gas temperatures during a quick transient was found to be as high as 1.7 K when halving the soil thermal conductivity. The parameter sensitivities are in good agreement with those reported in Helgaker [10]. The soil thermal conductivity and seawater temperature were found to be the most sensitive parameters for the gas temperature (varied parameters are soil thermal conductivity, heat capacity, burial depth, burial length, air temperature and seawater temperature). The sensitivity of the gas pressure to the parameters was also Helgaker [10] found to be small.

The effect of the inner film coefficient must be noted here. During some transients, changing the inner film coefficient by 50% resulted in a gas temperature difference of 0.8 K. Even a change of 25% was found to result in temporary differences as large as 0.4 K. The Dittus-Boelter correlation is used to describe the heat transfer from the turbulent gas flow to the pipe inner wall. In the original paper from Dittus and Boelter [18] the data used as basis of the correlation shows a large spread. According to Winterton [20], the original correlation also uses two different coefficients; 0.0243 for cooling and 0.0265 for heating the fluid that are different from the coefficient of 0.023 (Equation 2.14) introduced by McAdams [19]. As discussed in Langelandsvik [8], during steady state flow, the value of the inner film coefficient is so high compared to the overall heat transfer coefficient that the uncertainty of this do not change overall heat transfer rates significantly. With an unsteady thermal model and quick changes in gas temperature, the instantaneous heat flux at the pipe inner wall is so large that the inner film coefficient starts to be a sensitive parameter. This will particularly be the case with during a large drop in mass flow rate. The value of the inner film coefficient will then be relatively low (it is directly correlated to the Reynolds number of the flow)

Discussion

while the heat transfer rate is highest. Another issue is that the Dittus-Boelter correlation uses the isobaric specific heat (in the Prandtl number) to calculate the film coefficient representing the wall heat transfer between the pipe wall and the turbulent gas. The pipe flow calculations use an energy equation based on internal energy and therefore uses the isochoric heat capacity. It would be interesting to explore if any differences occur with use of an energy equation based on enthalpy, and if a theoretical formulation for the film coefficient can be derived that is consistent within the framework of one dimensional pipe flow rather than the experimental value based correlation used today.

As discussed already in the previous chapter, the unsteady heat transfer models allow for heat storage of the wall and surrounding soil layers. The soil around the pipe has a combination of low thermal conductivity and high thermal capacitance. At the time scales of the gas temperature fluctuations, the soil domain has a low Fourier number, even when considering heat transfer over very small distances; the heat transfer regime is dominated by heat storage. A gas temperature change inside the pipe results in an immediate heat transfer at the pipe inner wall. Dependent on the direction of the heat transfer, heat is either stored in, or released from the pipe wall and surrounding soil at a high rate. This dampens the gas temperature response in the pipeline compared to the 1D steady model. The resulting difference in gas temperature in turn alters the gas density and thus the gas velocity. At operational pipeline pressures, the sensitivity of the gas density for temperature changes is small. The gas density affects the pressure and gas velocity changes through the value of the friction factor, which is an implicit function of the Reynolds number of the flow, and the change in hydrostatic fluid forces. With only minor gas density and velocity changes in response to a noticeable gas temperature change, the resulting gas pressure change will also be small.

The data from the soil measurements validate that the heat transfer response to quick gas temperature changes obtained with both of the unsteady models is very close to the real case and that the 1D steady model severely under-predicts the heat transfer rates between gas and ambient.

Another interesting aspect of the results is that the heat transfer behaviour of the 1D radial unsteady and 2D unsteady model is so similar for the burial cases considered. This is fortunate, because it allows the use of the easier to implement and less calculation intensive 1D radial unsteady model. Some interesting observations are made regarding the underlying causes of this:

- The thermal capacitance (ρC_p) of the pipe wall and surrounding soil is an order of magnitude higher than that of the compressed natural gas inside the pipe. The thermal capacitance of the pipe wall is around $3.5 \times 10^6 \text{ J/m}^3\text{K}$, and $2 \times 10^6 \text{ J/m}^3\text{K}$ for the soil. Natural gas at pipeline conditions (100-200 bar and 273.15-303.15 K) has a thermal capacitance of $0.2-0.8 \times 10^6 \text{ J/m}^3\text{K}$. There is thus a lot of capacity to store/release thermal energy in the pipe wall and soil compared to that of the flowing gas.
- The Fourier number of the soil layer around the pipe is very small. In response to a rapid gas temperature change the soil will store/release the

Discussion

- heat rather than conducting it further out through the soil. The time to a new thermal steady state in response to a boundary temperature change for even a thin soil layer is much larger than the time scale of the gas temperature transient.
- The thermal diffusivity of the soil is very low, thus it takes a long time for heat to diffuse through the domain. Changes at the boundary take a long time to spread throughout the domain and the temperature rate of change becomes progressively smaller with increasing distance from the boundary. With the inner boundary (the pipe inner wall) being cylindrical and with sufficient burial depth the transient heat transfer in radial direction through the soil close to the pipe will be similar in all directions. At further distance from the pipe wall, the attenuation of temperature fluctuations depends on the radial direction. Both the model and experimental results show that this does not have a significant effect upon the inner pipe wall heat transfer and the resulting gas temperatures.
 - The experimental results also confirm that heat transfer response to the quick gas temperature changes are occurring predominantly in the pipe wall and the surrounding thin layer of soil. Most of the gas temperature transients that occur on a time scale of ten hours or less have attenuated within the first 50 cm distance from the pipe wall.

For a different combination of pipeline fluid and ambient medium, the balance between the thermal properties could be less favorable and the heat transfer difference between the 1D radial unsteady and 2D unsteady model larger. This has not been investigated further in this work.

6.3 Ambient boundary condition

Often the external heat transfer models assume an isothermal boundary condition at the soil surface, using the ambient air or seawater temperature to set the boundary temperature. For the experimental case, the isothermal assumption is valid; the differences in measured temperatures at various distances from the pipe location do not show systematic differences due to the presence of the warm pipe. The experimental results do show large differences between the air temperature and soil surface temperature. The results of the investigations presented in Chapter 5.6.1 show that the use of air temperature as boundary condition has a small but noticeable effect upon the heat transfer. Ideally the full surface energy balance should be used in the heat transfer model but this not the most practical solution for industrial real time models. Using measured soil surface boundary conditions leads to almost as accurate calculation of the of the soil thermal profiles. The results do show that with the latter boundary condition, a minor over-prediction of temperatures in the upper soil layer during the summer (< 1 K) occurs. A possible cause of this is the omission of heat transfer associated with soil moisture transport and evaporation at the soil surface in the model. The results show that this does not influence the accuracy of the temperatures lower down in the soil. Using measured air temperature as soil surface boundary condition results in a time varying error in the pipe wall heat transfer. These errors are significant when compared

Discussion

to the average heat transfer over longer periods of time (10-15%), but are small in relation to the peak heat transfer rates occurring during quick gas temperature fluctuations. The results of the sensitivity studies with the verification model (first 12 km of Europipe 2) using the 1D radial unsteady heat transfer model further support the relative importance of the thermal boundary conditions. The difference in pipe inner wall heat transfer, using measured air temperature versus measured soil surface temperature for the boundary condition shows similar results. For the 5 km long buried section, the long-term gas temperature error is 0.05 K, with peak values of 0.15 K during quick gas temperature changes. This effect should thus be accounted for pipelines with significantly longer buried sections.

The results of the surface boundary condition further show that using daily averages of the measured air temperatures does not reduce further the accuracy of the heat transfer calculations. For the Gassco online models, air temperature data retrieved from meteorological stations are used to define the upper soil boundary condition. In some cases, the historical air temperature data is used. Using monthly normal temperatures does lead to additional inaccuracy of the heat transfer calculation. The use of a convective boundary condition at the soil surface (using a heat transfer coefficient between the soil surface and air temperature) does not have a significant effect upon the pipe wall heat transfer and will not solve the basic problem of using the air temperature. To obtain on average higher soil surface temperatures during the summer months, a negative, and non-physical, heat transfer coefficient is needed. Using a time varying offset, as suggested by Nofziger and Wu [84], is only viable if the year to year variation in air temperature is small. At the measurement location, the variation of the temperature in relation to the day normal is at least as high as the averaged differences between the air and soil surface temperatures. No improvement is therefore to be expected from such a method.

6.4 Ability to represent the effect of the annual ambient temperature cycle

The diffusion of the surface temperature deeper down into the soil attenuates and phase delays its cyclic variation. Particularly the annual ambient temperature cycle is still noticeable at pipeline burial depths and influences the inner pipe wall heat transfer rates. In this work, the ability of the external heat transfer models to capture this effect, and the resulting effect on calculated gas temperatures and pressures was evaluated. The results show that the both the 1D steady model and the 1D radial unsteady model cannot properly account for this, where the 2D unsteady model can. Differences in the heat transfer errors with the 1D radial unsteady model are generally 30% less than those with the 1D steady model. For a typical gas export pipeline, this has a minor effect on the calculation of gas temperatures. The gas pressures are not noticeably affected. The smallest errors occur for the case of a large diameter pipe buried in soil with low thermal conductivity and, with small amplitudes of the ambient temperature cycle. In the scope of this work, no viable solution was found to adapt the 1D radial unsteady model to obtain the same heat transfer behaviour as the 2D model in response to an annual cyclic soil surface temperature. The periodic steady approach of Barletta et al. [43] was found to give a much better match of the resulting heat transfer rates to those

Discussion

of the 2D unsteady model. The drawback of this model is that it assumes that the gas temperatures are relatively constant over time, and that the heat transfer rate is still described using an overall heat transfer coefficient (although with a time dependent sine shaped component). The heat transfer related to quick gas temperature changes is not accurately calculated with this model, as is the case with 1D radial unsteady model. For practical purposes one would prefer to use the 1D radial unsteady model, due to its good performance with respect to transient flow, and the overall small temperature errors. The parameter sensitivities do show that for other pipeline configurations, the heat transfer and resulting gas temperature errors can be sizeable. This is especially the case for small pipe diameters, high soil thermal conductivity, and large amplitude of the ambient temperature cycle. For such cases, as a suggested possible approach is to make a hybrid model combining aspects of the 1D radial unsteady model and the Barletta model, instead of using the 2D unsteady model. The concept of the hybrid model is to use the 1D radial unsteady model only for the pipe wall layers and a surrounding thin layer of soil to capture only the heat storage occurring during quick gas temperature changes. The soil surface temperature outer boundary condition of the 1D radial unsteady model is replaced by an energy boundary condition. The Barletta model can be used to provide the input for the energy boundary condition of the 1D radial model. The radius in the Barletta model is set equal to the outer radius of the 1D radial model. The thickness of the soil layer can in this hybrid model be used as tuning parameter to reduce the overall error of the gas temperature. This still untested.

6.5 Soil thermal properties

The parametric model and sensitivity studies demonstrate the importance of the soil thermal properties for the heat transfer problem and the correct calculation of the flow. This is both the case for the heat transfer response to the gas temperature transients induced by the flow transients and the time delayed propagation of the annual ambient air temperature cycle into the soil. Particularly soil thermal conductivity was found to be an important parameter; when flow conditions results in quick changes of gas temperature, changing the value of the soil thermal conductivity affects the gas temperature significantly. The value of the thermal capacitance is also important, although not to the same extent as the thermal conductivity. The same is the case for the heat transfer response to the annual ambient air temperature cycle. The agreement between the modelled soil thermal properties, measured values of soil samples and the long term onsite measurement is quite good. The continuous soil property measurements at the experimental site show that the thermal properties of both the fill sand in the ditch and the clay-like soil follow the soil moisture content. The relationship between soil moisture content and thermal properties is qualitatively similar to that obtained with the measurements on the soil samples. The measurements of soil humidity and thermal properties in the clayey soil show relatively continuous values over time, with variations within 10%. The thermal properties and soil humidity measurements in the sand surrounding the pipe are mostly constant over time. Only during the summer of 2014, there is a significant change in soil humidity, but only at the side of the pipe. The measured thermal properties at this location show a larger coinciding change. These results do indicate that thermal properties in the sand are not

Discussion

always constant over time. The measured soil thermal profiles can be quite accurately reproduced with the measurement site 2D model, using constant values for the soil thermal properties. The match between the Europipe 2 verification model and the measurement based pipe inner wall heat transfer rates and gas temperatures, using constant thermal properties show a good agreement. For the measurement period, the thermal conductivity and diffusivity are more than 10% different from the mean value during two occurrences. The effect of these occurrences upon gas temperature was not found to be significant with the verification model.

6.5.1 The role of soil moisture in gas to ambient heat transfer

In the standard external heat transfer models heat conduction is assumed the only mode of heat transfer. As discussed above, the soil moisture content affects the soil thermal properties. Movement of the moisture through the pores can also influence the heat transfer through forced and natural convection. The grain size measurements show that the clay at the experimental location has high mud content, restricting flow through the pores. The resulting low intrinsic permeability of the clay indicates that heat transfer due to soil moisture migration will be negligible. The measured intrinsic permeability values of the sand inside the ditch are within a wide range due to the uncertainty inherent in the measurement method. The measured values at the top of the range were high enough to suspect a contribution from convection heat transfer. This was investigated by model analysis. The results show that at the lower value there is no noticeable contribution of convective heat transfer. This is both the case for forced convection due to the ground water flow under the pipe as well as natural convection. At the upper value of the intrinsic permeability, the heat transfer contribution from ground water flow is still minimal, but natural convection becomes significant.

Adding natural convection heat transfer to the heat conduction 2D model from the experimental location does not significantly improve the fit to the measurements. There are therefore other sources of uncertainty underlying the deviations between modelled and measured temperatures. A complete understanding of these causes was not obtained from the investigations. Only limited information is available regarding the local geology around the pipe. The type and distribution of soil components and their thermal properties below the pipe are largely unknown and can be another cause of the deviations. It will for example make a difference to assume if bedrock is present lower down in the soil domain or not. The temperature measurements being lower than modelled at the side and below the pipe could for example be related to the bedrock level locally being much higher than for the rest of the soil domain. Local ground water movement like springs and subterranean streams can also be a source of the deviations. For a pipeline thermal model, it is not realistic to obtain this level of detail knowledge about the conditions all the way along the pipeline route, nor is this easily implemented in an external heat transfer model.

In the available literature, the effect of natural convection is primarily assessed for steady state flow conditions. Heat transfer correlations exist based upon exact solutions. These can be used to enhance the 1D steady heat transfer model. Regarding the effect of

Discussion

natural convection on the gas to ambient heat transfer, there is a reasonable agreement between the simulations and the approximated exact solution from Himsekhar and Bau [42]. Their exact solution predicts higher Nusselt numbers and quicker onset of the contribution of convective heat transfer at lower permeability values, but the overall trend is the same. For the 1D radial model, no extensions were found in the literature. In this study, the effect of porous media convection heat transfer upon the gas to ambient heat transfer could only get limited attention. How the addition of convective heat transfer to the heat conduction model affects the calculation of gas pressures, mass rates, and temperatures during transient flow was not studied systematically. How, and if, this can be represented in the 1D radial unsteady model is thus not clear. The same is the case for forced convection heat transfer due to Darcian flow of ground water. For the offshore sections of the pipeline ground water convection maybe an important aspect of the actual heat transfer problem. In case offshore sections are trenched, the trench could have been back filled with a porous medium. In some cases, offshore pipeline segments bury themselves due to sediment transport under influence of currents. In those cases, one can expect that the porous medium surrounding the pipeline will be water saturated. The flow patterns around the pipe in such case can be influenced by the residual wave action at the seabed (causing a periodical vertical pumping action of the water in the porous medium) or the effect of the tides. Forced convection due to Darcian flow of water in the soil around a pipeline, being primarily in vertical direction could have an additional dampening effect on the attenuation of the gas temperature fluctuations radially outwards from the pipe. This could possibly be emulated by using a smaller value for the soil thermal diffusivity in a ‘heat conduction only’ model. This is however at this stage speculation and requires further study.

With respect to soil moisture migration in vertical direction in the clay, the measurements show that there is a hydraulic gradient deeper down into the soil approaching saturation levels. The permeability of the clay is so small that downward movement of water into the clayey soil occurs on much larger time scale compared to the heat transfer and flow problem. This is supported by the good match between the calculated and the measured soil temperature profiles at ten meters lateral distance from the pipe wall, as shown in Chapter 5.7.1. The calculation model uses pure heat conduction heat transfer and constant thermal properties; significant vertical moisture migration would reduce the agreement of results.

6.6 Implications

Of the three external heat transfer models, the 2D unsteady model provides the best representation of the ambient heat transfer for a buried pipeline. This model provides the most correct spatial representation of the thermal domain. The 2D unsteady model also allows for physically more correct boundary conditions. The effect of soil layers/regions with different thermal properties also can easily be included. The effect of natural convection heat transfer in porous water saturated soil can be included with a porous media model as discussed in Chapter 4.4. The experience with the models used in the investigations is that where a 1D radial unsteady model uses minutes for calculating a certain case, the 2D unsteady model uses several hours. For real time

Discussion

operational control purposes, the 2D unsteady model is therefore not practical to use; the penalty on the calculation time is too large. The remaining uncertainty of other governing parameters, like soil thermal properties, local geology, and ambient temperatures is also large. These reasons limit the benefits of the 2D unsteady model over the 1D radial unsteady model regarding an accurate representation of the heat transfer. The results with the verification model show that the sensitivity for these parameters is significantly larger than for the choice between the 1D radial unsteady and 2D unsteady heat transfer model.

For transient pipe flow, the 1D radial unsteady model is thus the model of choice. The results show that this model results in a good trade-off between accurate representation of the soil heat transfer and model simplifications. The reduced computational effort outweighs the small errors introduced through the assumption of 1D radial heat transfer for a 2D geometry. The verification results show that the uncertainty in the other governing parameters can be so large that the 2D unsteady model will not provide an additional improvement on accuracy of flow calculation.

When the pipe flow conditions are very close to steady state, it is rational to use the 1D steady model. Near steady conditions occur when the time scales over which the changes in flow boundary conditions occur are at least on the same order of magnitude as the thermal time constant of the soil domain.

7 Conclusion and outlook

When calculating pipe flow in large gas networks, certain assumptions and simplifications of the pipe fluid thermal model are necessary. In this thesis, the assumptions and simplifications related to the external heat transfer part of the thermal model were studied in detail for pipelines containing buried sections.

7.1 Conclusions

The largest improvement in the accuracy of transient pipe flow calculation is achieved by using an unsteady external heat transfer model instead of a steady model. The effect of on calculated gas temperatures of using an unsteady model unsteady of a steady model is an order of magnitude larger compared to the other governing parameters of the heat transfer models. The results further show that varying the choice of model, and the parameters, only has a minor effect on the pressure profiles.

The results confirm that replacing the 1D steady model with either the 1D radial unsteady or the 2D unsteady models leads to a major improvement in accuracy of calculated gas temperatures during transient flow conditions. The differences in calculated pressures were found to be comparably minor. The results further show that using the geometrically more correct 2D unsteady model does not provide a noticeable additional improvement over the 1D radial model for a buried pipeline. Only when the pipe is partially buried (partially exposed to air or seawater), do differences in heat transfer rates and resulting gas temperatures become apparent. These differences increase with higher values of soil thermal conductivity.

The difference in heat transfer between the three external heat transfer models can be explained through the effect of heat storage in the pipe wall and soil layers upon the inner pipe wall heat transfer response. The experimental results show high instantaneous heat transfer rates between the gas and the pipe inner wall in response to a gas temperature change resulting from transient flow conditions at the pipeline inlet. The two unsteady heat transfer models are shown to accurately reproduce this response, where the 1D steady model does not. Both unsteady models allow for both conduction and storage of heat in the thermal domain. This is not the case with the 1D steady model, giving at all times the steady state conduction heat transfer rate over the entire thermal domain. This results in heat transfer rates that are an order of magnitude too small during rapid fluctuations in gas temperature. The subsequent cooling/heating of the gas, as it travels further downstream in the pipeline, is underestimated, causing noticeable deviations in the temperature profile. The validity of the 1D steady model is therefore limited to flow scenarios where changes in inlet conditions (mass rates and gas temperatures) occur at time scales of several hours to days.

Of the three external heat transfer models, only the 2D unsteady heat transfer model can accurately predict the delayed effect on the gas-to-ambient heat transfer of the annual

Conclusion and outlook

ambient temperature cycle. Both the 1D steady and 1D radial unsteady model cannot properly account for the attenuated and phase delayed effect on the gas-to-ambient heat transfer. The periodic steady heat transfer correlation from Barletta et al.[43] was found to give a good agreement with the 2D unsteady model results may be used with steady gas temperatures. For the pipe and soil configuration typical for an export gas pipeline, both the 1D steady and 1D radial unsteady model result in a small, gas temperature error while the significance of this for the calculation of the pipe flow pressures is negligible. Sensitivity analysis of the governing parameters showed that the heat transfer errors increase with decreasing pipe diameter, increased soil thermal conductivity, and larger amplitude of the ambient temperature cycle. There are therefore other pipeline configurations where the effect on gas temperatures is significant.

The energy balance at the soil surface was determined both experimentally and by modelling. This can be captured in different ways by the boundary conditions used in the thermal models. The effect of different boundary condition approaches on the temperature development and pipe inner wall heat transfer was determined. The results show that for the studied case, using measured soil surface temperatures as boundary condition is almost as accurate as using the full energy balance. A small, time varying, error in heat transfer is introduced when measured air temperatures are used to describe the soil surface boundary condition. The effect of this on the gas temperatures is minor, but could be significant for pipelines with much longer buried sections. The time resolution of these measurements is not influencing the results noticeably. No differences were found between using temperature data at five-minute intervals, and daily averages. This error is larger when historic air temperature data is used. These results warrant the conclusion that the best practical approach is to use measured daily average air temperatures for the soil surface boundary condition.

A verification model was run with one year of experimental data. The 1D radial unsteady and 1D steady model were compared to each other and against the measurement data. Regarding inlet pressures, both models result in accurate overall calculations but during large inlet mass rate transients both models result in temporary pressure differences as large as one bar to the measurements. With both models, the occurrence and magnitude of the deviations are close to each other. Therefore, these differences cannot be attributed to the choice of external heat transfer model. The cause of these pressure deviations was not identified. Regarding gas temperatures and pipe inner wall heat transfer, the results confirm the poor performance of the 1D steady model under transient flow conditions. The results also show that there are still sizeable gas temperature deviations (≈ 2 K) with the 1D radial model. These occur when the flow conditions are most transient. It is not quite clear what causes these differences. Parameter sensitivity of the 1D radial unsteady model shows that a parameter change results in a larger gas temperature change during the most transient flow events compared to when the flow is closer to steady state. The uncertainty in the model of the real soil thermal properties, burial depths, and ambient temperatures can thus be the cause of these deviations. During quick changes in gas temperature, the heat transfer rates are also sensitive for the value of the inner film coefficient. The results also show that soil thermal properties are important influencing parameters of the heat transfer model. The soil thermal property measurements at the experimental location show that

Conclusion and outlook

in the sand around the pipe the thermal properties are mostly constant over time, but that occasionally a large change can occur in the sand surrounding the pipe. The results with the verification model do not show a clear correlation between these changes in thermal properties and the gas temperature deviations. The overall good fit between calculated and measured soil temperatures obtained with the 2D model of the experimental site, thus support the use of time constant thermal properties in the models.

For the experimental case, within the range of measured soil intrinsic permeability, the effect of both forced and natural convection upon gas to ambient heat transfer is small. This is bolstered by the overall good fit between calculated and measured soil temperatures obtained with the 2D model of the experimental site. This model considers heat conduction only. For pipeline cases with higher soil intrinsic permeability, the role of natural convection will play a significant role. The steady state simulation results of natural convection heat transfer are in agreement with the approximate solution from in overall trend but with lower overall values. This approximate solution of Himsekhar and Bau [42] can be used to extend the 1D steady model. How this can be further extended to the 1D radial unsteady model was not investigated in detail.

For a short period, the seawater bottom temperatures along the case study pipeline were measured. During the measurement period, there was a very good agreement between the measured seawater temperatures and the Norkyst 800 model data.

Both the parametric modelling and experimental results show that the best trade-off between complexity and functionality is achieved with the 1D radial unsteady model with constant thermal properties. Analysis of the soil temperature measurements of the experimental site shows that the heat transfer response occurs predominantly in the soil layer close to the pipe wall, supporting the validity of the assumption of 1D radial unsteady heat transfer. The experimental results show that the temporal development of soil temperature profiles around the pipe is asymmetrical. This does not affect the heat transfer rates significantly within the accuracy of the measurements and calculations. Small heat transfer errors are introduced when using the 1D radial unsteady model due to the incorrect attenuation and phase delay of the annual ambient temperature cycle. For a typical gas export pipeline case, the gas temperature errors resulting from this are small in comparison to the uncertainties in the governing parameters of the heat transfer model. For other pipeline configurations, this will have to be re-evaluated.

7.2 Outlook

Significant progress is made towards understanding of the influence of the external heat transfer model upon the accuracy of the pipe flow calculations during transient flow conditions.

The results presented here demonstrate that including the heat storage term in the heat transfer model contributes to improved accuracy of the pipe flow calculation under transient flow conditions. Using the 1D radial unsteady model instead of the 1D steady

Conclusion and outlook

model, results in a large overall improvement in the accuracy of calculated gas temperatures. Occasionally there still occur deviations of significant magnitude in calculated gas temperatures and pressures. These are in connection with rapid changes in the inlet boundary conditions. These remaining deviations may be due to the accumulative uncertainty in the other governing parameters. The results obtained so far do not indicate that the assumption of 1D radial heat transfer for an essentially 2D geometry contributes significantly to these errors. A systematic investigation into the cause of these remaining errors, and how they correlate to the inlet transients, should be undertaken. This could include a new verification of the accuracy of thermal property correlations of the gas. Of particular interest is to investigate the effect of the inner film coefficient. The used correlation for the heat transfer between pipe wall and turbulent gas flow is based on experimental data with a significant spread. In addition, there is an inconsistency; the isobaric heat capacity is used in this correlation, while the isochoric heat capacity is used in the energy equation for the flow.

More research is needed to increase the understanding of the influence of soil moisture movement upon the gas to ambient heat transfer, as this change the soil thermal properties and add convective heat transfer. The effect of soil moisture migration on pipe flow calculation during transient flow will be both relevant for buried pipes on land and subsea. A trenched subsea pipeline will be surrounded by water saturated backfilled material. For the first part of an offshore pipeline route, with gas temperatures higher than the surroundings, natural convection heat transfer may also play a role. The varying water pressure at seabed level in shallow waters due to the effect of waves and tides can also be a cause of vertical water movement in the porous medium surrounding the pipe.

8 Summary of research articles

Article [a]

J.F.Helgaker, A.Oosterkamp, T. Ytrehus. Transmission of Natural Gas through offshore pipelines- effect of unsteady heat transfer model. MekIT'13: Seventh national conference on Computational Mechanics, pages 113-131, Akademia Publishing 2013.

In this paper, the effect of a heat transfer model with soil heat storage upon gas flow calculation is studied. Compared are 1D steady versus 1D radial unsteady heat transfer models. The external heat transfer models are coupled to the flow through a term in the energy equation of the set of one-dimensional Navier Stokes equations describing the pipe flow. For a buried pipeline, the results confirm that the use a steady state heat transfer model leads to over prediction of the amplitude of quick gas temperature changes during transient flow conditions. The 1D radial unsteady model is shown to improve upon this. The results are compared against a pipe flow case from industry. In the paper, the observation is made that the 1D radial unsteady model leads to incorrect definition of the ambient boundary condition. In the one-dimensional external heat transfer model, the heat flow is assumed the same in all radial directions. One can achieve more representative boundary conditions with a two-dimensional model. The heat transfer rate from a two-dimensional model was calculated and shown to differ approximately 50% compared the 1D radial unsteady model. This can be improved upon by adjusting the assumed thickness of the soil surrounding the pipe in the 1D radial unsteady model.

Article [b]

A.Oosterkamp, J.F. Helgaker, T.Ytrehus. Modelling of natural gas pipe flow with rapid transients-case study of effect of ambient model. In Energy Procedia, 3rd Trondheim Gas Technology Conference, TGTC-3, Trondheim, 2014.

The effect of different external heat transfer models on pipe flow calculation is investigated. Studied are steady, one-dimensional unsteady and two-dimensional unsteady models of the pipe wall and soil. Flow conditions at the pipeline inlet are varied. The effects of rapid changes in gas mass flow rate and temperature at the pipeline inlet are studied. The case presented is representative for export natural gas pipelines, containing offshore and buried sections along the route. Results are compared to experimental data from an existing export natural gas pipeline. The response to an inlet gas mass rate transient is shown to be different to that of gas temperature transient at the inlet. The results demonstrate that a steady state model of the ambient and soil cannot accurately represent the ambient heat exchange when rapid transients in the inlet flow occur. The reason is that inlet flow transients result in rapid temperature changes of the gas inside the pipeline. These can only be dissipated in the surrounding pipe wall and soil at a rate determined by the thermal resistance of the entire thermal domain. For both transients, the heat exchange during transient flow is underestimated. The unsteady models allow heat storage in the pipe wall and soil resulting in higher instantaneous heat exchange rates. This dampens the temperature response of the gas inside the

Summary of research articles

pipeline in response to the inlet transient. The results show that inclusion of the soil heat storage term in the heat exchange model has a large influence on the thermal accuracy of the calculated pipe hydraulic flow subject to an inlet flow transient. The effect on pressure calculation was found to be minor. The choice between a 1D radial versus 2D unsteady heat transfer model has a much smaller impact: for this case both models shows a similar response to the transients. Significant improvements in thermal calculation accuracy of transient pipe flow can be achieved by implementing a 1D radial unsteady heat transfer model of the soil instead of the currently used steady state model. The experimental results agree; the experimental verification demonstrates the improvement potential the 1D radial unsteady model has over the steady state model. The remaining temperature deviations are related to the peaks of the gas temperature inside the pipe in response to the inlet transients.

Article [c]

J.F. Helgaker, A.Oosterkamp, L.I.Langelandsvik, T.Ytrehus. Validation of 1D Flow model for transmission of natural gas through offshore pipelines. *Journal of Natural Gas Science and Engineering*, 2014

This paper deals with the numerical models for flow in high-pressure large diameter offshore pipelines. The paper describes the effect of different models that numerically solve the governing equations for one-dimensional compressible pipe flow using implicit finite difference methods. The pipeline model case has a diameter of 1 m and length of approximately 650 km. The effect of some key physical parameters are studied, the friction factor, equation of state and heat transfer model. The results show that the selection of the equation of state is important. The newer GERG 2004 is compared to the more traditional SRK, Peng–Robinson, and BWRS equations of state. The effect of using a unsteady heat transfer model of the pipeline and surrounding soil gives improved results for the calculated gas temperature in case of transient flow conditions. The flow model is validated by using a real pipeline case, showing that calculated gas temperatures noticeably improve compared to using a steady heat transfer model.

Article [d]

F.Sund, A.Oosterkamp, S.M. Hope. Pipeline modelling – impact of ambient temperature and heat transfer modelling. ISOPE-2015, Proceedings of the Twenty-fifth (2015) International Offshore and Polar Engineering Conference, Kona, Hawaii Big Island, USA, June 21–26, 2015, vol. 2, pp. 303-309.

The impact of different methods for modelling heat transfer between a pipeline and the ambient is investigated. The differences in outlet temperatures between a steady and an unsteady heat transfer model are quantified, as well as the effects of simulating the annual oceanic temperature cycle over several years. A seasonal difference between measured and modeled outlet temperature is found. The results show that the absence of the heat storage term in the heat transfer model may only be a small contributing factor to this difference. Assuming the error is caused by inaccuracies in the ambient

Summary of research articles

temperature, the impact on the capacity is found to be between 0.1 and 0.5 %. By using an analytical model for partially buried pipelines instead of the typical model that assumes that pipelines are either fully exposed or fully buried, and by tuning the ambient temperature and the corresponding hydraulic roughness according to the outlet temperature in the steady-state simulations, increases the maximum capacity of three investigated pipelines by between 0.3 and 0.5 %. An 2D unsteady, heat transfer model was used to model the annual heat cycle in the soil surrounding a pipe. The results show that the annual temperature cycle in the ocean, is expected lead to a change in the gas temperature of approximately 0.3 K per 100 km of offshore buried pipeline, compared to using steady-state heat transfer between the gas and ocean. This indicates that incorrect modelling of the annual heat cycle in the soil surrounding a pipe can only give a minor contribution to the 1-2 K outlet temperature discrepancy seen in the three investigated subsea pipelines.

The results from the analysis of operational data, the 1D unsteady heat transfer model, and the 2D heat storage model indicates that there is a seasonal inaccuracy in the oceanographic sea bottom temperature data used as input to the pipeline simulations. This inaccuracy can be reduced by improving the oceanographic models, and by improving the input data to the oceanographic model.

Article [e]

A.Oosterkamp, T.Ytrehus, S. Galtung. ‘Effect of the choice of boundary conditions on modelling ambient to soil heat transfer near a buried pipeline’, International Journal of Applied Thermal Engineering, vol.100, pp. 367-377.

The work presented here is studied the effect of the soil surface boundary on soil temperature profiles and the heat transfer between the ambient and the gas flowing inside a buried pipeline. Measurements were made of the radiation balance, key weather data parameters, and the temperature profiles in the soil near a natural gas pipeline. The soil heat conduction has been modelled with both one- dimensional and two-dimensional models. The measurement data was used to determine the soil energy balance and the heat transfer rates between the pipe and the soil. The numerical models were used to study the effects of different boundary condition assumptions upon the calculation accuracy of the soil temperature profile. The effect of typical simplifications of the soil surface boundary conditions upon the pipe-to-soil heat transfer rate was assessed thereafter. The best prediction of the soil temperature profile is obtained by using measured soil surface temperature as boundary condition, or the full surface energy balance. A reduction in predictive accuracy occurs by using simpler boundary conditions. Forcing the top node of the model to follow the ambient air temperature provides reduces the accuracy of the temperature predictions significantly in soil surface and to a lesser extent deeper down in the soil. Using daily or monthly averaged values of the measured air temperature does not change this accuracy significantly. For the pipe-to-soil heat transfer, simplification of the boundary conditions shows a difference in the long term, ‘near steady’ level heat transfer rates. Using the ambient air temperature as soil boundary condition instead of the measured soil surface temperatures resulted in a maximum difference of 16% in pipe to soil heat transfer for our model.

Summary of research articles

Article [f]

A.Oosterkamp. ‘Modelling and Measuring Soil Thermal Properties and Soil Heat Transfer of a Natural Gas Pipeline’, Submitted to the International Journal of Polar and Offshore Engineering, September 2015.

This work presents a study on the soil heat transfer from a buried natural gas pipeline. An export gas pipeline from Norway to the continent was subject to detail investigation. The aim was to improve the understanding of the heat exchange with the surrounding soil. The spatio-temporal development of soil temperatures in response to the presence of the warmer pipe was both measured and modelled. The thermal and hydraulic properties of the soil were determined through experimental methods and physical correlations/predictive modelling. The pipeline and the surrounding soil were instrumented with an array of temperature and soil moisture sensors providing the in-situ measurements. A CFD model of the experimental set-up was developed, applying the achieved soil thermal properties and local geology. In the model, measured soil surface and pipe wall temperatures were used as time dependent boundary conditions. The transient development of the thermal regime of the soil surrounding the pipeline was compared to the actual temperature measurement values. The model was used to assess the validity of the commonly used assumption that conduction is the prevailing heat transfer model. The contribution of forced and natural convection heat transfer from ground water was also assessed. The results show that, given the thermal properties determined for the soil surrounding the instrumented section of the pipeline, a numerical calculation model using heat conduction only, can represent the soil temperatures accurately at some distance to the pipe. Close to the pipe wall, the predictions are less accurate. The role ground water plays in forced and natural convection was demonstrated and found to be of minor significance for the case at hand.

Article [g]

A.Oosterkamp, ‘Heat transfer modelling of natural gas pipe flow-effect of yearly ambient temperature cycles’, Accepted for presentation at ISOPE 2016, the Twenty-sixth International Offshore and Polar Engineering Conference, Rhodes, Greece.

Correct modelling of external heat transfer in pipe flow is important for several areas of application. Examples are pipeline transmission of hydrocarbons or underground heat exchangers. In this paper, the case of non-isothermal, one-dimensional, unsteady, compressible pipe flow of natural gas is considered. The heat transfer between the gas inside the pipeline and the ambient is dependent on both the gas temperature fluctuations and the temperature variations at the upper soil boundary. Of interest is the heat transfer across the pipe wall and the effect of soil heat storage due to the annual ambient temperature cycle on this. In the study generic pipeline models are used. The models describe full one-dimensional, unsteady, compressible flow, coupled to an external heat transfer model. Four external heat transfer models are used. The first represent pipe and soil for each one-dimensional pipe calculation element as a two-dimensional (2D) cross-section in ANSYS Fluent. The second, simpler, model is a

Summary of research articles

discretization of the one-dimensional (1D) heat conduction equation in radial coordinates. The third model is a 1D steady model representing pipe and soil thermal domain as an overall heat transfer coefficient. The fourth model is an 1D periodic steady model. With negligible thermal gradients along the pipeline, the heat transfer problem has a 2D nature. It is expected that the 1D models cannot represent heat transfer accurately due to the 2D nature of the temporal development of the temperature profiles in response to the longer-term upper soil boundary temperature fluctuations.

The errors introduced by using simplified external heat transfer models are evaluated for a range of key parameter values. The results show the sensitivity for the governing parameters as well as the resulting effect upon the gas temperature and pressure.

The results show that using a 1D steady heat transfer model gives the largest heat transfer deviation. In comparison, the 1D radial unsteady model reduces the deviations by 1/3. The deviation magnitude is most sensitive for the pipe diameter, followed by the thermal conductivity and the temperature difference between gas and environment, and the pipe radius. The resulting effect on gas temperatures for the typical gas export pipeline case is 0.2-0.3 K over a 10 km buried length. The worst case pipeline scenario shows significantly larger gas temperature differences.

References

1. C.L.M.H.Navier, *Memoire sur les lois du mouvement des fluides*. Mem. Acad. Sci. Inst. France, 1822. **6**: p. 389-440.
2. G.G.Stokes, *On the theories of the internal friction of fluids in motion*. Transactions of the Cambridge Philosophical Society, 1845. **8**: p. 287-305.
3. K.J.Devlin, *The Millennium Problems: The Seven Greatest Unsolved Mathematical Puzzles of Our Time*. 2002, New York: Basic Books.
4. S.A.Orszag, *Analytical theories of turbulence*. J.Fluid.Mech, 1970. **41**: p. 363-386.
5. A.N.Kolmogorov, *The Local Structure of Turbulence in Incompressible Viscous Fluid for Very Large Reynolds Numbers*. Dok. Akad. Nauk. SSSR, 1941. **40**(4).
6. O.C.Zienkiewicz, R.L.Taylor, and P.Nitheratsu, *The Finite Element Method for Fluid Dynamics*. 2014, Oxford: Butterworth-Heinemann.
7. M.Abbaspour and K.S.Chapman, *Non-isothermal transient flow in natural gas pipeline*. J. Appl. Mech., 2008. **75**(3): p. 0310181-0310188.
8. L.I.Langelandsvik, *Modeling of natural gas transport and friction factors for large scale pipelines*. 2008, Ph.D thesis, Norwegian University of Science and Technology, Trondheim, Norway.
9. F.Sund, A.Oosterkamp, and S.Hope, *Pipeline modeling – impact of ambient temperature and heat transfer modeling*, in *ISOPE-2015-Proceedings of The Twenty-fifth (2015) International Offshore and Polar Engineering Conference*. 2015, ISOPE: Kona, Hawaii.
10. J.F.Helgaker, *Modelling Transient Flow in Long Distance Offshore Natural Gas Pipelines*. 2013: Ph.D thesis, Norwegian University of Science and Technology, Trondheim, Norway.
11. A.R.D.Thorley and C.H.Tiley, *Unsteady and transient flow of compressible fluids in pipelines - a review of theoretical and some experimental studies*. Int. J. Heat Fluid Fl., 1987. **8**(1).
12. M.Chaczykowsky, *Sensitivity of pipeline gas flow model to the selection of Equation of State*. Chem. Eng. Res. Des., 2009: p. 1596-1603.
13. C.F.Colebrook, *Turbulent flow in pipes, with particular reference to the transition region between the smooth and rough pipe laws*. J. Inst. Civil Eng., 1939. **11**: p. 133-156.
14. K.E.Starling, *Fluid Thermodynamic Properties for Light Petroleum Systems*. 1973, Gulf Publishing Company.
15. A.L.Lee, M.H.Gonzalez, and B.E.Eakin, *The Viscosity of Natural Gas*. J. Petrol. Technol. , 1966. **18**(8).
16. C.Whitson and M.Brûle, *Phase Behaviour*, in *Monograph Vol.20*, S.o.P. Engineers, Editor. 2000.
17. D.L.Katz, et al., *Handbook of Natural gas Engineering*. 1959: McGraw Hill Book Company.
18. F.W.Dittus and L.M.K.Boelter, *Heat Transfer in Automotive Radiators of Tubular Type*. University of California Publications in Engineering, , 1930. **2**(1): p. 443-461.

References

19. W.H.McAdams, *Heat Transmission*. 2nd ed. 1942, New York: McGraw-Hill.
20. R.H.S.Winterton, *Where did the Dittus and Boelter equation come from?* . Int. J. Heat Mass Tran., 1998. **41**(4-5): p. 809-810.
21. A.Zukauskas and C.Ziugzda, *Heat transfer of a cylinder in cross flow*. 1985, New York: Hemisphere Publishing.
22. D.A.Nield and A.Bejan, *Convection in Porous Media*,. 2013, New York: Springer Science+Business Media New York.
23. M.Kaviany, *Principles of Heat Transfer in Porous Media*. 1991, New York: Springer.
24. P.J.Williams and C.W.Smith., *The frozen earth*. 1989, New York: Cambridge University Press.
25. G.Mihalakakou., et al., *On the Application of the Energy Balance Equation to Predict Ground Temperature Profiles*. Sol. Energy, 1997. **60**(3/4): p. 181-190.
26. W.R.Herb, et al., *Ground surface temperature simulation for different ground covers*. J. of Hydrol., 2008. **356**: p. 327-343.
27. M.N.Ozisik, *Boundary Value Problems in Heat Conduction*. 1968, Canada: General Publishing Company.
28. H.Bau, *Heat Losses from a Fluid Flowing in a Buried Pipe*. Int. J. Heat Mass Trans., 1982. **25**(11): p. 1621-1629.
29. C.Ouworrie, *Steady-State Heat Transfer Models For Fully and Partially Buried Pipes*, in *CPS/SPE International Oil and Gas Conference and Exhibition*. 2010, SPE: Beijing.
30. J.C.Morud and A.Simonsen, *Heat transfer from partially buried pipes*, in *16th Australasian Fluid Mechanics Conference*. 2007: Gold Coast Australia. p. 1182-1186.
31. R.A.Archer and M.J.O'Sullivan, *Models for Heat Transfer from a Buried Pipe*. SPE Journal, 1997. **2**.
32. OLGA Burial of Pipes in OLGA.
33. J.Ramsen, et al., *Important Aspects of Gas Temperature Modeling in Long Subsea Pipelines*, in *Proceedings Pipeline Simulation Interest Group*. 2009, PSIG: Galveston.
34. J.Modisette, *Pipeline Thermal Models*, in *Proceedings of the PSIG The 34th Annual Meeting*. 2002, PSIG: Portland.
35. M.Chaczykowsi, *Transient flow in natural gas pipeline-the effect of pipeline thermal model*. Applied Mathematical Modelling, 2010. **34**: p. 1051-1067.
36. E.Nicholas, *The impact of pipe and ground on pipeline temperature transients*, in *Pipeline Simulation Interest Group*. 2011, PSIG: California.
37. J.F.Helgaker, A.Oosterkamp, and T.Ytrehus, *Transmission of Natural Gas through Offshore Pipelines - Effect of Unsteady Heat Transfer Model*, in *MEKIT '13*. 2013, Tapir: Trondheim.
38. A.Barletta, et al., *Transient heat Transfer from an offshore Buried Pipeline during Start-up Working Conditions*. Heat Transfer Engineering, 2008. **29**(11): p. 942-949.
39. X.Lu, P.Tervola, and M.Viljanen, *An efficient analytical solution to transient heat conduction in a one-dimensional hollow composite cylinder*. J. Phys. A. Math. Gen., 2005. **38**: p. 10145-10155.

References

40. W.W.Martin and S.S.Sadhal, *Bounds on transient temperature distribution due to a buried cylindrical heat source* Int. J. Heat Mass Trans., 1977. **21**: p. 783-789.
41. H.Bau, *Convective heat losses from a pipe buried in a semi-infinite porous medium*. Int. J. Heat Mass Trans., 1984. **27**(11): p. 2047-2056.
42. K.Himasekhar and H.Bau, *Thermal convection associated with hot/cold pipes buried in a semi-infinite saturated porous medium*. Int. J. Heat Mass Trans., 1985. **30**(2): p. 263-273.
43. A.Barletta, et al., *Numerical study of heat transfer from an offshore buried pipeline under steady-periodic thermal boundary conditions*. Appl. Therm. Eng., 2008. **28**: p. 1168-1176.
44. Snamprogetti, *Europipe 2 and Åsgard onshore pipeline –drawing nr LC-D-82001*. 1997, Snamprogetti.
45. A.Oosterkamp, *Modelling and Measuring Soil Thermal Properties and Soil Heat Transfer of a Natural Gas Pipeline*. submitted to the International Journal of Offshore and Polar Engineering (IJOPE), 2015.
46. C.S.Campbell, et al., *Application note: Calibration and evaluation of an improved low-cost soil moisture sensor*, D. Devices, Editor.: Pullmann, USA.
47. Sensors, H.T., *TP01 Thermal Properties Sensor User Manual*, in *TP01 Manual version 0608*. Hukseflux Thermal Sensors: Netherlands.
48. Huskeflux-Thermal-Sensors, *Instruction Manual NR01 Four-ComponentNet Radiation Sensor*. 2011, Huskeflux Thermal Sensors: Delft.
49. D.A.DeVries, *The Thermal Conductivity of Soil*. Mededelingen van de Landbouw Hogeschool te Wageningen, 1952. **52**(1): p. 1-73.
50. G.S.Campbell and J.M.Normann, *An Introduction to Environmental Biophysics*. 1998, United States: Springer Science and Business Media Inc.
51. J.Westermann, *Sensitivity of permafrost*. 2010: Ph.D thesis, University of Heidelberg, Germany.
52. P.M.Huang, Y.Li, and M.E.Sumner, *Handbook of Soil Sciences: Properties and Processes*. 2011, New York: CRC.
53. DecagonDevices, *KD2 Pro Thermal Properties Analyzer*, in *Operator's Manual*. 2014, Decagon Devices inc.: Pullman, USA.
54. A.D.Ward and S.D.Trimble, *Environmental Hydrology*. 2003: CRC Press.
55. H.S.Carslaw and J.C.Jaeger, *Conduction of Heat in Solids*. 1959, Oxford: Oxford Science Publications.
56. Hukseflux-Thermal-Sensors, *User manual including thermal diffusivity and volumetric heat capacity measurement*. 2008: Netherlands.
57. ASTM-International, *Book of Standards Volume: 04/02*, in *ASTM C136-06: Standard Test Method for Sieve Analysis of Fine and Coarse Aggregates*. 2006, ASTM International: West Conshohocken USA.
58. P.C.Carman, *Fluid flow through granular beds*. T. I. Chem. Eng-Lond., 1937. **15**: p. 150-166.
59. W.David Carrier III, *Goodbye, Hazen; Hello, Kozeny-Carman*. Journ. of Geotechnical and Geoenvironmental Eng., 2003. (Tech. Notes): p. 1054-1056.
60. K.Urumović and K.Urumović-sr., *The effective porosity and grain size relations in permeability functions*. Hydrol. Earth Syst. Sc., 2014. **11**: p. 6675–6714.

References

61. K.Yazdchi, S.Srivastava, and S.Luding, *On the validity of the Carman-Konzeny equation in random fibrous media*, in *II International Conference on Particle-based Methods – Fundamentals and Applications*. 2011.
62. R.P.Cchapuis and M.Aubertin, *Predicting the coefficient of permeability of soils using the Kozeny-Carman equation*. 2003, Ecole Polytechnique de Montreal: Canada.
63. J.Aguilar, *Analysis of Grain Size Distribution and Hydraulic Conductivity for a Variety of Sediment Types with Application to Wadi Sediments*. 2013: Thesis, King Abdullah University of Science and Technology, Thuwal, Kingdom of Saudi Arabia.
64. E.Gutierrez-Miravette, *Heat Conduction in Cylindrical and Spherical Coordinates*, in *Conduction Heat Transfer*, Rensselær, Editor. 2006: Hartford. p. 14.
65. F.P.Incropera and D.P.DeWitt, *Heat and Mass Transfer*. 2002, Indiana: Wiley and sons.
66. J.Albretsen, et al., *NorKyst-800 Report No. 1: User Manual and technical descriptions*. 2011, Havforsknings Institutet: Bergen Norway.
67. A.F.Shchepetkin and J.C.McWilliams, *The Regional Ocean Modeling System: A split-explicit, free-surface, topography following coordinates ocean model*. Ocean Modelling, 2005. **9**: p. 347-404.
68. Norwegian-Meteorological-Institute. *Numerical ocean models: MI-POM*. 2014; Available from: http://met.no/Numerical+ocean+models%3A+MI-POM.b7C_w7nW3z.ips.
69. J.E.Haugen, et al. *Operasjonell Hirlam med 12km, 8km og 4km gitter*. 2011.
70. T.Løthe and A.Oosterkamp, *Cruise report from S/Y Sirene on the deployments T1 and Mooring1 – 6 near Kårstø and Bokn, Rogaland*. 2014, Uni-Research Polytec: Haugesund, Norway.
71. A.J.Wheeler and A.R.Ganji, *Introduction to Engineering Experimentation*. 1996, New Jersey: Pearson.
72. C.Ouworrie. *Steady-state Heat Transfer Models for Fully and Partially Buried Pipelines*. in *CPS/SPE International Oil & Gas Conference and Exhibition*. 2010. Beijing.
73. ANSYS, *ANSYS FLUENT Theory Guide*, in *ANSYS FLUENT Theory Guide*. 2014, ANSYS Inc.: Canonsburg PA.
74. A.Oosterkamp, J.F.Helgaker, and T.Ytrehus, *Modelling of natural gas pipe flow with rapid transients-case study of effect of ambient model in Energy Procedia* 2015, Elsevier.
75. Statoil, S.a., *Alignment Sheet Europipe 2 and Åsgard*, D.-A.-P.F.X. nnn, Editor. 1997, Snamprogetti-Statoil: Italy.
76. Statoil, *Pipeline Position, Cross Profiles and Longitudinal Profile-P105 42" Gas Export Pipeline*, D052-SO-P105-F-XY-nnn, Editor. 2011, Statoil: Stavanger.
77. J.F.Helgaker, et al., *Validation of 1D Flow Model for High Pressure Offshore Natural Gas Pipelines*. Journal of Gas Science and Engineering, 2014. **16**(January 2014): p. 44-56.

References

78. A.Oosterkamp, *Heat transfer modelling of natural gas pipe flow-effect of yearly ambient temperature cycles in accepted for presentation at ISOPE2016*. 2016, ISOPE: Rhodes, Greece.
79. NMI, *eKlima*, in www.eklima.no.
80. A.Oosterkamp, T.Ytrehus, and S.Galtung, *Experimental investigation of ambient to soil heat transfer near a buried pipeline; effect of boundary conditions on the modelling of soil temperature profiles and pipeline heat transfer*. Appl. Therm. Eng., 2016. **100**: p. 367-377.
81. A.Salazar, *Energy propagation of thermal waves*. Eur.J.Phys., 2006. **27**: p. 1349-1355.
82. Norwegian-Meteorological-Institute, *eKlima*. 2014, Norwegian Meteorological Institute: www.eklima.no.
83. M.Huysmans and A.Dassargues, *Review of the use of Peclet numbers to determine the relative importance of advection and diffusion in low permeability environments*. Hydrogeol. J., 2004.
84. D.L.Nofziger and J.Wu, *Soil Temperature Variations With Time and Depth*, in *Soil Physics*, O.S. University, Editor. 2003: Oklahoma, USA.
85. F.M.White, *Fluid Mechanics*. 2011, New York: McGraw Hill.
86. T.Ytrehus, *Gas Transport*. 2009, Norwegian University of Science and Technology.
87. T.Ytrehus, *Notat om Energiligningen i Strømningsmekanikken*. 1996.
88. T.Ytrehus and J.F.Helgaker, *Energy Dissipation Effect in the One-Dimensional Limit of the Energy Equation in Turbulent Compressible Flow* J. Fluids Eng., 2013. **135**(6).

Appendix A: Selected papers

Article [a]

**Transmission of Natural Gas through Offshore Pipelines - Effect of
unsteady heat transfer model**

J.F. Helgaker, A. Oosterkamp and T. Ytrehus

In B. Skallerud and H. Andersson, editors, MekIT'13: Seventh national conference
on Computational Mechanics, pages 113-131, Akademika Publishing 2013.

Appendix

Transmission of Natural Gas through Offshore Pipelines - Effect of unsteady heat transfer model

Jan Fredrik Helgaker^{*1,2}, Antonie Oosterkamp^{1,2} and Tor Ytrehus²

¹Polytec Research Institute, Haugesund, Norway

²Department of Energy and Process Engineering

The Norwegian University of Science and Technology, Trondheim, Norway

*e-mail: jan.fredrik.helgaker@ntnu.no

Summary Transportation of natural gas through large diameter high pressure pipelines is modeled by numerically solving the governing equations for one-dimensional compressible viscous heat conducting flow. The heat exchange between the gas and the pipeline surroundings is modeled using two different approaches. In the first case a steady state heat transfer model is investigated. This is compared to an unsteady heat transfer model which accounts for heat accumulation in the ground. Comparison of the two models show that the steady state heat transfer model over predicts the amplitude of temperature changes in the flow. Also, during large transients, a significant difference in modeled pressure and mass flow rate is observed between the two models. The models are validated using operational data from an offshore natural gas pipeline.

Introduction

Gassco is a state owned Norwegian company responsible for the operation of a network consisting of 8000 km of high pressure large diameter natural gas pipelines on the sea bed across the North Sea. Natural gas is transported from the continental shelf to processing terminals on the Norwegian mainland. After the gas has been processed and unwanted components are removed, it is fed into long export pipelines and transported to continental Europe and the UK. These pipelines on the seabed can be up to 1000 km in length. The state of the gas is only known at the inlet and outlet. Between these points one has to rely on computer models to predict the flow conditions in the pipeline. An overview of the North Sea natural gas transport system which Gassco operates is shown in Fig.1.

Gassco uses one-dimensional compressible flow models to simulate the flow of natural gas through their pipelines. These have several important applications which include designing, monitoring and operating natural gas pipelines. They are also used to predict the pipeline hydraulic capacity and are an important part of pipeline leak detection systems. Modeling the transmission of natural gas through high pressure pipelines involves finding the numerical solution to a system of initial valued partial differential equations representing continuity, momentum and energy conservation. These equations form a system of hyperbolic partial differential equations.

An overview of different numerical techniques commonly used to solve such a system of equations can be found in the base literature article by Thorley and Tiley [14]. These include the method of characteristics, finite difference, finite volume and finite element methods. Finite difference methods are the most commonly used methods to model unsteady flow in high pressure pipelines. Explicit finite difference methods are easy to implement, but allow only for small time steps due to the CFL stability criteria. Implicit finite difference methods are unconditionally stable and allow for large time steps. These are therefore often used in commercial tools. Implicit finite difference methods were used by Kiuchi [13], Abbaspour and Chapman [7] and Chaczykowski [9]. Kiuchi solves the isothermal model, which means solving the continuity and momentum equation to find the pressure and mass flow rate in the pipeline. For short

Appendix

pipelines operating at low pressures it is admissible to assume an isothermal model. However, for large pipelines operating at high pressures one has to, as shown by Osiadacz [2], solve the non-isothermal model.



Figure 1: Overview of the Norwegian natural gas transport system in the North Sea which Gassco operates. Figure courtesy of Gassco.

Modeling the correct temperature in long subsea natural gas pipelines is of great importance when predicting the pipeline hydraulic capacity [5]. Calculating the correct temperature is quite complex as there are several different terms in the energy equation which have to be modeled in approximate ways. These include the change in internal energy, Joule-Thomson effect, dissipation term and the heat exchange with the surroundings. The temperature in the pipeline depends on several thermodynamic properties which are often calculated from a real gas equation of state. The sensitivity of the pipeline gas flow model to the selection of the equation of state was investigated by Chaczykowski [8]. Modeling the heat transfer between the gas and the pipeline surroundings for offshore pipelines has typically been done by using a total heat transfer coefficient [6]. The heat transfer coefficient is found from a combination of three steps and consists of heat transfer between the gas and the inner pipeline wall, transfer through the pipe wall and transfer between the surrounding and the outer pipe wall. This is a steady state process and does not allow for heat accumulation in the ground surrounding the pipeline. In the article by Chaczykowski [9] the effect of an unsteady heat transfer model, where heat accumulation in the ground is taken into account, is investigated. This model was compared to a traditional steady state heat transfer model. It was found that a steady state heat transfer model overestimates the amplitude of the temperature changes in transient flow. The unsteady heat transfer model was only investigated for on-shore pipelines buried under the ground. Also, the inlet pressure of the pipeline considered was 8.4 MPa, which is a lot lower compared to those operated by Gassco, which can have an inlet pressure of up to 20 MPa.

The purpose of this work is to investigate the effect of the unsteady heat transfer model as suggested by Chaczykowski [9] for an offshore natural gas pipeline operating at high pressure. This model will be compared to the steady state heat transfer model which has typically been

Appendix

used for offshore pipelines. As the unsteady model is one-dimensional, the computed heat flux will be compared to that of a two-dimensional heat transfer model in order to verify the one-dimensional approximation. The models will be validated using operational data from one of Gasscos offshore natural gas pipelines.

Theory

Governing Equations

The governing equations for one-dimensional compressible viscous heat conducting flow are found by averaging the three dimensional versions over the pipe cross-section. The result is:

Continuity

$$\frac{\partial \rho}{\partial t} + \frac{\partial(\rho u)}{\partial x} = 0 \quad (1)$$

Momentum

$$\frac{\partial(\rho u)}{\partial t} + \frac{\partial(\rho u^2 + p)}{\partial x} = -\frac{f \rho u |u|}{2D} - \rho g \sin \theta \quad (2)$$

Energy

$$\rho c_v \left(\frac{\partial T}{\partial t} + u \frac{\partial T}{\partial x} \right) + T \left(\frac{\partial p}{\partial T} \right)_p \frac{\partial u}{\partial x} = \frac{f \rho u^3}{2D} - \frac{4U}{D}(T - T_a) \quad (3)$$

The continuity and momentum equations are expressed in the conservative form, while the energy equation is in the non-conservative internal energy form. In the energy equation the second term on the left hand side represents the Joule Thomson effect, which is cooling upon expansion. On the right hand side the first term is the dissipation term, which is the breakdown of mechanical energy to thermal energy. The last term is the heat exchange between the gas and the pipeline surroundings where the total heat transfer coefficient U has the usual definition

$$U = \frac{Q}{A(T - T_a)} \quad (4)$$

where Q is the heat flow, A the pipeline cross-section and T_a the ambient temperature. The density can be related to the pressure through a real gas equation of state

$$\frac{p}{\rho} = ZRT \quad (5)$$

where $Z = Z(p, T)$ is the compressibility factor. In this work the BWRS (Benedict-Webb-Rubin-Starling) [12] equation of state was used to determine the compressibility factor Z . The friction factor f can be determined from the Colebrook-White correlation [3]

$$\frac{1}{\sqrt{f}} = -2 \log \left(\frac{\epsilon}{3.7D} + \frac{2.51}{Re\sqrt{f}} \right) \quad (6)$$

where ϵ is the equivalent sand grain roughness, D the pipe inner wall diameter and Re the Reynolds number of the flow. Introducing the mass flow rate $\dot{m} = \rho u A$ and replacing the density ρ with the pressure p in Equations (1) - (3) the partial differential equations for p , \dot{m} and T are developed into

$$\frac{\partial p}{\partial t} = \left[\frac{1}{p} - \frac{1}{Z} \left(\frac{\partial Z}{\partial p} \right)_T \right]^{-1} \left(\left[\frac{1}{T} + \frac{1}{Z} \left(\frac{\partial Z}{\partial T} \right)_p \right] \frac{\partial T}{\partial t} - \frac{ZRT}{pA} \frac{\partial \dot{m}}{\partial x} \right) \quad (7)$$

Appendix

$$\begin{aligned}\frac{\partial \dot{m}}{\partial t} &= \frac{\dot{m}ZRT}{pA} \left(-2\frac{\partial \dot{m}}{\partial x} + \dot{m} \left[\frac{1}{p} - \frac{1}{Z} \left(\frac{\partial Z}{\partial p} \right)_T \right] \frac{\partial p}{\partial x} - \dot{m} \left[\frac{1}{T} + \frac{1}{Z} \left(\frac{\partial Z}{\partial T} \right)_p \right] \frac{\partial T}{\partial x} \right) \\ &- A \frac{\partial p}{\partial x} - \frac{fZRT\dot{m}|\dot{m}|}{2DAp} - \frac{pA}{ZRT} g \sin \theta\end{aligned}\quad (8)$$

$$\begin{aligned}\frac{\partial T}{\partial t} &= -\frac{\dot{m}ZRT}{pA} \frac{\partial T}{\partial x} - \frac{\dot{m}(ZRT)^2}{pAc_v} T \left[\frac{1}{T} + \frac{1}{Z} \left(\frac{\partial Z}{\partial T} \right)_p \right] \\ &\times \left(\frac{1}{\dot{m}} \frac{\partial \dot{m}}{\partial x} - \left[\frac{1}{p} - \frac{1}{Z} \left(\frac{\partial Z}{\partial p} \right)_T \right] \frac{\partial p}{\partial x} + \left[\frac{1}{T} + \frac{1}{Z} \left(\frac{\partial Z}{\partial T} \right)_p \right] \frac{\partial T}{\partial x} \right) \\ &+ \frac{f}{2c_v D} \left(\frac{ZRT|\dot{m}|}{pA} \right)^3 - \frac{ZRT}{pc_v} \frac{4U}{D} (T - T_a)\end{aligned}\quad (9)$$

The procedure of deriving Equations (7)-(9) can be found in the article by Chaczykowski [9]. In the natural gas industry, measured quantities at the pipe inlet and outlet are often pressure p and mass flow rate \dot{m} . The rewrite of Equations (7)-(9) is beneficial as the measured flow values at the boundaries can be incorporated directly into the model, opposed to Equations (1)-(3) which require density ρ and velocity u as measured values at the boundaries.

Steady state heat transfer model

Gassco currently uses a steady state heat transfer model to predict the heat exchange between the gas and the pipeline surroundings [5]. For a buried pipeline, like that in Fig.2, the heat exchange between the gas and the pipeline surroundings is a combined mode of three different heat transfer processes.

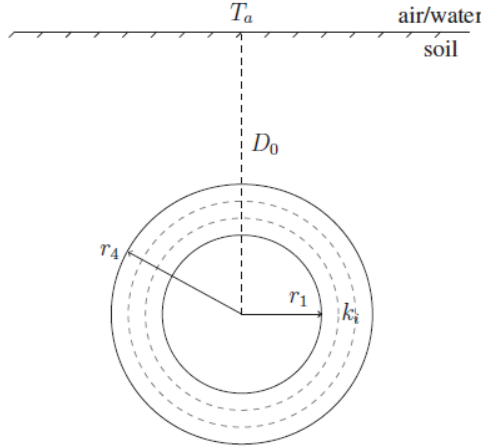


Figure 2: Cross-section of a buried pipeline consisting of three wall layers with inner radius r_1 and outer radius r_4 . Each pipe layer has its specific thermal conductivity k_i . D_0 is the burial depth from ground level to the pipe centerline. T_a is the ambient temperature of either air or water.

Appendix

The first process is the heat transfer between the gas and the inner wall, which is modeled using a film transfer coefficient determined from the Dittus-Boelter relation [4]

$$Nu = \frac{hL}{k} = 0.023 \cdot Re^{0.8} \cdot Pr^n \quad (10)$$

where Nu , Re and Pr are the Nusselt, Reynolds and Prandtl numbers respectively. h is the film transfer coefficient, L the characteristic length and k the thermal conductivity of the gas. When the gas is cooled by the ambient, $n = 0.4$, and in the reverse case $n = 0.3$. Heat transfer through the pipe wall is modeled as a conductive process. In Fig.2 the pipe wall consists of three different wall layers, each with a thermal conductivity k_i . The final process is the heat transfer between the outer wall and the surroundings which is modeled using an outer film coefficient determined from either a deep or shallow burial correlation, depending on the burial depth D_0 . To compute the total heat transfer coefficient U , each heat transfer process is assigned a thermal resistance, and the total heat transfer coefficient is equal to the sum of all thermal resistances. The following expression can be derived for the pipeline in Fig.2 [1]

$$U = \left(\frac{1}{h_i} + r_1 \frac{\ln(r_2/r_1)}{k_1} + r_1 \frac{\ln(r_3/r_2)}{k_2} + r_1 \frac{\ln(r_4/r_3)}{k_3} + \frac{r_1}{r_3 h_o} \right)^{-1} \quad (11)$$

where h_i is the inner film coefficient, h_o the outer film coefficient and k the thermal conductivity of each layer.

Unsteady heat transfer model

While the steady state heat transfer model using the total heat transfer coefficient U allows for simple calculations of the heat exchange between the pipeline and the surroundings, it does not take into account time dependent heat accumulation in the ground and in the pipe wall. In the work by Chaczykowski [9] the heat transfer from the gas to the surroundings is considered as unsteady, so that the effect of heat accumulation is taken into account. Transient heat conduction in the solid surrounding the pipeline is now modeled by solving the one-dimensional radial heat conduction equation. Assuming azimuthal symmetry, the unsteady one-dimensional heat conduction equation takes the form

$$\rho c_p \frac{\partial T}{\partial t} = \frac{k}{r} \frac{\partial}{\partial r} \left(r \frac{\partial T}{\partial r} \right) \quad (12)$$

The model is axial symmetric where each thermal layer is represented by a coaxial cylindrical shell, which is now considered as a thermal capacitor, and not a thermal resistance as in the steady heat transfer model. Fig.3 shows the half plane of the cross-section of a buried pipeline with different thermal elements. Equation (12) is discretized using an implicit finite difference scheme

$$\rho_i c_{pi} \frac{T_i^{n+1} - T_i^n}{\Delta t} = \frac{(kr)_{i-1/2}}{r_i} \left(\frac{T_{i-1}^{n+1} - T_i^{n+1}}{\Delta r^2} \right) - \frac{(kr)_{i+1/2}}{r_i} \left(\frac{T_i^{n+1} - T_{i+1}^{n+1}}{\Delta r^2} \right) \quad (13)$$

where $r_{i+1/2}$ is the radial position located halfway between r_i and r_{i+1} . ρ_i and c_{pi} is the density and heat capacity of element i , while $k_{i+1/2}$ is the heat transfer coefficient between elements $i+1$ and i . In order to couple the one-dimensional radial heat equation with the one-dimensional flow model, the heat flow Q between the gas and the inner wall is defined as

$$Q = \frac{k_0 D}{4} (T - T_1) \quad (14)$$

Appendix

where k_0 is the heat transfer coefficient between the the gas and the inner wall which, as in the steady heat transfer model, is determined by the film transfer coefficient in Equation (10). T_1 is the temperature of the first cylindrical shell in Fig.3. At the outer domain the ambient temperature T_a is set as the boundary condition. When solving the one-dimensional flow equations at a new time level, the heat flow Q from the previous time step is used in the energy equation to model the heat exchange between the gas and the surroundings. For an updated gas temperature, the radial heat equation (Equation (12)) is solved together with Equation (14) to update the temperature field around the pipeline and determine the heat flow Q between the gas and the surroundings.

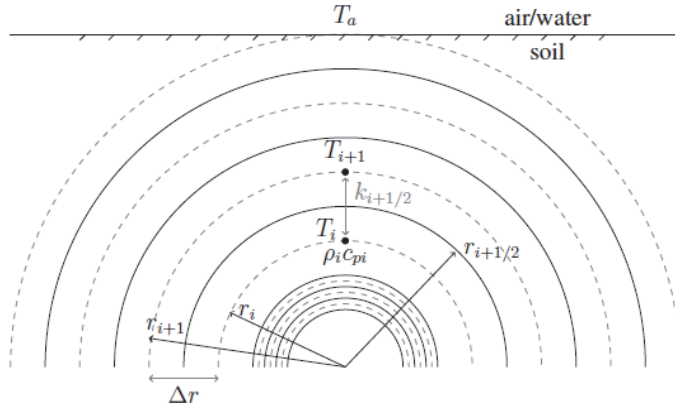


Figure 3: Half plane of the cross-section of a buried pipeline. Thermal elements are represented by coaxial cylindrical layers.

Numerical scheme

Equations (1)-(3) form a system of hyperbolic partial differential equations which have to be solved numerically. In this work an implicit finite difference scheme is used, which is preferred over an explicit scheme, as it is stable for any CFL number. Explicit methods are only stable for a CFL number less than 1. For transportation of natural gas through high pressure pipelines, the CFL number is $(u + c)\Delta t/\Delta x$, where c is the speed of sound, u the velocity of the gas and Δx and Δt the spatial and temporal step. The numerical value of $u + c$ is approximately 400 m/s. The spatial step between grid points Δx can vary, and depends on the inclination angle. For steep inclination a short Δx is required, while for little or no inclination a larger grid size may be used. In the case of an explicit method with a short grid space of $\Delta x = 100$ m, a time step of $\Delta t = 0.25$ s or less is required to ensure stability. During steady state periods one would typically use time steps much greater than this. When using an implicit method, the time step can be set to any reasonable value, regardless of what the spatial step is. This illustrates why it is advantageous to use an implicit method compared to an explicit method when modeling the flow of natural gas through long distance pipelines.

The numerical stencil is presented in Fig.4. The pipeline is divided into N grid points with Δx being the distance between points i and $i + 1$. Δt is the time step between time level $n + 1$ and n . Flow values are stored at the grid points, but are computed at the midpoint between two grid points.

Appendix

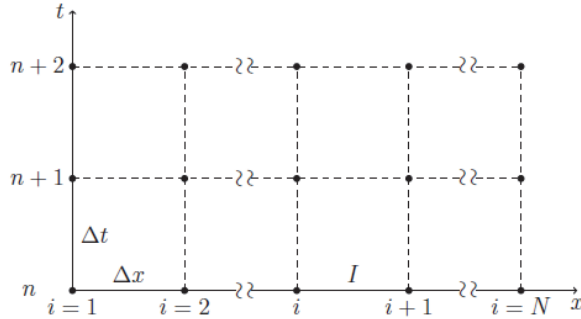


Figure 4: Stencil used in the finite difference method

For pipe section I , which is the section between points i and $i + 1$, the partial derivative of a variable Y with respect to time is approximated by

$$\frac{\partial Y(x_I, t_{n+1})}{\partial t} = \frac{Y_{i+1}^{n+1} + Y_i^{n+1} - Y_{i+1}^n - Y_i^n}{2\Delta t} + \mathcal{O}(\Delta t) \quad (15)$$

the spatial derivative by

$$\frac{\partial Y(x_I, t_{n+1})}{\partial x} = \frac{Y_{i+1}^{n+1} - Y_i^{n+1}}{\Delta x} + \mathcal{O}(\Delta x^2) \quad (16)$$

and the individual term by

$$Y(x_I, t_{n+1}) = \frac{Y_{i+1}^{n+1} + Y_i^{n+1}}{2} + \mathcal{O}(\Delta x^2) \quad (17)$$

This method is first order correct in time and second order correct in space. When discretizing all terms in a fully implicit way, the governing equations form a system non-linear equations. Solving such a system can be computationally expensive, especially for long pipelines and complicated pipe networks. To simplify the computations the non-linear terms are linearized about the previous time step to give a system of linear equations. The procedure can be found in the article by Luskin [10]. The resulting system can be solved in an efficient way using simple linear algebra. This has been done in the following.

In the case where an unsteady heat transfer model is used, the radial heat equation is solved in the solid domain surrounding the pipeline at every grid point and time step. The number of thermal elements surrounding the pipeline depends on whether the pipeline is buried under ground or exposed to sea water. For the case where the pipeline is buried under ground each wall layer is assigned a thermal element, and the surrounding soil is divided into four layers. When exposed to sea water each wall layer is assigned a thermal element, while the heat transfer between the outer wall and the sea water is modeled using a film transfer coefficient, as there is no heat accumulation in the surrounding sea water.

Results

In the following a 650 km horizontal pipeline with an inner diameter of 1.016 m will be considered. Simulations will be run for both an on-shore and offshore pipeline. Offshore pipelines

Appendix

are usually buried under the ground for the first and final lengths of the pipeline where the gas departs the processing terminal and arrives at the receiving terminal, as shown in Fig.5. This has been included in the offshore pipeline simulations.

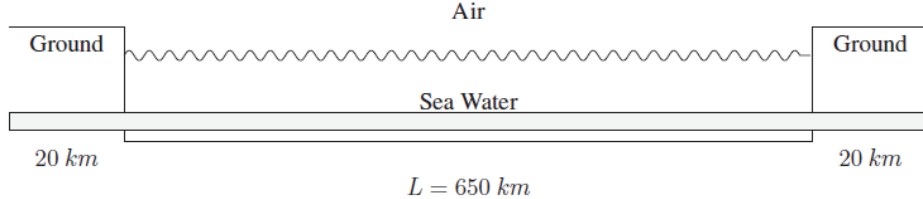


Figure 5: Offshore natural gas pipeline which is buried under ground for first and last 20 km. Pipeline is lying on seabed exposed to the sea water.

The following boundary conditions were used

$$\begin{aligned} p(L, t) &= 9 \text{ MPa} \\ T(0, t) &= 30^\circ\text{C} \\ \dot{m}(0, t) &= f(t) \text{ kg/s} \end{aligned} \quad (18)$$

where $f(t)$ is shown in Fig.6.

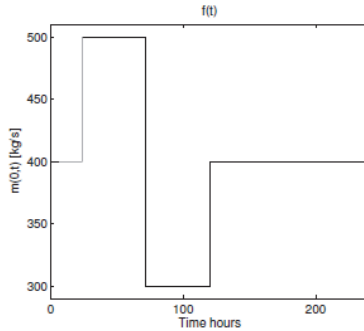


Figure 6: Inlet boundary condition for the mass flow rate.

The gas composition (in mol%) was set to: $CH_4 = 89.1704\%$, $C_2H_6 = 7.3513\%$, $C_3H_8 = 0.5104\%$, $iC_4H_{10} = 0.0251\%$, $nC_4H_{10} = 0.0311\%$, $N_2 = 0.6980\%$ and $CO_2 = 2.2209\%$. The pipe wall consists of a single steel layer with a thickness of 25 mm. The steel layer has a density of $\rho = 7850 \text{ kg/m}^3$, heat capacity $c_p = 500 \text{ J/(kg K)}$ and thermal conductivity $k = 45 \text{ W/(m K)}$. For the buried pipeline the surrounding soil was assumed to have a density of $\rho = 2650 \text{ kg/m}^3$, heat capacity of $c_p = 950 \text{ J/(kg K)}$ and thermal conductivity $k = 3 \text{ W/(m K)}$. All simulations were performed using both the steady and unsteady heat transfer model.

The pipeline was divided into 101 grid points with a grid spacing $\Delta x = 6.5 \text{ km}$. A time step of $\Delta t = 60 \text{ s}$ was used. The convergence of the numerical scheme presented in the previous

Appendix

section and the discretization errors were investigated, with the local error defined as

$$e = \frac{1}{N} \left(\sum_{i=1}^N \left(\frac{Y_i - Y_{i,hi}}{Y_{i,hi}} \right)^2 \right)^{1/2} \quad (19)$$

where Y represents p , \dot{m} and T at point i . The summation is done over all grid points N , where $Y_{i,hi}$ is the numerical solution computed using the finest grid and shortest time step (high resolution solution). Results are presented in Fig.7. The spatial discretization error as a function of grid points N is shown to the left. As the numerical method is second order correct in space, a line with slope -2 is indicated. Both the mass flow and temperature converge to order second order, while the pressure converges to an order of approximately 2.5 . The temporal discretization errors as a function of time step Δt are shown to the right in Fig.7. The numerical method is first order correct in time. Both mass flow and temperature converge to first order, while the pressure converges to an order of approximately 1.5 . The local errors for pressure, mass flow and temperature are small and results indicate that a grid consisting of 101 points and a time step of $\Delta t = 60$ s is sufficient to run simulations on long distance natural gas pipelines.

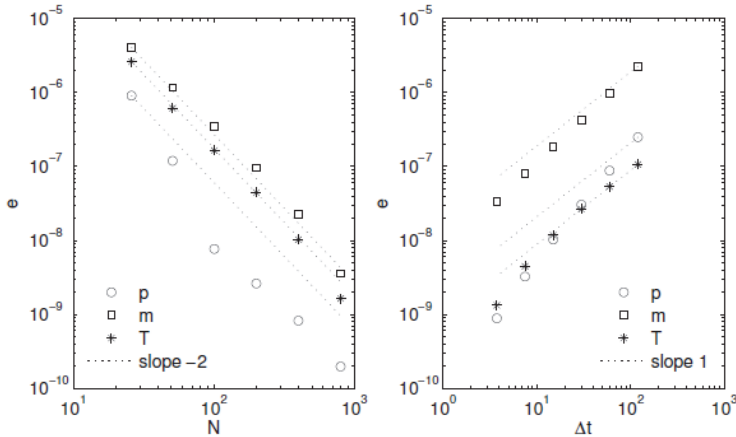


Figure 7: Local errors. Left: Local error for pressure, mass flow and temperature as a function of grid points N . Right: Local error for pressure, mass flow and temperature as a function of time step Δt .

On-shore pipeline

For the on-shore pipeline the distance from the ground surface to the pipe centerline was 2 m. The ambient air temperature was set to 5°C . Results for inlet pressure, outlet mass flow rate and outlet temperature using both the steady and unsteady heat transfer models are presented in Fig. 8. During steady state conditions there is no difference between the two solution strategies. However, when the flow conditions are transient a small difference in computed inlet pressure and outlet mass flow rate can be observed. But these differences are small compared to that of the outlet temperature which is shown at the bottom of Fig.8. During transient conditions a difference of up to 1°C was observed, with the steady state heat transfer model over predicting the amplitude of the temperature changes in the flow, which can clearly be seen in Fig. 8. At the final time step there is a small difference in outlet temperature between the two solution

Appendix

strategies. The computed outlet temperatures will eventually converge to the same value, but because the thermal response of the unsteady heat transfer model is considerably slower than that of the steady heat transfer model, the time it takes for the temperature profiles in Fig. 8 to converge is longer than the simulation time.

Offshore pipeline

The offshore natural gas pipeline schematics is shown in Fig.5. For the first and final 20 km the pipeline is buried under ground, while for the remaining part it is lying on the seabed fully exposed to the sea water. The total length is the same as for the on-shore pipeline and the boundary conditions are unchanged. The ambient air temperature is 5°C while the ambient sea bottom temperature is 4°C. Because the sea water has a high heat capacity and currents on the sea bottom constantly move the water across the pipeline, it is assumed that there is no heat accumulation in the sea water. The heat transfer from the outer pipe wall to the surrounding sea water is modeled using a film coefficient which is computed from a Nusselt-number relation. The surrounding sea water is assumed to have a velocity of 0.5 m/s across the pipeline.

Results for inlet pressure and outlet mass flow rate are almost identical to those in Fig.8 for the on-shore case. Under the given operating conditions there was no significant difference in inlet pressure and outlet mass flow using the two different heat transfer models. There was however a small difference in outlet temperature which is presented in Fig.9.

Appendix

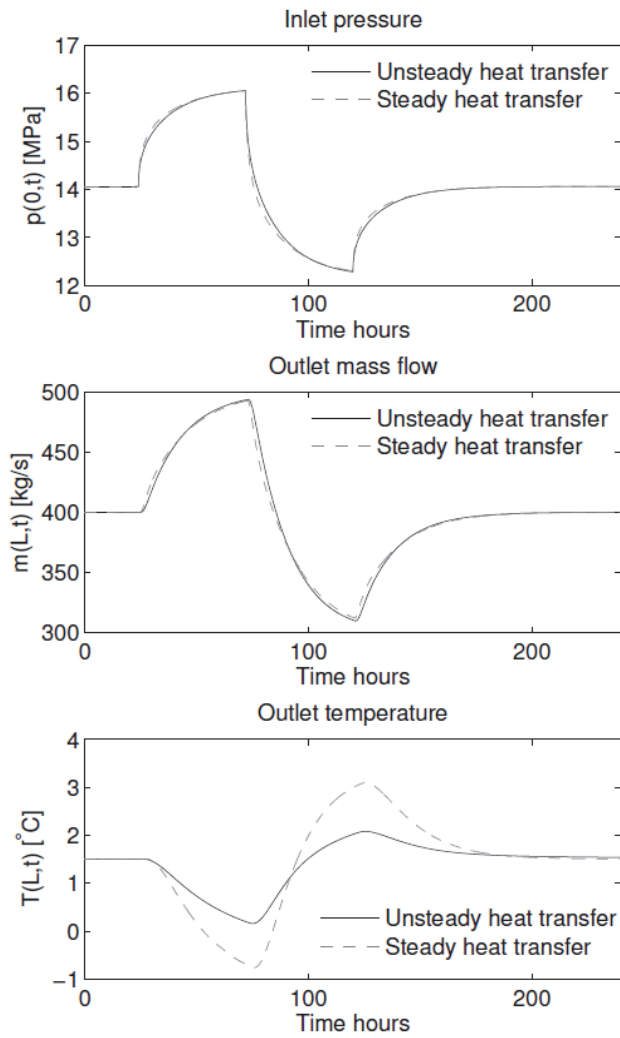


Figure 8: Results on-shore pipeline using the two different heat transfer models. Top inlet pressure, middle outlet mass flow and bottom outlet temperature. The steady heat transfer model over predicts the amplitude of temperature changes in the flow compared to the unsteady heat transfer model.

Appendix

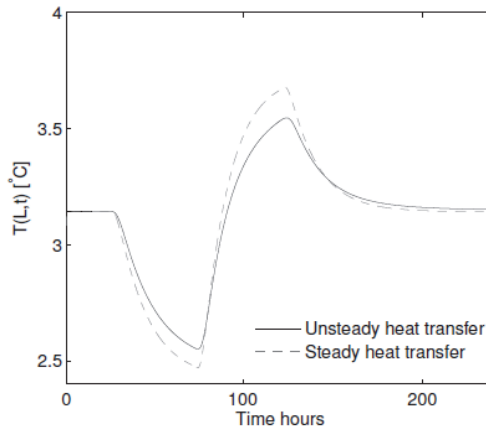


Figure 9: Outlet temperature for offshore pipeline using both unsteady and steady heat transfer model. Difference between the two temperature profiles is less than for the on-shore pipeline as there is no heat accumulation in the surrounding sea water.

Model validation

So far only a change in inlet mass flow rate has been considered, while the inlet temperature has been kept constant. In this section a change in both inlet mass flow rate and temperature will be considered. Boundary conditions are taken from operational data from a 650 km offshore pipeline operated by Gassco. The pipeline was buried under ground for the first and final 20 km. The effect of an unsteady heat transfer model on Gasscos pipelines will be investigated.

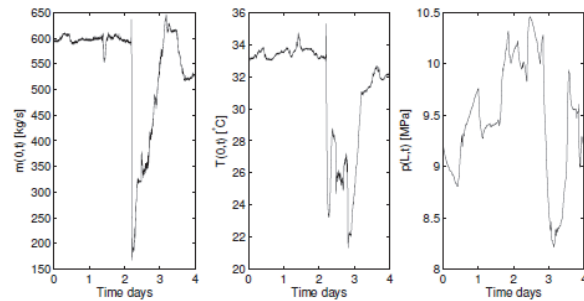


Figure 10: Boundary conditions for model validation. Left inlet mass flow, middle inlet temperature and right outlet pressure. Data courtesy of Gassco.

The pipeline diameter is approximately 1 m. The boundary conditions for outlet pressure, inlet mass flow rate and inlet temperature are given in Fig.10. After approximately 2 days a large transient occurs with a large reduction in inlet mass flow rate and temperature. The pipeline was discretized by 98 grid points with a varying Δx and $\Delta t = 60$ s. The data is from the winter season and the ambient temperature is approximately 6°C. Results are presented in Fig.11.

Appendix

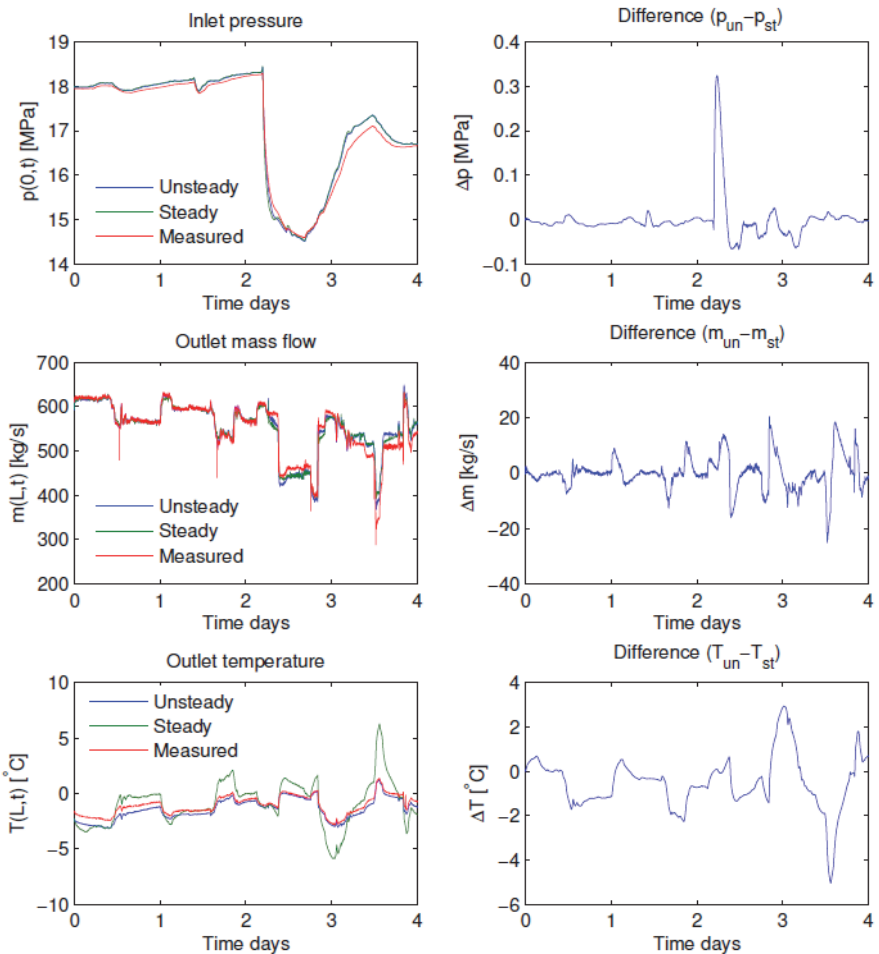


Figure 11: Results model validation. Top left: Computed inlet pressure found using unsteady and steady heat transfer model compared to measured inlet pressure. Top right: Difference inlet pressure between unsteady and steady heat transfer model. During transient a difference of 0.3 MPa can be observed. Middle left: Computed outlet mass flow using different heat transfer models compared to measured value. Middle right: Difference outlet mass flow between different heat transfer models. Bottom left: Outlet temperature using two different heat transfer models compared to measured outlet temperature. Steady heat transfer model over predicts temperature changes compared to unsteady. Bottom right: Difference outlet temperature using different heat transfer models.

Appendix

Results for inlet pressure, outlet mass flow rate and outlet temperature in Fig.11 are compared to measured values from the offshore pipeline. For the inlet pressure (top Fig.11) a small difference during steady state conditions can be observed between the unsteady and steady heat transfer model. However, during transient conditions there is a considerable difference in inlet pressure. This difference is approximately 0.3 MPa and occurs at the beginning of the transient. For the outlet mass flow small differences are seen in Fig.11, although these small differences are present during both transient and steady state conditions. In agreement with Chaczykowski [9] the steady heat transfer model over predicts the amplitude of temperature changes in the flow. This is clearly visible in the outlet temperature (bottom Fig.11). Although Chaczykowski only investigated on-shore buried pipelines, results in Fig.11 demonstrate that a steady heat transfer model also over predicts the amplitude of temperature changes in the flow for offshore pipelines. Even though the pipeline investigated here was buried under the ground only for the first and final part of the pipe length, an unsteady heat transfer model for these short pipeline sections gives improved results for the computed outlet temperature.

Discussion

Unsteady heat transfer

The reason why there is such a considerable difference in inlet pressure between the two heat transfer models in Fig.11 during the transient can be interpreted as follows. In the steady state heat transfer model the heat exchange term between the gas and the pipeline surroundings in Equation (4) is proportional to the product of the total heat transfer coefficient U and the temperature difference ($T - T_a$) between the gas and the ambient. As the ambient temperature in the model validation case was approximately 6°C and the inlet temperature in Fig.10 is never less than 20°C the temperature difference will always be positive. The total heat transfer coefficient U is also positive, implying that the heat exchange between the gas and the surroundings will always be modeled as a positive energy flux out of the pipeline. In the unsteady heat transfer model the temperature at each thermal layer is computed at every time step. After a steady state period the inner pipe wall is assumed to have the same temperature as the gas, while the outer pipe wall and soil layers further away have a lower temperature. When a transient occurs, and there is a large drop in inlet temperature like that in Fig.10, the gas temperature drops below the temperature of the inner wall. For a short period of time, before thermal equilibrium is reached, an energy flux will be transferred from the wall to the gas. By computing the temperature at each thermal layer the unsteady heat transfer model allows for energy to be transferred from the wall to the gas. This gives a higher gas temperature at points close to the inlet compared to a steady state heat transfer model, which in turn gives a higher inlet pressure during transients like the one observed in Fig.11.

The relation between heat conduction and heat storage can be determined by considering the Fourier number

$$Fo = \frac{\alpha t}{L^2} \quad (20)$$

where $\alpha = k/\rho c_v$ is the thermal diffusivity, t the characteristic time and L the characteristic length through which heat conduction occurs. For the on-shore pipeline the characteristic length is the burial depth, which is approximately 1.5 m. The time for the ramp up or ramp down to occur in Fig.8 is approximately 50 hours, and the thermal diffusivity of the soil is $1.2 \cdot 10^{-6}$ m²/s, giving a Fourier number of 0.1. The physical meaning of this is that the heat conduction rate is an order of magnitude less than the heat storage rate, and the transient thermal response upon the change in the mass flow rate is predominantly dictated by the heat storage effect, even

Appendix

on a two day time scale as is the case here. For shorter characteristic time scales, the larger the effect of heat storage compared to the effect of heat conduction. In this case, the value of the Fourier number underlines that the steady state approach for heat transfer is not valid. In such case it should be much larger than 1.

The Biot number gives the ratio of the heat transfer resistances inside of and at the surface of a body, and is defined as

$$Bi = \frac{hL}{k} \quad (21)$$

where h is the heat transfer film coefficient at the boundary of the body, L is the characteristic length and k is the thermal conductivity of the body. The Biot number determines whether or not the temperature inside a body will vary significantly in space when heated or cooled over time as a result of thermal gradients applied to its surface. For small Biot numbers (0.1 or less) the heat conduction inside the body is much faster than the heat convection at the surface, meaning that temperature gradients inside the body are negligible. For the on-shore pipeline the characteristic length L can be chosen as the volume of the body divided by the surface area. For the circular system of the pipeline buried under ground with ambient boundary condition there are two Biot numbers. At ground level, at a radius of 2 meters from the pipe centerline, the ambient temperature can be coupled with a heat transfer coefficient of 50 W/(mK). The characteristic length is $L = 4.5$ and the soil thermal conductivity $k = 3$ W/(m²K). The Biot number is then 75. On the outer pipe wall we can consider the outer film coefficient as the heat transfer coefficient, or alternatively the combined wall resistance and inner wall film coefficient. This will also give a high Biot number. These high Biot numbers show that for a change of ambient temperature and heat transfer conditions at the pipe wall, the surrounding soil will react by developing time dependent temperature gradient. This further supports the need for an unsteady heat transfer model.

One-dimensional approximation

The unsteady heat transfer model is a simple and straightforward way to include heat accumulation in the ground. However, the model does have limitations. Because it is an axial-symmetric one-dimensional model, it has symmetric boundary conditions, implying that the ambient boundary condition which is set above the pipeline is automatically set for the entire circular domain surrounding the pipeline. This is not correct, as boundary conditions on each side and below generally differ from that of the ambient temperature boundary on top. This can only be set correctly using a two-dimensional model.

To verify the computed heat flux in the one-dimensional unsteady heat transfer model it is compared to the computed heat flux from a two-dimensional model, which was made in ANSYS Fluent. In this model, the soil and pipe are represented by a 2D finite volume grid, and the calculations incorporate solving the energy equation on the solid domain. The soil domain is 50 meters deep and extends 25 meters sideways in each direction from the pipe centerline, and consisted of approximately 35000 computational cells. Symmetric boundary conditions are employed at the left and right side of the soil domain. At the bottom of the soil domain a constant temperature boundary conditions is used which is set at 10 °C. At the top of the soil domain the ambient temperature is coupled through a heat transfer coefficient of 50 W/(m²K). The gas temperature is connected to the inner wall of the pipe though the film transfer coefficient in Equation (10).

The following two cases were considered:

Appendix

- 1) Gas temperature 30 °C, ambient temperature 5 °C
- 2) Gas temperature 1.5 °C, ambient temperature 5 °C

These two cases correspond to the conditions at the inlet and outlet of the on-shore pipeline during steady state conditions. The pipe setup and thermal data are the same as in the on-shore pipeline case. For case 1, the Reynolds and Prandtl number were $3.06 \cdot 10^7$ and 0.72 respectively. For case 2 these values were $3.69 \cdot 10^7$ and 0.71 respectively. The thermal conductivity of the gas was 0.0521 W/(m K) in the first case and 0.042 W/(m K) in the second. The calculated heat flux in W/m for both cases are presented in Table.1. The computed heat flux in the 1D model was approximately 50% more than the 2D model for both case 1 and 2. The temperature field around the pipeline for case 1 and 2 is shown in Fig.12 and 13 respectively. Results in Table.1 suggest that the 1D heat transfer model under the given operating conditions predicts too large values of the heat flux between the gas and the surroundings, owing to the one-dimensional axial-symmetric assumption.

	Case 1	Case 2
1D heat transfer model	353 W/m	-49 W/m
2D heat transfer model	230 W/m	-33 W/m

Table 1: Calculated heat flux in W/m using the 1D and 2D heat transfer model. The calculated heat flux in the 1D case was approximately 50% greater than in the 2D case.

The heat flux in the one-dimensional model can be adjusted to match that of the two-dimensional model by introducing the equivalent soil radius, as is done in other compressible flow models [11]. This should be investigated in more detail for the examples shown above.

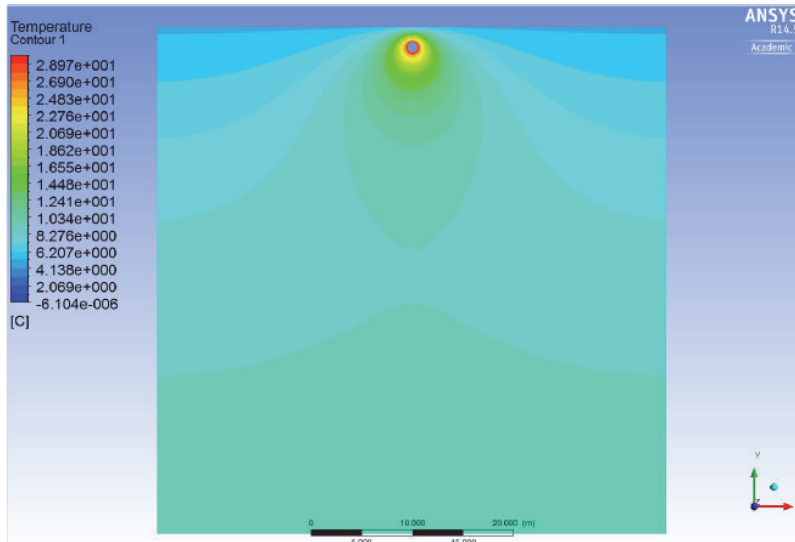


Figure 12: Contour lines for the temperature around the pipeline for case 1. The gas temperature is 30 °C and the ambient 5 °C.

Appendix

Conclusion

An unsteady heat transfer model has been compared to a steady state heat transfer model for transmission of natural gas through high pressure large diameter pipelines. This model allows for heat accumulation in the pipe wall and ground surrounding the pipeline. Results for the on-shore buried pipeline demonstrate that the steady heat transfer model over predicts the amplitude of temperature changes in the flow. The same model was applied to an offshore natural gas pipeline. Even though heat accumulation is only present at beginning and end of the pipeline where it is buried under ground, and not along the main part which is exposed to sea water, the unsteady heat transfer model still has an effect on the flow conditions in the pipeline. For large transients considerable differences were observed between the two heat transfer models. As with the on-shore pipeline, the steady state heat transfer model for offshore pipelines over predicts the amplitude of temperature changes in the flow. Also, a significant difference in modeled inlet pressure was observed between the two models under transient conditions. The computed heat flux is compared to that of a two-dimensional heat transfer model. For the considered case the one-dimensional model over predicts the heat flux by 50% compared to the two-dimensional model. In order to investigate how this affects the flow, a detailed two-dimensional heat transfer model should be used at every grid point and be compared to the one-dimensional case. The presented models were validated using operational data from an offshore natural gas pipeline. Results suggest that an unsteady heat transfer model should be used for offshore natural gas pipelines.

Acknowledgment

This work has been financed by Gassco as part of a project to improve flow modeling in off-shore natural gas pipelines. The authors would like to thank Professor Bernhard Müller (NTNU)

Appendix

and Principal Scientist Stein Tore Johansen (SINTEF Materials and Chemistry) for their guidance and feedback.

Nomenclature

c_p	heat capacity constant pressure [J/(kg·K)]
c_v	heat capacity constant volume [J/(kg·K)]
D	pipe inner wall diameter [m]
f	friction factor
g	gravitational acceleration [m/s ²]
h	film transfer coefficient [W/(m ² ·K)]
k	heat transfer coefficient [W/(m·K)]
L	characteristic length [m]
\dot{m}	mass flow [kg/s]
Nu	Nusselt number
Pr	Prandtl number
p	pressure [Pa]
Q	heat flow [W]
T	temperature [K]
T_a	ambient temperature [K]
R	gas constant [J/(kg·K)]
r	pipe radius [m]
Re	Reynolds number
t	time [s]
U	total heat transfer coefficient [W/(m ² ·K)]
u	gas velocity [m/s]
x	spatial coordinate [m]
Z	compressibility factor
α	thermal diffusivity [m ² /s]
ϵ	equivalent sand grain roughness [m]
ρ	density [kg/s]
θ	pipe inclination angle

References

- [1] A.F. Mills *Heat and Mass Transfer* Irwin, 1995.
- [2] A.J. Osiadacz, M. Chaczykowski Comparison of isothermal and non-isothermal pipeline gas flow models *Chemical Engineering Journal*, vol.81, 41–51, 2001.
- [3] C.Colebrook Turbulent flow in pipes, with particular reference to the transition region between the smooth and rough pipe laws *J. Inst. Civil Eng.*, vol.11, 133–156, 1939.
- [4] F.P. Incropera, D.P. DeWitt, T.L. Bergman, A.S. Lavine *Fundamentals of Heat and Mass Transfer* Wiley, 6 edition, 2007.
- [5] J. Ramsen, S.E. Losnegård, L.I. Langelandsvik, A.J. Simonsen, W. Postvoll Important Aspect of Gas Temperature Modeling in Long Subsea Pipelines *Proceedings to 40th PSIG Annual Meeting in Galveston Texas*, 2009.

Appendix

- [6] L.I. Langlands *Modeling of natural gas transport pipeline and friction factor for large-scale pipelines* PhD thesis, NTNU, 2008.
- [7] M. Abbaspour, K.S. Chapman Nonisothermal Transient Flow in Natural Gas Pipeline *Journal of Applied Mechanics*, vol.75, 031018-1–8, 2008.
- [8] M. Chaczykowski Sensitivity of pipeline gas flow model to the selection of the equation of state *Chemical Engineering Research and Design*, vol.87, 1596–1603, 2009.
- [9] M. Chaczykowski Transient flow in natural gas pipeline - The effect of pipeline thermal model *Applied Mathematical Modelling*, vol.34, 1051–1067, 2009.
- [10] M. Luskin An approximate procedure for non-symmetric nonlinear hyperbolic systems with integral boundary conditions *SIAM Journal on Numerical Analysis*, vol.16(1), 145–164, 1979.
- [11] SPT Group *OLGA 5 User Manual* Kjeller, Norway, 2010.
- [12] K. Starling *Fluid Thermodynamic Properties for Light Petroleum Systems* Gulf Publishing Company, 1973.
- [13] T. Kiuchi An implicit method for transient gas flows in pipe networks *International Journal of Heat and Fluid Flow*, vol.15(5), 378–383, 1994.
- [14] A.Thorley and C.Tiley Unsteady and transient flow of compressible fluid in pipelines - a review of theoretical and some experimental studies *International Journal of Heat and Fluid Flow*, vol.8(1), 3–15, 1987.

Appendix

Article [b]

Modelling of natural gas pipe flow with rapid transients-case study of effect of ambient model.

A.Oosterkamp, J.F. Helgaker, T.Ytrehus.

Energy Procedia, 3rd Trondheim Gas Technology Conference, TGTC-3,
Trondheim, 2014, vol. 64, pp. 101-110.



Available online at www.sciencedirect.com

ScienceDirect

Energy Procedia 64 (2015) 101 – 110

Energy
Procedia

3rd Trondheim Gas Technology Conference, TGTC-3

Modelling of natural gas pipe flow with rapid transients-case study of effect of ambient model

A.Oosterkamp^{a,b,*}, J.F.Helgaker^{a,b}, T.Ytrehus^b

^aPolytec Research Institute, Sørhauggate 128, 5524 Haugesund, Norway

^bNorwegian University of Science and Technology, Kolbjørn Hejes vei 1b, 7491 Trondheim, Norway

Abstract

The paper presents a study of gas pipeline to soil heat transfer. The effect of simplifications of the heat transfer model is investigated. Studied are steady, one dimensional unsteady and two dimensional unsteady models of the pipe wall and soil. Flow conditions at the pipeline inlet are varied. The effects of rapid changes in gas mass flow rate and temperature at the pipeline inlet are studied. The case presented is representative for export natural gas pipelines, containing offshore and buried sections along the route. Results are compared to experimental data from an existing export natural gas pipeline.

© 2015 The Authors. Published by Elsevier Ltd. This is an open access article under the CC BY-NC-ND license (<http://creativecommons.org/licenses/by-nc-nd/4.0/>).

Peer-review under responsibility of the Scientific Committee of TGTC-3

Keywords: pipeline transmission; pipe hydraulic flow; heat transfer; natural gas

1. Introduction

The effect of simplifications in the heat transfer model of a gas pipeline and the ambient soil is investigated. Of interest is the accuracy of hydraulic flow calculation when rapid transient flow conditions occur at the pipeline inlet. The aim of the study is to determine the relative importance of the heat storage term and the enhancement of such a non-steady heat transfer model from one dimensional radial to a two dimensional domain. The studied cases are for the same pipeline layout. Both the effects of rapid changes in mass flow rate and temperature of the gas at the pipeline inlet are studied. The pipeline case is characteristic for gas export pipelines from the Norwegian Continental Shelf. Experience with such pipelines is that during transient flow the calculation results from the models are less accurate than desired, Helgaker [1]. The transients studied in this work are changes in flow, pressure

* Corresponding author. Tel.: +47-90981031; fax: +0-000-000-0000 .

E-mail address: oosterkamp@polytec.no

and temperature due to the packing and unpacking of the pipeline originating from fluctuations in demand. Understanding the causes of the deviations during transient flow is highly significant. The network is likely to be in a transient state, steady state is the exception. Transients are occurring on the minute time scale; the period of interest to follow a single transient to the system ranges from hours to several days.

Nomenclature

σ	2H/D, H=Distance from top of soil to centerline of pipe (m), D=Internal pipediameter (m)
H_{amb}, H_{sea}	Heat transfer coefficient between thermal domain and ambient air, respectively sea (W/m ² K)
k_s	Soil thermal conductivity (W/mK)
α_s	Thermal diffusivity (m ² /s)
ρ	Density (kg/m ³)
p	Pressure (Pa)
Z	Compressibility factor
T	Temperature (K)
\dot{m}	Mass flow rate (kg/s)
u	Gas velocity (m/s)
θ	Angle of incline (pipe element)
f	Darcy-Weissbach friction factor
A	Pipeline internal cross sectional area (m ²)
x	Distance along pipeline (m)
C_v	Gas specific heat at constant volume (J/kgK)
C_p	Specific heat at constant pressure (J/kgK)
h	Enthalpy (J)
q	Rate of heat-transfer per unit time and unit mass of the gas (W/kg)
q_b	Heat flux at boundary (W)
U	Overall heat transfer coefficient to ambient (W/m ² K)
h_i	Inner wall film coefficient (W/m ² K)
h_w	Conductive term for the thermal resistance of the pipe wall layers (W/m ² K)
h_o	Film coefficient representing heat transfer to the ambience, acting on pipe outer wall (W/m ² K)
r_s	Radial thickness of soil domain (m)
r_e	Equivalent soil radius (m)
SCADA	Supervision Control And Data Acquisition
KP	Kilometer Post: distance in km from pipeline inlet

2. Modelling Case

The study uses a generic model of a natural gas pipeline representing the characteristics of export gas pipelines on the Norwegian Continental Shelf. The 40 inch carbon steel pipe has a 44 mm thick steel wall with a 6 mm outer plastic anti corrosion coating. The length of the offshore pipeline is 100 km. The pipeline elevation profile is kept horizontally level. The first and final 10 km of the pipeline is onshore and buried to a depth of 2 m (top of soil to pipe centre line). The middle section of the pipeline is lying on the seabed exposed to an ocean current. The ambient air temperature is 278.15 K. Sea water temperature is 277.15 K, the current velocity across the pipeline is 0.1 m/s. Two types of transients are studied (Figure 1). The first is a step change in mass flow rate at the pipeline entrance. Ramp-up and ramp down times are 60 seconds with several days of steady mass flow rate levels. Inlet gas temperature is kept constant. The second transient is a step change in inlet temperature (from 303.15 K to 308.15 K), while keeping the inlet mass flow constant. These transients represent extreme cases of real inlet transients. Soil thermal conductivity $k_s = 3$ W/mK and thermal diffusivity $\alpha_s = 1.2 \times 10^{-6}$ m²/s. The flow model is recently published by Helgaker [1], Langelandsvik [2], and Chazcykowski [3]. It is a compressible flow model suitable for single phase gas mixtures. The model is an implicit finite difference discretization of the Navier Stokes equations. The governing equations for one-dimensional compressible flow result from averaging the 3-dimensional equations

across the pipe cross section. The derivation of these equations is described by Helgaker [1] and Langelandsvik [2] (eq.1 to eq.3).

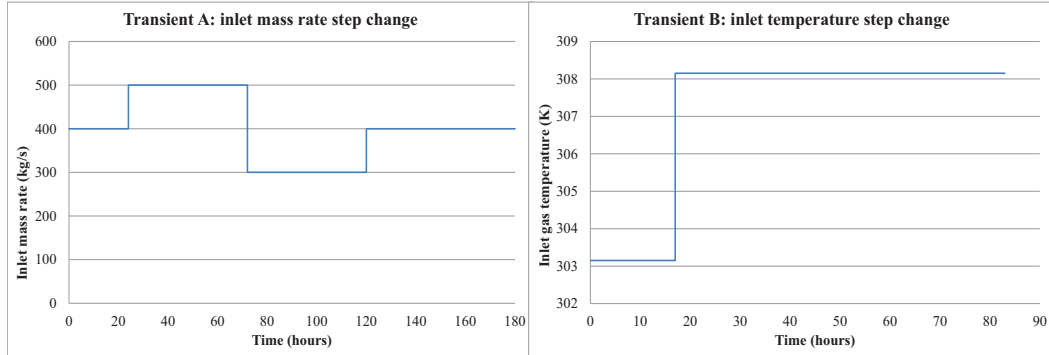


Figure 1: inlet mass flow rate and temperature transients used in the numerical study.

$$\frac{\partial \rho}{\partial t} + \frac{\partial}{\partial x} (\rho u) = 0 \quad (1)$$

$$\rho \frac{\partial u}{\partial t} + \rho u \frac{\partial u}{\partial x} = - \frac{\partial p}{\partial x} + \rho g \sin \theta - \frac{1}{2} \rho u^2 \frac{f}{D} \quad (2)$$

$$\rho C_v \left(\frac{\partial T}{\partial t} + u \frac{\partial T}{\partial x} \right) + u \left(\frac{\partial p}{\partial T} \right)_\rho \frac{\partial u}{\partial x} = \frac{f \rho u^3}{2D} - \frac{4U}{D} (T - T_a) \quad (3)$$

Heat transfer between the gas inside the pipe and the ambient is represented in the final term of the energy equation (eq. 3). Through defining q as the rate of heat-transfer per unit time and unit mass of the gas (W/kg) for the thermal exchange with the environment, the energy equation can be rewritten as:

$$\rho C_v \left(\frac{\partial T}{\partial t} + u \frac{\partial T}{\partial x} \right) + u \left(\frac{\partial p}{\partial T} \right)_\rho \frac{\partial u}{\partial x} = \frac{f \rho u^3}{2D} - \rho q \quad (4)$$

The advantage of using the energy equation in this form is that the flow domain can be coupled directly to the thermal domain by exchange of thermal energy at the pipe wall, instead of using an overall heat transfer coefficient for the entire thermal domain. It is worth noticing that the first term on the right hand side of equation 3 is the internal energy dissipation due to the turbulent wall friction of the gas while the second term represents the energy exchange with the environment. The pipe flow model uses calculation elements with a length of 1 km each. Based on previous work in Helgaker et al. [4], a grid spacing of 1 km has been shown to be sufficient when modelling the flow of gas through long distance export pipelines. The following boundary conditions apply: the inlet mass rate and temperature are specified (base line 400 kg/s and 30 °C), and at the outlet pressure is specified (9 MPa). Thermo-physical properties of the flow are calculated using the BWRS equation of state as described by Starling [5].

2.1 Heat exchange models

Three different models of the thermal domain are compared. Underlying assumption for the models is that soil heat transfer in axial direction may be neglected; radial heat transfer is dominant.

Steady state model: the steady state model is similar to the model described in Langelandsvik [2]. This model is commonly used for modelling the ambient in gas pipe flow. The heat flux from the gas in the pipeline to the ground and vice versa is represented as a single heat transfer coefficient solely based upon the thermal resistance of the pipe wall layers and the soil. The Dittus Boelter correlation shown in Incropera and DeWitt [6] is used for the inner film coefficient h_i . The conduction through the wall layers, Langelandsvik [2], can be expressed as follows:

$$h_w = \sum_{i=1}^n \ln(r_{oi} / r_{ii}) / k_i \quad (5)$$

In this formula, n is the number of wall layers, k_i is the thermal conductivity of wall layer i and r_{oi} and r_{ii} are the outer and inner radius of wall layer i respectively. The outer film coefficient h_o is based upon an exact steady state solution of 2D heat conduction equation, using the appropriate shape factor as shown in Incropera and DeWitt [6]. Another configuration is when the pipe is lying on the seabed exposed to sea water currents. In such case h_o can be expressed in terms of the Nusselt number. The correlation as proposed by Zukauskas [7] is used. The resulting expression for U is according to Langelandsvik [2]:

$$U = 1 / (1/h_i + r_i h_w + r_i / (r_o h_o)) \quad (6)$$

An assumption of equation 6 is that the soil surface boundary condition is isothermal as described in Ouvorrie [8].

1D radial unsteady model: few relevant studies about unsteady heat transfer of long buried pipelines can be found in the literature. In these studies the heat conduction through the soil is often considered as a 1D radial problem. On the other side, unsteady conductive heat transfer for the case of a hollow cylinder is studied extensively, offering exact as well as numerical solutions. Examples of pipeline specific studies, using numerical approximations, are Osiadacz [9] and Nicholas [10]. Particularly the latter work is of interest, studying the propagation of thermal fronts through a buried pipeline and the impact of neglecting the ground storage term in the heat transfer model. The work from Nicholas [10] uses a 1D radial unsteady thermal conduction model of the ambience together with a 1D pipe flow model. Here the case is made that the use of a single heat transfer coefficient may be adequate for the steady state approach but not when thermal transients are present in the pipeline. To verify this, the ground is represented as a series of concentric shells. Each shell has uniform thermal properties and the thickness of the shells increase with radial distance from the pipe. Unfortunately, this work does not fully disclose the numerical methods used to solve the ground thermal problem, but appears in approach similar to the 1D radial unsteady model presented in this paper. The conclusions of Nicholas [10] are that representing the heat flux between soil and gas as a steady state heat transfer coefficient when modelling transient pipe flow, leads to inaccuracies of gas temperatures and pipeline inventories. The initial thermal response of gas inside the pipeline is over/under predicted when a steady state thermal model is employed. Heat transfer inside the pipe wall can be ignored when time scales of flow changes are larger than 30 seconds, but not the heat capacity of the wall.

Our 1D radial unsteady model solves the 1D radial form of the unsteady heat equation using a finite difference scheme. An extensive description of this model and its coupling with the flow model is provided in Chaczykowsky [3] and Helgaker et al. [11]. The model consists of coaxial cylindrical layers surrounding the pipe. The gas temperature is coupled through the film heat transfer coefficient at the inner wall of the innermost layer (the pipe wall) and the ambient temperature is imposed as surface temperature on the outermost layer. The temperature field varies both in time and in the radial spatial dimension, but not angularly. For the transient problem, the flow parameters and the ambient heat exchange model are calculated separately during each time step. Each simulation is started by setting up a steady state flow condition and corresponding thermal gradient in the pipe wall and soil layers. The steady state is achieved by running the transient model with constant boundary conditions over a sufficient number of time steps. In each time step, the changes in the thermal model are calculated first, using the gas temperature of the previous time step as input. The resulting values for q for each pipe element are subsequently used in the flow calculation. One problem arising is how to define the total radial thickness, r_s , of the soil domain. An initial approach is to set r_s equal to the depth of burial from the top of the soil to the pipe most outer layer. As discussed in Helgaker et al [11], this approach gives a smaller thermal domain compared to the 2D case and a too short steady state conduction path. The energy exchange between gas inside the pipe and the ambience in steady

state is then overestimated. A known way to improve upon the latter is to use a so-called equivalent, or effective soil layer radius. This is for example used by the multiphase flow simulation software OLGA as documented in OLGA documentation [12]. The equivalent soil layer radius, based upon isothermal boundary conditions is:

$$r_e = 0.5D\left(\sigma + \sqrt{\sigma^2 - 1}\right) \quad (7)$$

2D unsteady model: published work of a two dimensional approach to soil heat transfer of buried pipelines are mostly limited to steady state case. Barletta et al. [13], studied the steady periodic heat transfer of buried offshore pipelines numerically. The transient case is the annual temperature variation on the seabed in shallow water. In this work the periodical non-steady heat 2D heat conduction problem is transformed and solved numerically as a steady problem. In Gu et al. [14], the effect of soil heat storage on a case of alternating hot-cold fluid entering a buried oil pipeline is modeled numerically. This paper does not clarify how the heat transfer is coupled to the flow and how oil temperatures inside the pipeline are calculated. The paper studies the effect of moisture transfer and moisture phase change upon the temperature distribution in the ground. In Barletta et al.[15], 2D unsteady heat transfer of a completely buried pipeline is investigated. Both step-rise (rapid transient) and smooth rising case (slow transient) are studied and compared with an 1D radial unsteady model. In the model, only the soil heat transfer is modelled, not the flow of the gas inside the pipe. The problem investigated is that of pipeline start-up; i.e. initially the flow is at standstill and the thermal domain at equilibrium. The start-up of flow through the pipeline is then modelled by changing the pipe wall temperatures accordingly in one 2D plane. The response of the soil domain upon the temperature change at the wall is then evaluated through the dimensionless thermal power exchange at the wall per unit length.

The contribution and novelty presented in our work is that we investigate the unsteady heat transfer for a buried pipeline using full thermal coupling between compressible fluid flow and the thermal domain over an entire pipeline length, and, using a 2D representation of the pipe wall and soil. The 2D unsteady model couples the thermal soil domain to the energy equation of the flow model similar to the 1D radial unsteady model, using the gas temperature and resulting pipe wall heat flux. For buried sections, each pipe flow calculation element has a corresponding 2D thermal model of the pipe wall and soil through the plane perpendicular to the pipe axis. The system is shown schematically in Figure 2.

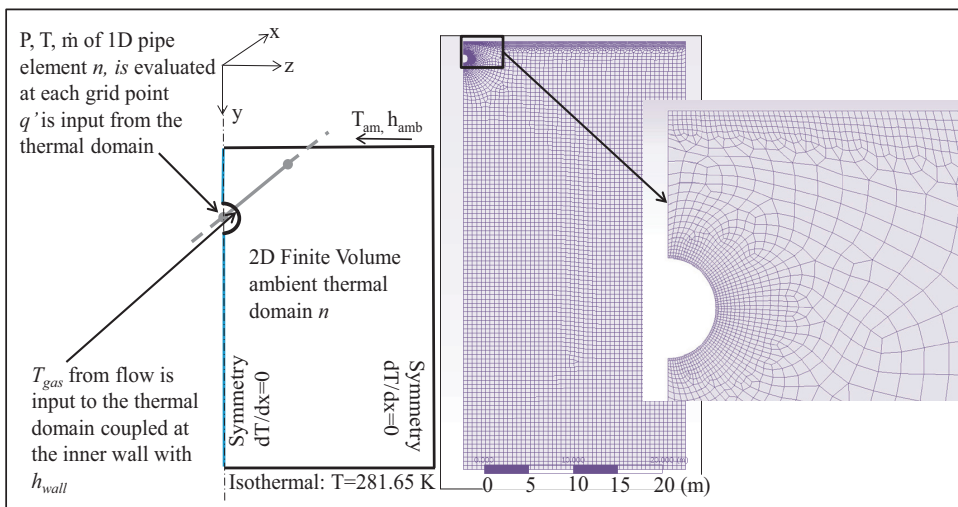


Figure 2: 2D model description and detail of finite volume grid of each soil slice.

The 2D thermal domains form 2D ‘slices’ of the soil, discretized using a Finite Volume grid with the program FLUENT. The physical dimensions of these 2D soil domains are 50*25 meters and the pipe wall layer is modelled

with perfect thermal contact to the soil. The size of the domain is chosen sufficiently large for the thermal gradients to be near zero at the vertical and lower borders. The symmetry along the y-axis is utilized to reduce the size of the model. On the lower and right hand side border of the domain, Neumann boundary conditions are employed with zero heat flux. Ambient temperature is coupled to the top border of the domain through a convective boundary condition employing heat transfer coefficient of $50 \text{ W/m}^2\text{K}$. The grid was refined until the steady state heat transfer rate at the inner wall for $T_{\text{gas}}=303.15 \text{ K}$ and $T_{\text{ambient}}=278.15 \text{ K}$ did not change more than 1% with further refinement. This was evaluated after letting the solution converge to a residual of the energy equation of $1*10^{-9}$. Only the energy equation for the solid domains is solved. In Fluent, the discretization scheme for the energy equation is second order upwind in space and first order implicit in time. The under relaxation factor for the energy equation is set to one, and the V cycle multigrid solver is used. At the pipeline inner wall, a convective heat transfer boundary condition is used. The gas temperature is defined as the fluid temperature and a fixed value for the film coefficient ($1650 \text{ W/m}^2\text{K}$). Radiative heat transfer is ignored, as gas temperatures are low. The resulting heat transfer through the boundary is calculated in Fluent [16] by summation of the net heat exchanged at each element on the boundary.

3 Results

In the pipeline scenario studied here, there are three distinct heat transfer regimes along the pipeline (as discussed in Ramsen et al.[17]. For the initial buried part (10 km), the gas is hotter than the environment; heat is transferred from gas to environment. The second part of the pipeline (80 km) is subsea and subjected to much higher heat transfer rates. The gas will cool down to ambient seawater temperature and then start to receive heat from the seawater to balance a drop in the internal energy due to the expansion of the gas (second term to the left of eq. 3) as the gas pressure drops downstream along the pipeline. At the end of the subsea part, the gas temperature will be approximately 0.5 K below the seawater temperature. The locations of interest to evaluate the response of the flow parameters upon the transients are at the end of the first buried part of the pipeline, the end of the offshore part and the pipeline exit. The case of a fully buried pipeline with $\sigma=3.58$ (soil surface to centre line of pipe is 2 m) is used. From eq. 5 and eq. 6, the overall heat transfer coefficient U is calculated to be $2.9 \text{ W/m}^2\text{K}$. The equivalent soil layer radius of the 1D radial unsteady model is 4.2 m.

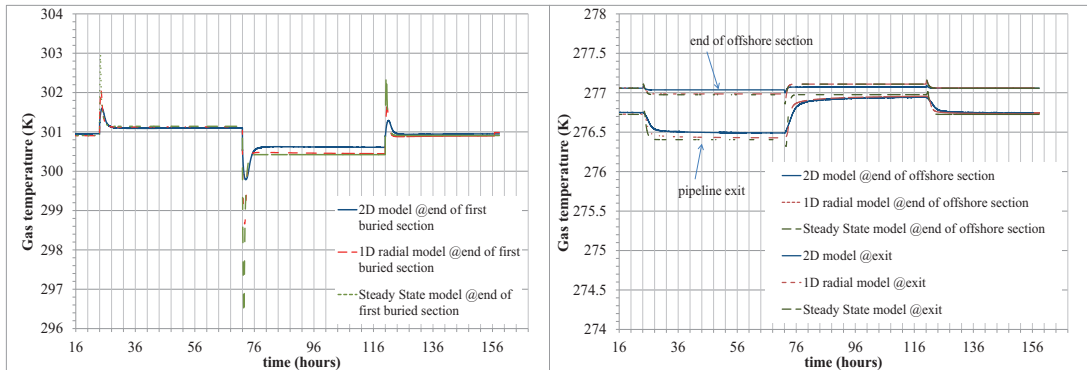


Figure 3: Left:gas temperature response on inlet mass rate transients at end of first buried section (upper three curves in left graph), end of offshore section (top three curves in right graph) and pipeline exit (lower three curves in right graph).

Figure 3 and Figure 4 show that there is a significant difference in gas temperature response to the inlet mass transients but **not** in gas pressure. In the first buried section, the difference in gas temperature between the three heat transfer models is the largest. For the second mass rate change, the difference between the steady and 2D unsteady model is as large as 4K. At the end of the offshore section, the temperature differences are much smaller, 0.3K. At the pipeline exit the differences between the models increases to 0.5 K. At the first location, the difference is 2.7 K, at the exit 1.5 K. We look in more detail at the response in the first buried part, where the differences between the models are largest. Considering the initial mass rate change (at $t=24 \text{ hrs}$), the sudden increase in inlet gas velocity

will lead to compression of the gas already inside the pipeline and thus a resulting sharp temperature increase. Initially, more gas per time unit will flow into the inlet than can flow out at the outlet (fixed outlet pressure). The pipeline inventory increases first and maximally at the pipeline inlet side and gradually declines towards the exit. The initial compression and temperature rise is than at maximum at the first buried section and declining towards the exit. This is the main reason that the spike in the temperature response at the end of the offshore section and pipeline exit is small compared to the first location. The qualitative and quantitative differences in calculated gas temperature between the 1D radial unsteady model and the 2D unsteady model are small compared to the difference with the 1D steady model. The difference between the steady and non-steady models can be explained from the heat storage capacity of the pipe wall and nearby soil layers. The difference in gas temperature response between the models can be explained as follows: For the steady state model, the U value remains constant in time. Therefore the thermal energy exchange over the pipe wall with the environment will still be governed by the term $4U/D^*(T_{\text{gas}} - T_{\text{ambient}})$. The film coefficient U is based on steady conduction throughout the entire soil domain, and has a long thermal time constant. The sudden increase in the gas temperature will result in a modest increase in the heat flux between gas and environment according to the last term in the energy equation. For the unsteady thermal models, the instant thermal response of the pipe wall and surrounding soil layers to the change in gas temperature leads to a much higher heat flux at the pipe inner wall. This inner wall heat flux is directly coupled to the heat equation, as the term $4U/D^*(T_{\text{gas}} - T_{\text{ambient}})$ is replaced with thermal energy change of the gas due to the instantaneous inner wall heat flux. The pipe wall and soil immediately around it are allowed to respond to the gas temperature change by storing the thermal energy before conducting it further out through the soil domain. This difference in energy exchange is shown in Figure 4 at the right hand side.

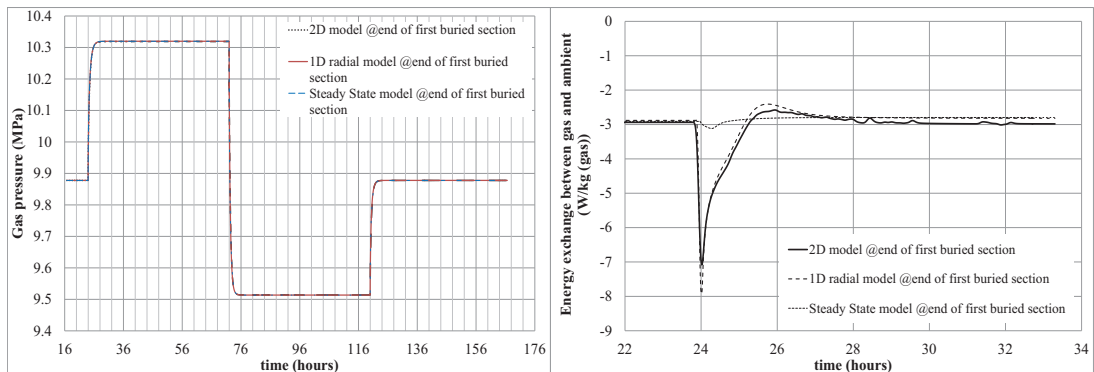


Figure 4: Right: gas pressure response to inlet mass rate transient at end of first buried section. Note that the all three models result in pressure profiles so close to each other that the lines are indistinguishable. Left: Energy exchange between gas and ambient at KP10 during the first inlet temperature transient at end of first buried section.

The difference between the models is smallest at the end of the offshore section. Because the heat transfer coefficient between the pipe and the seawater is so high, the differences in energy exchange between the models in response to the mass rate transient is reduced at this location.

For the inlet temperature transient, calculated temperature and pressure response are shown in Figure 5. The unsteady models both have a similar pressure and temperature response and show that including heat storage in the surrounding pipe wall layers and soil delay the gas temperature response following a thermal inlet transient. The energy exchange between the gas and the environment is also in this case an order of magnitude higher for the unsteady models compared with the steady model in response to the inlet temperature transient. It takes longer for the gas flowing through the pipeline to achieve a new steady state temperature at each location along the buried parts of the pipeline when ambient heat storage is allowed; the first gas at higher temperature streaming into the inlet is cooled down by the colder pipe wall and soil until these are gradually heated up to a new steady state equilibrium with the streaming gas. Again, there are no significant differences between the 1D and 2D unsteady model. The two dimensional geometrical aspect of a buried pipe is also in this transient case of limited importance compared to the effect of including the heat storage term in the thermal domain. At the end of the offshore section, the high heat

exchange rate with the seawater has cooled down to ambient the gas that entered the pipeline at higher temperature; the models therefore show no significantly different response at this location and at the exit. The response in pressure at the end of the first buried part shows a small, but noticeable pressure peak. This caused by the hotter gas entering the pipeline having a lower density. In order to maintain the same mass rate, momentarily the flow velocity increases. The new hotter gas entering the pipeline experiences some compression due to the inertia of the slower, colder gas already inside the pipeline. With the unsteady models, the hotter gas flowing into the pipeline is initially cooled down due to heat storage in the wall and soil in the first buried section, which is not the case with the steady model. This small bump in pressure is therefore less with the unsteady models. The difference amounts to 25 KPa.

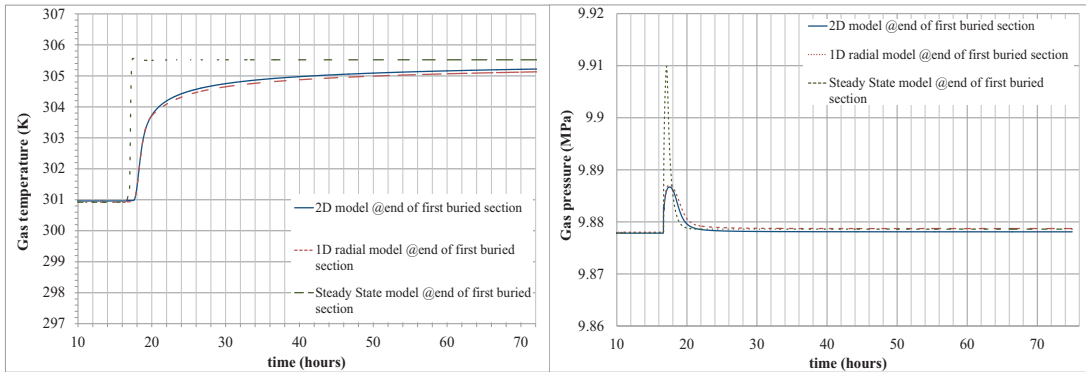


Figure 5: 2 m burial depth. Left:gas temperature response on inlet temperature transients at the end of the first buried section (upper three curves, left hand y-axis. Right: gas pressure response to inlet temperature transient at the end of the first buried section .

4 Experimental verification with real pipeline case.

The real pipeline case is that of an export gas pipeline. The 1016 mm bore pipeline has a length of 658 km (642 km is offshore). The first part of the pipeline, from inlet to the offshore landfall has been modelled using the 1D radial unsteady model. The pipeline elevation profile is shown in Figure 6.

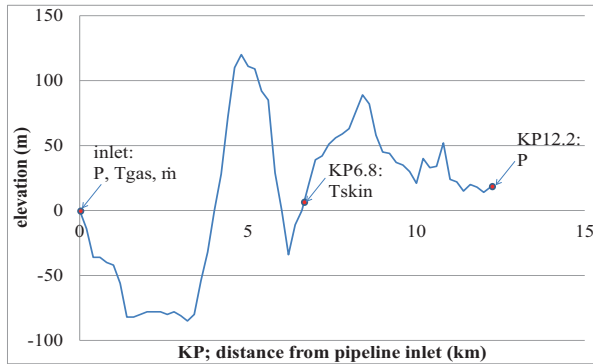


Figure 6: Pipeline elevation profile and measurement locations

For part of this route, the pipeline goes through two short subsea sections (sounds). For the majority of the subsea section, the pipeline lies buried under the seabed. On the land sections, the pipeline is buried in sand filled ditches to an average depth of 2 m. The thickness of the soil layer is based upon pipeline design and recent survey data. Real pipeline data is obtained from the SCADA system at Gassco AS at the pipeline entrance (Pressure, temperature and

flow rate) and at the offshore landfall at KP12.2 (gas pressure). Pipe skin temperature (pipe outer wall) measurement is available at KP6.8. The pipeline elevation profile is shown in Figure 6.

The following real case of Figure 7, containing both rapid inlet mass rate and inlet gas temperature changes is used in the flow model with both the 1D steady and 1D radial unsteady heat transfer model. The calculated inlet pressures from the models are compared to the measured pressure, as shown in Figure 7. With both models, the inlet pressure calculations match the measurements almost exactly. In Figure 8, the calculated skin temperature response versus measured temperature response at KP7 is shown to the left, while to the right the relative differences for both models is shown. The results clearly demonstrate the ability of the 1D radial unsteady heat transfer model to predict the gas temperatures more accurate than the steady state model in response to inlet mass rate and temperature transients. The steady state model has a maximum deviation of 2.5 K in calculated temperature in response to rapid changes in inlet conditions, with the 1D radial model this is less than 0.5 K. It is worth noticing that the temperature deviations with the steady state model are occurring because the gas temperature rises/sinks too fast in response to a transient. This is in full agreement with the results from the modelling study. The temperature deviations with the 1D radial unsteady model are over-predictions occurring at the peaks in the gas temperature inside the pipe in response to the transients at the inlet. Further study is needed to identify the cause of these peaks, e.g. inaccurate thermal properties in the model or other influencing factors like convective heat transfer due to soil moisture.

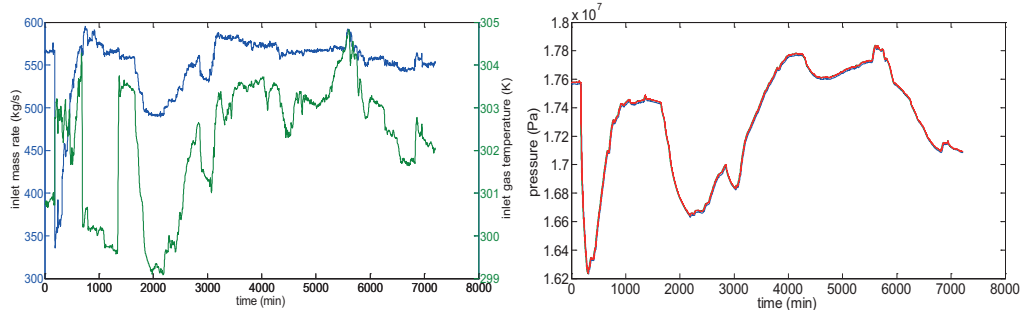


Figure 7:Left:inlet mass flow rate (blue line) and inlet temperature (green line) of real case 1. Right: inlet pressure; blue is measured, red calculated with steady state thermal model, the green line is the pressure calculated with unsteady 1D radial thermal mode; this is coinciding with that of the steady state thermal model (red line).

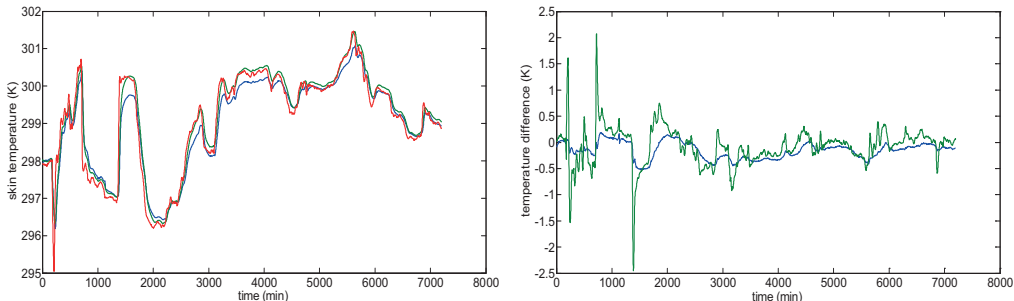


Figure 8: Pipe skin measurement KP6.8; blue line is measured skin temperature, red line is skin temperature calculated with steady state thermal model, green line is skin temperature calculated with unsteady 1D radial thermal model. Right:difference between measured and calculated skin temperature at KP6.8; green line is steady state model, blue line is 1 D radial model.

4 Conclusions

Studied is the effect of the heat transfer model on pipe flow calculation during transient. The response to an inlet gas mass rate transient is shown to be different to that of an inlet gas temperature transient. The results demonstrate that a steady state model of the ambient and soil cannot accurately represent the ambient heat exchange when rapid transients in the inlet flow occur. The reason is that inlet flow transients result in rapid temperature changes of the gas inside the pipeline. These can only be dissipated in the surrounding pipe wall and soil at a rate determined by the thermal resistance of the entire thermal domain. For both transients, the heat exchange during transient flow is underestimated. The unsteady models allow heat storage in the pipe wall and soil resulting in higher instantaneous heat exchange rates. This dampens the temperature response of the gas inside the pipeline in response to the inlet transient. The results show that inclusion of the soil heat storage term in the heat exchange model has a large influence on the thermal accuracy of the calculated pipe hydraulic flow subject to an inlet flow transient. The effect on pressure calculation was found to be minor. The choice between a 1D radial versus 2D unsteady heat transfer model has a much smaller impact: for this case both models shows a similar response to the transients. Significant improvements in thermal calculation accuracy of transient pipe flow can be achieved by implementing a 1D radial unsteady heat transfer model of the soil instead of the currently used steady state model. The experimental results are in agreement; the experimental verification demonstrates the improvement potential the 1D radial unsteady model has over the steady state model. The remaining temperature deviations are related to the peaks of the gas temperature inside the pipe in response to the inlet transients. Further study is needed to identify the cause(s) of this.

Acknowledgment

This work is funded by the Norwegian gas transmission operator Gassco as part of a project to improve flow modeling in gas pipelines. We acknowledge the contributions of Willy Postvoll and Leif Idar Langelandsvik from Gassco AS.

References

- [1] Helgaker JF. *Modelling Transient Flow in Long distance Offshore Natural Gas Pipelines*. PhD Thesis Trondheim: Norwegian University of Science and Technology; 2013.
- [2] Langelandsvik LI. *Modeling of natural gas transport and friction factors for large scale pipelines*. PhD Thesis Trondheim: Norwegian University of Science and Technology; 2008.
- [3] Chaczykowski M. Sensitivity of pipeline gas flow model to the selection of the equation of state. *Chemical Engineering Research and Design* 2009; pp. 1596-1603.
- [4] Helgaker JF, Oosterkamp A, Langelandsvik LI, Ytrehus T. Validation of 1D flow model for high pressure offshore natural gas pipelines. *Journal of Natural Gas Science and Engineering* 2014; vol 16: pp. 44-56.
- [5] Starling KE. *Fluid Thermodynamic Properties for Light Petroleum Systems*. Gulf Publishing Company; 1973.
- [6] Dewitt DP , Incropera F P. *Fundamentals of Heat and Mass Transfer*. New York: Wiley; 2000, pp. 193, 491.
- [7] Zukauskas A, Ziugzda C. *Heat transfer of a cylinder in cross flow*. New York: Hemisphere Pub; 1985.
- [8] Ouworrie C. Steady-state Heat Transfer Models for Fully and Partially Buried Pipelines. *CPS/SPE International Oil & Gas Conference and Exhibition*, Beijing, 2010.
- [9] Osiadacz AJ, Chaczykowski M. Comparison of isothermal and non-isothermal pipeline gas flow. *Chemical Engineering Journal* 2001; vol. 81: pp. 41-51.
- [10] Nicholas E. The impact of the pipe and ground on pipeline temperature transients. *Proceedings Pipeline Simulation Interest Group*, Galveston, 2011.
- [11] Helgaker JF, Oosterkamp A, Ytrehus T. Transmission of Natural Gas through Offshore Pipelines - Effect of Unsteady Heat Transfer Model. *MEKIT 2013*, Trondheim, 2013.
- [12] SPT-Group. *User documentation: Olga Heat Transfer Review Modelling of Buried Pipelines with Standard Olga Model*.
- [13] Barletta A, et al. Numerical study of heat transfer from an offshore buried pipeline. *Applied Thermal Engineering* 2008; vol. 28: pp. 1168-1176.
- [14] Gu F, et al. A Numerical Calculation of Soil Moisture and Heat Couple Temperaure Field around Pipelines in The Process of Alternate Transportation of Cool-Hot Crude Oil. *ICPTT*, 2009.
- [15] Barletta A, et al. Transient Heat Transfer from an Offshore Buried Pipeline during Start-up Working Conditions. *Heat Transfer Engineering* 2008; vol. 29 nr. 11: pp. 942-949.
- [16] ANSYS. *ANSYS FLUENT Theory Guide*. Canonsburg PA: ANSYS Inc.; 2014.
- [17] Ramsen J, et al. Important Aspects of Gas Temperature Modeling in Long Subsea Pipelines. *Proceedings Pipeline Simulation Interest Group*, Galveston, 2009.

Appendix

Article [c]

Validation of 1D Flow model for transmission of natural gas through offshore pipelines.

J.F. Helgaker, A.Oosterkamp, L.I.Langelandsvik, T.Ytrehus.

Journal of Natural Gas Science and Engineering, 2014, vol. 16, pp. 44-56.

Appendix

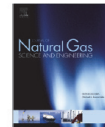
Journal of Natural Gas Science and Engineering 16 (2014) 44–56



Contents lists available at ScienceDirect

Journal of Natural Gas Science and Engineering

journal homepage: www.elsevier.com/locate/jngse



Validation of 1D flow model for high pressure offshore natural gas pipelines



Jan Fredrik Helgaker ^{a,b,*}, Antonie Oosterkamp ^{a,b}, Leif Idar Langelandsvik ^c, Tor Ytrehus ^b

^a Polytec Research Institute, 5527 Haugesund, Norway

^b Norwegian University of Science and Technology, Department of Energy and Process Engineering, 7491 Trondheim, Norway

^c Gassco AS, 4250 Koppervik, Norway

ARTICLE INFO

Article history:

Received 24 June 2013

Received in revised form

28 October 2013

Accepted 18 November 2013

Available online 14 December 2013

Keywords:

Transportation

Offshore pipelines

Compressible flow

Friction factor

Equation of state

Heat transfer model

ABSTRACT

Transportation of natural gas through high pressure large diameter offshore pipelines is modeled by numerically solving the governing equations for one-dimensional compressible pipe flow using an implicit finite difference method. The pipelines considered have a diameter of 1 m and length of approximately 650 km. The influence of different physical parameters which enter into the model are investigated in detail. These include the friction factor, equation of state and heat transfer model. For high pressure pipelines it is shown that the selection of the equation of state can have a considerable effect on the simulated flow results, with the recently developed GERG 2004 being compared to the more traditional SRK, Peng–Robinson and BWRS equations of state. Also, including heat accumulation in the ground is important in order to model the correct temperature at the outlet of the pipeline. The flow model is validated by comparing computed results to measured values for an offshore natural gas pipeline.

© 2013 Elsevier B.V. All rights reserved.

1. Introduction

Natural gas may be transported over long distances through high pressure transmission pipelines. An overview of the Norwegian natural gas transport system lying in the North Sea is shown in Fig. 1. The network is operated by the Norwegian state owned company Gassco. After the gas has been processed and unwanted components are removed it is fed into long export pipelines and transported from Norway to continental Europe and the UK. The pipelines have a diameter of approximately 1 m and can be between 600–800 km in length. Measurements of the state of the gas such as pressure, mass flow, temperature and composition are available only at the inlet and outlet. To know the state of the gas between these two points one has to rely on computer models.

Transmission of natural gas through high pressure pipelines can be modeled by numerically solving the governing equations for one-dimensional compressible viscous heat conducting flow. Such mathematical models have several important applications in the

gas industry. These include designing, operating and monitoring natural gas pipelines and predicting the pipeline hydraulic capacity. High accuracy in transport capacity is important to ensure optimal utilization of the network, as failure to deliver the forecasted capacity can result in penalties and a poor reputation as a gas network operator (Langelandsvik et al., 2009). They also play an integral part in software based leak detection systems. It is therefore crucial that these models are as accurate as possible, but at the same time fast and efficient as conditions in the pipeline are usually transient.

An overview of different numerical techniques used to solve the governing flow equations can be found in basic literature articles (Thorley and Tiley, 1987). These include the method of characteristics, finite difference, finite volume and finite element methods. Finite difference methods have commonly been used to model the flow of natural gas through pipelines (Abbaspour and Chapman, 2008; Chaczykowski, 2010; Kiuchi, 1994), with implicit methods being preferred to explicit, as these are stable for any choice of time and spatial step.

In order to accurately model the flow through high pressure pipelines one has to solve the full non-isothermal model (Osadacz and Chaczykowski, 2001), which implies solving the continuity, momentum and energy conservation equations for the flow. As well as solving the governing flow equations, several physical processes have to be modeled in appropriate ways. These include

* Corresponding author. Norwegian University of Science and Technology, Department of Energy and Process Engineering, 7491 Trondheim, Norway. Tel.: +47 48077450.

E-mail addresses: jan.fredrik.helgaker@polytec.no, jan.fredrik.helgaker@ntnu.no (J.F. Helgaker).

Appendix

Nomenclature	
A	pipe cross section [m^2]
c_p	heat capacity at constant pressure [$\text{J}/(\text{kg K})$]
c_v	heat capacity at constant volume [$\text{J}/(\text{kg K})$]
D	pipe diameter [m]
Fo	Fourier number
f	friction factor
g	gravitational constant [m/s^2]
h	film transfer coefficient [$\text{W}/(\text{m}^2 \text{K})$]
k	heat transfer coefficient [$\text{W}/(\text{m K})$]
\dot{m}	mass flow rate [kg/s]
p	pressure [Pa]
p_c	critical pressure [Pa]
p_r	reduced pressure
Q	heat flow [W]
R	gas constant [$\text{J}/(\text{kg K})$]
Re	Reynolds number
r	pipe radius [m]
T	Temperature [K]
T_a	Ambient temperature [K]
T_c	critical temperature [K]
T_r	reduced temperature
t	time [s]
U	total heat transfer coefficient [$\text{W}/(\text{m}^2 \text{K})$]
u	gas velocity [m/s]
x	spatial coordinate [m]
Z	compressibility factor
ϵ	equivalent sand grain roughness [m]
λ	thermal conductivity [$\text{W}/(\text{m K})$]
ρ	density [kg/m^3]
ρ_m	molar density [kg mol/m^3]
θ	pipe inclination angle

the friction factor, equation of state and heat exchanges between the gas and the surrounding environment. Previous research has looked into the sensitivity of the pipeline gas flow model to the selection of the equation of state (Chaczykowski, 2009) and the effect of the pipeline thermal model (Chaczykowski, 2010). However, in both these cases the investigated pipeline had an inlet pressure of 8.4 MPa, which is typical that of an on-shore distribution network. Offshore pipeline like those in Fig. 1 can have an inlet pressure of up to 20 MPa, well above that typically considered in the literature.

The objective of this study is to validate the one-dimensional flow model for high pressure offshore natural gas pipelines. An implicit finite difference method is used to solve the governing flow equations. The model is validated by running simulations on an offshore natural gas pipeline and comparing numerical results to measured values. Different physical processes which enter into the one-dimensional flow model will be investigated and discussed in detail. These include the friction factor, equation of state and heat transfer between the gas and the surrounding environment. For the equation of state the recently developed GERG 2004 will be compared to the more traditional SRK, Peng–Robinson and BWRS equations of state currently used today. The heat exchange between the gas and the surroundings will be modeled using both a steady and unsteady external heat transfer model. The main difference between these two approaches is that the unsteady heat transfer model takes into account heat accumulation in the ground surrounding the pipeline.

2. Theory

2.1. Governing equations

The governing equations for one-dimensional compressible viscous heat conducting flow are found by averaging the three-dimensional versions across the pipe cross section. The result is:

Continuity

$$\frac{\partial \rho}{\partial t} + \frac{\partial (\rho u)}{\partial x} = 0 \quad (1)$$

Momentum

$$\frac{\partial(\rho u)}{\partial t} + \frac{\partial(\rho u^2 + p)}{\partial x} = -f \rho u |u| - \rho g \sin \theta \quad (2)$$

Energy

$$\rho c_p \left(\frac{\partial T}{\partial t} + u \frac{\partial T}{\partial x} \right) + T \left(\frac{\partial p}{\partial T} \right)_p \frac{\partial u}{\partial x} = \frac{f \rho u^3}{2D} - \frac{4U}{D}(T - T_a) \quad (3)$$

In the momentum equation the first term on the right hand side is the friction term, where f is the friction factor. The final term is the gravity term where θ is the pipe inclination angle. In the energy equation the second term on the left hand side represents the Joule–Thomson effect, which is cooling upon expansion. On the right hand side the first term is the dissipation term, which is breakdown of mechanical energy to thermal energy. The final term represents the heat exchange between the gas and the surroundings.

The density can be related to pressure and temperature by using a real gas equation of state

$$\frac{p}{\rho} = ZRT \quad (4)$$

where $Z = Z(p, T)$ is the compressibility factor. When working with natural gas pipelines, one is often interested in knowing the pressure and mass flow at the inlet and outlet. By replacing the density with pressure and introducing the mass flow rate $\dot{m} = \rho u A$, where A is the pipeline cross section, Equations (1)–(3) can be developed into partial differential equations for p , \dot{m} and T (Chaczykowski, 2010). The result is:

$$\begin{aligned} \frac{\partial p}{\partial t} &= \left[\frac{1}{T} + \frac{1}{Z} \left(\frac{\partial Z}{\partial T} \right)_p \right] \left[\frac{1}{p} - \frac{1}{Z} \left(\frac{\partial Z}{\partial p} \right)_T \right]^{-1} \frac{\partial T}{\partial t} \\ &\quad - \frac{ZRT}{pA} \left[\frac{1}{p} - \frac{1}{Z} \left(\frac{\partial Z}{\partial p} \right)_T \right]^{-1} \frac{\partial \dot{m}}{\partial x} \end{aligned} \quad (5)$$

$$\begin{aligned} \frac{\partial \dot{m}}{\partial t} &= \frac{\dot{m} ZRT}{pA} \left(-2 \frac{\partial \dot{m}}{\partial x} + \dot{m} \left[\frac{1}{p} - \frac{1}{Z} \left(\frac{\partial Z}{\partial p} \right)_T \right] \frac{\partial p}{\partial x} \right. \\ &\quad \left. - \dot{m} \left[\frac{1}{T} + \frac{1}{Z} \left(\frac{\partial Z}{\partial T} \right)_p \right] \frac{\partial T}{\partial x} \right) - A \frac{\partial p}{\partial x} - \frac{f ZRT \dot{m} |\dot{m}|}{2D A p} - \frac{pA}{ZRT} g \sin \theta \end{aligned} \quad (6)$$

Appendix

46

J.F. Helgaker et al. / Journal of Natural Gas Science and Engineering 16 (2014) 44–56

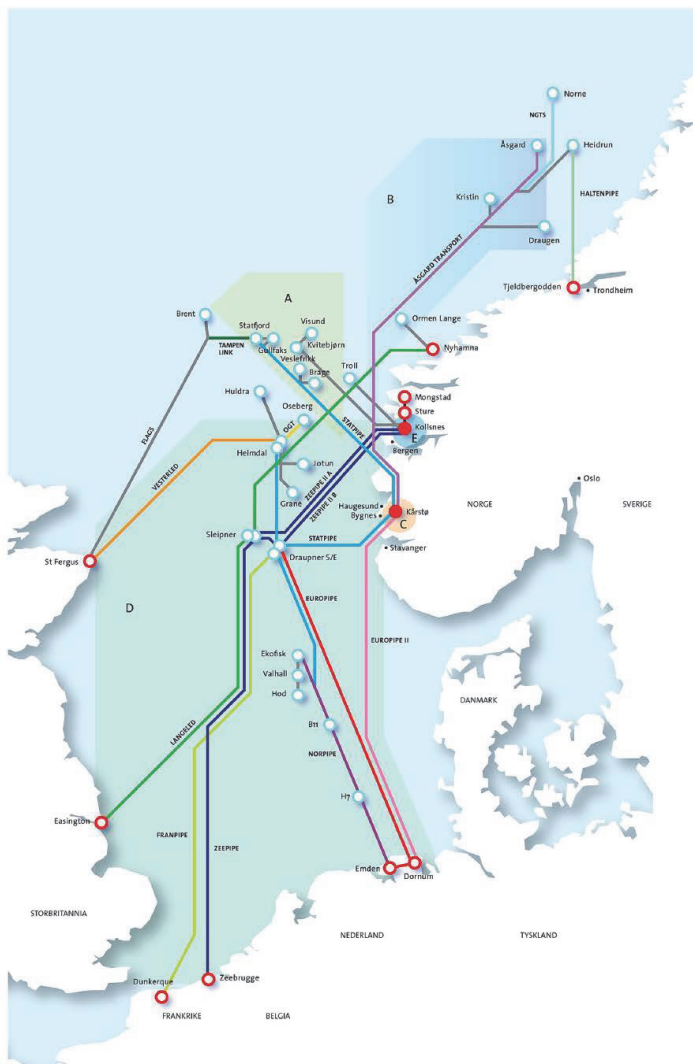


Fig. 1. Overview of the Norwegian natural gas transport system in the North Sea. Figure courtesy of Gassco.

Appendix

$$\begin{aligned} \frac{\partial T}{\partial t} = & -\frac{\dot{m}ZRT}{pA}\frac{\partial T}{\partial x} - \frac{\dot{m}(ZRT)^2}{pAc_v}T\left[\frac{1}{T} + \frac{1}{Z}\left(\frac{\partial Z}{\partial T}\right)_p\right] \times \left(\frac{1}{\dot{m}}\frac{\partial \dot{m}}{\partial x}\right. \\ & \left.- \left[\frac{1}{p} - \frac{1}{Z}\left(\frac{\partial Z}{\partial p}\right)_T\right]\frac{\partial p}{\partial x} + \left[\frac{1}{T} + \frac{1}{Z}\left(\frac{\partial Z}{\partial T}\right)_p\right]\frac{\partial T}{\partial x}\right) \\ & + \frac{f}{2c_v D}\left(\frac{ZRT|\dot{m}|}{pA}\right)^3 - \frac{ZRT}{pc_v D}4U(T - T_a) \end{aligned} \quad (7)$$

2.2. Friction factor

The friction factor accounts for the frictional force between the fluid and the pipe wall. The friction factor f for a pipe, commonly denoted the Darcy–Weisbach friction factor, is defined as

$$f = \frac{-dp/dx}{\frac{1}{2}\rho u^2} \quad (8)$$

This is a semi-empirical parameter, meaning that no analytical description of these forces has been developed. For pipeline flow with high turbulence intensity (described by the Reynolds number), it is also impossible to fully calculate this parameter by computational simulations.

Today the Colebrook–White formula is the most widespread relation for determining f , which combines the two main regions for the friction factor. For low Reynolds numbers the friction factor is solely dependent on Reynolds number (smooth turbulent flow), whereas for higher Reynolds numbers the friction factor becomes independent of Reynolds number and only depends on the internal roughness (rough turbulent flow). Colebrook–White is a mathematical combination of these two expressions that was developed in the 1930s (Colebrook, 1939)

$$\frac{1}{\sqrt{f}} = -2\log\left(\frac{\epsilon}{3.7D} + \frac{2.51}{Re\sqrt{f}}\right) \quad (9)$$

where ϵ is the equivalent sand grain roughness, D the diameter of the pipe and Re the Reynolds number of the flow. Later, several modifications to the smooth turbulent law have been suggested (McKeon et al., 2005), while how to determine the roughness elements on the inner wall by means of measurement has been

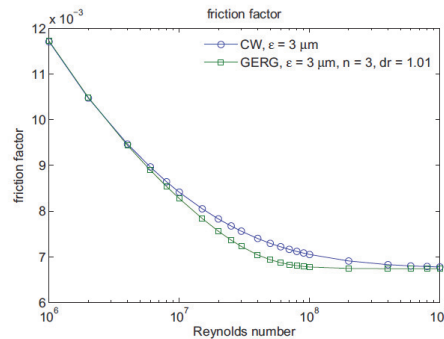


Fig. 2. Friction factor f computed using the Colebrook–White (CW) and GERG friction factor correlation. The GERG friction factor formula predicts a more abrupt transition from smooth to fully rough turbulent flow compared to Colebrook–White.

discussed based on recent experiments (Langelandsvik et al., 2008; Shockling et al., 2006). For transportation of natural gas through offshore pipelines, the Reynolds number is typically of the order 10^7 , meaning the friction factor lies in the region between smooth and fully rough turbulent flow. Based on operational data from natural gas pipelines, it is stated that the transition from smooth to fully rough turbulent flow is more abrupt than that suggested by Colebrook–White, and that the friction factor in this region bears significant uncertainty (Langelandsvik et al., 2005). A modified friction factor formula was proposed by the European Gas Research Group (GERG) (Gersten et al., 2000)

$$\frac{1}{\sqrt{f}} = \frac{2}{n} \log \left[\left(\frac{1.499}{dr Re \sqrt{f}} \right)^{0.942 \cdot n \cdot dr} + \left(\frac{\epsilon}{3.7D} \right)^n \right] \quad (10)$$

where dr is the draught factor which accounts for other pressure losses such as curvature and pipe joints, and n is used to control the shape of the transition, $n = 1$ corresponds to a smooth Colebrook–White transition while $n = 10$ a more abrupt transition.

In Fig. 2 the friction factor f computed using the Colebrook–White and GERG friction factor formulas for an equivalent sand grain roughness of $3 \mu m$ is shown. In the GERG formula the draught and transition factor were set to $dr = 1.01$ and $n = 3$ (Piggott et al., 2002). The GERG friction factor formula gives a more abrupt transition from smooth to fully rough turbulent flow compared to Colebrook–White, with the friction factor in the transition region being considerably lower. However, limited information is available as to what values of dr and n should be used in high pressure pipelines. It is therefore difficult to conclude whether the GERG friction factor formula is any significant improvement of the traditional Colebrook–White correlation.

2.3. Equation of state

The equation of state is the relationship between state variables. Several different equations of state, including SRK, Peng–Robinson, BWRS, AGA-8, GERG 88 and GERG 2004, are applied in the industry today. The sensitivity of the gas pipeline flow model to the selection of the equation of state has been investigated previously (Chaczkowski, 2009) for the SRK, BWR, AGA-8 and GERG 88 equations of state. These did not influence the computed flow parameters and line-pack values in any significant way. However, the inlet pressure in the considered pipeline was only 8.4 MPa, which is typical that of an on-shore distribution network. Offshore natural gas pipelines can have inlet pressures in the range 18–20 MPa. The sensitivity of the selection of the equation of state for high pressure pipelines will therefore be investigated in the following. The equations of state considered are SRK, Peng–Robinson, BWRS, GERG 88 and GERG 2004.

2.3.1. SRK

The Soave–Redlich–Kwong (SRK) is a modification of the Redlich Kwong equation of state and was first published in 1972 (Soave, 1972). It is a cubic equation of state, and in the original article by Soave it is validated up to 12 MPa. It can conveniently be expressed as

$$Z^3 - Z^2 + Z(A - B - B^2) - AB = 0 \quad (11)$$

where A and B are constants which depend on reduced pressure and temperature

Appendix

48

J.F. Helgaker et al. / Journal of Natural Gas Science and Engineering 16 (2014) 44–56

$$A = 0.427 \frac{\alpha p_r}{T_r} \quad (12)$$

$$B = 0.08664 \frac{p_r}{T_r} \quad (13)$$

where the subscript r denotes reduced state variables ($p_r = p/p_c$, $T_r = T/T_c$, p_c and T_c being critical pressure and temperature). The parameter α is a function which depends on the reduced temperature and the acentric factor. Mixing rules are applied to gas mixtures.

2.3.2. Peng–Robinson

Peng–Robinson is also a cubic equation of state and is structurally similar to SRK. It was first published in 1976 and is claimed to predict the liquid phase densities more accurately compared to SRK (Peng and Robinson, 1976). On polynomial form it can be expressed as

$$Z^3 - (1 - B)Z^2 + (A - 3B^2 - 2B)Z - (AB - B^2 - B^3) = 0 \quad (14)$$

where

$$A = 0.45724 \frac{\alpha p_r}{T_r} \quad (15)$$

$$B = 0.07780 \frac{p_r}{T_r} \quad (16)$$

As with SRK α is a function of reduced temperature and acentric factor. Owing to their simple mathematical structure, cubic equations of state such as SRK and Peng–Robinson along with their modifications are still frequently used in the industry today. However, they have proven to be inaccurate, especially for pressures above 12 MPa (Modisette, 2000).

2.3.3. BWRS

The Benedict–Webb–Rubin–Starling (BWRS) equation of state is based on a virial expansion in density. It was published in 1973 and is a modification of the BWR equation of state (Starling, 1973). The BWRS equation of state is formulated as

$$\begin{aligned} p = & \rho_n RT + \left(B_0 RT - A_0 - \frac{C_0}{T^2} + \frac{D_0}{T^3} - \frac{E_0}{T^4} \right) \rho_n^2 + \left(bRT - a - \frac{d}{T} \right) \rho_n^3 \\ & + \alpha \left(a + \frac{d}{T} \right) \rho_n^6 + \frac{c\rho_n^3}{T^2} (1 + \gamma\rho_n) \exp(-\gamma\rho_n^2) \end{aligned} \quad (17)$$

In total it contains 11 coefficients. Values and mixing rules can be found in the literature. Because of its ability to cover both liquid and gases the BWRS is widely used for simulations of pipelines with high density hydrocarbons (Modisette, 2000). For the offshore network in Fig. 1, the operator Gassco currently uses a BWRS equation of state with coefficients which are especially tuned for hydrocarbons, which will be denoted as BWRS*. In the following, BWRS* has the same form and mixing rules as BWRS. The only difference is that the numerical values of the coefficients are different.

2.3.4. GERG88

The European Gas Research Group (GERG) has performed an extensive research into compressibility factor measurements. The GERG 88 virial equation of state was developed to accurately predict the compressibility factor of natural gas mixtures (Jaeschke et al., 1991). It takes the form

$$Z = 1 + B_M(T)\rho_m + C_M(T)\rho_m^2 \quad (18)$$

$$B_M(T) = \sum_{i=1}^n \sum_{j=1}^n x_i x_j B_{ij}(T) \quad (19)$$

$$C_M(T) = \sum_{i=1}^n \sum_{j=1}^n \sum_{k=1}^n x_i x_j x_k C_{ijk}(T) \quad (20)$$

where $B_M(T)$ and $C_M(T)$ are the second and third virial coefficients which depend on temperature and gas composition. x_i , x_j and x_k represent the mole fractions of the i th, j th and k th component. For compressibility factor calculations GERG 88 is claimed to have an uncertainty of less than 0.1% for pressures up to 12 MPa and temperatures in the range 265–335 K.

2.3.5. GERG 2004

GERG has since published the GERG 2004 equation of state which accurately predicts compressibility factors for pressures and temperatures up to 30 MPa and 365 K respectively (Kunz et al., 2007). The GERG 2004 is explicit in Helmholtz free energy a with density and temperature as independent variables. As a function of reduced density δ and temperature τ the compressibility factor is determined from

$$\frac{p(\delta, \tau)}{\rho RT} = 1 + \delta \alpha_\delta^\tau \quad (21)$$

where α_δ^τ is the dimensionless Helmholtz free energy. The GERG 2004 equation of state can also conveniently be used to predict other thermodynamical properties such as enthalpy, internal energy, heat capacity and Joule–Thomson coefficients to mention a few. An expansion of GERG 2004, referred to as GERG 2008, has also recently been published (Kunz and Wagner, 2012). The only difference between GERG 2004 and GERG 2008 is that GERG 2008 includes components which were not considered in GERG 2004, namely n-nonane, n-decane and hydrogen sulfide. These components were not considered in this work.

The compressibility factor as a function of pressure and temperature for a typical North Sea natural gas mixture was calculated using all the equations of state mentioned above. The composition of the gas in mol% was set to the following: CH_4 –89.16%, C_2H_6 –7.35%, C_3H_8 –0.51%, $n\text{C}_4\text{H}_{10}$ –0.03%, $i\text{C}_4\text{H}_{10}$ –0.03%, $n\text{C}_5\text{H}_{12}$ –0.002%, $i\text{C}_5\text{H}_{12}$ –0.001%, N_2 –0.70%, CO_2 –2.22%. In the 1D flow model (Equations (5)–(7)) the partial derivatives of Z with respect to temperature and pressure are required. These are found by taking the derivative of the expression for Z with respect to p and T . In Fig. 3 the compressibility factor Z as a function of pressure at different temperatures is presented. Up to 10 MPa the different equations of state predict almost the same value of the Z factor. Above 10 MPa a more noticeable difference is observed. Partial derivatives of Z with respect to temperature and pressure are presented in Figs. 4–6. In Figs. 4 and 5 the computed values agree well with each other over the entire pressure range. In Fig. 6 some deviations above 20 MPa are observed.

2.4. Heat transfer model

The final term in the energy equation (Equation (7)) represents the heat exchange between the gas and the surrounding environment, where the total heat transfer coefficient U has the usual definition

Appendix

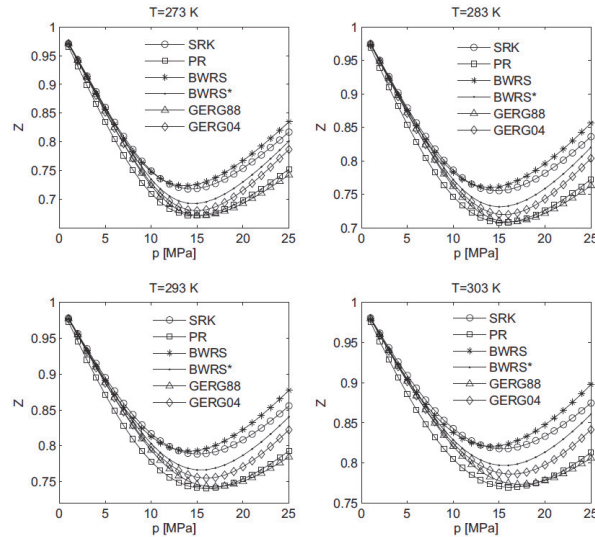


Fig. 3. Compressibility factor Z as a function of pressure at different temperatures. For pressures below 10 MPa only small differences between the different equations of state are observed. For pressures above 10 MPa a considerable difference can be seen.

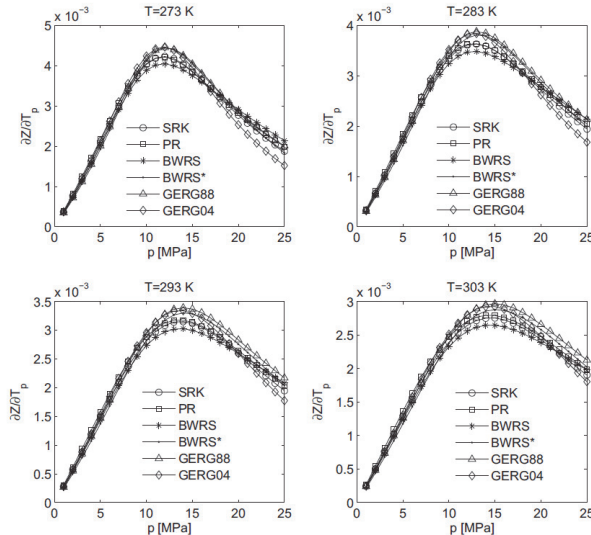


Fig. 4. Partial derivative of Z with respect to temperature at constant pressure ($\partial Z / \partial T_p$).

Appendix

50

J.F. Helgaker et al. / Journal of Natural Gas Science and Engineering 16 (2014) 44–56

$$U = \frac{Q}{A(T - T_a)} \quad (22)$$

Q is the heat flow and A the area through which heat transfer takes place. Gassco has previously modeled the heat exchange between the gas and the surroundings using a total heat transfer coefficient U (Ramsen et al., 2009). The total heat transfer coefficient for a pipeline consisting of multiple wall layers is

$$U = \left[\frac{r_o}{r_i} \frac{1}{h_i} + \sum_{n=1}^N \left(\frac{r_o}{\lambda_n} \ln \left(\frac{r_n}{r_{n-1}} \right) \right) + \frac{1}{h_o} \right]^{-1} \quad (23)$$

where r_o is the outer radius of the pipe, r_i the inner radius, r_n outer radius of wall n , λ_n the thermal conductivity of wall n , h_i the inner wall film heat transfer coefficient and h_o the outer film heat transfer coefficient. This is a steady state approach which does not allow for heat accumulation in the ground. To include heat accumulation in the ground one has to solve the unsteady heat transfer model (Chaczkykowski, 2010). In the unsteady heat transfer model the one-dimensional radial heat equation is solved in the domain surrounding the pipeline.

$$\rho c p \frac{\partial T}{\partial t} = \frac{\lambda}{r} \frac{\partial}{\partial r} \left(r \frac{\partial T}{\partial r} \right) \quad (24)$$

The radial heat equation can be expressed on dimensionless form as

$$\frac{\partial T^*}{\partial t^*} = \frac{Fo}{r^*} \frac{\partial}{\partial r^*} \left(r^* \frac{\partial T^*}{\partial r^*} \right) \quad (25)$$

where $*$ represents a dimensionless variable. Fo is the Fourier number which is defined as

$$Fo = \frac{\alpha t}{L^2} \quad (26)$$

where $\alpha = \lambda/\rho c_p$ is the thermal diffusivity, t the characteristic time and L the characteristic length through which heat conduction occurs. The Fourier number is the ratio of the heat conduction rate to the heat storage rate. For small Fourier numbers (much less than 1) the heat storage rate is greater than the heat conduction rate, underlining that heat accumulation should be included in the model. The radial heat conduction equation is solved on the domain shown in Fig. 7. The model is axial symmetric, where each thermal layer is represented by a coaxial cylindrical shell. Equation (24) is discretized using finite differences. The following equations are solved for the unsteady external heat transfer model (Chaczkykowski, 2010)

$$\begin{aligned} Q &= \frac{k_0 D}{4} (T - T_1^{n+1}) \\ \rho_1 c p_1 \frac{T_1^{n+1} - T_1^n}{\Delta t} &= \frac{k_1}{A_1} (T_2^{n+1} - T_1^{n+1}) - \frac{k_0}{A_1} (T_1^{n+1} - T) \\ \rho_1 c p_1 \frac{T_1^{n+1} - T_1^n}{\Delta t} &= \frac{k_1}{A_1} (T_{i+1}^{n+1} - T_i^{n+1}) - \frac{k_{i-1}}{A_i} (T_i^{n+1} - T_{i-1}^{n+1}) \\ \rho_N c p_N \frac{T_N^{n+1} - T_N^n}{\Delta t} &= \frac{k_N}{A_N} (T_a - T_N^{n+1}) - \frac{k_{N-1}}{A_N} (T_N^{n+1} - T_{N-1}^{n+1}) \end{aligned} \quad (27)$$

The first line represents the heat exchange between the gas and the temperature at point 1, where k_0 is the heat transfer coefficient between these two points. k_0 depends on the inner wall film heat transfer coefficient and the heat conduction between the inner wall and point 1. k_i is the heat transfer coefficient between points $i+1$ and i , while k_N is the heat transfer coefficient between the ambient and T_N and depends on the outer film heat transfer coefficient. For

an updated gas temperature in the pipeline, the system of equations above are solved in the domain surrounding the pipeline to determine the updated temperature field. For an updated temperature field the heat flow Q between the gas and the surroundings is computed. This value is then used to model the heat exchange between the gas and surroundings at the next time step, using the fact that $U = Q/(A(T - T_a))$. The radial heat equation is only solved for sections where the pipeline is buried under ground. When it is exposed to sea water, the heat transfer between the outer wall and the sea water is modeled using a film heat transfer coefficient, as there is assumed to be no heat accumulation in the surrounding sea water.

3. Numerical scheme

Transportation of natural gas through high pressure natural gas pipelines is modeled by numerically solving the governing equations for one-dimensional compressible flow. Equations (5)–(7) form a system of hyperbolic partial differential equations which are solved using finite differences, with the discretization being implicit in time. The numerical stencil is presented in Fig. 8.

A pipeline is divided into N grid points. The distance between point i and $i+1$ is the discretization length Δx , while the time step between time level $n+1$ and n is Δt . Flow values are stored at grid points, but are computed at the midpoints between two grid points. For pipe section i , being the pipe section between points i and $i+1$, the partial derivative of a flow variable Y with respect to time is approximated by

$$\frac{\partial Y(x_i, t_{n+1})}{\partial t} = \frac{Y_{i+1}^{n+1} + Y_i^{n+1} - Y_{i+1}^n - Y_i^n}{2\Delta t} + \mathcal{O}(\Delta t) \quad (29)$$

the spatial derivative by

$$\frac{\partial Y(x_i, t_{n+1})}{\partial x} = \frac{Y_{i+1}^{n+1} - Y_i^{n+1}}{\Delta x} + \mathcal{O}(\Delta x^2) \quad (30)$$

and the individual terms by

$$Y(x_i, t_{n+1}) = \frac{Y_{i+1}^{n+1} + Y_i^{n+1}}{2} + \mathcal{O}(\Delta x^2) \quad (31)$$

This is method is first order correct in time and second order correct in space, and is the same method as in the work by Kiuchi (1994) and Abbaspour and Chapman (2008). When discretizing all terms in a fully implicit way, the governing equations form a system of non-linear equations. Kiuchi and Abbaspour and Chapman solve the system of non-linear equations using the Newton–Raphson method. This can however be time consuming, especially for long pipelines and complicated networks, and would not be feasible for real time applications. To simplify the computations the non-linear terms are linearized about the previous time step to give a system of linear equations. This system can be solved in an efficient way using simple linear algebra, which is done in the following.

4. Results

The influence of the friction factor, equation of state and heat transfer model on the transmission of natural gas through offshore pipelines is investigated. A 650 km offshore pipeline is considered, with a slightly simplified setup shown in Fig. 9. For the first and final 25 km, where the gas departs the processing terminal and arrives at the receiving terminal, the pipeline is buried under ground. For the 600 km between this it is an offshore pipeline lying at a depth of

Appendix

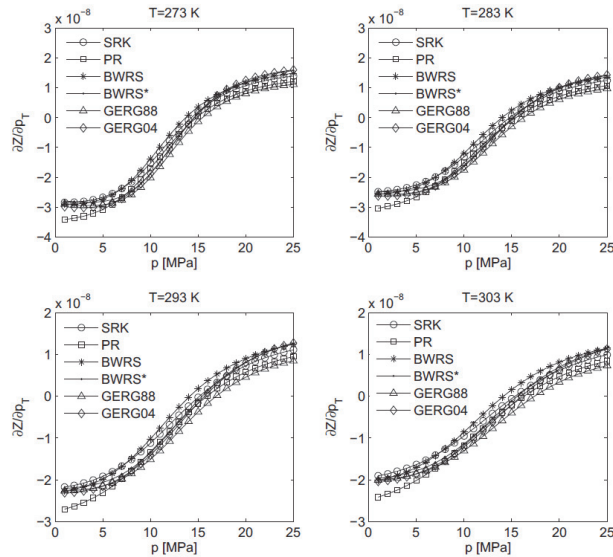


Fig. 5. Partial derivative of Z with respect to pressure at constant temperature ($\partial Z/\partial p_T$).

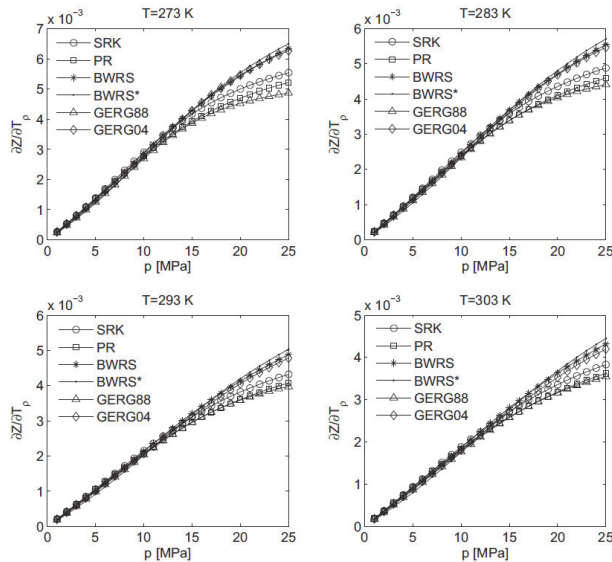


Fig. 6. Partial derivative of Z with respect to temperature at constant density ($\partial Z/\partial T_p$).

Appendix

52

J.F. Helgaker et al. / Journal of Natural Gas Science and Engineering 16 (2014) 44–56

approximately 300 m. The pipeline is assumed to be lying on the seabed completely exposed to the seawater. The ambient sea water temperature is in the region 4–6 °C, depending on location along the pipeline. The pipeline was divided into 101 grid points, with an average grid spacing of $\Delta x = 6.5$ km. The time step was $\Delta t = 60$ s.

The composition of the gas was kept constant and was set to (in mol%): CH₄–89.16%, C₂H₆–7.35%, C₃H₈–0.51%, nC₄H₁₀–0.03%, iC₄H₁₀–0.03%, nC₅H₁₂–0.002%, iC₅H₁₂–0.001%, N₂–0.70%, CO₂–2.22%. Inlet mass flow, inlet temperature and outlet pressure were given as boundary conditions.

4.1. Discretization errors

When using finite differences the governing equations are transformed into algebraic expressions in discrete time and space. Such a process introduces discretization errors in the solution. As the numerical method presented in Section 3 is first order correct in time and second order correct in space, the discretization errors will be proportional to Δt and Δx^2 respectively. In order to investigate the discretization errors in the model, simulations were run with different grid sizes and spatial steps. Flow values which represent typical transient conditions were used as boundary conditions. The local error is defined as

$$e = \frac{1}{N} \left(\sum_{i=1}^N \left(\frac{Y_i - Y_{i,hi}}{Y_{i,hi}} \right)^2 \right)^{1/2} \quad (32)$$

where Y represents p , m and T at point i . The summation is done over all grid points N , where $Y_{i,hi}$ is the numerical solution computed using the finest grid and the shortest time step (high resolution solution). Results for the local error are presented in Fig. 10.

To the left in Fig. 10 the spatial discretization error as a function of grid points N is presented, while the temporal discretization error as a function of time step Δt is presented to the right. Corresponding values are given in Tables 1 and 2. As the numerical method is first order correct in time and second order correct in space, the 1 and –2 slopes are included. The numerical method converges approximately to the expected order. The local discretization errors are small, and will for a correct choice of time and spatial step not effect the flow field solution in any significant way.

In the remaining sections operational data from high pressure pipelines will be used, with computed results being compared to measured values. Boundary conditions are inlet mass flow, inlet temperature and outlet pressure, which are presented in Fig. 11.

4.2. Influence of friction factor

The two different friction factor formulas presented in Section 2.2 were investigated for the flow. A change in friction factor is most noticeable in the modeled inlet pressure. The equivalent sand grain roughness was set to 3 μm. The effect of the draught factor and transition shape factor in the GERC formula was investigated in Fig. 12. To the left the draught factor was kept constant at $dr = 1.01$ while the transition shape factor varied. To the right the transition shape factor was kept constant at $n = 3$ while the draught factor varied. All results are compared to measured data. Results in Fig. 12 suggest that the draught factor should be in the region 1.01–1.03, while the transition shape factor in the region 3–4. These values are in agreement with those in the literature (Piggott et al., 2002; Sletfjording, 1998).

When using the Colebrook–White friction factor formula with an equivalent sand grain roughness of 3 μm, the modeled inlet pressure is considerably higher compared to the GERC formula and

the measured values, as shown in Fig. 13. This can be explained by considering the Moody diagram in Fig. 2. As the GERC formula predicts a more abrupt transition from smooth to fully rough turbulent flow, the friction factor in the Reynolds number range 10^7 – 10^8 is higher in the Colebrook–White formula compared to the GERC formula for the same equivalent sand grain roughness. When reducing the equivalent sand grain roughness to 1.5 μm in the Colebrook–White formula in Fig. 13, the modeled inlet pressure matches that of the GERC formula and the measured inlet pressure.

4.3. Influence of equation of state

The influence of the equation of state on the flow model was investigated by running simulations with SRK, Peng–Robinson, BWRS, GERC 88 and the GERC 2004 equation of state. The most noticeable difference between the different equations of state was observed in the modeled inlet pressure, which is shown in Fig. 14. To the left the modeled inlet pressure during the entire four day period is presented, while a close up view after one day is presented to the right. Modeled values are compared to the measured inlet pressure. Gassco currently uses the BWRS equation of state with coefficients especially tuned for hydrocarbons, denoted as BWRS*. The modeled inlet pressure is in the region 15–18 MPa. GERC 2004 is the only equation of state in the literature which is stated to be valid for such high pressures. The difference between the GERC 2004 equation of state and the tuned BWRS* is approximately 0.1 MPa. The measured inlet pressure lies between the modeled pressure using the GERC 2004 and BWRS* equation of state. The standard BWRS equation of state predicts an inlet pressure which is too high compared to the measured pressure, while the tuned BWRS* matches closely that of the measured pressure. Considering the equations of state available in the literature, GERC 2004 would be the preferred choice, as it gives the most accurate results for high pressure pipelines. The tuned BWRS* also gives similar results for the modeled inlet pressure. It should be noted that GERC 2004 is computationally demanding compared to all other equations of states considered here, with the increase in computational time being almost a factor 10.

4.4. Heat transfer model

Using the same boundary conditions, the model was run using both the steady and unsteady external heat transfer models. Results for inlet pressure, outlet mass flow and outlet temperature for two different cases are presented in Figs. 15 and 16. Note that boundary conditions for Fig. 15 are given in Fig. 11, while boundary conditions for Fig. 16 are not included. For the outlet temperature the steady heat transfer model over predicts the amplitude of temperature changes in the flow compared to the unsteady heat transfer model which takes into account heat accumulation in the pipe wall and ground. Heat accumulation in the ground is only considered where the pipeline is buried under ground, and not where it is exposed to sea water. Where the pipeline is buried under ground, heat accumulation in the ground is more important than heat accumulation in the pipe wall. There is also an observable difference in computed outlet mass flow between the two heat transfer models. After abrupt changes in outlet mass flow, the unsteady heat transfer model agrees better with measured values compared to the steady heat transfer model.

5. Discussion

When considering the friction factor, results computed using the Colebrook–White and GERC friction factor formulas differ considerably from each other, which can be explained by

Appendix

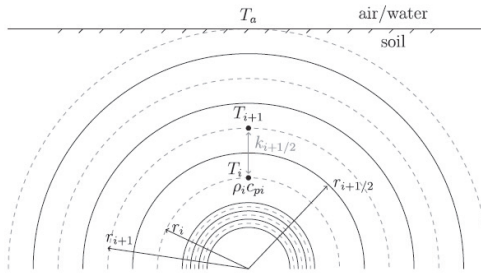


Fig. 7. Half plane of the cross-section of a buried pipeline. Thermal elements are represented by coaxial cylindrical layers, with each element assigned a temperature T_b , heat capacity c_{pi} and density ρ_i . $k_{i+1/2}$ is the heat transfer coefficient between elements i and $i + 1$.

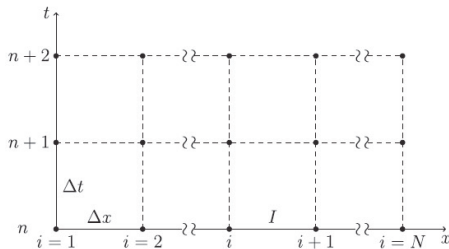


Fig. 8. Stencil used in the finite difference method.

considering the friction factor as a function of Reynolds number in Fig. 2. It has previously been reported that the transition from smooth to fully rough turbulent flow is more abrupt than that predicted by Colebrook–White (Langelaarsvik et al., 2005). In the Reynolds number range 10^7 – 10^8 the GERP friction factor formula predicts a lower friction factor f compared to Colebrook–White, which in turn results in a lower modeled inlet pressure. It has previously been reported that for pipelines operated by Gassco, the measured surface roughness of the pipe is higher compared to that which has been used in online models in order to model the correct inlet pressure (Langelaarsvik, 2008). In order to model the same inlet pressure using the Colebrook–White and GERP formulas, the equivalent sand grain roughness had to be reduced from 3 to $1.5\text{ }\mu\text{m}$ in the Colebrook–White formula. Owing to the more abrupt transition from smooth to fully rough turbulent flow, the GERP friction factor formula would be more suited to model the flow of natural gas through pipelines for Reynolds numbers in the range 10^7 – 10^8 . However, more validation and preferably a large scale laboratory test should be conducted before drawing any conclusions on

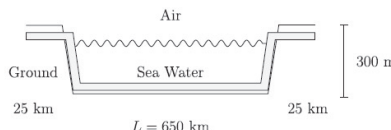


Fig. 9. Offshore natural gas pipeline which is buried under ground for the first and final 25 km. The total length is 650 km.

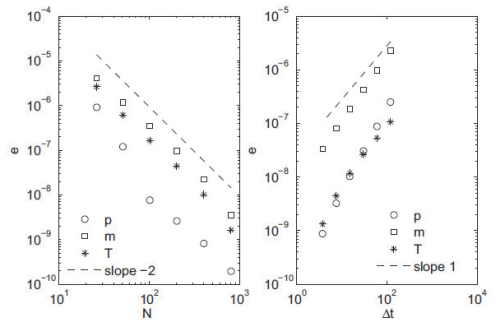


Fig. 10. Local discretization errors for pressure p , mass flow \dot{m} and temperature T . Left: Spatial discretization error as a function of grid points N . Right: Temporal discretization error as a function of time step Δt .

Table 1
Values for the spatial discretization error to the left in Fig. 10 as a function of grid points N . e is the local error and O the order.

N	Δx [km]	p		\dot{m}		T	
		e	O	e	O	e	O
26	26	$9.1177 \cdot 10^{-7}$		$4.0748 \cdot 10^{-6}$		$2.6242 \cdot 10^{-6}$	
51	13	$1.1964 \cdot 10^{-7}$	3.01	$1.1655 \cdot 10^{-6}$	1.86	$6.1345 \cdot 10^{-7}$	2.16
101	6.5	$7.6746 \cdot 10^{-9}$	3.52	$3.4679 \cdot 10^{-7}$	1.82	$1.6496 \cdot 10^{-7}$	2.04
201	3.25	$2.6177 \cdot 10^{-9}$	2.86	$9.6424 \cdot 10^{-8}$	1.83	$4.4347 \cdot 10^{-8}$	2.00
401	1.625	$8.2002 \cdot 10^{-10}$	2.56	$2.2285 \cdot 10^{-8}$	1.90	$1.0205 \cdot 10^{-8}$	2.03
801	0.825	$1.9715 \cdot 10^{-10}$	2.46	$3.5674 \cdot 10^{-9}$	2.05	$1.6375 \cdot 10^{-9}$	2.15

whether the GERP friction factor formula is an improvement of the Colebrook–White formula.

For the different equations of states considered in Section 4.3, the biggest influence was observed in the modeled inlet pressure. As the inlet pressure lies in the region 15–18 MPa, this is also the region where the different equations of state differ most from each other, as was observed in Fig. 3. As GERP 2004 is the only equation of state which is explicitly stated to be valid for such high pressures, it is also believed to be the best reference. At the outlet the difference in computed outlet mass flow and temperature was small. As the outlet pressure was in the region of 9 MPa, the different equations of state agree well with each other in this pressure region in Fig. 3. Therefore, the difference in computed flow variables at the outlet is not that significant.

The tuned BWRS equation of state currently used by Gassco matches the results of the GERP 2004 quite well. The GERP 88 equation of state also gives adequate results for the modeled inlet pressure. Owing to the fact that GERP 2004 is validated for pressures up to 30 MPa and temperatures up to 365 K, and that it can

Table 2
Values for the temporal discretization error to the right in Fig. 10 as a function of time step Δt . e is the local error and O the order.

Δt [s]	p		\dot{m}		T	
	e	O	e	O	e	O
120	$2.4966 \cdot 10^{-7}$		$2.2741 \cdot 10^{-6}$		$1.0633 \cdot 10^{-7}$	
60	$8.8016 \cdot 10^{-8}$	1.50	$9.8274 \cdot 10^{-7}$	1.21	$5.3836 \cdot 10^{-8}$	0.98
30	$3.0543 \cdot 10^{-8}$	1.52	$4.2808 \cdot 10^{-7}$	1.20	$2.6541 \cdot 10^{-8}$	1.00
15	$1.0289 \cdot 10^{-8}$	1.53	$1.8693 \cdot 10^{-7}$	1.20	$1.1811 \cdot 10^{-8}$	1.06
7.5	$3.2524 \cdot 10^{-9}$	1.57	$8.0447 \cdot 10^{-8}$	1.21	$4.4550 \cdot 10^{-9}$	1.14
3.75	$8.8397 \cdot 10^{-10}$	1.63	$3.3314 \cdot 10^{-8}$	1.22	$1.3276 \cdot 10^{-9}$	1.26

Appendix

54

J.F. Helgaker et al. / Journal of Natural Gas Science and Engineering 16 (2014) 44–56

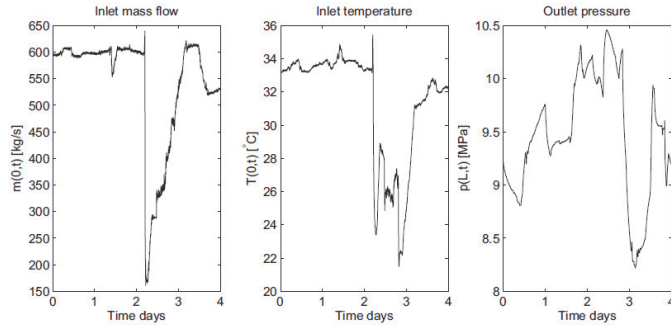


Fig. 11. Boundary conditions in the model. Left inlet mass flow, middle inlet temperature and right outlet pressure.

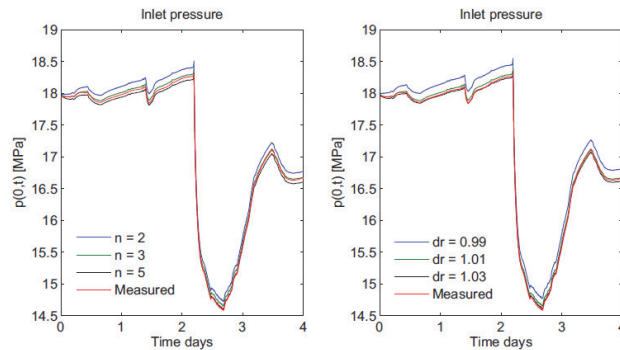


Fig. 12. Modeled inlet pressure using the GERG friction factor formula. Left: $dr = 1.01$ and varying transition shape factor n . Right: $n = 3$ and varying draught factor dr . Computed values are compared to measured values.

conveniently be used to determine physical properties such as heat capacity, enthalpy, entropy and internal energy, it would be the preferred equation of state when modeling the flow through high pressure natural gas pipelines. However, compared to all other equations of states considered here, GERG 2004 is the most computationally demanding. For the examples considered above, the computational time for the entire simulation using GERG 2004 was found to be approximately 10 times greater compared to other equations of state. This significant increase in computational time is likely due to all coefficients which are required in the case of GERG 2004. Because of this great increase in computational time, the tuned BWRS equation of state is still the preferred choice for real time applications. The difference in computed inlet pressure between GERG 2004 and the tuned BWRS was approximately 0.1 MPa.

It is shown by example how the heat exchange between the gas and the surroundings should be modeled using an unsteady heat transfer model which accounts for heat accumulation in the ground. Results in Fig. 15 for the outlet temperature illustrate how a steady heat transfer model over predicts the amplitude of temperature changes in the flow, while the unsteady heat transfer model shows a better agreement with measured values. Heat accumulation in the ground is only considered important where the pipeline is buried under ground, and not where it exposed to sea water. In the examples above, the pipeline was only buried

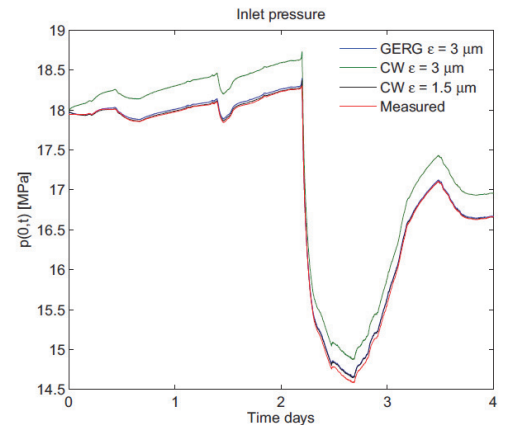


Fig. 13. Modeled inlet pressure using the Colebrook–White (CW) and GERG friction factor formulas. For the Colebrook–White formula, the equivalent sand grain roughness ϵ had to be reduced to $1.5 \mu\text{m}$ in order to match the measured inlet pressure.

Appendix

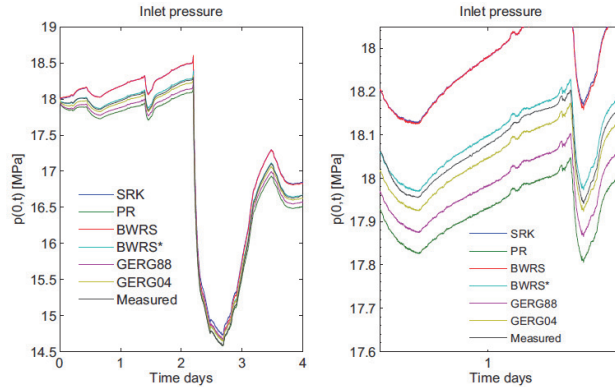


Fig. 14. Influence of the equation of state on the modeled inlet pressure. Results found using the SRK, Peng–Robinson, BWRS, BWRS*, GERG 88 and GERG 04 equations of state. Right figure is a close up view of the left after one day of operation.

under ground at the beginning and end of the pipeline where the gas leaves the processing terminal and arrives at the receiving terminal. Both of these lengths are approximately 25 km. Even for such a short section of pipeline, an unsteady heat transfer model should be used. In the example in Section 4.3, the relation between

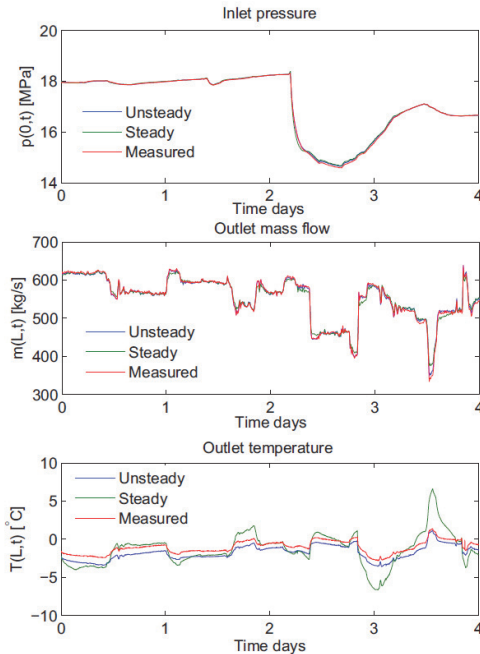


Fig. 15. Simulated results compared to measured values using both the steady and unsteady external heat transfer models for boundary conditions in Fig. 11. Top inlet pressure, middle outlet mass flow, bottom outlet temperature.

heat conduction and heat storage can be determined by considering the Fourier number. The thermal diffusivity of the soil is approximately $1.2 \cdot 10^{-6}$. The characteristic length, in this case the burial depth, is 1.5 m, while the characteristic time is the time for ramp down to occur in Fig. 15. The Fourier number is determined to be 0.1. The physical meaning of this is that the heat conduction rate is an order of magnitude less than the heat storage rate, and the transient thermal response upon the change in the mass flow rate is predominantly dictated by the heat storage effect, even on a day time scale as is the case here. For shorter characteristic time scales,

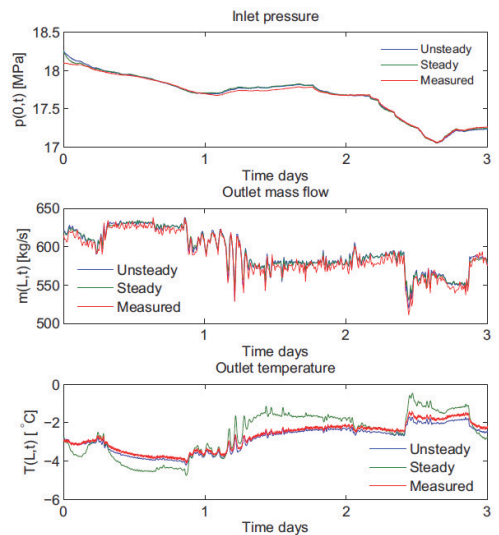


Fig. 16. Simulated results compared to measured values using both the steady and unsteady external heat transfer model. Top inlet pressure, middle outlet mass flow, bottom outlet temperature.

Appendix

56

J.F. Helgaker et al. / Journal of Natural Gas Science and Engineering 16 (2014) 44–56

the larger the effect of heat storage compared to the effect of heat conduction. This underlines that the steady state approach for heat transfer is not valid, and that an unsteady heat transfer model should be used.

In general the computed inlet pressure and mass flow agree well with measured values. For the outlet temperature, an unsteady heat transfer model gives better results for the amplitude of temperature changes in the flow compared to a steady heat transfer model. However, the modeled temperature lies slightly below the measured temperature. The reason for this deviation between measured and modeled temperature arises either because of an incorrect ambient temperature or that the assumed burial depth is not correct. As it is an offshore pipeline, the ambient sea bottom temperature along the pipeline is determined from oceanographic models. In order to accurately model the flow, it is important to know the correct ambient temperature along the whole pipeline.

6. Conclusion

The flow of natural gas through high pressure offshore pipelines is modeled by numerically solving the governing equations for unsteady one-dimensional compressible viscous heat conducting flow. The numerical discretization errors are shown to be small, and discrepancies between modeled and measured flow values is most likely due to physical approximation errors, and not numerical errors. The selection of the equation of state for high pressure pipelines is studied in detail. The different equations of state gave different results for inlet pressure, with the recently developed GERG 2004 believed to be the best reference. However, as it is computationally demanding to solve, the BWRS equation of state is still used for compressibility factor calculations in offshore pipelines. The difference in computed inlet pressure between GERG 2004 and the tuned BWRS was approximately 0.1 MPa. It is shown by example how an unsteady heat transfer model which takes into account heat accumulation in the ground greatly improves the modeled outlet temperature compared to a steady heat transfer model which has traditionally been used when modeling the flow through offshore pipelines. Some discrepancies between the modeled and measured outlet temperature are still present, which most likely are due to an incorrect ambient temperature.

Acknowledgment

This work has been funded by the Norwegian gas operating company Gassco as part of a project to improve flow modeling in offshore natural gas pipelines. The contributions of Willy Postvoll (Gassco) are greatly acknowledged.

References

- Abbaspour, M., Chapman, K.S., 2008. Nonisothermal transient flow in natural gas pipeline. *J. Appl. Mech.* 75, 031018.
- Chaczkyowski, M., 2009. Sensitivity of pipeline gas flow model to the selection of the equation of state. *Chem. Eng. Res. Des.* 87, 1596–1603.
- Chaczkyowski, M., 2010. Transient flow in natural gas pipeline – the effect of pipeline thermal model. *Appl. Math. Model.* 34, 1051–1067.
- Colebrook, C., 1939. Turbulent flows in pipes, with particular reference to the transition region between the smooth and rough pipe laws. *J. Inst. Civil Eng.* 81, 133–156.
- Gersten, K., Papenfuss, H.D., Kurschat, T.H., Genillon, P.H., Fernandes Perez, F., Revell, N., Feb 2000. New transmission-factor formula proposed for gas pipelines. *Oil Gas J.*, 58–62.
- Jaeschke, M., Audibert, S., Caneghem, P.v., Humphreys, A.E., Rosmalen, R.J., Pellel, Q., Schouten, J.A., Michels, J.P., Aug 1991. Accurate Prediction of Compressibility Factors by the GERG Virial Equation. Society of Petroleum Engineers, pp. 343–349.
- Kiuchi, T., 1994. An implicit method for transient gas flows in pipe networks. *Int. J. Heat Fluid Flow* 15, 378–383.
- Kunz, O., Klimeck, R., Wagner, W., Jaeschke, M., 2007. The GERG-2004 Wide-range Equation of State for Natural Gases and Other Mixtures. In: GERG Technical Monograph.
- Kunz, O., Wagner, W., 2012. The GERG-2008 wide-range equation of state for natural gases and other mixtures: an expansion of GERG-2004. *J. Chem. Eng. data* 57, 3032–3091.
- Langelandsvik, L.L., Postvoll, W., Svendsen, P., Øverli, J.M., Ytrehus, T., 2005. Evaluation of the friction factor formula based on operational data. In: Proceedings of the 37th PSIG Annual Meeting, San Antonio Texas 2005.
- Langelandsvik, L.L., Kunkel, G.J., Smits, A.J., 2008. Flow in a commercial steel pipe. *J. Fluid Mech.* 595, 323–339.
- Langelandsvik, L.L., 2008. Modeling of Natural Gas Transport and Friction Factor for Large-scale Pipelines (PhD thesis). Norwegian University of Science and Technology, Trondheim, Norway.
- Langelandsvik, L.L., Postvoll, W., Aarhus, B., Kaste, K.K., 2009. Accurate calculations of pipeline transport capacity. In: Proceedings to 24th World Gas Conference, Buenos Aires Argentina.
- McKeon, B.J., Zagariola, M.V., Smits, A.J., 2005. A new friction factor relationship for fully developed pipe flow. *J. Fluid Mech.* 538, 429–433.
- Modisette, J.L., 2000. Equation of state tutorial. In: Proceedings of the 32nd PSIG Annual Meeting, Savannah Georgia 2000.
- Osiadacz, A.J., Chaczkyowski, M., 2001. Comparison of isothermal and non-isothermal pipeline gas flow model. *Chem. Eng. J.* 81, 41–51.
- Peng, D.Y., Robinson, D.B., 1976. A new two-constant equation of state. *Ind. Eng. Chem. Fundam.* 15, 59–64.
- Piggott, J., Revell, N., Kurschat, T., 2002. Taking the rough with the smooth – a new look at transmission factor formulae. In: Proceedings to 34th PSIG Annual Meeting Portland Oregon.
- Ramsen, J., Losnegård, S.E., Langelandsvik, L.L., Simonsen, A.J., Postvoll, W., 2009. Important aspects of gas temperature modeling in long subsea pipelines. In: Proceedings to 40th PSIG Annual Meeting Galveston Texas.
- Shockling, M.A., Allen, J.J., Smits, A.J., 2006. Roughness effects in turbulent pipe flow. *J. Fluid Mech.* 564, 267–285.
- Slettjærden, E., 1998. Friction Factor in Smooth and Rough Gas Pipelines (PhD thesis). Norwegian University of Science and Technology, Trondheim, Norway.
- Soave, G., 1972. Equilibrium constants from a modified Redlich-Kwong equation of state. *Chem. Eng. Sci.* 27, 1197–1203.
- Starling, K.E., 1973. Fluid Thermodynamic Properties for Light Petroleum Systems. Gulf Publishing Company.
- Thorley, A.R.D., Tiley, C.H., 1987. Unsteady and transient flow of compressible fluids in pipelines – a review of theoretical and some experimental studies. *Int. J. Heat Fluid Flow* 8, 3–15.

**Pipeline modelling – impact of ambient temperature and heat transfer
modelling.**

F.Sund, A.Oosterkamp, S.M. Hope

ISOPE-2015, Proceedings of the Twenty-fifth (2015) International Offshore and
Polar Engineering Conference, Kona, Hawaii Big Island, USA, June 21–26, 2015,
vol. 2, pp. 303-309.

Is not included due to copyright

Appendix

Article [e]

'Effect of the choice of boundary conditions on modelling ambient to soil heat transfer near a buried pipeline'

A.Oosterkamp, T.Ytrehus, S. Galtung.

International Journal of Applied Thermal Engineering, vol.100, 2016.

Appendix

Applied Thermal Engineering 100 (2016) 367–377



Contents lists available at ScienceDirect

Applied Thermal Engineering

journal homepage: www.elsevier.com/locate/apthermeng



Research Paper

Effect of the choice of boundary conditions on modelling ambient to soil heat transfer near a buried pipeline



Antonie Oosterkamp *, Tor Ytrehus, Sondre T. Galtung

Uni Research Polytec, Sorhauggate 128, Haugesund 5527, Norway

HIGHLIGHTS

- Study of the effect of surface boundary conditions on soil heat conduction models.
- The modelled results are compared to the experimental data of a buried pipeline case.
- Comparison of soil temperature profiles and pipe to ambient heat transfer.
- Accuracy is reduced when using measured air temperatures as the soil surface boundary.
- Best accuracy with real soil surface temperatures or full surface energy balance.

ARTICLE INFO

Article history:

Received 5 February 2015

Accepted 9 January 2016

Available online 11 February 2016

Keywords:

Heat transfer

Soil energy balance

Soil thermal regime

Pipeline

Geothermics

ABSTRACT

The soil temperature distribution influences the thermal interaction between the ambient and subsurface objects. This paper shows the effect of the soil surface boundary conditions on heat transfer calculations around a buried pipeline. The results are compared to measurements from an experimental installation. Measurements include soil temperatures, the soil surface radiation balance, and weather parameters. The heat conduction problem is modelled with one- and two-dimensional models. The models were used to find the sensitivity for different soil surface boundary condition assumptions. The results are compared to the measured soil thermal profiles and the pipeline to ambient heat transfer. Using both the measured soil surface temperature and the full surface energy balance provides similar and accurate soil temperature prediction. A reduction in predictive accuracy of soil temperatures occurs when using measured air temperatures for the soil surface boundary condition. This has an effect on the long term pipeline to ambient heat transfer.

© 2016 Elsevier Ltd. All rights reserved.

1. Introduction

The heat transfer between the fluid in a gas pipeline and the environment is an influencing factor on the calculation of gas pressures, temperatures, and mass flow rate. To describe the soil surface boundary of a heat transfer model properly, the full surface energy balance needs to be used. Important aspects include solar, atmospheric, soil surface radiation, and convection heat transfer to the air surface layer. The migration of moisture into and out of the soil due to precipitation, condensation, and evaporation is an additional factor needed to describe fully the heat transfer problem. Due to the large length of export gas pipelines, the external ambient heat transfer model is desired to be as simple as possible in pipe flow calculations. The heat transfer problem of a buried gas pipeline is described in detail in Archer and O'Sullivan [1], Bau [2], and Sund et al. [3].

Typically, the models are limited to steady state conduction. In such models, the two-dimensional aspect of heat transfer of a buried pipe is made one-dimensional by using a steady state conduction shape factor, as shown in Incropera and DeWitt [4]. The heat transfer from the gas to the ambient is captured in an overall heat transfer coefficient, U , coupling the ambient heat transfer to the energy equation governing the pipe flow. This overall heat transfer coefficient combines the convective heat transfer from gas to pipe wall and the thermal resistance of the pipe wall layers and the soil. In Bau [5], the steady state one dimensional(1D) heat transfer model is extended to include convective heat transfer due to soil moisture migration around the pipe. Non-steady heat transfer models are normally restricted to 1D radial heat conduction, as described in Chacykowski [6], Nicholas [7], and Helgaker et al. [8]. The use of two dimensional (2D) heat transfer models in connection with pipe flow is discussed in Oosterkamp et al. [9] and Yu et al. [10]. The effect upon calculated gas pressures and temperatures of the heat transfer model is described in detail in the above mentioned publications and an overview is provided in Sund et al. [3].

* Corresponding author. Tel.: +47 90981031; fax: +47 52700470.
E-mail address: Oosterkamp@polytec.no (A. Oosterkamp).

Appendix

368

A. Oosterkamp et al./Applied Thermal Engineering 100 (2016) 367–377

In all these models, the detailed aspects of the ambient to soil energy balance are ignored. The heat transfer models used in modelling gas pipe flow used simplified boundary conditions. The full surface energy balance is not considered; it is not practical to measure this everywhere along the land-based sections of a pipeline route. Detailed knowledge of the soil surface temperatures above the buried pipeline is usually not available either. In the heat transfer models it is common practice that the soil surface temperature is either set equal to the air temperature or through a convective boundary condition. The air temperatures along the pipeline route are normally not measured directly. These are often obtained from a nearby meteorological station or derived from historical weather data. There is limited information available in the literature on the effect of the simplifications of the external heat transfer models as used in the flow modelling of gas and oil pipelines. In for example Yu et al. [10], an unsteady 2D heat transfer model is coupled to the flow equations of pipe flow in an oil pipeline. The model uses a convective boundary condition at the soil surface, with the air temperature approximated by a sine function of time. The analysis focuses on the boundary conditions at the pipe wall and the numerical methods that are employed to solve the heat transfer problem.

The problem of heat transfer of a buried gas pipeline has analogies with that of underground heat exchangers. In the literature, several publications can be found dealing with the effect of the model assumptions. In Florides and Kalogirou [11], a review of heat transfer models for ground heat exchangers is provided, discussing 1D, 2D and 3D heat transfer models. Some of these include the effect of soil moisture migration. The effect of the boundary conditions is given little attention. In Ozgener et al. [12] measured air temperature is used together with the analytical solution of one dimensional heat conduction (Hillel [13]) to predict the subsurface soil temperatures. The amplitude and phase shift of the annual soil surface temperature is approximated by fitting a sine with a one-year period to the air temperature data. Comparison with measured soil temperatures at 5, 10, 20 and 300 cm depth leads to maximum soil temperature errors as large as 6 K in the upper soil layer. The effect of the boundary condition on the resulting heat transfer rates is not reported but the notion is made that for more accurate calculations the soil surface temperature should be used.

In Liu et al. [14], a 1D radial unsteady model is used to model heat transfer between soil and flowing air in an underground tunnel. In this case, the outer boundary condition is considered to have constant temperature for a soil radius exceeding 10 m. The rationale provided here is that at depths of more than 10 m, the periodic variation of the air temperature does not affect the resulting heat transfer with the air inside the tunnel. The outer node of the soil model is set at the value of the undisturbed soil temperature at the corresponding depth. This concept is further explained in Kartti and Kreider [15].

Analytical solutions exist for the soil temperature profiles through a column of soil. In their most basic form these assume one dimensional conduction heat transfer, the soil extending as an infinite domain downwards and assume a known, annual, sinusoidal surface temperature cycle, as shown in for example Carslaw and Jaeger [16]. Often, detailed information on the soil surface temperatures cycle is not available, and only local air temperature data may be used to estimate soil surface temperatures. In the literature, methods have been presented to correlate the soil surface temperature to the measured air temperature or other more easily measured parameters [17,18]. In Jin and Mullen [19] a recent experimental study of the relation between soil surface temperature and air temperatures is provided. The results show that the diurnal air temperature and soil temperature peaks in the upper soil layer lag the soil surface temperature by 2 hours. The findings also show that the diurnal temperature variations are barely noticeable at 25 cm depth into the soil. The notion is made that the relationships between soil mois-

ture, soil temperature, soil surface temperature, and air temperature are not well understood. The results show that there is a low correlation between upper level soil moisture and soil surface temperature and that the correlation between air temperature and upper soil layer temperature is higher than that between air temperature and soil surface temperature.

In Cleall and Munoz-Criollo [20], an analytical solution is provided using the full soil surface energy balance. The derived equations include the effects of soil moisture at the surface. Simplified mathematical expressions are provided for evaporative and convective heat transfer coefficients at the surface, the diurnal and annual solar radiation, and air temperature variation. Their conclusion is that using the full heat balance with a 1D analytical heat conduction model provides a reasonable estimate of soil thermal behaviour.

In Jang and Choi [21], the surface boundary condition is simplified using a convective heat transfer coefficient to the air temperature. The surface heat transfer coefficient is set to 9 W/m²K. The authors claim excellent agreement between numerical results and experiments for soil temperature profiles using this boundary condition (depth restricted to 60 cm).

In our study, we investigated the effect of different approaches to the soil surface boundary conditions on the prediction of the thermal regime in the ground. We subsequently looked at the effect of the boundary conditions on the heat transfer between the pipeline fluid and the surrounding soil. In the study, we used measurement data from the soil around a pipeline for verification purposes. The sensitivity of the soil thermal profile to the soil-to-atmosphere boundary conditions was first investigated with a 1D heat conduction model of the soil. This was compared to the measured soil temperature at different depths. The full surface energy balance was estimated from correlations using measured weather data and net radiation measurements. The effect of the choice of soil surface boundary condition representation on the heat transfer between pipe and soil was thereafter determined using a 2D heat transfer model of the soil and pipe. It was a specific objective of the study to determine the effect of using measured air temperature as soil surface boundary condition on the resulting heat transfer between the gas inside the pipeline and the ambient.

2. Methodology

2.1. Background theory and mathematical expressions used

In elementary soil heat transfer, the ground is considered a homogeneous medium into which heat flows vertically through conduction. Fourier law describes heat flow as

$$q_g = -\lambda \frac{dT}{dz} \quad (1)$$

This 1D assumption is only valid if conduction is the sole form of energy transfer and horizontal energy transport does not play a significant role. In reality, the problem is more complex due to the effect of groundwater movement and phase changes occurring during freezing/thawing of soil layers. The presence of the warm pipe (28–30 °C) may affect the assumption of purely vertical heat conduction. The expectation is that at sufficient lateral distance from the pipe the effect is small enough to allow the use of a 1D model.

The temperature regime in the soil upper layer governs the ground thermal regime. This is the zone influenced by the climatic conditions [22]. The basic to understanding this regime is the surface energy balance, defined as

$$q^* = q_h + q_e + q_g \quad (2)$$

Here q^* is the net exchange of radiation from the atmosphere to the soil surface, q_h is the transfer of sensible heat from soil surface

Appendix

to the air, q_{le} is the transfer of latent heat from the soil surface to the air, and q_g is the conduction of heat into the ground (positive z-direction). The energy balance is such that, during the day, more radiation energy is absorbed than reflected/emitted. Heat is transported away from the soil surface by convection and evaporation, and conduction into deeper layers. During the night, there is a net loss due to long wave radiation from the surface, and a net transfer from the sum of q_h , q_c and q_g [22].

The boundary condition for the heat conduction equation at the ground surface (the vertical z-axis has a positive direction into the soil) is obtained by combining Eqs. (1) and (2):

$$-\lambda \frac{dT}{dz} \Big|_{z=0} = q^* - q_h - q_{le} \quad (3)$$

The sensible heat, q_h , is approximated as convection heat transfer between atmosphere and soil temperature. It can be determined from the air temperature profile just above the surface [23]:

$$q_h = h_s(T_s - T_a) \quad (4)$$

Several correlations for the convection heat transfer coefficient are found in the literature. In simple form it is expressed as a function of ground level wind velocity [24]. Cleall and Munoz [20] give an expression using air density, ρ_{air} (kg/m^3), air specific heat capacity, $C_{p,air}$ ($\text{J/kg}\cdot\text{K}$), and aerodynamic resistance, r_a (s/m):

$$h_s = \frac{\rho_{air} C_{p,air}}{r_a} \quad (5)$$

A more elaborate way to estimate h_s is provided in Herb et al. [25], with h_s at the soil surface composed of a forced and natural convection term:

$$h_s = \rho_{air} C_{p,water} (C_{fc} u_s + C_{nc} \Delta T_v^{1/3}) \quad (6)$$

The form of the equations shown here is for soil surfaces bare for vegetation. In Herb et al. [25] scaling extensions to the equations are provided for plant coverage. C_{fc} and C_{nc} are constants (<1) for forced and natural convection. ΔT_v is the difference between virtual air and soil surface temperature, u_s is the wind velocity at ground level (here the wind speed at ten metres height (u_{10}) multiplied by the wind sheltering coefficient). The virtual temperature is defined as the temperature dry air must be heated to for having the same density and pressure as a given sample of moist air [26]. Proper estimation of the term q_h depends on accurate measurement of moisture loss due to evaporation at the surface during dry periods, and moisture transfer to the surface during conditions of high air humidity and precipitation. This implies measurement of the moisture profile in the air boundary layer right above the soil. In this study, we relied on indirect estimations of this term. In Herb et al. [25] a correlation is provided for the latent heat q_{le} :

$$q_{le} = \rho_{air} C_{p,water} (C_{fc} u_s + C_{nc} \Delta T_v^{1/3}) * (r_{sat} - r_a) \quad (7)$$

Here r_{sat} and r_a are saturation and ambient specific humidity ($\text{kg}_{\text{water}}/\text{kg}_{\text{air}}$).

2.2. Experimental system

The experimental station is located on Bokn on the west coast of Norway. This is approximately 7 km from the inlet of a pipeline exporting natural gas to the continent. The pipeline has a diameter of 1 m and 2.3 m burial depth from the pipe centre. At the site, the pipeline and soil are instrumented with temperature and soil humidity sensors, and weather data are collected. Fig. 1 shows the measurement setup schematically.

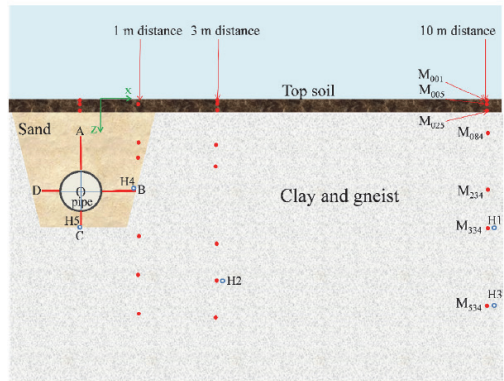


Fig. 1. Schematic setup of soil measurement system. The red dots show the temperature measurement locations. The red lines O–A, O–B, O–C and O–D indicate temperature sensor booms. The blue dots represent the locations of the soil volumetric water content sensors. M₀₀₁ to M₃₃₄ identify the measurements at 10 m from the pipe wall. The index indicates their respective depths in the soil in centimetres; i.e. M₀₀₁ is at 1 cm depth, M₀₀₅ is at 5 cm depth, etc. (For interpretation of the references to colour in this figure legend, the reader is referred to the web version of this article.)

In the soil, close to the pipe wall, the installation consisted of four sensor booms, placed in the radial directions O–A, O–B, O–C, and O–D. Radial sensor spacing is similar on each of the booms. Similar sensors were installed at 1 m, 3 m and 10 m distance from the pipe outer wall to measure the soil depth profiles. The temperature sensors were PT100's with a 4 mm diameter stainless steel sheath. The data-logger connection was a four-wire configuration (full bridge). The resolution of the measurement was 0.01 K. For each measurement point, the calibration of the data-logger channel, measurement-bridge, connectors, leads, and sensors was as one connected system. The calibration procedure comprised a series of multiple comparative measurements in the temperature interval from 0 to 30 °C. The sensors were tested in a hot bath calibrator (Hart 7103 Microbath) against a calibrated reference PT100 temperature measurement probe. The estimated accuracy after calibration exceeds ± 0.05 K within the measurement interval.

The measurement programme further contained ambient air temperature, air humidity measurement, and a four component net radiometer from Huskflux Thermal Sensors [27]. This instrument measures the incoming hemispherical solar and long wave radiation, as well as the outgoing (reflected solar) and upward long wave radiation.

In this investigation, we looked primarily at the measurements performed at the farthest distance (10 m) from the pipe wall. Here the soil temperature profile will be least influenced by the presence of the warm pipe. At the far field (10 m lateral distance from the pipe wall), the temperature sensors are located at the following depths: 1 cm (M₀₀₁), 5 cm (M₀₀₅), 25 cm (M₀₂₅), 84 cm (M₀₈₄), 234 cm (M₂₃₄), 334 cm (M₃₃₄) and 534 cm (M₅₃₄). Sensors measuring soil volumetric water content (Decagon EC5) are located at 334 cm and 534 cm depth. The sensor response is calibrated to the soil type.

The sensors were installed after drilling a 10 cm diameter hole to a depth of 6 metres. Soil samples were taken to measure the thermal properties of the soil. In this area, the available geological maps show that the bedrock is predominantly consisted of gneiss. The soil consists of a 25–30 cm thick top soil layer, followed by clay

Appendix

370

A. Oosterkamp et al./Applied Thermal Engineering 100 (2016) 367–377

Table 1
Soil thermal properties.

Soil constituent	Thermal conductivity (W/m·K)	Thermal diffusivity (m ² /s)
Top soil	1.5	0.40–0.50*10 ⁻⁶
Clay	1.8	0.80–1.0*10 ⁻⁶
Bedrock	2.4	1.0*10 ⁻⁶ [29]

containing a range of smaller and larger pebbles, on top of the bedrock. The depth to which the clay layer extends is unknown.

The thermal properties of the soil samples (top soil and clay) were measured at different soil moisture contents with the thermal needle probe technique, using a Decagon KD2 Pro with SH-1 dual needle. The correlation between volumetric water content and relevant thermal properties (thermal conductivity λ and thermal diffusivity α) was thus determined. These measurements are reported in Oosterkamp [28]. The soil volumetric water content measurements show that the soil volumetric water contents at 334 cm depth is nearly constant at 0.27 m³/m³. The soil volumetric water content at 534 cm depth is nearly 0.32 m³/m³. Table 1 shows the values for thermal conductivity λ and thermal diffusivity α used in the study:

The measurement data were collected from 16-May-2013 to 03-Sep-2014. There is a four week gap in the data during January 2014 due to equipment malfunctioning. Weather data from preceding years are obtained from two meteorology stations near the measurement site: Haugesund Airport station (18 km distance) and Kvitsøy station (18 km distance). The historical air temperature data from the Kvitsøy station are used to set up the initial soil temperature profile for the numerical models. Only during a limited time period could wind speed, air humidity and dew point measurements be measured at the Bokn site; the missing data are complemented with data from the Kvitsøy station. The data from the Haugesund Airport station are used to fill (rare) gaps in the data from the Kvitsøy station.

3. Computational models

Numerical models were made of a one-dimensional column of the soil and a 2D cross-section of the soil with the buried pipeline. The one-dimensional finite difference model was used to test the different boundary conditions and the effect of simplifications of the surface energy balance against the experimental results. The two dimensional finite volume model was used to assess the effect of the boundary condition simplifications on the pipe wall heat transfer.

The one-dimensional model is a finite difference discretization of the one-dimensional unsteady heat conduction equation:

$$\rho C_p \frac{\partial T}{\partial t} = \frac{\partial}{\partial z} \left(\lambda \frac{\partial T}{\partial z} \right) \quad (8)$$

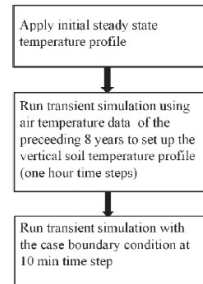
The discretization scheme is central in space, and the resulting set of equations was solved both explicitly and implicitly. For the explicit model care was taken that the time step is chosen to fill the CFL stability criterion $\alpha \Delta t / (\Delta z)^2 \leq 1/2$. The implicit model used a Crank–Nicholson scheme [30], where the thermal profile is defined as

$$T_m^n = T(z_m, t_n), \quad z_0 = 0, \quad z_M = L \quad (9)$$

and where L is the spatial extent of the domain. The resulting scheme (using trapezoid rule to approximate the integral) is

$$\frac{1}{\alpha} \frac{T_m^{n+1} - T_m^n}{\Delta t} = \frac{T_{m+1}^n - 2T_m^n + T_{m-1}^n}{2(\Delta z)^2} + \frac{T_{m+1}^{n+1} - 2T_m^{n+1} + T_{m-1}^{n+1}}{2(\Delta z)^2} \quad (10)$$

One-dimensional model of a vertical soil column



Two-dimensional model of a soil cross-section with buried pipeline

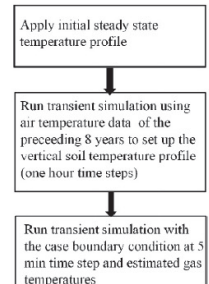


Fig. 2. Modelling scheme used to set up the model simulations.

It is well established practice to put the resulting set of equations in matrix form $[A] \times [T] = [D]$, where $[T]$ is the new temperature field at $t + \Delta t$ and $[D]$ contains solely terms of the known temperature field at t . The solution in each time step is found by using matrix inversion in Matlab. In the model, the lower boundary condition is implemented as $\frac{\partial T}{\partial z}|_{z=L} = 0$ and $L = 25$ m. The discrete difference approximation of this is $\frac{T_{m+1} - T_{m-1}}{2\Delta z} = 0$. As T_{m+1} is a fictitious node, it is substituted by T_{m-1} and inserted into the last equation of the difference scheme. Secondly, an implicit Euler scheme was implemented; this has the following form:

$$\frac{1}{\alpha} \frac{T_m^{n+1} - T_m^n}{\Delta t} = \frac{T_{m+1}^{n+1} - 2T_m^{n+1} + T_{m-1}^{n+1}}{(\Delta z)^2} \quad (11)$$

Also the explicit Euler scheme was tried:

$$\frac{1}{\alpha} \frac{T_m^{n+1} - T_m^n}{\Delta t} = \frac{T_{m+1}^n - 2T_m^n + T_{m-1}^n}{(\Delta z)^2} \quad (12)$$

All three schemes are second order accurate in space. The Euler schemes are of first order, and the Crank–Nicholson scheme is second order accurate in time. Comparing the three models provided no significant calculation time or accuracy improvement. The numerical study of the effect of the top boundary condition was therefore performed using the explicit discretization. The models were run with uniform grid size of 0.05 m. Refinement of the grid did not lead to significant change of the resulting temperature profiles.

Prior to each run the calculation domain is given an initial steady state temperature profile. This initial temperature profile is obtained by running the model using the day normal air temperatures for a 25 year period. This also provides the value of the soil temperature at the lower boundary of the domain. It is important during initial setup that the influence of the annual temperature cycle has propagated all the way to the lower boundary of the domain; otherwise, the initial temperature profile of the domain will influence the results of the subsequent transient simulation. When the initial temperature profile is set up, the hourly ambient temperatures (Kvitsøy station, NMI [31]) from 16-May-2005 until 16-May-2013 are applied as upper boundary condition. The resulting temperature profile is used as initial condition for each model case. Fig. 2 shows this schematically.

The one-dimensional model is used to study the effect of the definition of the upper boundary condition on the temporal development of the vertical soil temperature profile. Different boundary condition cases are applied to the upper node of the model, at

Appendix

Table 2
Boundary condition cases.

Boundary condition	Expression	Description
BC1: Base case	$T(0,t) = M_{00}(t)$	Dirichlet, top node follows soil surface temperature
BC2: Air temperature	$T(0,t) = T_a(t)$	Dirichlet, top node follows air temperature
BC3: Convection	$-\lambda \frac{\partial T}{\partial Z} \Big _{z=0} = -h(T(0,t) - T_a(t))$ $h = 100 \text{ W/m}^2\text{K}$	Neumann, heat conduction rate into the soil surface is equal to the heat transfer between soil surface and air
BC4: Convection plus radiation	$-\lambda \frac{\partial T}{\partial Z} \Big _{z=0} = -h(T(0,t) - T_a(t)) + q^*$ $h = 100 \text{ W/m}^2\text{K}$	Neumann, heat conduction rate into the soil surface is equal to the sum of the heat transfer between soil surface and air and the soil surface radiation balance
BC5: Full surface energy balance	$-\lambda \frac{\partial T}{\partial Z} \Big _{z=0} = -h(T(0,t) - T_a(t)) + q^* - q_{le}$	Neumann, heat conduction rate into the soil surface is equal to the full soil surface energy balance
BC6: Daily average air temperatures	$T(0,t) = T_d \text{ (daily averages)}$	Dirichlet, top node follows daily averaged air temperature measurements
BC7: Monthly average air temperatures	$T(0,t) = T_m \text{ (monthly averages)}$	Dirichlet, top node follows monthly averaged air temperature measurements
BC8: Monthly normal air temperatures	$T(0,t) = T_n \text{ (monthly normal values)}$	Dirichlet, top node follows monthly normal air temperature from the Kvitsøy station statistics (eKlima) [31]

position $z = 0$. This node represents the soil surface. Table 2 shows the different boundary condition cases for the upper node. The lowest node at $z = 25 \text{ m}$ is set at 8.4°C .

The third boundary condition, BC3, used the following discretization in the explicit models:

$$-\lambda \left(\frac{T_2^n - T_1^n}{dz} \right) = h(T_1^n - T_a^n) \quad (13)$$

For BC3 and BC4, a heat transfer coefficient of $100 \text{ W/m}^2\text{K}$ is used. For the fourth and fifth boundary cases, the right hand term of Eq. (12) is extended with the respective contributions of q^* , q_{le} , and q_{le} . The values of q^* , q_{le} , and q_{le} are updated in each time step. The net radiation q^* are measurement values. For the case of BC5, the convective heat transfer coefficient h is calculated according to Eq. (6), and the latent heat, q_{le} , according to Eq. (7) [25].

For each boundary condition case, the accuracy of fit of the calculated temperature depth profiles in relation to the measured values is used to evaluate the results. The used criteria are the normal root mean square error (NRMSE) of the fit, the maximum difference, and the mean and standard deviation of the difference. The NRMSE of the fit is calculated with the MATLAB routine using the following general scheme:

$$\text{NRMSE} = 1 - \frac{\|x(1:N) - x_{ref}(1:N)\|}{\|x(1:N) - \text{mean}(x_{ref}(1:N))\|} \quad (14)$$

If the NRMSE is one, the fit is perfect. A NRMSE of zero implies that the fit is no better than that obtained with fitting a straight line. The larger negative value of NRMSE is, the worse the fit is.

The 2D model is a cross section of the soil and the pipe at the measurement site at Bokn. This model, shown in Fig. 3, is made with Ansys Fluent ([32]). The model uses the Fluent as a server option. This allows a third part application to take control of Fluent by executing commands in the text console. A dedicated Matlab script controls the execution of the model in Fluent. The Matlab script reads the measurement data of the top soil layer temperature and pipe gas temperature. These are used as boundary conditions in the Fluent case and refreshed at the beginning of each 5 min transient time step. At the end of each time step simulation, the resulting soil temperatures and pipe wall heat-transfer rate are collected in Matlab. The transient Fluent case obtains its initial temperature field in the same manner as the one-dimensional models, as seen in Fig. 2. Thermal soil properties are based upon measurements of the soil samples [28].

Ansys Fluent uses the following energy transport equation in the solid domain:

$$\frac{\partial}{\partial t} \left(\rho \int_{T_{ref}}^T C_p dT \right) + \nabla(\bar{v} \rho H) = \nabla(\lambda \nabla T) + S_h \quad (15)$$

Here \bar{v} is a velocity vector, H is enthalpy, and S_h is an energy source term. The second term on the left represents the convective energy transfer due to rotational or translational motion of solids. In our model, the solid domain is stationary, and source terms S_h (for example internal heating) are absent; therefore Eq. (15) reduces to the 2D heat conduction equation. The discretization scheme for the energy equation is second order upwind in space and first order implicit in time. A V-cycle multigrid solver is used [32].

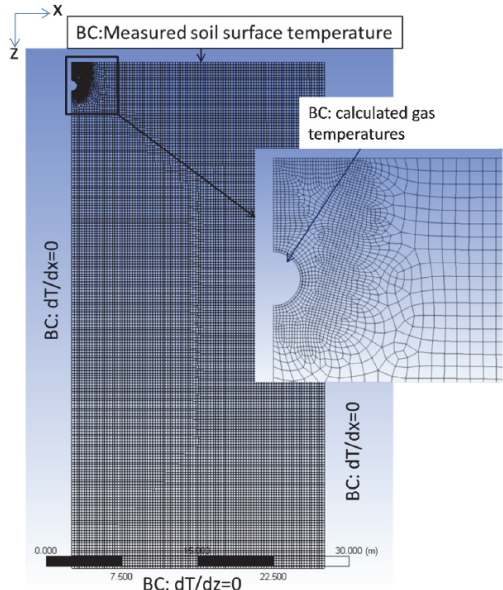


Fig. 3. 2D computational grid and boundary conditions for the numerical model of the Bokn measurement location. (For interpretation of the references to colour in this figure legend, the reader is referred to the web version of this article.)

Appendix

372

A. Oosterkamp et al./Applied Thermal Engineering 100 (2016) 367–377

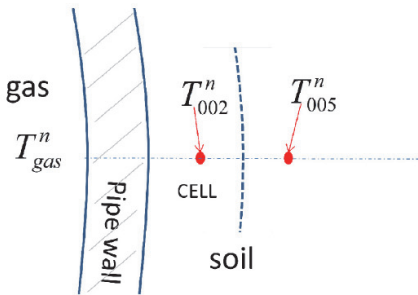


Fig. 4. Schematic of the system used for calculating gas temperatures from the soil measurements close to the pipe wall.

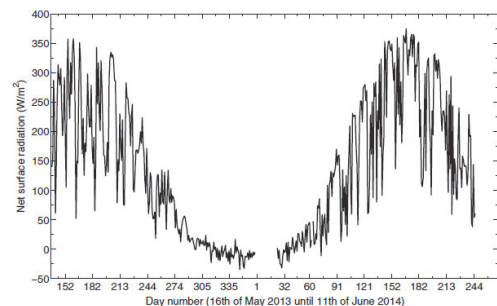


Fig. 5. Daily averaged measurement values of net surface radiation (16 May 2013 until 11 June 2014).

Care was taken that the boundary condition cases for this model were consistent with those shown in Table 1. For case BC1, the measured temperatures from the sensors at 1 cm depth in the soil are applied at the soil surface nodes. For case BC2, the soil surface nodes follow the measured air temperatures. Case BC5 is implemented as a heat flux boundary condition at the soil surface. Cases BC6 and BC7 use the averages of measured air temperatures to set the soil surface node temperatures. For all boundary condition cases, the boundary conditions at the vertical and lower edges of the model domain, as well as at the pipe inner wall, are the same:

- vertical edges: $dT/dx = 0$
- lower edge: $T = 8.4^\circ\text{C}$
- pipe inner wall: $-\frac{dT}{dr}|_{r=0} = -h_f(t)(T(r, 0) - T_{\text{gas}})$

The inner film coefficient h_f is calculated from the operational gas flow conditions using the Dittus–Boelter correlation [33], having typical values of 1400–1600 W/m²K.

The measurement set-up did not allow for direct measurement of gas temperature T_{gas} . The soil temperature measurements closest to the pipe outer wall are used to approximate the gas temperature from the measurements. This is based upon the thermal energy balance of a radial 1D calculation cell surrounding these measurement points, as shown in Fig. 4.

The calculation cell stretches 3 cm in the radial direction from the pipe wall, with the temperature measurement point at the center. The thermal energy change from time step $n - 1$ to n ($\Delta t = 300$ s) is balanced with the energy flux over the cell boundaries in time step n . Thermal energy storage in the pipe wall is neglected, so that the thermal energy flux over the inner cell boundary can be expressed as

$$q'' = U(T_{\text{gas}}^t - T_{002}^t) \quad (16)$$

Here U is the overall heat transfer coefficient combining the thermal resistances of the inner wall film coefficient, the pipe wall layer and the first 2 cm of soil. T_{gas}^t is the unknown gas temperature and T_{002}^t is the measurement at the center cell at time step t . By using the temperature measurement T_{005}^t at five centimetre distance from the pipe wall, the thermal energy flux over the outer cell boundary can be calculated. T_{gas}^t follows from

$$T_{\text{gas}}^t = T_{002}^t + \frac{0.03\rho C_p}{U\Delta t}(T_{002}^t - T_{005}^t) - \frac{\lambda}{0.03U}(T_{005}^t - T_{002}^t) \quad (17)$$

4. Results and discussion

4.1. Evaluation of surface energy balance

The energy balance at the soil surface consists of the sum of the heat conducted into the soil q_g , the net radiation q' , the latent heat q_{le} and the sensible heat q_h . The latter three components are derived from the measurements. The net radiometer measurements include both the incoming and outgoing long wave and short wave radiation energy at 600 s intervals and are combined to provide the net radiation q^* at the soil surface. The sensible heat q_h and latent heat q_{le} are derived from Eqs. (6) and (7) using air humidity, air temperature, air pressure and air speed measurements. The constants C_f and C_{nc} are set to 0.003 and 0.0015 as suggested in Herb et al. [25]. The equations are not scaled to the presence of vegetation and thus provide the upper-bound values for q_h and q_{le} . The virtual temperature, T_v , used in Eqs. (6) and (7) is calculated using the saturation vapour pressure correlation given in Flatau et al. [34]. The necessary values for air humidity, air pressure and wind velocity (u_{10}) are taken from the historical records of the Kvitsøy station (eKlima [31]). Because the experimental site is in an open field, the wind-sheltering coefficient is assumed unity. Fig. 5 shows the resulting daily averaged net radiation.

4.2. Effect of boundary conditions on soil temperature profiles with the one-dimensional model

The thermal diffusivities of the numerical model were first tuned to obtain the best fit to the measurements when employing the base case boundary condition BC1: $T(0, t) = M_{001}(t)$. The following values give the best fit: for the top soil (0–0.30 m), $\alpha = 0.60 \times 10^{-6} \text{ m}^2/\text{s}$ and for the lower soil layers (0.30–25.00 m): $\alpha = 0.90 \times 10^{-6} \text{ m}^2/\text{s}$. These values are within the range of the measured thermal diffusivity of the soil samples. The thermal conductivity in the top soil layer is set to 1.5 W/m·K.

For each of the boundary condition cases from Table 2, a transient simulation was run with the one-dimensional model. Fig. 6 shows the accuracy of fit of the temperature depth profiles in terms of normal root mean square errors (NRMSE) and max deviation for each boundary condition case. The mean and standard deviation of the difference between calculated and measured temperatures are also shown.

The results of the base case, BC1, show generally a good match with low maximum deviations and an average difference of less than one degree. Deeper down in the soil the accuracy is less, the deepest measurement M_{534} showing on average one degree higher mea-

Appendix

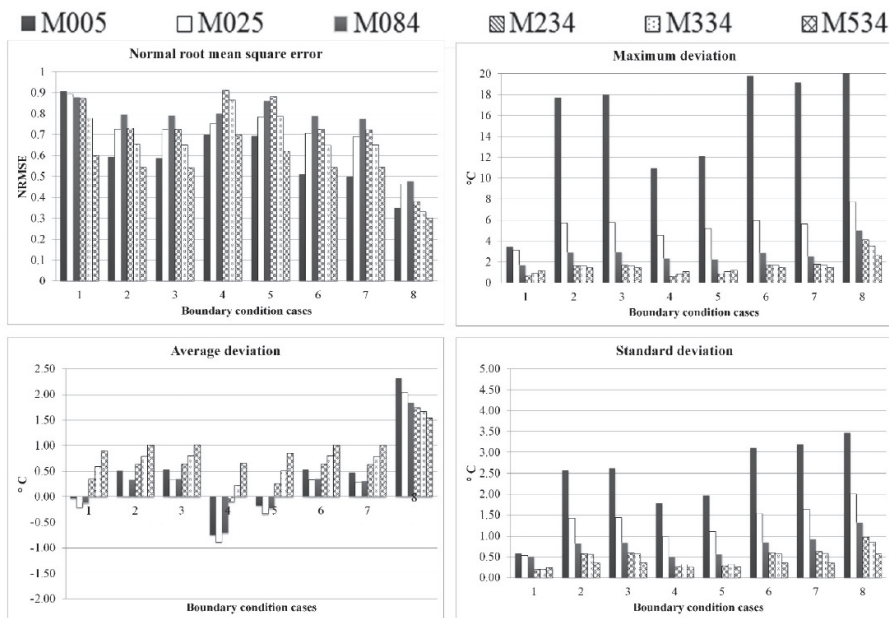


Fig. 6. Results from the boundary case studies with the one-dimensional model. The deviation is defined as measured value minus calculated value.

sured temperatures compared to the calculation. Note that the calculated temperature in the soil surface layers is slightly higher than the measurements. Using the air temperature as boundary condition, BC2 reduces the accuracy of the fit significantly, but still provides almost as accurate results in the lower soil layers. As expected, at the upper measurement positions (top soil layer) the resulting accuracy is significantly lower. This is reflected in a high maximum temperature deviation in the upper soil layers, especially at M005.

Using a convective boundary condition at the soil surface incorporating the air temperature (BC3) leads to almost identical calculated temperature profiles as those obtained when forcing the surface temperature to follow the measured air temperatures (BC2). When choosing the heat transfer coefficient at the lower value of nine W/m²·K as used by Jang and Choi [21], the fit in the soil surface becomes less accurate.

The combination of convective and net radiation at the surface (case BC4) gives a large improvement in the fit lower down in the soil compared to boundary condition (case BC2). The extra energy added to the soil by including the net radiation balance boosts the soil temperatures during the summer months. The fit of the two lowest measurement positions improves compared to case BC1, except in the soil surface layer. The surface temperatures in this case are overestimated. Using the full energy balance (case BC5) has a similar effect on the temperatures lower down in the soil as with case BC4, but the additional heating of the soil surface is less because the latent heat is included. The results are in accordance with the findings of Cleall and Munoz-Criollo [20], who concluded that using the full heat balance in an 1D analytical model leads to calculations that match well with measurements. In our case, a somewhat better accuracy is achieved both at moderate depth (less than 1

degree versus over 2 degrees) as well as in the soil surface. The difference with the approach of Cleall is that they used correlations for the components of the soil surface energy balance based upon average values of relevant weather parameters. Since we used onsite measurements, the resulting predictions can be expected to be better. In our results, the general trend of the calculated temperature profile in the soil surface follows the measurements, but shows spikes with non-physically high temperature values. The probable cause is related to the calculation of the convective heat transfer coefficient h using Eq. (6). Low values of h lead to overestimation of the effect of net solar radiation. Due to the discretization of the top boundary condition in the numerical scheme, the heating effect of the net solar radiation with a near zero value for h becomes so large that the upper calculation cell gets a non-physical high temperature during that time step. This error will propagate further down into soil domain over time. Using a minimum cut-off value for the convective heat transfer coefficient reduces this effect. Even with a minimum value of $h = 50 \text{ W/m}^2\text{·K}$, the soil surface temperatures are periodically overestimated. Using the easier to implement boundary conditions of case BC6 (daily averaged air temperatures) and BC7 (monthly averaged air temperatures) leads to very similar results as with BC2 (measured air temperatures at 10 min intervals), demonstrating that for the temperature development in the soil the temporal resolution of the boundary condition is of less importance. For pipeline models, often real air temperature data are unavailable and statistical weather data are used instead. Often the monthly normal temperatures are used to define the soil boundary condition. In boundary condition case 8, the monthly normal temperatures of the Kvitsøy station are used as input (eKlima [31]). This gives the worst prediction of soil temperature profiles at all depths. The average deviations are doubled to 1.5–2.0 °C.

Appendix

374

A. Oosterkamp et al./Applied Thermal Engineering 100 (2016) 367–377

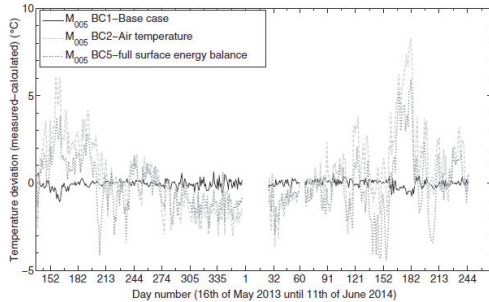


Fig. 7. Deviation between measured and calculated temperatures close to soil surface for three different boundary condition cases: base case BC1, air temperature BC2, and full surface energy balance BC5.

Fig. 7 shows the daily averaged temporal development of the deviation between measured and calculated temperatures in the soil surface layer for three boundary cases. For the base case (**BC1**), during the summer, the calculated temperatures are slightly too high, while during the winter they are too low. This could be an indication that moisture transport in the upper soil layer plays a minor role in the soil heat transfer at this location. For the other two cases, the seasonally dependency is opposite, during the summer the calculated temperatures are too low. For the air temperature boundary condition case (**BC2**) this can be explained from soil surface layer temperature reaching higher temperatures compared to the air temperature during summer day time. For the full surface energy boundary condition case (**BC5**), this difference during the summer is much less than with **BC2**. The probable cause here is an overestimation of the latent and sensible heat or a season dependent measurement error of the radiation balance. During the winter months, the calculated soil surface layer temperature is too high. For the **BC2** case, this is associated with the air temperature being higher than the soil surface layer temperature. For the **BC5** case, a probable cause is underestimation of the latent and sensible heat or a seasonable dependent measurement error of the radiation balance.

Fig. 8 shows the comparison between the daily averaged sum of q_e and q_h as derived from the surface balance in the base case

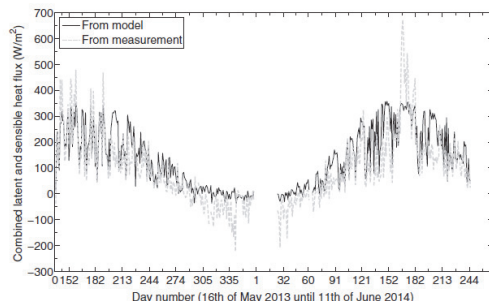


Fig. 8. Comparison between the sum of q_e and q_h as derived from the surface balance in the base case simulation and the measurement-derived values.

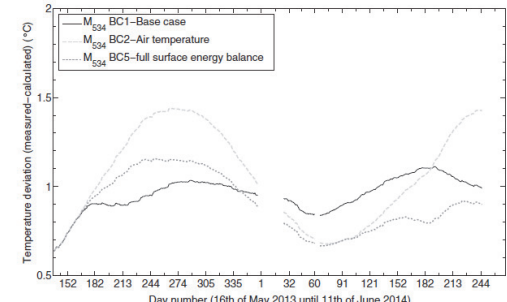


Fig. 9. Deviation between measured and calculated soil temperatures at 5.34 m depth for three different boundary condition cases: base case BC1, air temperature BC2 and full surface energy balance BC5.

simulation and the measurement-derived values. Clearly, during the summer the measured values are higher and during the winter lower than the model derived values.

Fig. 9 shows the effect of these three boundary condition cases on the temporal development of the soil temperatures at 5.34 m depth. The deviations are clearly sine shaped with a relatively similar mean of 0.8–1.0 °C but different amplitudes for the three cases. For the base case (**BC1**), the peak-to-peak amplitude is 0.3 °C. For the air temperature case (**BC2**) it is 0.5 °C, and for the full energy balance case (**BC5**) it is 0.7 °C.

The mean deviation could be a systematic error caused by the presence of the warm pipe. At the measurement location, the pipeline fluid (natural gas) has a higher temperature than the soil. The effect of the presence of the pipeline on the soil temperature profiles was studied with the 2D numerical model. Over distance the amplitude of the gas temperature fluctuations attenuates exponentially. For distances several metres away from the pipe, the temperature of the gas flowing inside the pipe can be considered constant. During the simulation, the gas temperature is kept at the average of 27 °C. The initial temperature profile is set up in a similar way as that of the 1D numerical model and the other boundary conditions remain the same. **Fig. 10** shows the soil temperature profiles at different times during the year at 10 m and 24 m lateral distance from the pipe outer wall. From **Fig. 10**, it can be seen that at 10 m lateral distance there is still some influence of the pipe wall temperature upon the soil temperature profile. During February and November, the soil temperatures at 5 m depth are 1–1.2 °C higher at 10 m distance from the pipe, reducing to 0.5–0.8 °C during May and August. This is in good agreement with the deviations obtained with the 1D simulation using the base case boundary conditions. Largely, the deviations between the 1D model and the measurements deeper in the soil can be explained by the presence of the warmer pipe.

4.3. Effect of soil surface boundary conditions on the pipe to soil heat transfer

The 2D Ansys model was used to evaluate the effect of different soil surface boundary conditions on the heat transfer over the pipe wall. When modelling pipe flow, often only the daily average air temperature is available as input for the boundary condition (**BC6**). The resulting heat transfer over the pipe wall was compared to those obtained when using the base case boundary condition (**BC1**), employing the measured soil surface tempera-

Appendix

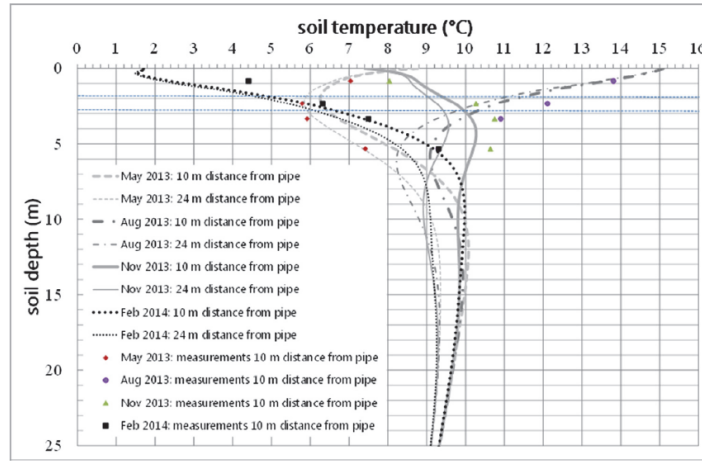


Fig. 10. Fluent Ansys simulations of two soil temperature profiles at different distances from the pipe wall and at different dates. The blue dashed horizontal lines indicate the upper and lower level of the pipe in the soil. The markers show the measured soil temperature values at the different dates. (For interpretation of the references to colour in this figure legend, the reader is referred to the web version of this article.)

tures. For each run of the model the measurement data derived gas temperatures, as described in the previous section, were used in the convective boundary condition at the pipe inner wall. In addition, the boundary case **BC8**, using monthly normal air temperatures was run. For both cases, the pipe wall heat transfer is compared to the base case, and the resulting deviations are shown in Fig. 11. The results show that during the summer months, using the air temperature as boundary condition increases the heat transfer between gas and the ambient by up to 6 W/m^2 . During the winter months, the resulting heat transfer is $0.5\text{--}3 \text{ W/m}^2$ less. The deviations are larger when using the monthly averaged air temperatures. Updating the air temperatures in each time step (**BC2**) does not improve accuracy compared to the use of daily averaged values.

With an average heat flux from gas to ambience of 30 W/m^2 , the effect of choosing air temperature as the soil surface boundary condition instead of measured soil surface temperatures leads in the summer months to a 15% too high heat flux with both **BC2** and **BC6** and a 20% too high heat flux with **BC8**. This is consistent with the air temperature during the summer being on average lower than the soil surface temperature. During the winter months, this is the opposite, with higher heat flux due to the choice of air temperatures as soil surface boundary condition.

5. Conclusions

When modelling the heat transfer between gas pipelines and the ambient, assumptions are made regarding the choice of thermal boundary condition at the soil surface. In this study, we looked at the effect of different approaches to define the boundary condition at the soil surface. The resulting accuracy of soil profile temperature prediction and pipe to ambient heat transfer rate were assessed, using both 1D and 2D numerical models for a specific buried pipeline case. In the simulations, measurements of the radiation balance, key weather parameters and soil surface temperatures were used to define cases with different soil surface boundary condition assumptions. The measured soil thermal profile was used to verify the calculations and to assess the effect of each boundary condition case. The results give rise to the following conclusions:

1. Using the measured soil surface temperature as boundary condition (base case) in the 1D numerical model provides the best prediction of the soil temperature profile. The model gives a minor over-prediction of temperatures in the upper soil layer during the summer ($<1^\circ\text{C}$). A possible cause of this is the omission of heat transfer associated with soil moisture transport and evaporation at the soil surface in the model. The temperature deviations in the deeper soil layers can be related to the presence of the warmer gas pipe in the soil.

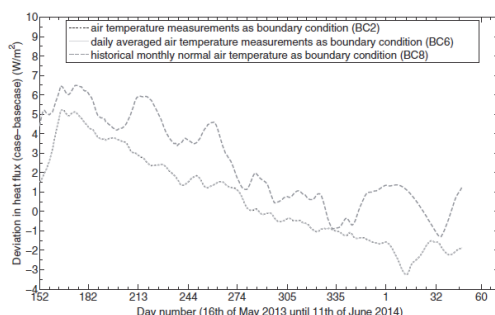


Fig. 11. Pipe wall heat transfer: deviation from base case (BC1) when using available air temperature data as boundary conditions. The black line is for monthly normal, and the grey line for daily averaged air temperature data. The start date is 1 June 2013.

Appendix

376

A. Oosterkamp et al./Applied Thermal Engineering 100 (2016) 367–377

2. Compared to the base case, using the full surface energy balance as soil surface boundary condition results in comparable calculation accuracy for the four lowest measurement positions in the soil. In the soil surface, the accuracy is reduced. The probable causes are errors in the estimation of the latent and sensible heat, or a reasonable dependent measurement error of the radiation balance.
3. When using the measured air temperature as soil surface boundary condition, the accuracy of the predicted soil temperature profiles is significantly reduced. The biggest differences are seen in the soil surface layer, the effect deeper down in the soil is less. During the summer months, the temperatures in the soil surface are under-predicted by as much as 8 °C, while during the winter the predicted soil surface temperature is too high by up to 3 °C. Using daily averaged or monthly averaged air temperature measurements in the soil surface boundary condition does not further reduce the calculation accuracy significantly. For the 2D model, applying the measured air temperature as soil surface boundary condition instead of the measured soil temperatures, the difference in the heat transfer rate between pipe and ambient is found to be as large as 16% and varying in time. Using daily averaged values of the measured air temperature does not change this difference noticeably.
4. Using historically based, monthly normal temperatures as the soil surface boundary condition do reduce the calculation accuracy. The resulting average deviations of the calculated soil temperature profiles are at least twice those obtained with the other boundary condition cases. The resulting error in heat transfer rate between pipe and ambient is found to be larger (up to 20%) and varying in time.
5. The one-dimensional numerical model was used to determine the soil energy balance and to derive the combined effects of latent and sensible heat due to convection and evaporation at the soil surface. This was compared to the calculated values based upon wind speed, air pressure, relative humidity and ambient temperature measurements using the correlations from Herb et al. [25]. Both approaches are in good agreement and follow each other in overall trend, but there are seasonal differences. The used correlation from Herb et al. [25] results in higher values during the summer months and lower values during the winter.
6. The fit between the one-dimensional numerical model and the data indicates that the influence of the pipe at 10 m lateral distance is in accordance with the calculations of the 2D numerical model. The influence increases from a minimum at the soil surface to a maximum at 10 m depth of approximately 1.0 °C. An error of the same magnitude is found for the lowest measurement position if the 1D numerical model is employed.

Acknowledgements

This work is funded by the Norwegian gas transmission operator Gassco AS as part of a project to improve flow modelling in natural gas pipelines. Special thanks go to Richard Markeson for his help in projecting and installing the measurement equipment.

Nomenclature

h	Heat transfer coefficient ($\text{W}/\text{m}^2 \cdot ^\circ\text{C}$)
k_v	Constant representing coverage of overgrowing vegetation
q^*	Net exchange of radiation (W/m^2)
q_h	Sensible heat transfer (W/m^2)
q_{le}	Latent heat transfer (W/m^2)
q_g	Soil conductive heat transfer (W/m^2)
r_{sat}	Saturation specific humidity ($\text{kg}_{\text{water}}/\text{kg}_{\text{air}}$)
r_a	Ambient specific humidity ($\text{kg}_{\text{water}}/\text{kg}_{\text{air}}$)

u_s	Wind velocity at ground level (m/s)
C_p	Specific heat ($\text{J}/\text{kg} \cdot ^\circ\text{C}$)
C_{fc}	Constant for forced convection
C_{nc}	Constant for natural convection
ΔT_v	Difference between virtual air temperature and soil surface temperature ($^\circ\text{C}$)
T	Temperature ($^\circ\text{C}$)
T_a	Ambient air temperature ($^\circ\text{C}$)
T_m	Mean soil surface temperature ($^\circ\text{C}$)
T_s	Soil surface temperature ($^\circ\text{C}$)
T_g	Ground temperature at depth ($^\circ\text{C}$)
T_v	Virtual temperature ($^\circ\text{C}$)
U	Overall heat transfer coefficient ($\text{W}/\text{m}^2 \cdot ^\circ\text{C}$)
BC	Boundary condition
NRMSE	Normal root mean square error
α	Thermal diffusivity (m^2/s)
λ	Thermal conductivity ($\text{W}/\text{m} \cdot ^\circ\text{C}$)
ρ	Density (kg/m^3)

References

- [1] R.A. Archer, M.J. O'Sullivan, Models for heat transfer from a buried pipe, SPE J. 2 (1997).
- [2] H.H. Bau, Heat losses from a fluid flowing in a buried pipe, Int. J. Heat Mass Tran. 25 (1982) 1621–1629.
- [3] F. Sund, A. Oosterkamp, S. Mongstad Hope, Pipeline modeling – impact of ambient temperature and heat transfer modeling, in: ISOPE 2015, ISOPE, Kona, Hawaii, 2015.
- [4] F.P. Incropera, D.P. DeWitt, Heat and Mass Transfer, Wiley & Sons, Indiana, 2002.
- [5] H. Bau, Convective heat losses from a pipe buried in a semi-infinite porous medium, Int. J. Heat Mass Tran. 27 (1984) 2047–2056.
- [6] M. Chaczkyowski, Transient flow in natural gas pipeline-the effect of pipeline thermal model, Appl. Math. Model. 34 (2010) 1051–1067.
- [7] E. Nicholas, The impact of pipe and ground on pipeline temperature transients, Pipeline Simulation Interest Group, PSIG, California, 2011.
- [8] J.F. Helgaker, A. Oosterkamp, L.I. Langelandsvik, T. Ytrehus, Validation of 1D flow model for high pressure offshore natural gas pipelines, J. Nat. Gas Sci. Eng. 16 (2014) 44–56.
- [9] A. Oosterkamp, J.F. Helgaker, T. Ytrehus, Modelling of natural gas pipe flow with rapid transients – case study of effect of ambient model, in: Energy Procedia TCTC2014, 2014.
- [10] G. Yu, B. Yu, D. Han, L. Wang, Unsteady-state thermal calculation of buried oil pipeline using a proper orthogonal decomposition reduced order model, Appl. Therm. Eng. 31 (2011) 177–189.
- [11] G. Florides, S. Kalogirou, Ground heat exchangers – a review of systems, models and applications, Renew. Energ. 32 (2007) 2461–2478.
- [12] O. Ozgener, L. Ozgener, J.W. Tester, A practical approach to predict soil temperature variations for geothermal (ground) heat exchangers applications, Int. J. Heat Mass Tran. 62 (2013) 473–480.
- [13] D. Hillel, Introduction to Soil Physics, Academic Press, New York, 1982.
- [14] X. Liu, Y. Xiao, K. Inthavong, J. Tu, A fast and simple numerical model for a deeply buried underground tunnel in heating and cooling applications, Appl. Therm. Eng. 62 (2014) 542–552.
- [15] M. Krati, J.F. Kreider, Analytical model for heat transfer in an underground tunnel, Energy Convers. Manag. 37 (1996) 1561–1574.
- [16] H.S. Carslaw, J.C. Jaeger, Conduction of Heat in Solids, Oxford Science Publications, Oxford, 1959.
- [17] W.J. Parton, Predicting soil temperatures in a short grass steppe, Soil Sci. 138 (1984) 93–101.
- [18] S. Brown, K. Pregitzer, D. Reed, A.J. Burton, Predicting daily mean soil temperature from daily mean air temperature in four northern hardwood forest stands, Forest Sci. 46 (2000).
- [19] M.S. Jin, T. Mullenens, A study of the relations between soil moisture, soil temperatures and surface temperatures using ARM observations and offline CLM4 simulations, Climate 2 (2014) 279–295.
- [20] P.J. Cleall, J.J. Munoz-Criollo, Analytical solutions for ground temperature profiles and stored energy using meteorological data, Transp. Porous Media 106 (2015) 181–199.
- [21] C. Jang, C. Choi, A prediction of ground temperature distribution using n-factor and convective coefficient, in: ISOPE 2014, ISOPE, Busan, Korea, 2014, pp. 587–591.
- [22] P.J. Williams, C.W. Smith, The Frozen Earth, Cambridge University Press, New York, 1989.
- [23] G. Mihalakakou, M. Santamouris, J.O. Lewis, D.N. Asimakopoulos, On the application of the energy balance equation to predict ground temperature profiles, Sol. Energy 60 (1997) 181–190.
- [24] M. Mostrel, B. Givoni, Windscreens in radiant cooling, Passive Solar Journal 1 (1982).

Appendix

- [25] W.R. Herb, B. Janke, O. Mohseni, H.G. Stefan, Ground surface temperature simulation for different ground covers, *J. Hydrol.* (Amst.) 356 (2008) 327–343.
- [26] R.B. Stull, *An Introduction to Boundary Layer Meteorology*, Kluwer Academic Publishers, 1950.
- [27] Huskeflux Thermal Sensors, Instruction Manual NR01 Four-Component Net Radiation Sensor, Huskeflux Thermal Sensors, Delft, 2011.
- [28] A. Oosterkamp, Modelling and measuring soil thermal properties and pipeline to soil heat transfer of a natural gas pipeline, in: ISOPE 2015, ISOPE, Kona, Hawaii, 2015.
- [29] L. Eplebaum, I. Kutsov, A. Pilchin, *Applied Geothermics*, Springer, 2014.
- [30] T.J. Chung, *Computational Fluid Dynamics*, Cambridge University Press, 2002.
- [31] Norwegian Meteorological Institute, eKlima, Norwegian Meteorological Institute, www.eklima.no, 2014 (accessed 31.07.14).
- [32] ANSYS, *ANSYS FLUENT Theory Guide*, ANSYS Inc., Canonsburg, PA, 2014.
- [33] R.H.S. Winterbottom, Where did the Dittus and Boelter equation come from?, *Int. J. Heat Mass Tran.* 41 (1998) 809–810.
- [34] P.J. Flatau, R.L. Walko, W.R. Cotton, Polynomial fits to saturation vapor pressure, *J. Appl. Meteorol.* 31 (1992) 1507–1513.

Article [f]

**'Modelling and Measuring Soil Thermal Properties and Soil Heat Transfer
of a Natural Gas Pipeline'**

A.Oosterkamp

Submitted to the International Journal of Polar and Offshore Engineering,
September 2015.

Is not included due to copyright

Article [g]

'Heat transfer modelling of natural gas pipe flow-effect of yearly ambient temperature cycles'

A.Oosterkamp

Accepted for presentation at ISOPE 2016, the Twenty-sixth International Offshore and Polar Engineering Conference, Rhodes, Greece.

Is not included due to copyright

Appendix

Appendix B: Derivation of governing equations for 1D flow

The equations used for 1D unsteady compressible viscous flow with external heat transfer are:

Conservation of mass:

$$\frac{\partial \rho}{\partial t} + \frac{\partial(\rho u)}{\partial x} = 0 \quad (1)$$

Conservation of momentum:

$$\frac{\partial(\rho u)}{\partial t} + \frac{\partial(\rho u^2 + p)}{\partial x} = -\frac{f \rho u |u|}{2D} - \rho g \sin \theta \quad (2)$$

Energy:

$$\rho c_v \left(\frac{\partial T}{\partial t} + u \frac{\partial T}{\partial x} \right) + T \left(\frac{\partial p}{\partial T} \right)_p \frac{\partial u}{\partial x} = \frac{f \rho u^3}{2D} - \frac{4q_w}{D} \quad (3)$$

Conservation of mass

How the conservation of mass equation is obtained in general form is described in for example White [85]. The derivation to 1D form shown here is taken from Ytrehus [86], using the integral form of a control volume. The net flux of mass entering the boundaries of a control volume is equal to the change of mass inside the control volume within a time interval. This can be expressed as:

$$\int_V \frac{\partial \rho}{\partial t} dV + \int_S \rho \vec{u} \cdot \vec{n} dS = 0 \quad (4)$$

Here ρ is the fluid density, and V and S are the volume and surface area of the control volume. The Reynolds transport theorem is used together with the transformation:

$$\int_V \frac{\partial \rho}{\partial t} dV = \frac{\partial}{\partial t} \int_V \rho dV \quad (5)$$

Together this result in (with system volume V passing through local control volume S^* :

Appendix

$$\frac{\partial}{\partial} \int_{V^*} \rho dV + \int_{S^*} \rho (\vec{u} - \vec{b}) \cdot \vec{n} dS = 0 \quad (6)$$

A fixed control volume is used in pipe flow, thus the control surface velocity vector, b , is set to zero. Further, the mean velocity u is defined as:

$$u = \frac{1}{A} \int_A u_r dA \quad (7)$$

Integration of Equation (6) over the pipe cross section A , assuming that the density ρ is constant over cross section , and using $dV=dAdx$ results in:

$$\frac{\partial \rho}{\partial t} + \frac{\partial(\rho u)}{\partial x} = 0 \quad (8)$$

In Thorley and Tiley [11], further steps are described. Firstly, the relationship between density ρ and pressure p is described through the compressibility Z , obtained from the Equation of State:

$$\rho = \frac{p}{ZRT} \quad (9)$$

This is rewritten as:

$$\ln \rho = \ln p - \ln Z - \ln R - \ln T \quad (10)$$

The time derivative of Equation (10) is:

$$\frac{1}{\rho} \frac{\partial \rho}{\partial t} = \frac{1}{p} \frac{\partial p}{\partial t} - \frac{1}{Z} \frac{\partial Z}{\partial t} - \frac{1}{T} \frac{\partial T}{\partial t} \quad (11)$$

The compressibility factor is a function of p and T and its derivative with respect to time is:

$$\frac{\partial Z}{\partial t} = \left(\frac{\partial Z}{\partial p} \right)_T \left(\frac{\partial p}{\partial t} \right) + \left(\frac{\partial Z}{\partial T} \right)_p \frac{\partial T}{\partial t} \quad (12)$$

Equation (8) can be rewritten as:

$$\frac{1}{\rho} \frac{\partial \rho}{\partial t} = \left[\frac{1}{p} - \frac{1}{Z} \left(\frac{\partial Z}{\partial p} \right)_T \right] \left(\frac{\partial p}{\partial t} \right) - \left[\frac{1}{T} + \frac{1}{Z} \left(\frac{\partial Z}{\partial T} \right)_p \right] \left(\frac{\partial T}{\partial t} \right) \quad (13)$$

Using the mass flow rate \dot{m} instead of velocity u :

Appendix

$$\dot{m} = \rho u A \quad (14)$$

Equation (8) can be rewritten as:

$$\frac{1}{\rho} \frac{\partial \rho}{\partial t} = - \frac{ZRT}{pA} \frac{\partial \dot{m}}{\partial x} \quad (15)$$

Combining Equations (13) and (15) gives:

$$\frac{\partial p}{\partial t} = \left[\frac{1}{T} + \frac{1}{Z} \left(\frac{\partial Z}{\partial T} \right)_p \right] \left[\frac{1}{p} - \frac{1}{Z} \left(\frac{\partial Z}{\partial p} \right)_T \right]^{-1} \frac{\partial T}{\partial t} - \frac{ZRT}{pA} \left[\frac{1}{p} - \frac{1}{Z} \left(\frac{\partial Z}{\partial p} \right)_T \right]^{-1} \frac{\partial \dot{m}}{\partial x} \quad (16)$$

Momentum equation

The starting point is Newton second law, stating that the sum of forces acting on a system of gas particles is equal to their momentum rate of change. The derivation of the momentum equation can be found in textbooks, like, White [85]. The derivation to the 1D form shown here is taken from Ytrehus [86]. The acting forces on the fluid are pressure forces, shear forces and body forces (gravity in case of pipe flow).

The linear momentum rate of change for a control volume can be written in integral form as:

$$\frac{d}{dt} (m\vec{u}) = \sum \vec{F} = \int_V \frac{\partial}{\partial t} (\rho\vec{u}) dV + \int_S \rho\vec{u} (\vec{u} \cdot \vec{n}) dS \quad (17)$$

Using the Reynolds control theorem together with Equation (17) gives:

$$\frac{\partial}{\partial t} \int_{V^*} \rho\vec{u} dV + \int_{S^*} \rho\vec{u} (\vec{u} - \vec{b}) \cdot \vec{n} dS = \sum \vec{F} \quad (18)$$

The sum of the forces in the pipe flow direction, with constant pipe cross-section D , is:

$$\sum F_x = pA - \left(p + \frac{\partial p}{\partial x} dx \right) A - \tau_w \pi D - \rho g A \sin \alpha \quad (19)$$

Using the general expression for a turbulent flow profile

Appendix

$$\beta u^2 A = \int_A u_r^2 dA \quad (20)$$

With $\beta=1$, and control surface velocity vector, b set to zero, combining and integrating Equation (18) and Equation (19) leads to:

$$\frac{\partial(\rho u)}{\partial t} + \frac{\partial(\rho u^2 + p)}{\partial x} = \tau_w \pi D - \rho g \sin \alpha \quad (21)$$

The shear force τ_w in Equation (21) can be expressed in terms of the Darcy friction factor, the result is Equation (2). This is developed further by Helgaker[10] in the steps below. Firstly, use the following expression for the gas velocity:

$$u = \frac{\dot{m}ZRT}{pA} \quad (22)$$

Partial differentiation of the logarithmic identity with respect to x gives:

$$\frac{1}{u} \frac{\partial u}{\partial x} = \frac{1}{\dot{m}} \frac{\partial \dot{m}}{\partial x} + \frac{1}{Z} \frac{\partial Z}{\partial x} + \frac{1}{T} \frac{\partial T}{\partial x} - \frac{1}{p} \frac{\partial p}{\partial x} \quad (23)$$

With fully written out partial derivation of Z with respect to x this becomes:

$$\frac{1}{u} \frac{\partial u}{\partial x} = \frac{1}{\dot{m}} \frac{\partial \dot{m}}{\partial x} + \left[\frac{1}{T} + \frac{1}{Z} \left(\frac{\partial Z}{\partial T} \right)_p \right] \frac{\partial T}{\partial x} - \left[\frac{1}{p} - \frac{1}{Z} \left(\frac{\partial Z}{\partial p} \right)_T \right] \frac{\partial p}{\partial x} \quad (24)$$

Using the mass flow rate \dot{m} instead of velocity u and Equation (24) in Equation (2) gives:

$$\begin{aligned} \frac{\partial \dot{m}}{\partial t} &= \frac{\dot{m}ZRT}{pA} \left(-2 \frac{\partial \dot{m}}{\partial x} + \dot{m} \left[\frac{1}{p} - \frac{1}{Z} \left(\frac{\partial Z}{\partial p} \right)_T \right] \frac{\partial p}{\partial x} - \dot{m} \left[\frac{1}{T} + \frac{1}{Z} \left(\frac{\partial Z}{\partial T} \right)_p \right] \frac{\partial T}{\partial x} \right) \\ &\quad - A \frac{\partial p}{\partial x} - \frac{fZRT\dot{m}|\dot{m}|}{2DAp} - \frac{pA}{ZRT} g \sin \theta \end{aligned} \quad (25)$$

Energy Equation

The energy equation used in the flow model is in the non-conservative internal energy form. The derivation is provided in for example White [85]. A derivation is also given in Ytrehus [87]. The derived form of the energy equation looks like this:

Appendix

$$\rho c_v \frac{DT}{Dt} + T \left(\frac{\partial p}{\partial T} \right)_\rho \frac{\partial u_j}{\partial x_j} = \tau_{ij} \frac{\partial u_i}{\partial x_j} + \frac{\partial}{\partial x_j} \left[k \frac{\partial T}{\partial x_j} \right] \quad (26)$$

To get to the one-dimensional form, this equation is integrated over the pipe cross-section. This has been detailed in Ytrehus and Helgaker [88]. The same steps are repeated here for the non-conservative internal energy form. The Reynolds decomposition for turbulent flow is used:

$$\begin{aligned} u_i &= \bar{u}_i + u'_i \\ T &= \bar{T} + T' \\ p &= \bar{p} + p' \end{aligned} \quad (27)$$

The Reynolds decompositions are inserted in Equation (26) and averaged over time.

The first term to the right, the dissipation term is developed as:

$$\bar{\Phi} = \tau_{ij} \frac{\partial \bar{u}_i}{\partial x_j} \rightarrow \left(\bar{\tau}_{ij} - \bar{\rho} \bar{u}_i \bar{u}_j' \right) \rightarrow \tau_{ij}^{total} \frac{\partial u_i}{\partial x_j} \quad (28)$$

All the time-averaged terms are subsequently averaged over the pipe cross-section. For the dissipation term, this leads to:

$$\langle \bar{\Phi} \rangle = \frac{1}{A} \int_A \tau \frac{\partial \bar{u}}{\partial y} dA \quad (29)$$

This needs an expression of the turbulent velocity profile. In Ytrehus and Helgaker [88], a classical expression for the velocity profile and shear layer in the core layer, overlap layer and viscous sub layer is used with the following results:

$$\langle \bar{\Phi} \rangle = \rho \frac{f u^3}{2D} \sqrt{\frac{C_f}{2}} \left[y_0^+ + \frac{1}{\kappa_k} \ln \frac{R^+}{y_0^+} - \frac{3}{2\kappa_k} + \frac{y_0^+}{R^+ \kappa_k} \right] \quad (30)$$

C_f is the Fanning friction factor, κ_k the Von Kármán constant and y_0^+ and R^+ are dimensionless sublayer thickness and pipe radius.

Expressed in one dimension, Equation (26) now becomes (analogous to Thorley and Tiley [11]):

$$\rho c_v \left(\frac{\partial T}{\partial t} + \frac{\partial x}{\partial t} \frac{\partial T}{\partial x} \right) + T \left(\frac{\partial p}{\partial T} \right)_\rho \frac{\partial u}{\partial x} = \frac{Wu + \Omega}{A} = \frac{\rho f u^3}{2D} - \frac{4q_w}{D} \quad (31)$$

Appendix

With W being the frictional force per unit length ($W=4\rho f|u|u/2D$) and \mathcal{Q} the heat flow per unit length ($\mathcal{Q}=4q_wA$) and time of the pipe.

The simple dissipation term ρfu^3 in Equation (31) is an extrapolation of that for laminar flow by replacing the laminar friction factor ($64/Re$) by the turbulent friction factor f . To include the turbulent structure it needs to be expanded according to Equation (30), resulting in:

$$\rho c_v \left(\frac{\partial T}{\partial t} + \frac{\partial x}{\partial t} \frac{\partial T}{\partial x} \right) + T \left(\frac{\partial p}{\partial T} \right)_p \frac{\partial u}{\partial x} = \rho \frac{4\tau_w}{\rho u^2 D} u^3 F - \frac{4q_w}{D} \quad (32)$$

Here F is the dissipation factor that is a function of the Reynolds number, following from Equation (30):

$$F = \sqrt{\frac{f}{8}} \left[y_0^+ + \frac{1}{\kappa_k} \ln \frac{R^+}{y_0^+} - \frac{3}{2\kappa_k} + \frac{y_0^+}{R^+ \kappa_k} \right] \quad (33)$$

According to Ytrehus and Helgaker [88], $R^+ = 0.5 * Re^{*} \sqrt{f/8}$ and y_0^+ is set to 10, and for typical Reynolds numbers and pipe roughness in natural gas pipe flow, F is close to 1.

The further derivation is shown in Helgaker[10] and summarized here. First, the ‘Joule-Thomson’, expressed as derivative of pressure with respect of temperature needs to be converted to an expression using the equation of state.

$$\left(\frac{\partial p}{\partial T} \right)_p = \rho R \left[Z + T \left(\frac{\partial Z}{\partial T} \right)_p \right] \quad (34)$$

Dividing by ρc_v gives:

$$\frac{\partial T}{\partial t} = -u \frac{\partial T}{\partial x} - \frac{R}{c_v} T \left[Z + T \left(\frac{\partial Z}{\partial T} \right)_p \right] \frac{\partial u}{\partial x} + \frac{1}{\rho c_v} \frac{f \rho u^3}{2D} - \frac{1}{\rho c_v} \frac{4U}{D} (T - T_a) \quad (35)$$

This leads to:

$$\begin{aligned} \frac{\partial T}{\partial t} &= -\frac{\dot{m}ZRT}{pA} \frac{\partial T}{\partial x} - \frac{R}{c_v} T \left[Z + T \left(\frac{\partial Z}{\partial T} \right)_p \right] \frac{\dot{m}ZRT}{pA} \\ &\times \left[\frac{1}{\dot{m}} \frac{\partial \dot{m}}{\partial x} + \frac{1}{Z} \left(\left(\frac{\partial Z}{\partial p} \right)_T \frac{\partial p}{\partial x} + \left(\frac{\partial Z}{\partial T} \right)_p \frac{\partial T}{\partial x} \right) + \frac{1}{T} \frac{\partial T}{\partial x} - \frac{1}{p} \frac{\partial p}{\partial x} \right] \\ &+ \frac{f}{2c_v D} \left(\frac{ZRT |\dot{m}|}{pA} \right)^3 - 4U \frac{ZRT}{pc_v D} (T - T_a) \end{aligned} \quad (36)$$

Appendix

This can be rewritten into:

$$\begin{aligned}
 \frac{\partial T}{\partial t} = & -\frac{\dot{m}ZRT}{pA}\frac{\partial T}{\partial x} - \frac{\dot{m}(ZRT)^2}{pAc_v}T\left[\frac{1}{T} + \frac{1}{Z}\left(\frac{\partial Z}{\partial T}\right)_p\right] \\
 & \times \left(\frac{1}{\dot{m}}\frac{\partial \dot{m}}{\partial x} - \left[\frac{1}{p} - \frac{1}{Z}\left(\frac{\partial Z}{\partial p}\right)_T \right]\frac{\partial p}{\partial x} + \left[\frac{1}{T} + \frac{1}{Z}\left(\frac{\partial Z}{\partial T}\right)_p \right]\frac{\partial T}{\partial x} \right) \\
 & + \frac{f}{2c_v D} \left(\frac{ZRT|\dot{m}|}{pA} \right)^3 - 4U \frac{ZRT}{pc_v D} (T - T_a)
 \end{aligned} \tag{37}$$

Appendix C: Calibration coefficients PT100 sensors.

SENSOR CALIBRATION FUNCTIONS-PT100's

01	CHANNEL 02	PT100	$y = -0.00000122 x^3 + 0.00002409 x^2 + 0.00471644 x - 0.24642669$
02	CHANNEL 03	PT100	$y = -0.00000074 x^3 + 0.00000680 x^2 + 0.00205917 x + 0.04563493$
03	CHANNEL 04	PT100	$y = -0.00000142 x^3 + 0.00003426 x^2 + 0.00414312 x - 0.18452533$
04	CHANNEL 05	PT100	$y = -0.00000123 x^3 + 0.00003562 x^2 + 0.00496058 x - 0.30402681$
05	CHANNEL 06	PT100	$y = -0.00000048 x^3 - 0.00001015 x^2 + 0.00346171 x - 0.10030988$
06	CHANNEL 07	PT100	$y = 0.00000048 x^3 + 0.00003265 x^2 + 0.00259816 x - 0.1575088407$
07	CHANNEL 08	PT100	$y = 0.00000038 x^3 + 0.00003651 x^2 + 0.0035942 x - 0.14918403$
08	CHANNEL 09	PT100	$y = -0.00000005 x^3 - 0.00004280 x^2 + 0.00299523 x - 0.16579518$
09	CHANNEL 10	PT100	$y = -0.00000021 x^3 - 0.00002527 x^2 + 0.00493347 x - 0.31638390$
40	CHANNEL 11	PT100	$y = 0.00000005 x^3 - 0.00003726 x^2 + 0.00424717 x - 0.29223761$
41	CHANNEL 12	PT100	$y = 0.00000036 x^3 - 0.00006213 x^2 + 0.00308612 x - 0.07950819$
42	CHANNEL 13	PT100	$y = -0.00000060 x^3 - 0.00001531 x^2 + 0.00433196 x - 0.23458843$
43	CHANNEL 14	PT100	$y = 0.00000044 x^3 - 0.00006742 x^2 + 0.00440558 x - 0.07495497$
44	CHANNEL 15	PT100	$y = -0.00000022 x^3 - 0.00003503 x^2 + 0.00396780 x - 0.11091219$
45	CHANNEL 16	PT100	$y = 0.00000049 x^3 - 0.00002726 x^2 + 0.00281120 x - 0.34081292$
46	CHANNEL 17	PT100	$y = 0.00000011 x^3 - 0.00005799 x^2 + 0.00340279 x - 0.02400151$
47	CHANNEL 18	PT100	$y = -0.00000144 x^3 + 0.00000959 x^2 + 0.00642954 x - 0.00418518$
48	CHANNEL 19	PT100	$y = 0.00000017 x^3 - 0.00004549 x^2 + 0.00298155 x - 0.03561348$
49	CHANNEL 20	PT100	$y = -0.00000042 x^3 - 0.00001606 x^2 + 0.00325945 x - 0.11008189$
50	CHANNEL 21	PT100	$y = 0.00000009 x^3 - 0.00003653 x^2 + 0.00264629 x - 0.10162142$
51	CHANNEL 22	PT100	$y = -0.00000032 x^3 - 0.00002486 x^2 + 0.00316119 x - 0.04127221$
52	CHANNEL 23	PT100	$y = -0.00000055 x^3 - 0.00000851 x^2 + 0.00406766 x - 0.46428427$
53	CHANNEL 24	PT100	$y = -0.00000114 x^3 + 0.00000871 x^2 + 0.00437463 x + 0.02023250$
54	CHANNEL 25	PT100	$y = -0.00000020 x^3 - 0.00002400 x^2 + 0.00496051 x - 0.29423479$
55	CHANNEL 26	PT100	$y = 0.00000005 x^3 - 0.00004991 x^2 + 0.00409063 x - 0.03724903$
56	CHANNEL 27	PT100	$y = 0.00000029 x^3 - 0.00004842 x^2 + 0.00331857 x - 0.02565265$
57	CHANNEL 28	PT100	$y = 0.00000013 x^3 - 0.00002149 x^2 + 0.00279092 x - 0.07050170$
58	CHANNEL 29	PT100	$y = 0.00000007 x^3 - 0.00004067 x^2 + 0.00080560 x + 0.00367090$
59	CHANNEL 30	PT100	$y = 0.00000064 x^3 - 0.00004016 x^2 + 0.00169238 x - 0.39334720$
60	CHANNEL 31	PT100	$y = -0.00000100 x^3 - 0.00001280 x^2 + 0.00461675 x + 0.02651559$
61	CHANNEL 32	PT100	$y = -0.00000021 x^3 - 0.00002126 x^2 + 0.00440945 x - 0.13212262$
62	CHANNEL 33	PT100	$y = -0.00000024 x^3 - 0.00001206 x^2 + 0.00110528 x - 0.07042931$
63	CHANNEL 34	PT100	$y = -0.00000164 x^3 + 0.00004465 x^2 + 0.00426603 x - 0.14084408$
64	CHANNEL 35	PT100	$y = -0.00000049 x^3 - 0.00001331 x^2 + 0.00473606 x - 0.08162772$
65	CHANNEL 36	PT100	$y = -0.00000100 x^3 - 0.00000331 x^2 + 0.00599948 x - 0.16060144$
66	CHANNEL 37	PT100	$y = -0.00000119 x^3 + 0.00000888 x^2 + 0.00476687 x - 0.01799079$
67	CHANNEL 38	PT100	$y = -0.00000090 x^3 + 0.00000677 x^2 + 0.00313502 x - 0.12050269$
68	CHANNEL 39	PT100	$y = -0.00000071 x^3 + 0.00000431 x^2 + 0.00336929 x - 0.05489964$
69	CHANNEL 40	PT100	$y = -0.00000004 x^3 - 0.00003311 x^2 + 0.00228083 x - 0.03195113$
74	CHANNEL 45	PT100	$y = 0.00000258 x^3 - 0.00026957 x^2 + 0.00212937 x + 0.30885919$
76	CHANNEL 47	PT100	$y = 0.00000201 x^3 - 0.00021626 x^2 + 0.00139483 x + 0.27583142$
80	CHANNEL 101	PT100	$y = -0.00002995 x^2 + 0.00089838 x + 0.00000899$
81	CHANNEL 102	PT100	$y=0$
82	CHANNEL 103	PT100	$y = -0.00002995 x^2 + 0.00089838 x + 0.00000899$
83	CHANNEL 104	PT100	$y = -0.00002995 x^2 + 0.00089838 x + 0.00000899$
84	CHANNEL 105	PT100	$y = -0.00004991 x^2 + 0.00149730 x + 0.00001498$
85	CHANNEL 106	PT100	$y=0$
86	CHANNEL 107	PT100	$y = -0.00002995 x^2 + 0.00089838 x + 0.00000899$
87	CHANNEL 108	PT100	$y = -0.00002995 x^2 + 0.00089838 x + 0.00000899$
88	CHANNEL 109	PT100	$y = -0.00002995 x^2 + 0.00089838 x + 0.00000899$

Appendix

Appendix D: Europipe 2- Flow Model Data

Pipe element	Elevation (m)	steel wall layer thick	pp wall layer thickness (mm)	concrete wall layer thickness (mm)	burial depth	U
1	0	29.8	6	50	0	33
2	-14	29.8	6	50	0	33
3	-36	29.8	6	50	0	33
4	-36	29.8	6	0	2.1	2.5
5	-40	29.8	6	0	2.1	2.5
6	-42	29.8	6	0	2.1	2.5
7	-56	29.8	6	0	2.1	2.5
8	-82	29.8	6	0	2.1	2.5
9	-82	29.8	6	0	2.1	2.5
10	-80	29.8	6	0	2.1	2.5
11	-78	29.8	6	0	2.1	2.5
12	-78	29.8	6	0	2.1	2.5
13	-78	29.8	6	50	0	33
14	-80	29.8	6	50	0	33
15	-78	29.8	6	50	0	33
16	-81	29.8	6	50	0	33
17	-85	29.8	6	50	0	33
18	-80	29.8	6	50	0	33
19	-54	29.8	6	50	0	33
20	-32	44	6	0	2.1	2.5
21	0	44	6	0	2.1	2.5
22	28	44	6	0	2.1	2.5
23	72	44	6	0	2.1	2.5
24	110	44	6	0	2.1	2.5
25	120	44	6	0	2.1	2.5
26	111	44	6	0	2.1	2.5
27	109	44	6	0	2.1	2.5
28	92	44	6	0	2.1	2.5
29	85	44	6	0	2.1	2.5
30	29	44	6	0 partial		53
31	0	44	6	0 partial		53
32	-34	44	6	0 partial		53
33	-11	44	6	0 partial		53
34	0	44	3	0	2.3	1.5
35	20	44	3	0	2.3	1.5
36	39	44	3	0	2.3	1.5
37	42	44	3	0	2.3	1.5
38	51	44	3	0	2.3	1.5
39	56	44	3	0	2.3	1.5
40	59	44	3	0	2.3	1.5
41	63	44	3	0	2.3	1.5
42	76	44	3	0	2.3	1.5
43	89	44	3	0	2.3	1.5
44	82	44	3	0	2.3	1.5
45	58	44	3	0	2.3	1.5
46	45	44	3	0	2.3	1.5
47	44	44	3	0	2.3	1.5
48	37	44	3	0	2.3	1.5
49	35	44	3	0	2.3	1.5
50	30	44	3	0	2.3	1.5
51	21	44	3	0	2.3	1.5
52	40	44	3	0	2.3	1.5
53	33	44	3	0	2.3	1.5
54	34	44	3	0	2.3	1.5
55	52	44	3	0	2.3	1.5
56	24	44	3	0	2.3	1.5
57	22	44	3	0	2.3	1.5
58	15	44	3	0	2.3	1.5
59	20	44	3	0	2.3	1.5
60	18	44	3	0	2.3	1.5
61	14	44	3	0	2.3	1.5
62	18	44	3	0	2.3	1.5

Appendix E: Results from parameteric model studies

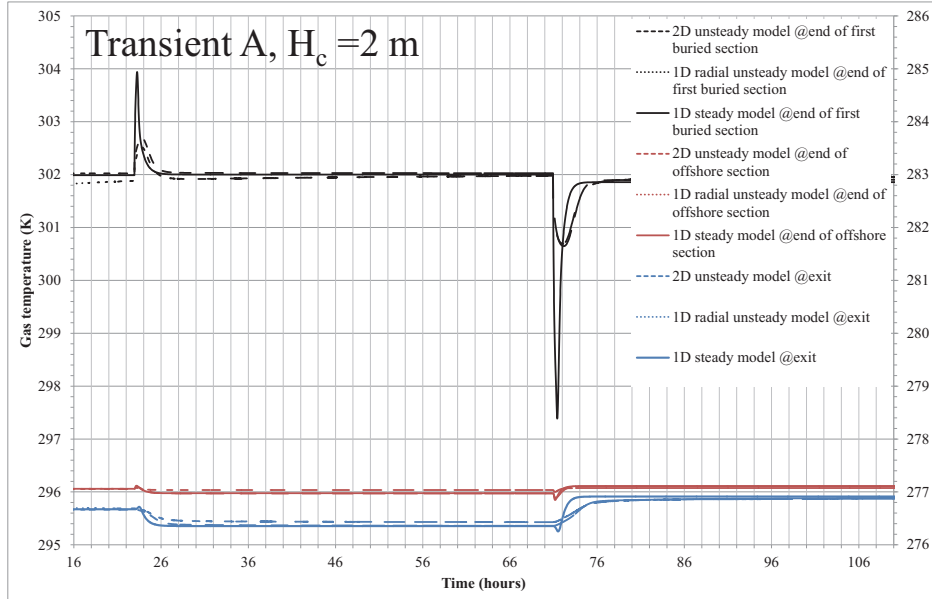


Figure E.1: Response to inlet mass transient (transient A). The soil thermal conductivity is reduced from 3 to 1 W/m²K.

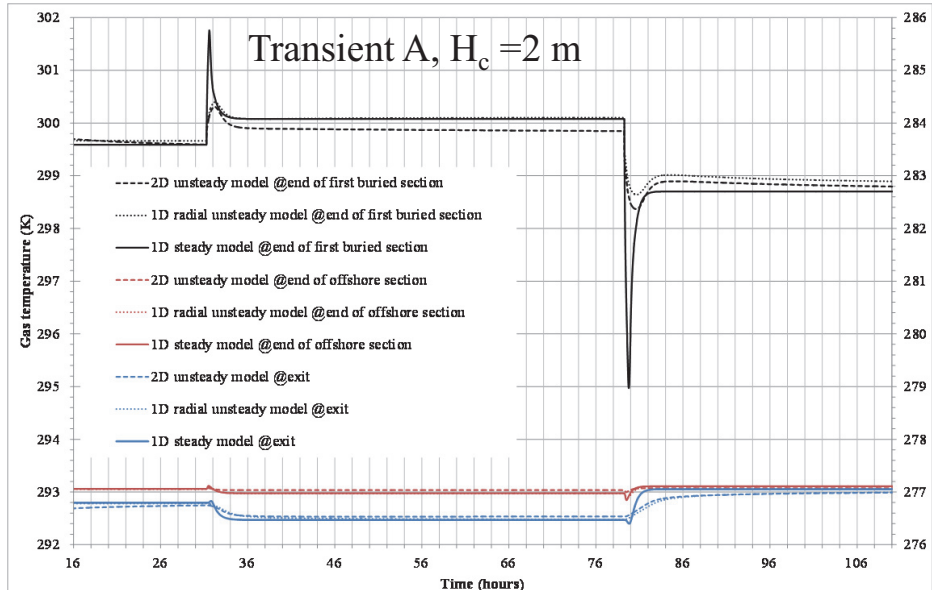


Figure E.2: Response to inlet mass transient (transient A). The soil thermal conductivity is increased from 3 to 6 W/m²K.

Appendix

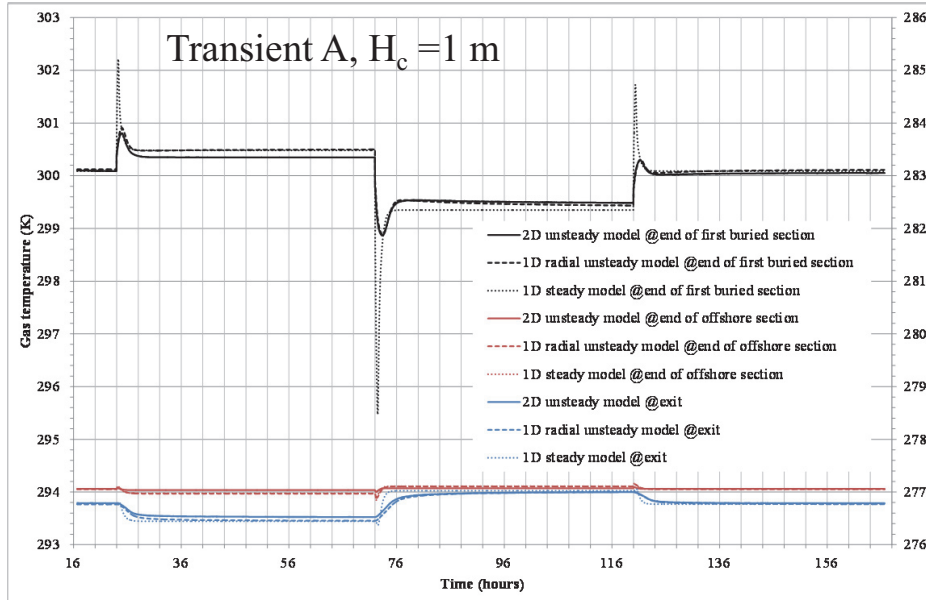


Figure E.3: One meter burial depth case. Gas temperatures in response to the inlet mass rate transient are shown at different locations along the pipeline route.

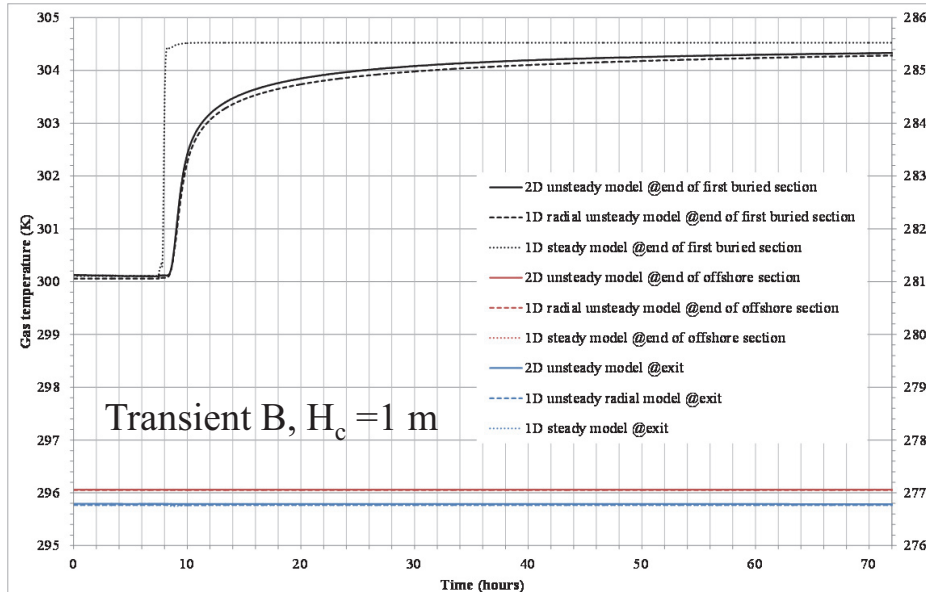


Figure E.4: One meter burial case: Gas temperatures in response to the inlet temperature transient are shown at different locations along the pipeline route.

Appendix

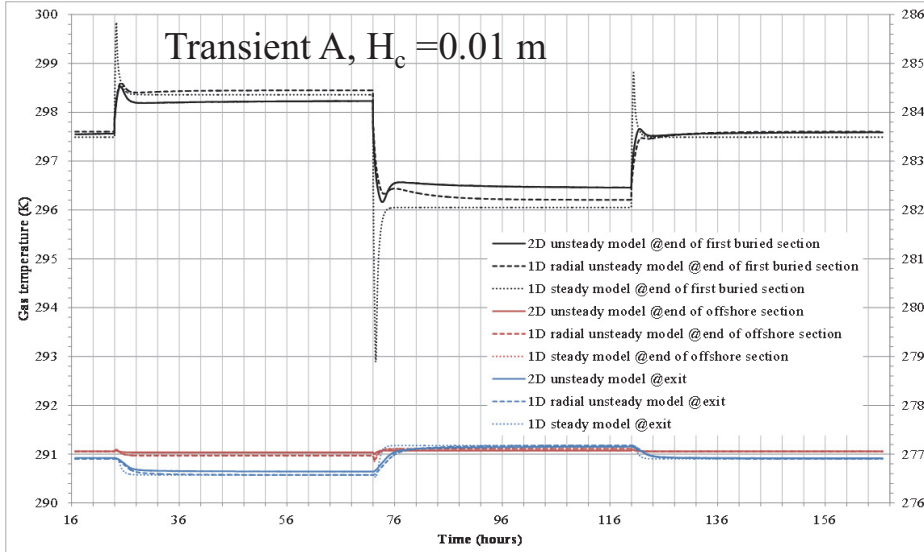


Figure E.5: One cm burial case: Gas temperatures in response to the inlet mass rate transient are shown at different locations along the pipeline route.

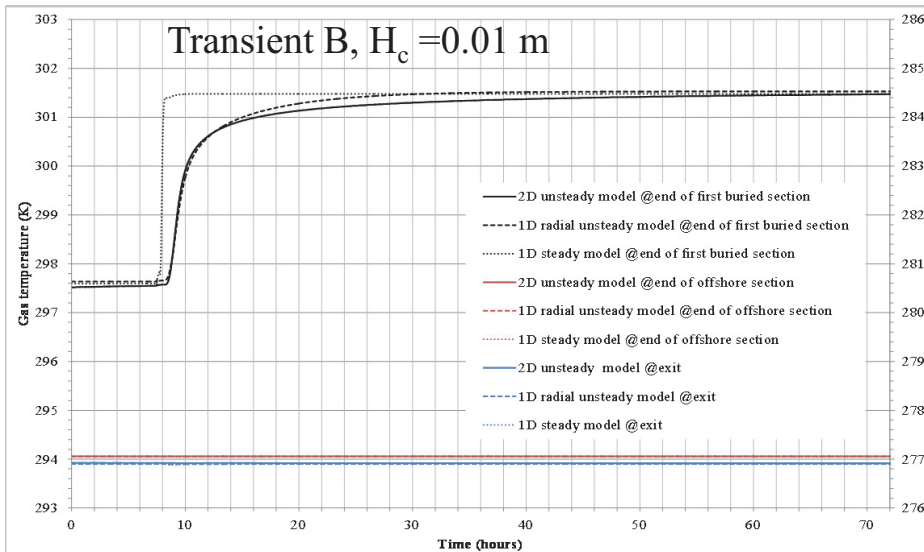


Figure E.6: One cm burial case. Gas temperatures in response to the inlet temperature transient are shown at different locations along the pipeline route.

Appendix

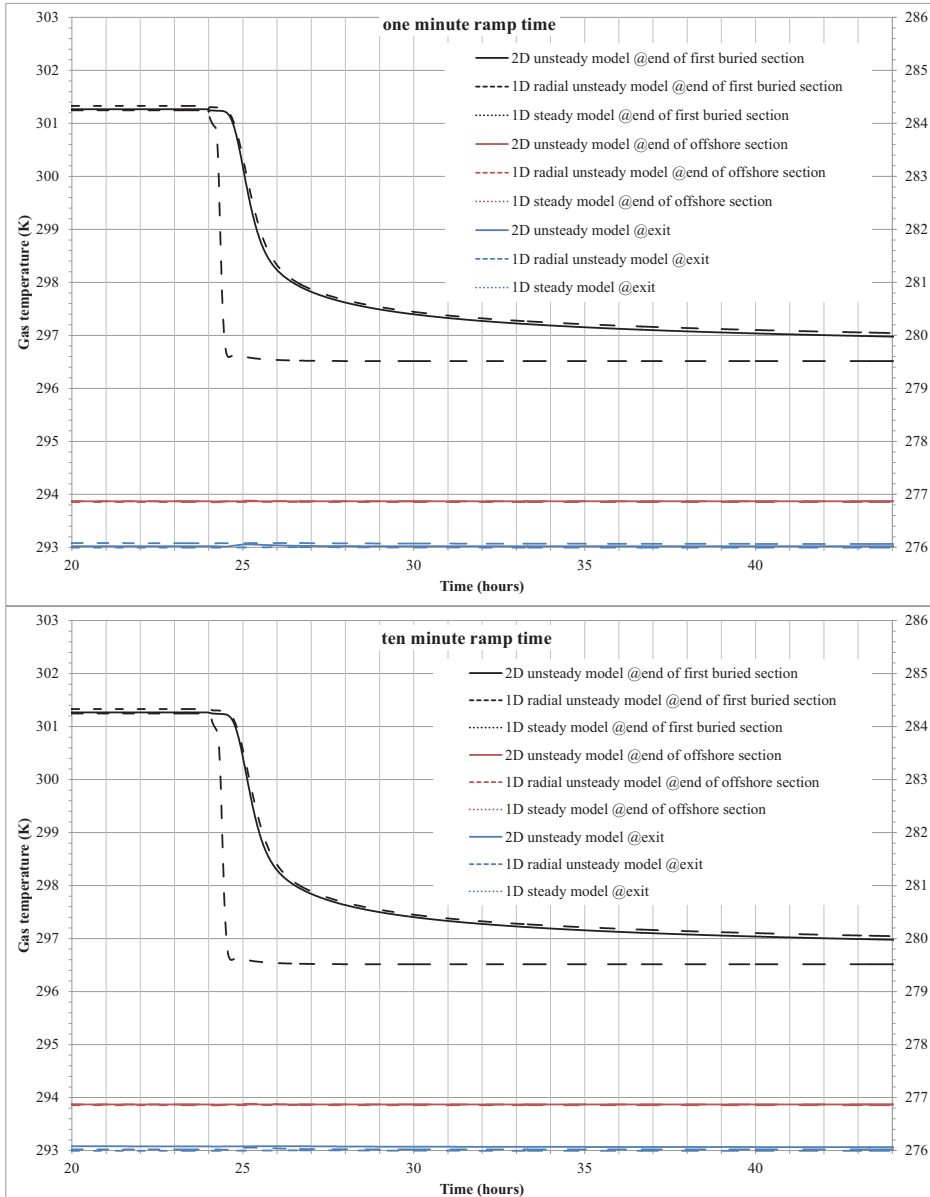


Figure E.7: Temperature response at different locations along the pipeline route in response to a sudden drop in gas temperature at the inlet. Shown are one minute ramp time (above) and ten minute ramp time (below).

Appendix

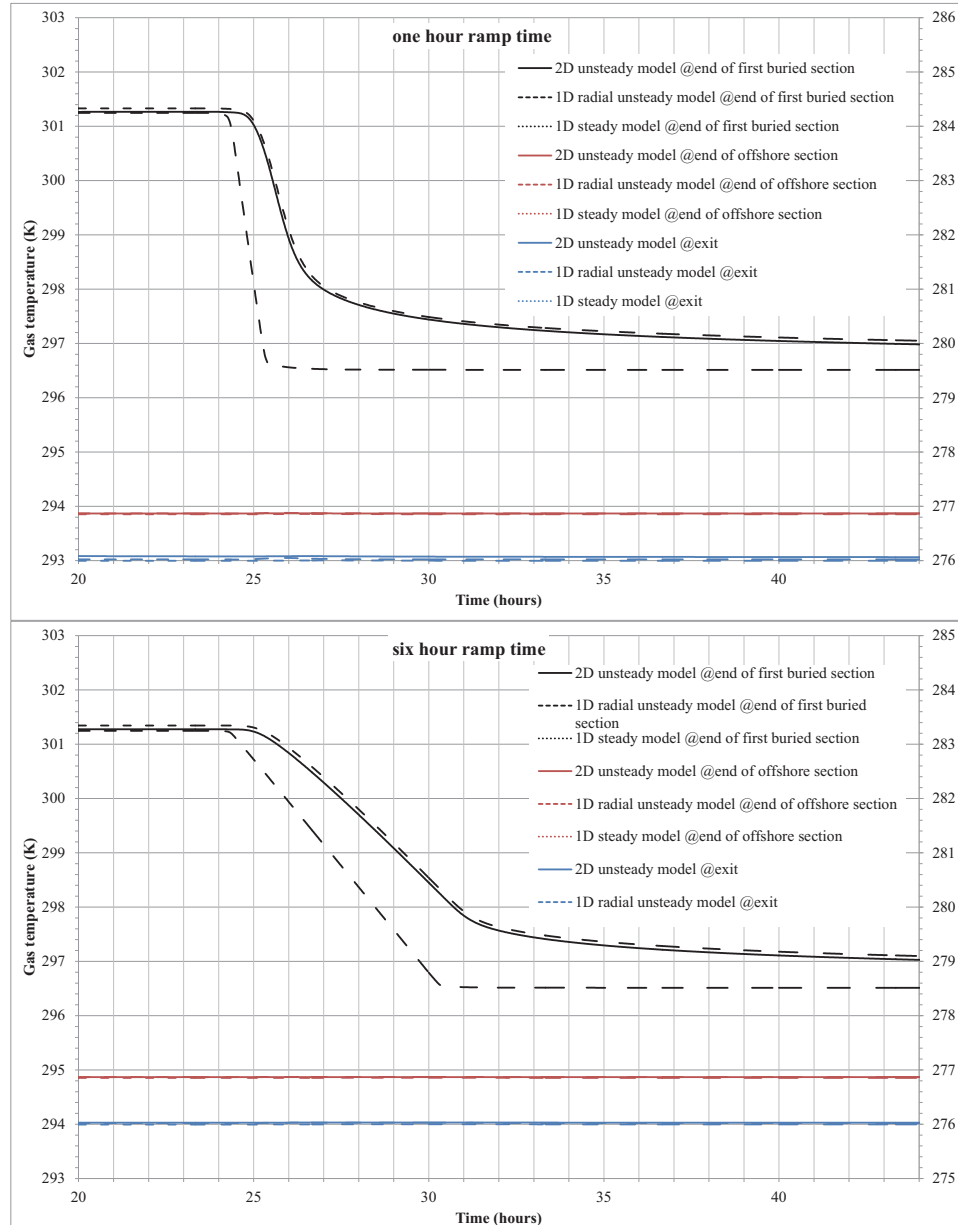


Figure E.8: Temperature response at different locations along the pipeline route in response to sudden drop in inlet gas temperature. Shown are one hour ramp time (above) and six hour ramp time (below).

Appendix

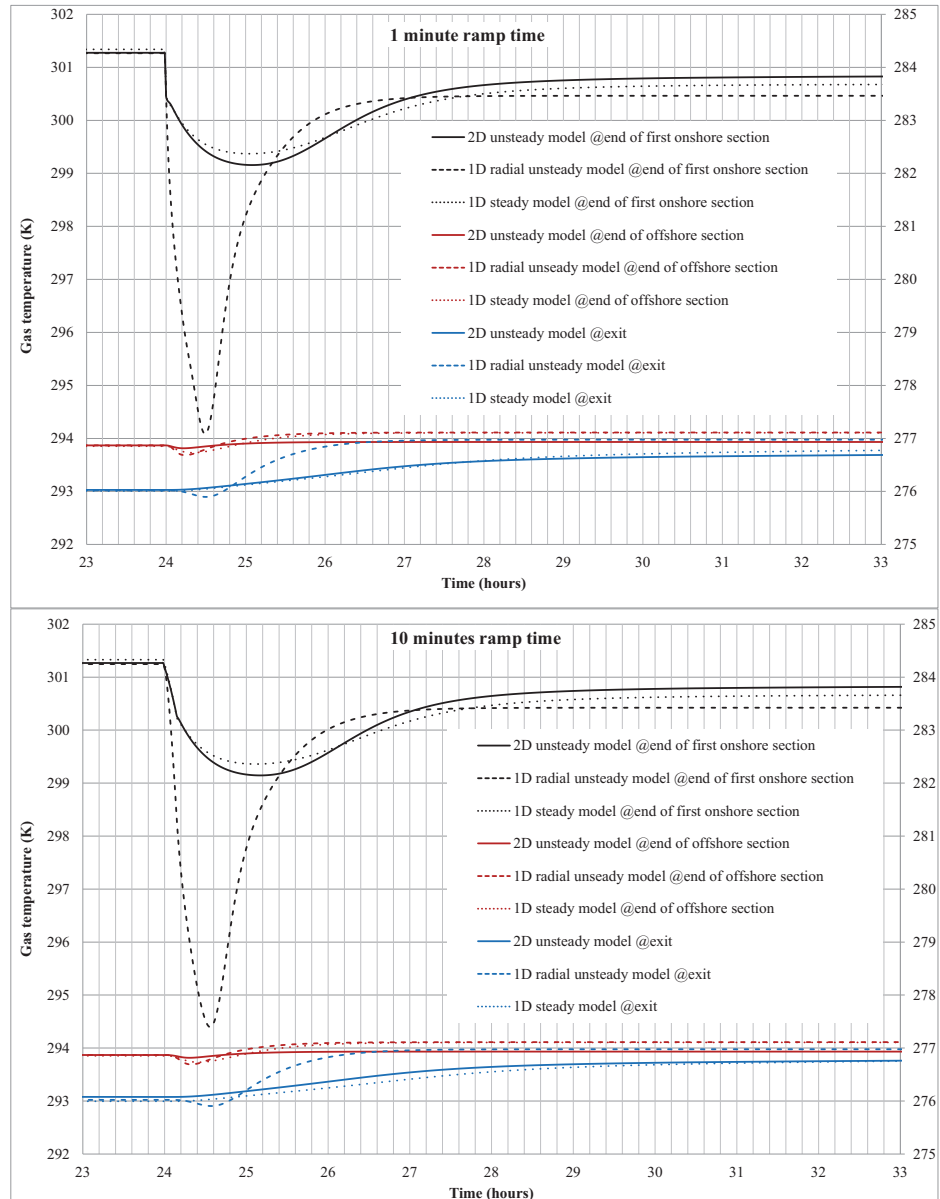


Figure E.9: Temperature response at different locations along the pipeline route in response to inlet mass flow rate change. Shown are one minute ramp time (above) and ten minute ramp time (below).

Appendix

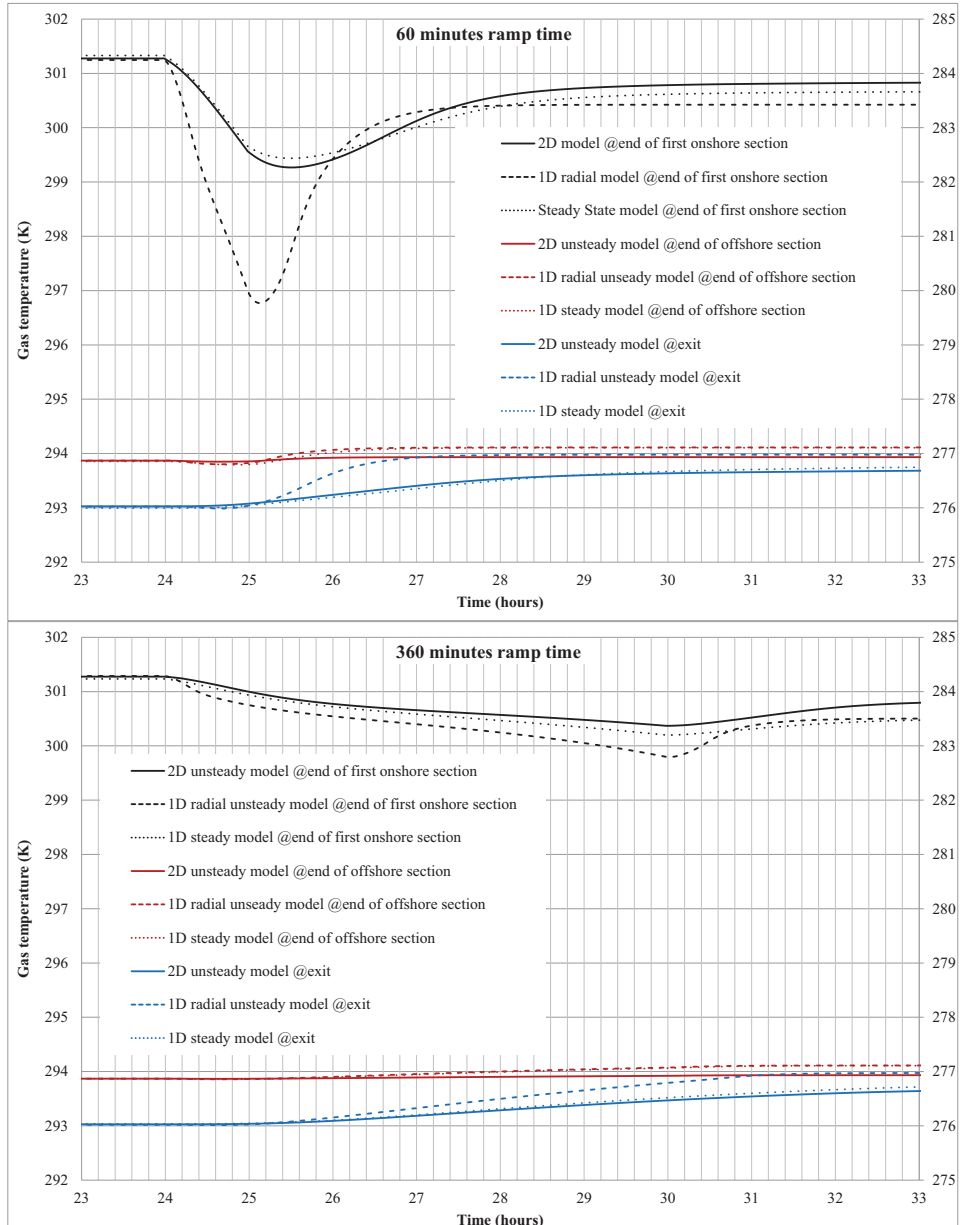


Figure E.10: Temperature response at different locations along the pipeline route in response to inlet mass flow rate change. Shown are one hour ramp time (above) and six hour ramp time (below).

Appendix F: Inner film coefficient

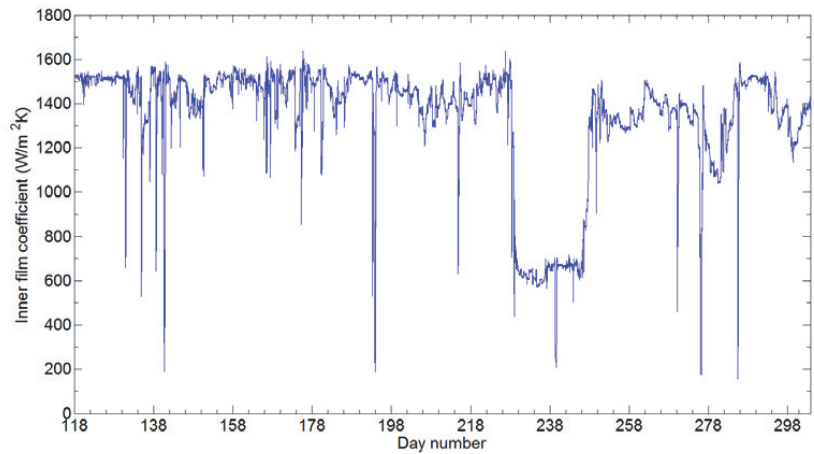


Figure F.1: Calculated innerfilm coefficient (from the 28th of April 2013 to the 27th of October 2013).

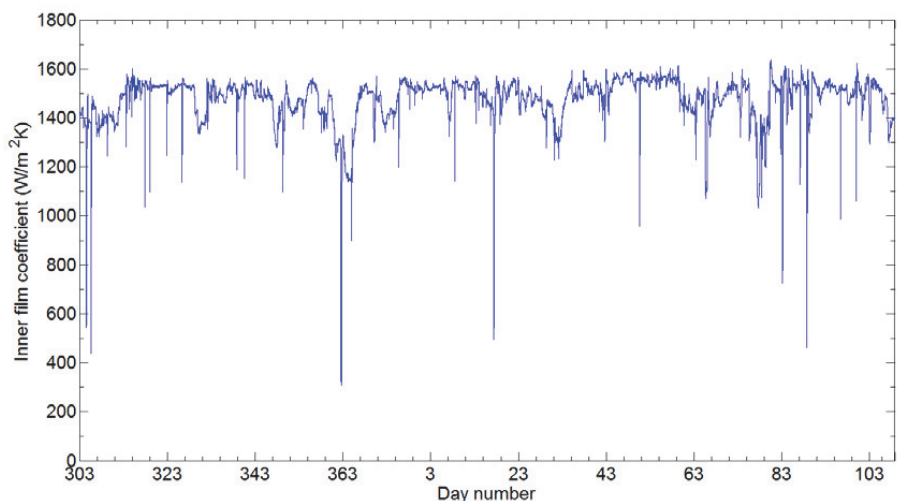


Figure F.2: Calculated innerfilm coefficient (from the 28th of October 2013 to the 28th of April 2014)

Appendix G: Measured temperature soil profiles

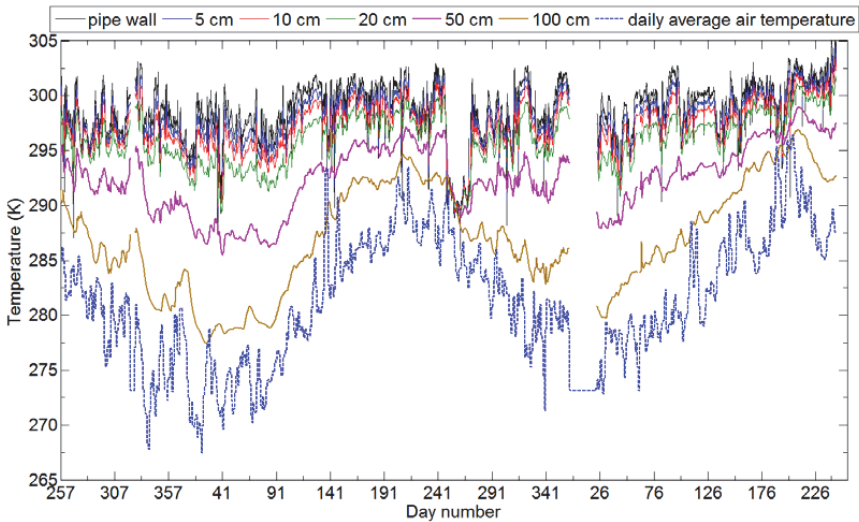


Figure G.1: Soil temperature measurements in vertical direction above the pipe (from the 14th of September 2013 to the 14th of September 2014).

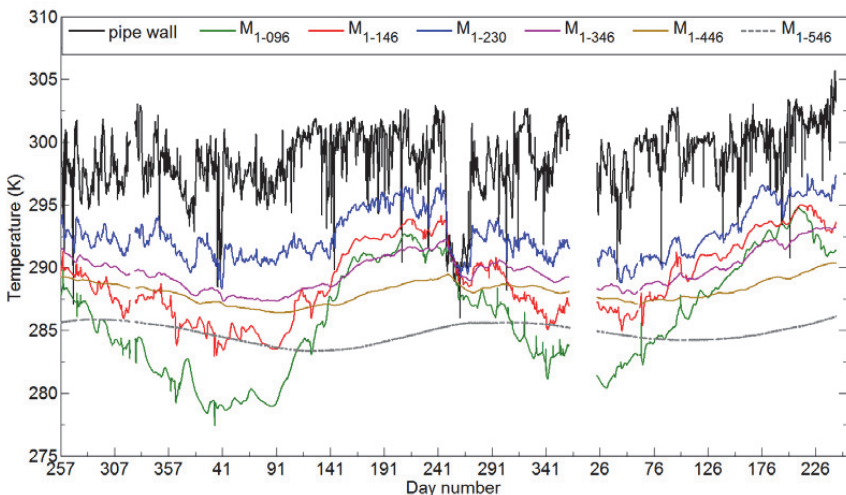


Figure G.2: Soil temperatures measurements along vertical line at 1 m lateral distance from the pipe wall. Temperature measurements in the soil at the pipe outer wall are shown by the black line (from the 14th of September 2013 to the 14th of September 2014).

Appendix

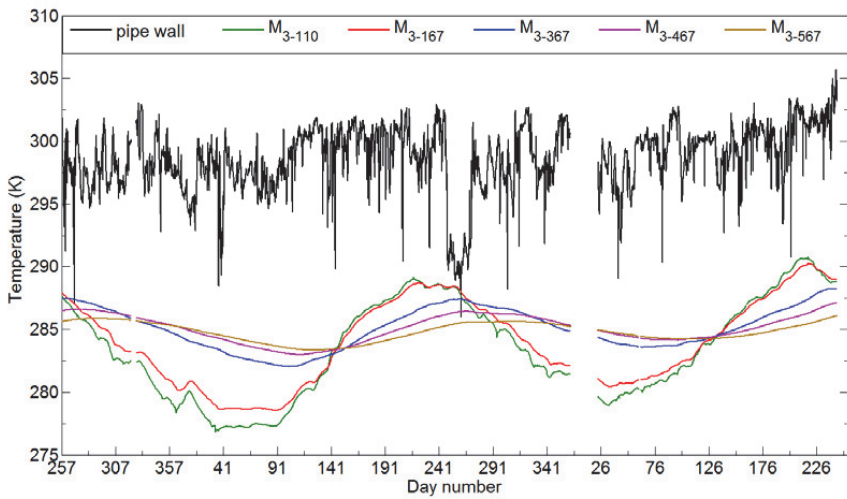


Figure G.3: Soil temperatures along vertical line at 3 m lateral distance from the pipe wall. Temperature measurements in the soil at the pipe outer wall are shown by the black line (from the 14th of September 2013 to the 14th of September 2014).

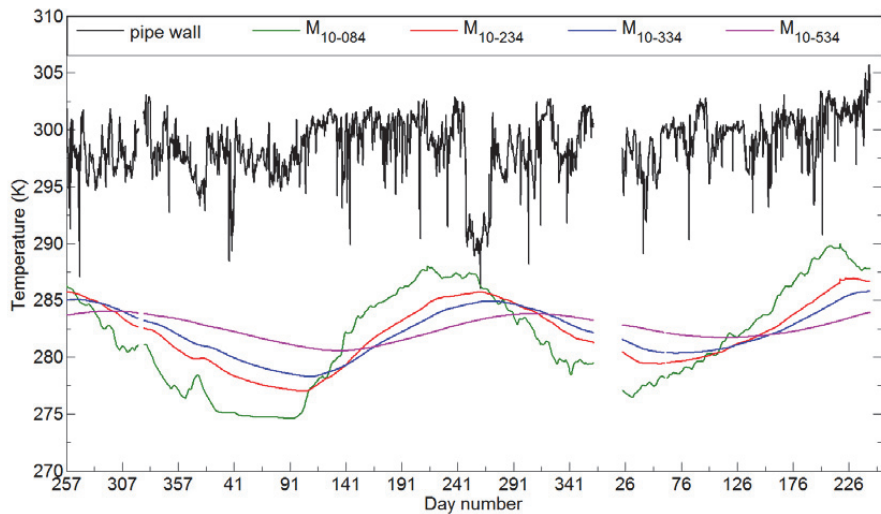


Figure G.4: Soil temperatures along vertical line at 10 m lateral distance from the pipe wall. Temperature measurements in the soil at the pipe outer wall are shown by the black line (from the 14th of September 2013 to the 14th of September 2014).

Appendix H: Measured and modelled temperature curves

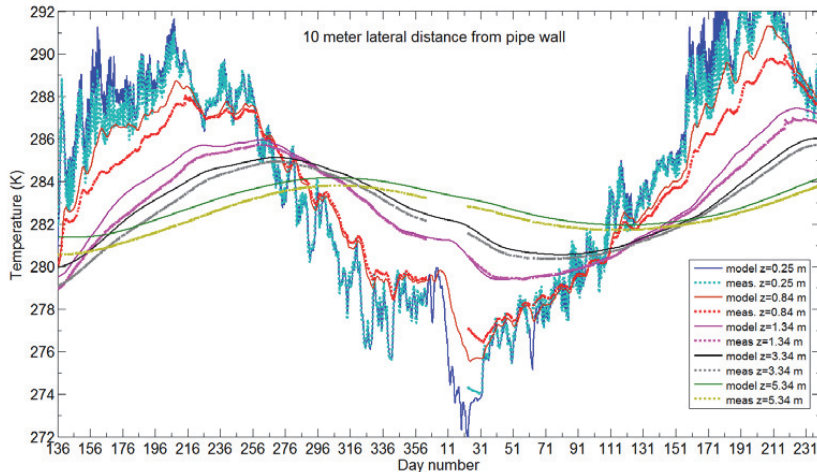


Figure H.1: Calculated versus measured temperatures. 10 m lateral distance from the pipe wall (from the 16th of May 2013 to the 20th of August 2014).

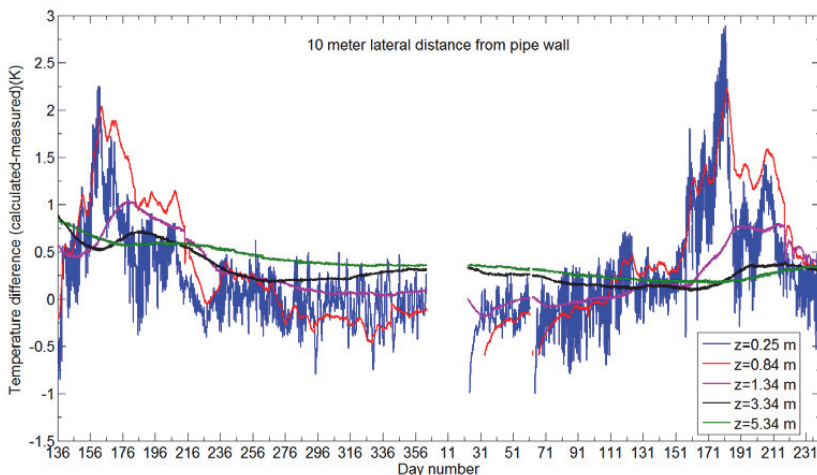


Figure H.2: Difference in calculated versus measured temperatures. 10 m lateral distance from the pipe wall (from the 16th of May 2013 to the 20th of August 2014).

Appendix

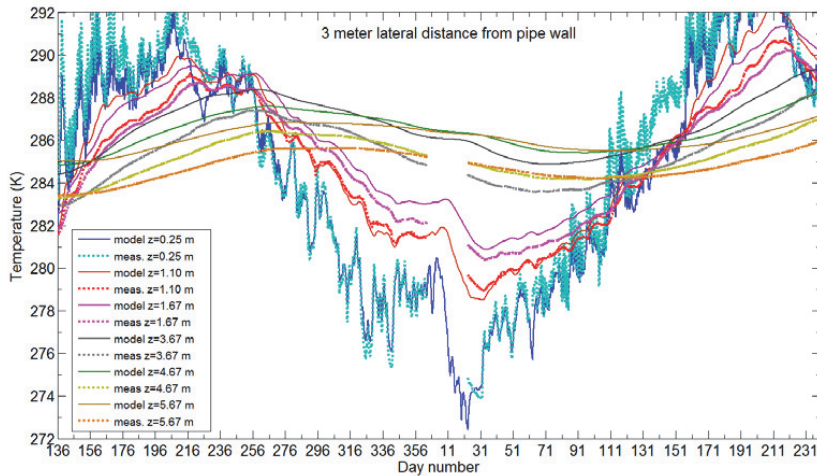


Figure H.3: Calculated versus measured temperatures. 3 m lateral distance from the pipe wall (from the 16th of May 2013 to the 20th of August 2014).

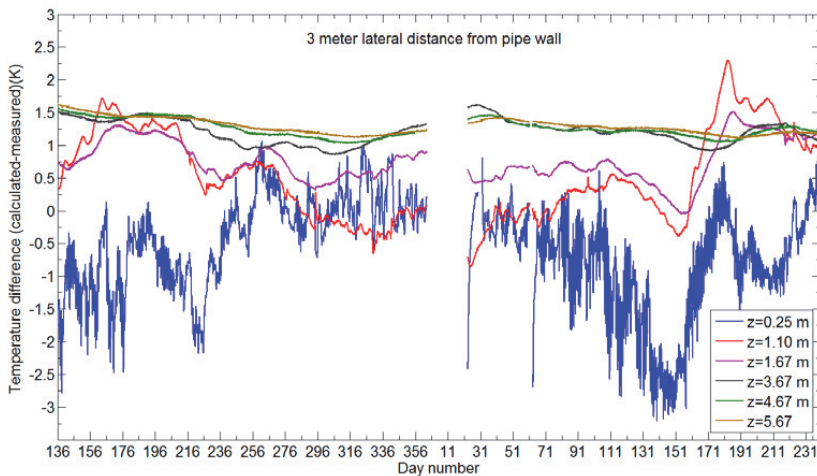


Figure H.4: Difference in calculated versus measured temperatures. 3 m lateral distance from the pipe wall (from the 16th of May 2013 to the 20th of August 2014).

Appendix

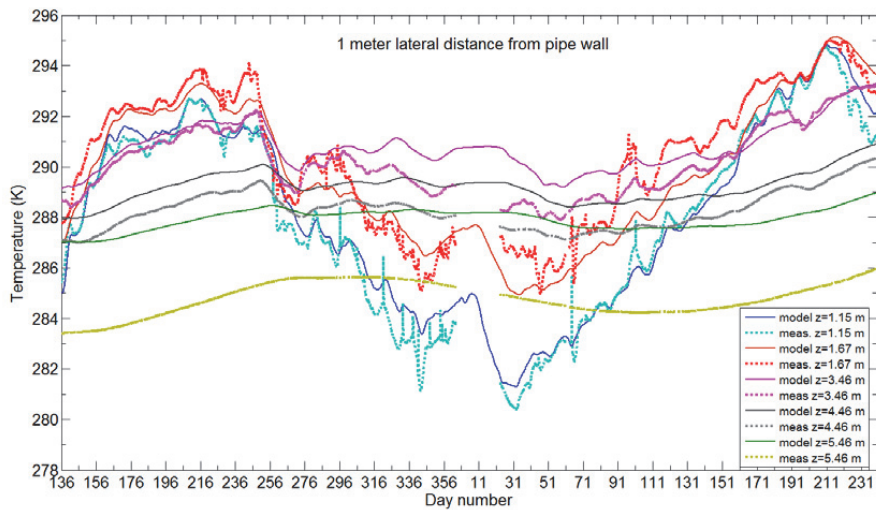


Figure H.5: Calculated versus measured temperatures. 1 m lateral distance from the pipe wall (from the 16th of May 2013 to the 20th of August 2014).

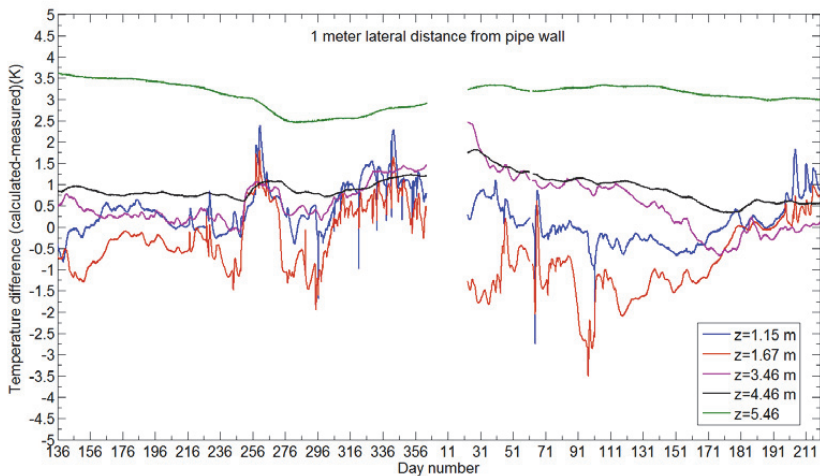


Figure H.6: Difference in calculated versus measured temperatures. 1 m lateral distance from the pipe wall (from the 16th of May 2013 to the 20th of August 2014).

Appendix

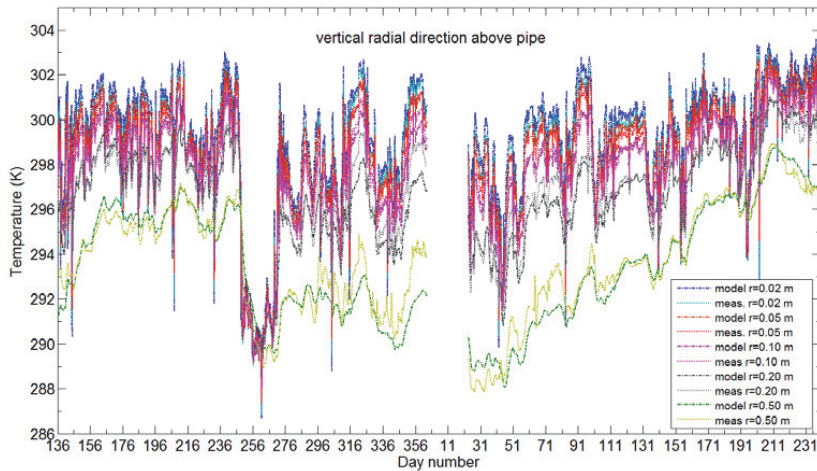


Figure H.7: Calculated versus measured temperatures. Vertical direction above pipe (from the 16th of May 2013 to the 20th of August 2014).

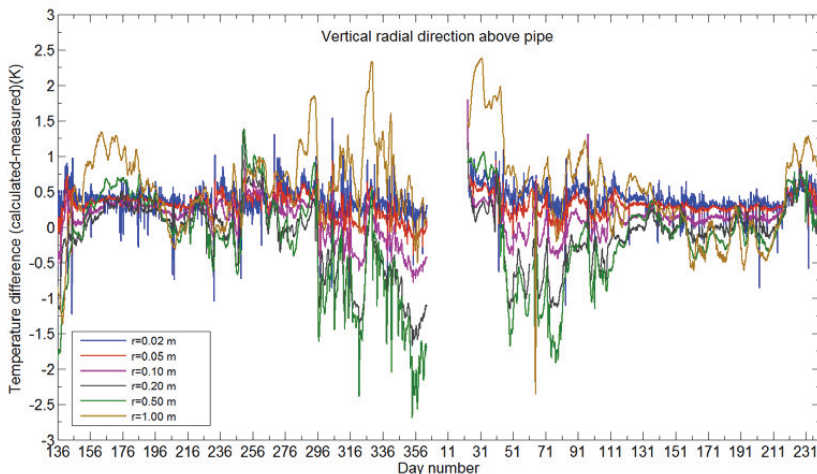


Figure H.8: Difference in calculated versus measured temperatures. Vertical direction above pipe (from the 16th of May 2013 to the 20th of August 2014).

Appendix

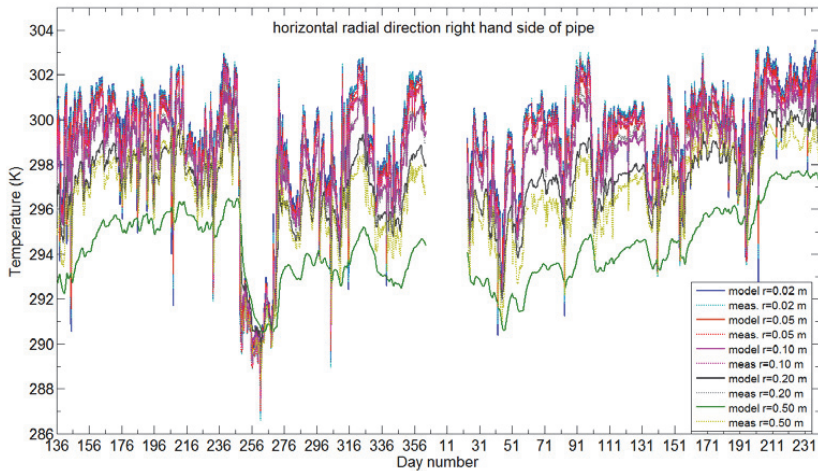


Figure H.9: Calculated versus measured temperatures. Horizontal direction from pipe (from the 16th of May 2013 to the 20th of August 2014).

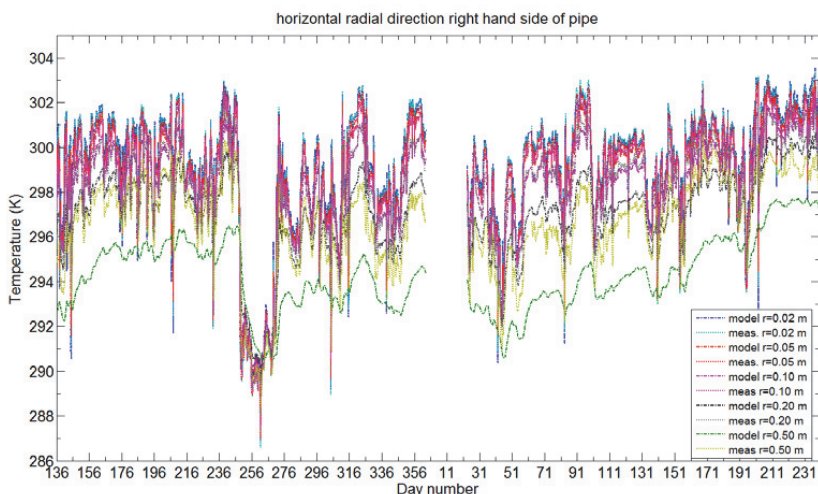


Figure H.10: Difference in calculated versus measured temperatures. Horizontal direction from pipe (from the 16th of May 2013 to the 20th of August 2014).

Appendix

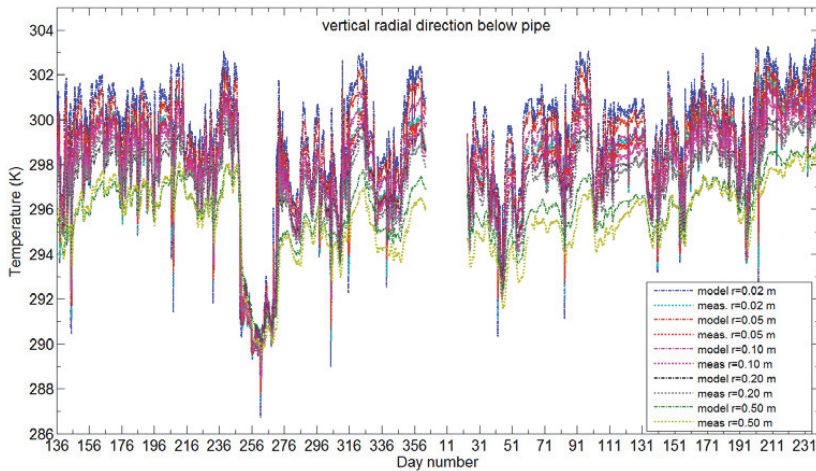


Figure H.11: Calculated versus measured temperatures. Vertical direction below pipe (from the 16th of May 2013 to the 20th of August 2014).

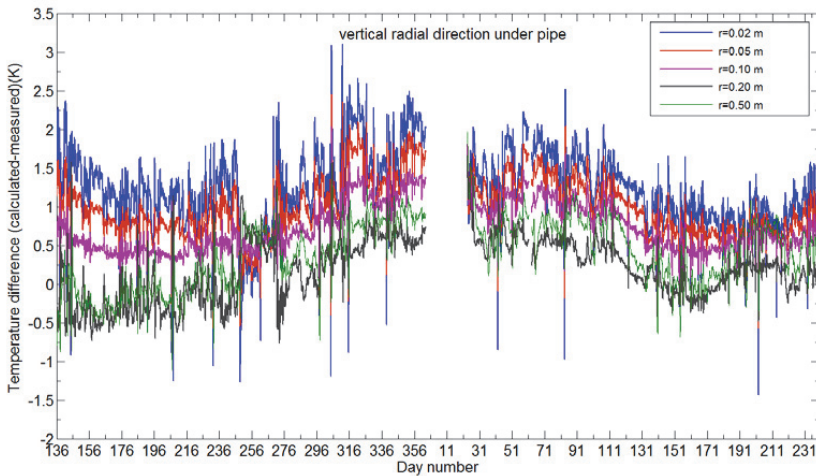


Figure H.12: Difference in calculated versus measured temperatures. Vertical direction below pipe (the 16th of May 2013 to the 9th of August 2014).

Appendix I: Results of sensitivity study on the verification model

The figure below shows the inlet gas mass rate and temperature used in the simulation (SCADA data).

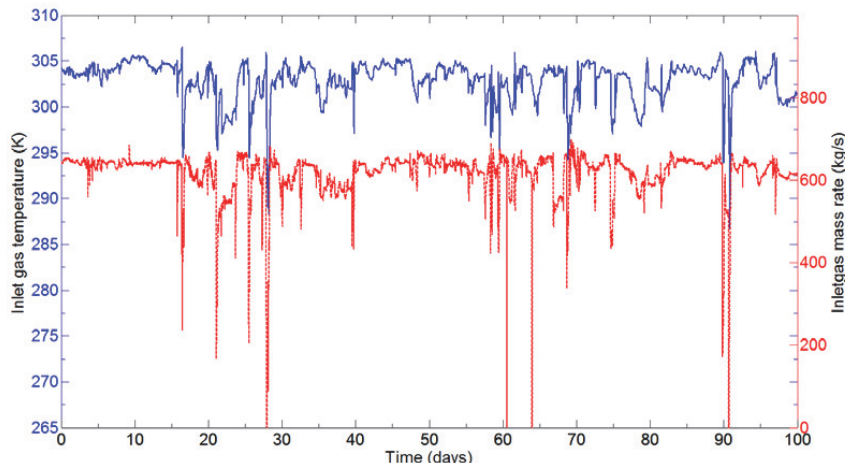


Figure I.1: Gas mass flow rate and temperature at the inlet.

The following figures show the difference in the gas temperature between the case and the base case at the measurement location for each parameter variation.

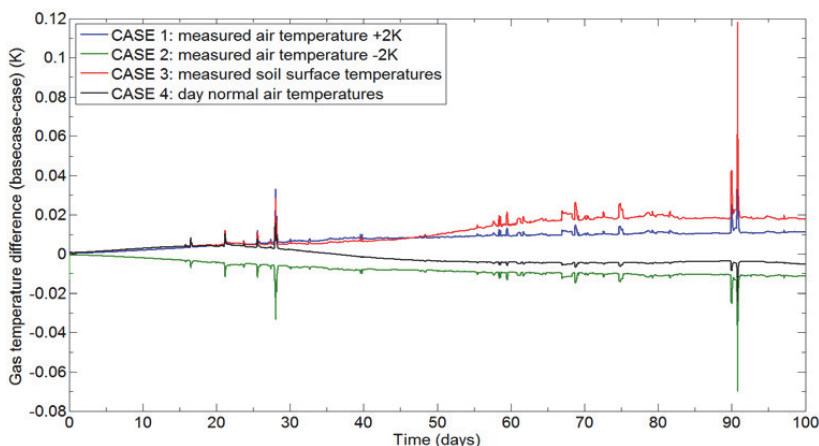


Figure I.2: Sensitivity cases for air and soil surface temperature (KP6.8).

Appendix

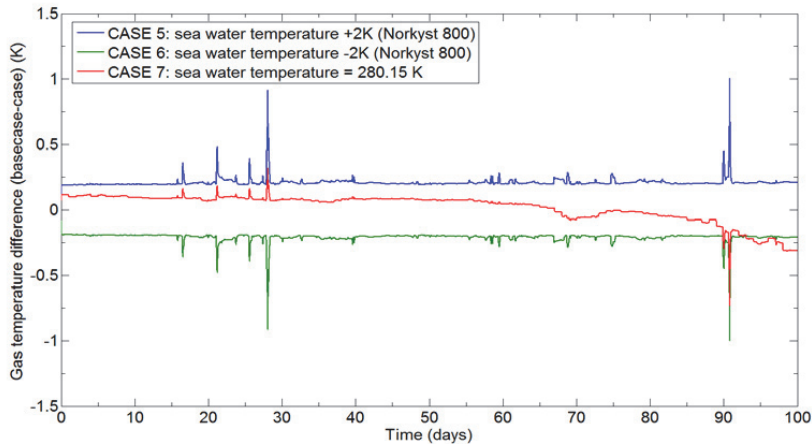


Figure I.3: Sensitivity cases for seawater temperature (KP6.8).

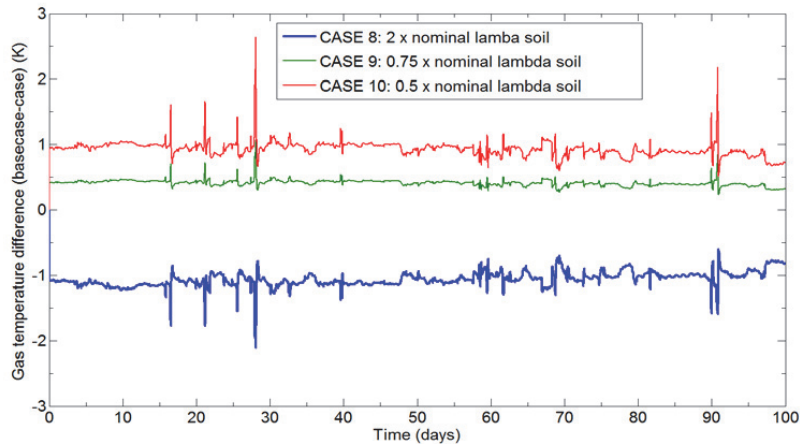


Figure I.4: Sensitivity cases for soil thermal conductivity (KP6.8).

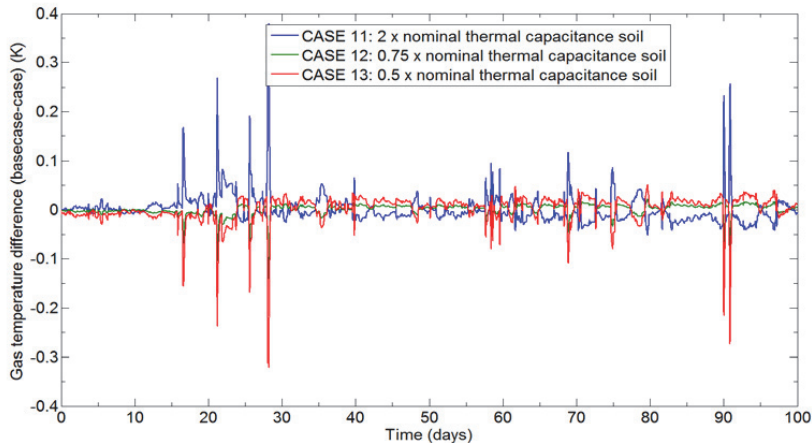


Figure I.5: Sensitivity cases for soil thermal capacitance (KP6.8).

Appendix

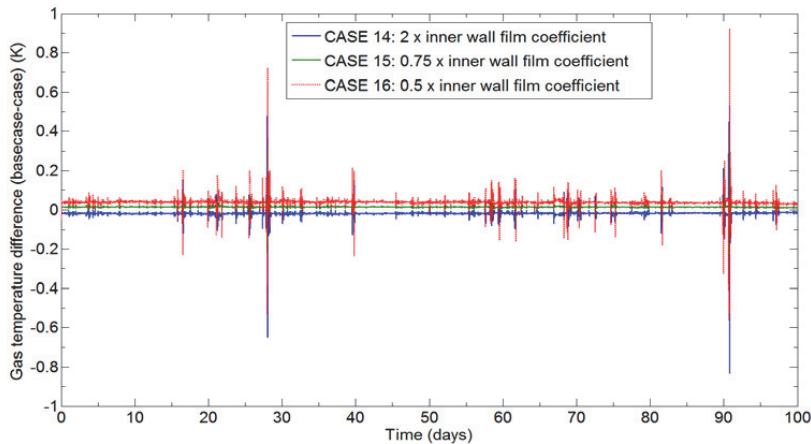


Figure I.6: Sensitivity cases for inner wall film coefficient (KP6.8).

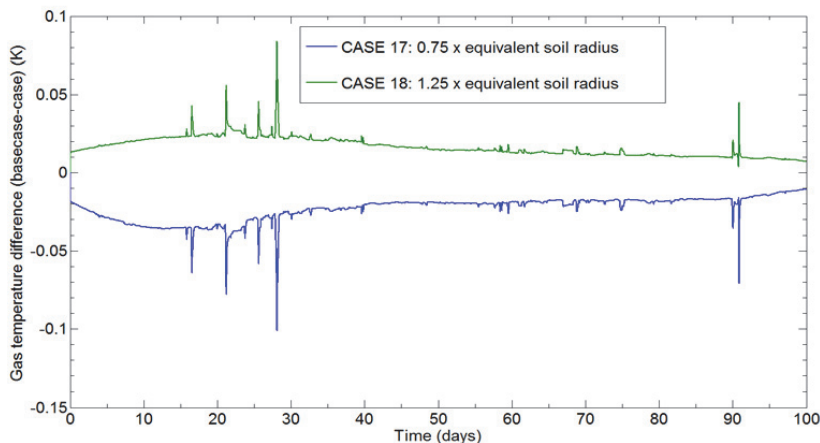


Figure I.7: Sensitivity cases for equivalent soil radius (KP 6.8).

The following figures show the difference in gas temperature between the case and the base case at KP12 for each varied parameter.

Appendix

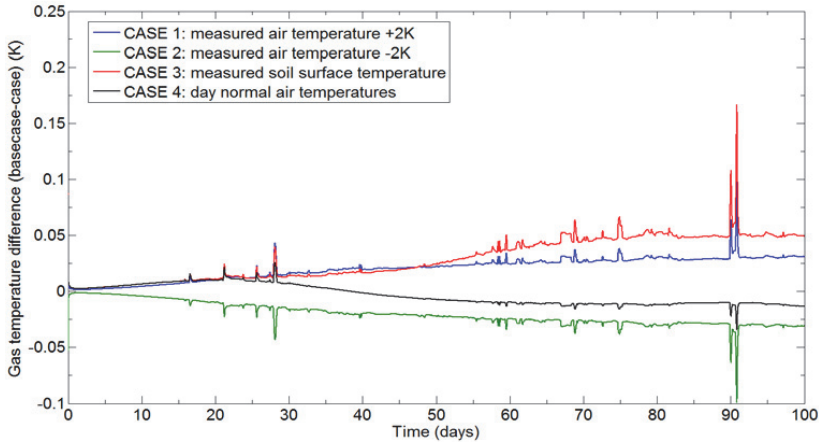


Figure I.8: Sensitivity cases for air and soil surface temperature (KP12).

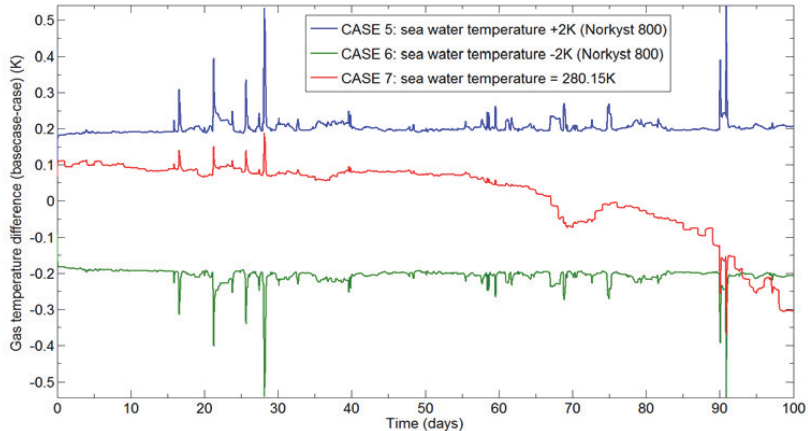


Figure I.9: Sensitivity cases for seawater temperature (KP12).

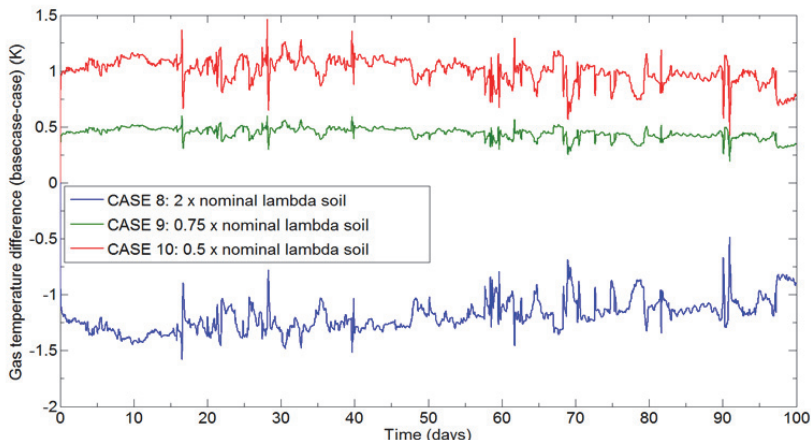


Figure I.10: Sensitivity cases for soil thermal conductivity (KP12).

Appendix

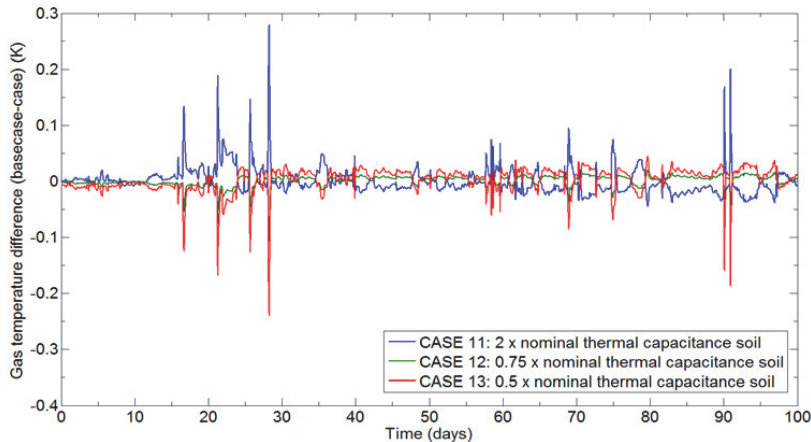


Figure I.11: Sensitivity cases for soil thermal capacitance (KP12).

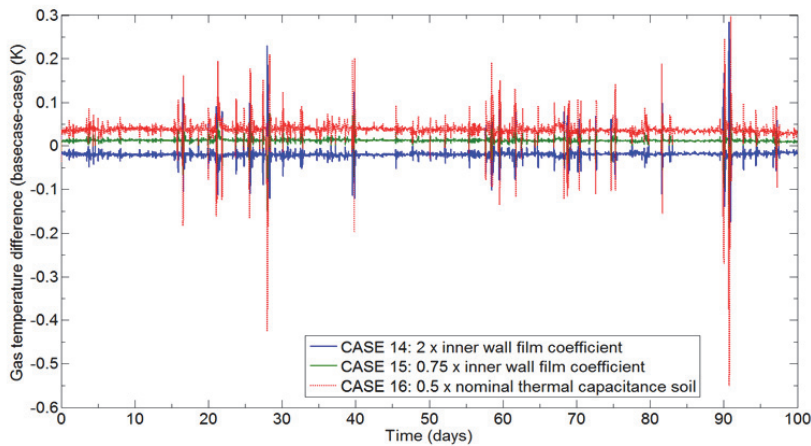


Figure I.12: Sensitivity cases for inner wall film coefficient (KP12).

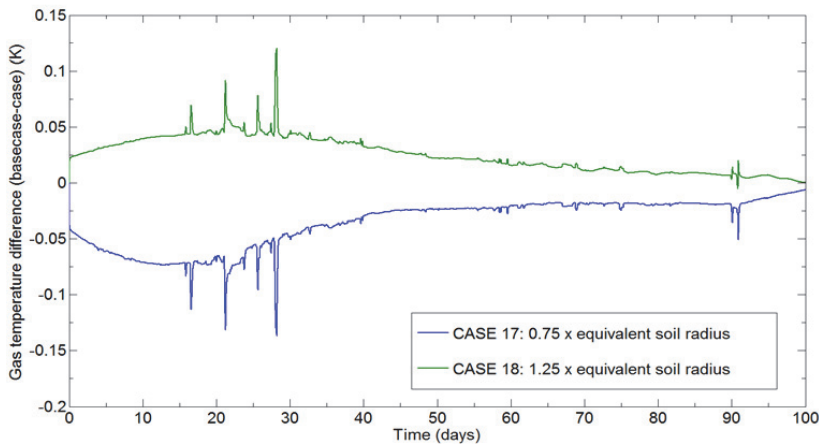


Figure I.13: Sensitivity cases for equivalent soil radius (KP 12).

Appendix

The following figures show the difference in inner wall heat exchange rate between the case and the base case at the measurement location for each varied parameter.

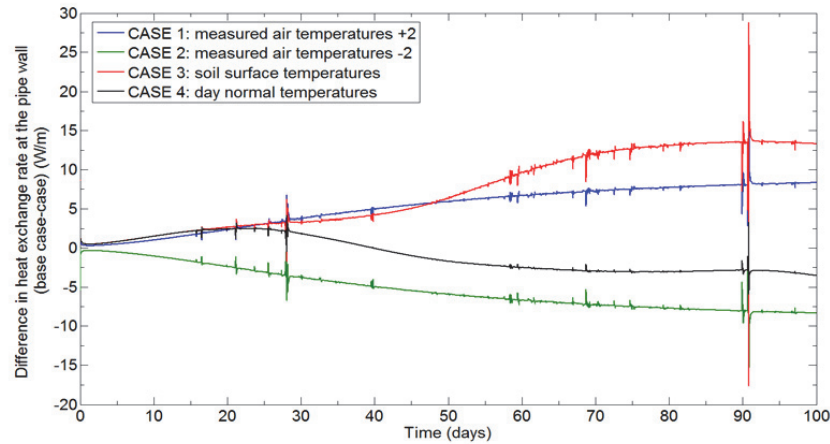


Figure I.14: Sensitivity cases for air and soil surface temperature (KP6.8).

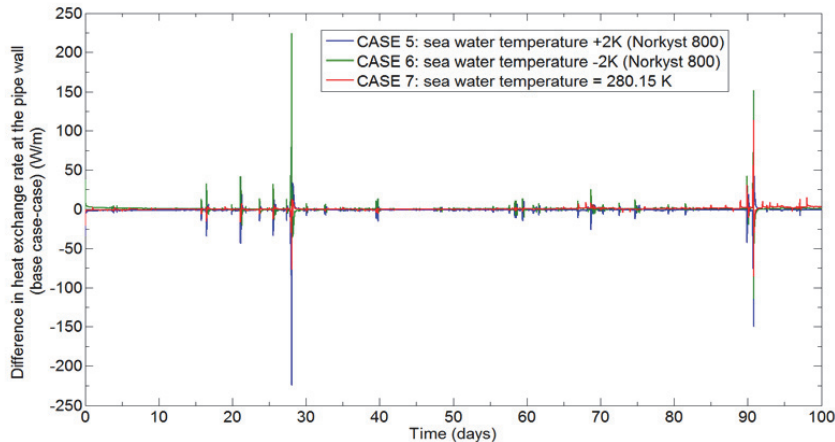


Figure I.15: Sensitivity cases for seawater temperature (KP6.8).

Appendix

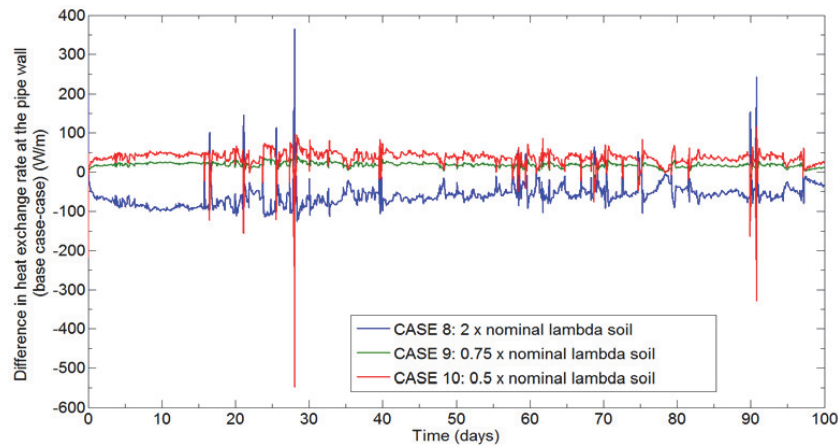


Figure I.16: Sensitivity cases for soil thermal conductivity (KP6.8).

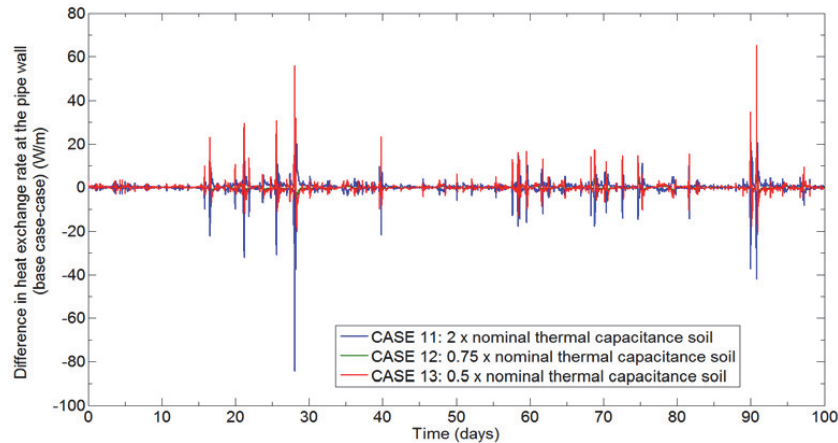


Figure I.17: Sensitivity cases for soil thermal capacitance (KP6.8).

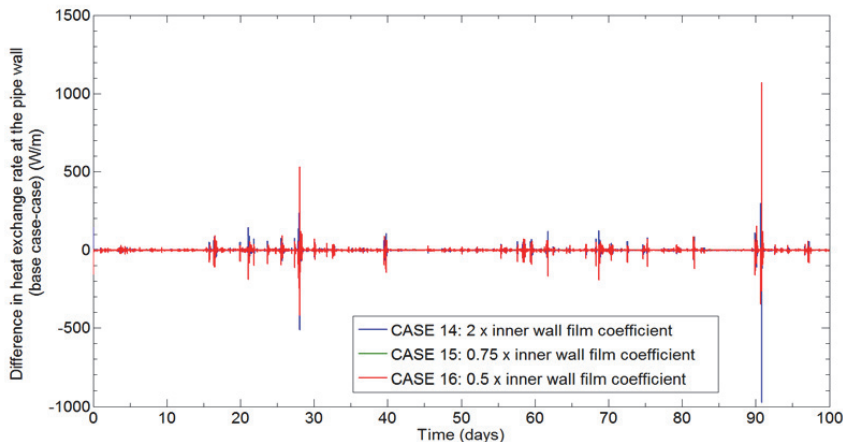


Figure I.18: Sensitivity cases for inner wall film coefficient (KP6.8).

Appendix

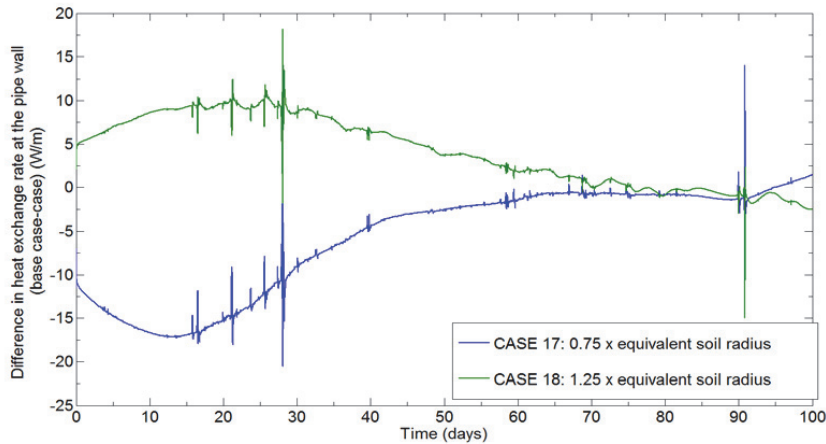


Figure I.19: Sensitivity cases for equivalent soil radius (KP 6.8).

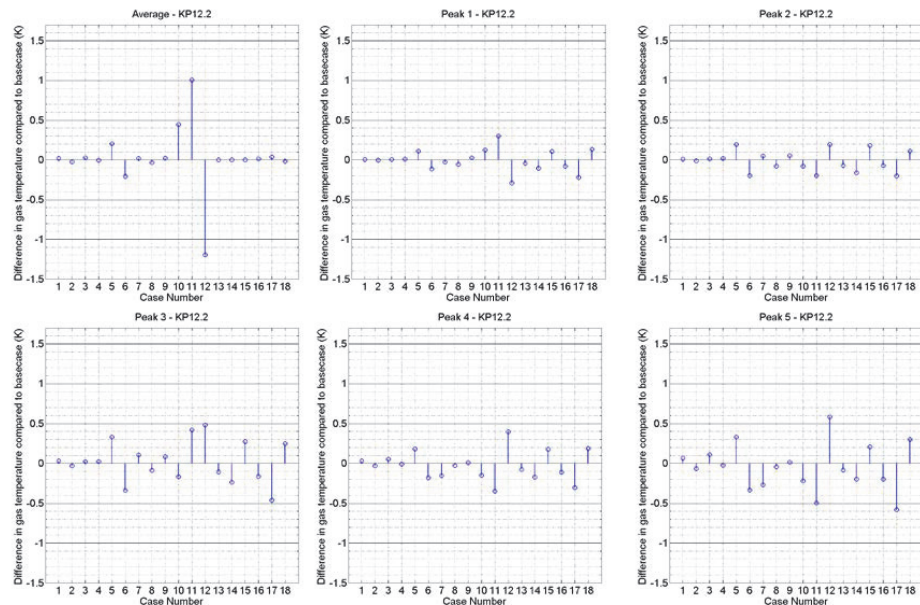


Figure I.20: Average gas temperature difference and peak gas temperature difference between each case and the base case (KP12).